Proceedings of the

2nd International Conference on Structural Engineering Research (iCSER2019)
4th GCSTMR World Congress

19-22 January 2019

Dhaka, Bangladesh

ISBN: 978-0-6482681-2-3

Fidelis R. Mashiri, Md Kamrul Hassan, Mahbuba Begum, Swapan Saha, Raquib Ahsan, Eds.

Global Circle for Scientific, Technological and Management Research (GCSTMR)

Proceedings of the 2nd International Conference on Structural Engineering Research,
4th GCSTMR World Congress, 19-22 January 2019, Dhaka, Bangladesh

Published by Science, Technology and Management Crest Australia (STAMCA)
in association with
Global Circle for Scientific, Technological and Management Research, Sydney, Australia

Editors:

Fidelis R. Mashiri
Associate Professor
School of Computing, Engineering and Mathematics
Western Sydney University, Australia

Md Kamrul Hassan
Post-Doctoral Research Fellow
Centre for Infrastructure Engineering,
Western Sydney University, Australia

Mahbuba Begum
Professor
Department of Civil Engineering
Bangladesh University of Engineering and Technology, Bangladesh

Swapan Saha
Associate Professor
School of Computing, Engineering and Mathematics
Western Sydney University, Australia

Raquib Ahsan
Professor
Department of Civil Engineering
Bangladesh University of Engineering and Technology, Bangladesh

Date published: 19 January 2019

Publisher:
Science, Technology and Management Crest
12 Boyer Pl, Minto, New South Wales 2565, Sydney, Australia

Abstract Review Process:
The submitted abstracts in iCSER-2019 were reviewed by the Technical Committee.

2nd International Conference on Structural Engineering Research (iCSER2019)
4th GCSTMR World Congress

19-22 January 2019, Dhaka, Bangladesh

Organized by:

LOGOS of Sponsoring Companies

Sponsors to three Engineering Conferences (iCSER2019, iCWEE2019, iCERP2019) are Shah Cement, Sevenrings Cement, and Bengal cement.

Welcome by Conference Chair and Co-Chairs

The 2nd International Conference on Structural Engineering Research aims to provide an international platform for effective exchange of ideas, reaffirming the existing collegial contacts, provide opportunities for establishing new ones as well as providing a forum for academics and researchers to present and share the results and findings of their latest research and practice on a wide range of topics relevant in structural engineering.

As the General Co-Chair of the 2nd International Conference on Structural Engineering Research, 19-22 January 2019, Dhaka (iCSER-2019), we would like to thank the Plenary Speakers, Keynote Speakers, Invited Speakers, Authors, Sponsors, Secretaries, IT Team Members, Authors, Conference Advisory Committee Members, Organising Committee Members, Technical Committee Members, Reviewers and Volunteers for making this conference successful.

Associate Professor Fidelis R. Mashiri
Chair

Associate Professor Swapan Saha
Co-Chair

Professor Raquib Ahsan,
Co-Chair

2nd International Conference on Structural Engineering Research (iCSER-2019)

CHIEF AND SPECIAL GUESTS

Chief Guest:

Mr K M Khalid, MP, Hon'ble State Minister, Ministry of Cultural Affairs, Government of Bangladesh

Senior Special Guest:

Professor Dr. Engr. Jamilur Reza Choudhury
National Professor, Vice-Chancellor, University of Asia Pasific (UAP), Past Advisor, Bangladesh Government

Special Guests:

Professor Dr. Abdul Mannan
Chairman, University Grants Commission (UGC)

Professor Dr. Engr. Saiful Islam
Vice-Chancellor, Bangladesh University of Engineering and Technology (BUET)

Professor Dr. M A Mannan
Vice-Chancellor, Bangladesh Open University (BAU)

Professor Dr. Mohammed Alauddin
Vice-Chancellor, Dhaka University of Engineering and Technology (DUET), Bangladesh

Professor Dr. Quazi Sazzad Hossain
Vice-Chancellor, Khulna University of Engineering and Technology (KUET), Bangladesh

Professor M A Hannan
Rector
Engineering Staff College Bangladesh, Dhaka, Bangladesh and
Past President, The Institution of Engineers, Bangladesh (IEB), Bangladesh

Professor Emeritus Dr. Engr. M. Shamim Z. Bosunia
Past President, The Institution of Engineers' Bangladesh (IEB)

Engr. Md Abdus Sabur
President, The Institution of Engineers, Bangladesh (IEB), Bangladesh

Mr. Md. Sabur Khan
Chairman & Founder, Daffodil International University (DIU)

Professor Dr. Gias U. Ahsan
Pro Vice-Chancellor, North South University (NSU), Bangladesh

PLENARY SPEAKERS

Plenary 1: Engr. Klaas Visser, Principal, KAV Consulting Pty Ltd, Australia
Title: Bypassing the HFC Phasedown by Using Highly Efficient CO_2 and Hydro Carbon Refrigeration for the Cooling of Buildings in Bangladesh.

Plenary 2: Prof. Dr. Taha B.M.J. Ouarda, National Institute for Scientific Research, Canada
Title: Impacts of Climate Change on Water Resources.

Plenary 3: Engr. Dr Rafiqul Islam, CEO, Solar-e-Technology, Sydney, Australia
Title: Educating Engineers with Personality as World Citizen Leading to Sustainable Development.

Plenary 4: Prof. Dr. Vivian Tam, Western Sydney University, Australia
Title: Construction Automation: A Concrete Perspective.

Plenary 5: Prof. Dr. Shams Rahman, RMIT University, Australia
Title: Brain Gain and Economic Development: How Strategic the Strategy Is?

Plenary 6: Prof. Dr. Ataur Rahman, Western Sydney University, Australia
Title: Bangladesh has so much rain, but so little for drinking: Is there any sustainable solution?

Plenary 7: Prof Dr. Md Jakariya, North South University, Bangladesh
Title: Groundwater Arsenic contamination in Bangladesh: Challenges and way forward to ensure sustainable safe water coverage.

Plenary 8: Prof. Dr. Tofail Ahmed, VC, Britannia University, Bangladesh
Title: Bangladesh - Nature and dimensions of rural transformation.

Keynote Speaker

****

Associate Professor Dr. Swapan Saha, Lead DAP - Construction Management, Engineering and Construction Management, Western Sydney University, Australia

Title of Presentation: Case Studies in Australian on Work Health and Safety Requirements during the Construction Process of Temporary Structures.

Biography: Swapan Saha received his Master of Engineering degree in Construction in 1989 from the Asian Institute of Technology in Bangkok, Thailand and obtained his PhD in 2003 from the University of Western Sydney. He currently works at Western Sydney University as the Lead Director of Academic Program (Construction Management). Swapan's teaching and research are mainly in the areas of construction management and simulation, construction information systems and construction technology. He worked in the construction industry in Australia and Thailand before joining as an academic member of staff with UWS. Swapan has worked on landmark projects including the Sydney Harbour Tunnel Project during 1990 and 1992, plus the Bangkok elevated expressway project in 1989. He has published papers in journals and conferences and is a member of Engineers Australia and the Fellow of the Australian Institute of Building.

Keynote Speaker

****

Professor Dr. Ahsanul Kabir, Head, Department of Civil Engineering, Bangladesh University of Engineering and Technology (BUET), Dhaka, Bangladesh

Title of Presentation: Developing Safety Assessment Procedure for Existing Buildings in Bangladesh.

Biography: Prof. Dr. Ahsanul Kabir is working in the department of Civil Engineering of Bangladesh University of Engineering and Technology (BUET) since 1977. He is currently serving as Head of the department of Civil Engineering. He is a Fellow of Institution of Engineers Bangladesh, Fellow Association of Civil and Environmental Engineering (ACEE), Member of International Society for Soil Mechanics and Foundation Engineering (ISSMFE), Member, Bangladesh Society of Geotechnical Engineering (BSGE) and former Member of American Concrete Institute (ACI). He has long experience of university teaching both at undergraduate and graduate levels. He is primarily involved in taking courses on structural engineering discipline of civil engineering. At postgraduate level he offered courses like Bridge Engineering, Finite Element Method, Advanced Concrete Technology and Design and Analysis of Concrete Shell Structures in different sessions. A number of technical and research publications have been made in different International and national journals that includes Masonry International, ACEE, ASCE, Institution of Engineers India, Institution of Engineers Bangladesh and others. Over forty papers have been published in different journals and in the proceedings of national and international conferences (at home and abroad). He received the Institution Gold Medal from the Indian Institution of Engineers for his outstanding journal paper on Finite Element Analysis of Skew RC Slabs in 1997. He held different administrative and academic positions at different times. Some of these are: Director of Bureau of Research Testing and Consultation, Provost and Assistant Provost of Students hall of residences, Member of Association of Universities in Bangladesh, Academic Council of BUET, Course Monitoring Committee BUET and many more. Besides teaching, he has worked as a consultant and design engineer for different project of national interest. As a member of the group of consultants of civil engineering department he has successfully completed a considerable number of (design and review) projects either individually or as a contributing member of a team. These include design of Buildings, RC and Prestressed Concrete Bridges, Pre-engineered steel buildings, Water tanks & reservoirs, Swimming pool,

RC shells, Water treatment plants, Marine Jetties, Microwave towers, folded plates, machine foundations and many other structural elements. He worked as one of the core member of the team to formulate an acceptable national guideline for safety assessment of existing Garment buildings formed by tripartite agreement between the government, garment factory owners and the sponsor International Labour Organisation (ILO).

Keynote Speaker

****

Associate Professor Dr Neaz Sheikh, School of Civil, Mining & Environmental Engineering, University of Wollongong, Australia

Title of Presentation: HSC Columns Reinforced with Glass Fiber-Reinforced Polymer Bars and Helices: Experimental Investigation.

Biography: Neaz Sheikh is an Associate Professor in the School of Civil, Mining and Environmental Engineering at the University of Wollongong. A/Prof. Sheikh obtained Bachelor of Science in Civil Engineering from Chittagong University of Engineering and Technology (CUET), Bangladesh. He obtained MPhil and PhD in Structural Engineering from the University of Hong Kong, Hong Kong SAR. A/Prof. Sheikh has authored over 150 articles in highly reputed international journals conference proceedings. He has supervised to graduation 11 Ph.D. graduates and currently supervising over 10 Ph.D. students His main research interests include reinforced concrete structures, composite structures, and structural dynamics.

Keynote Speaker

****

Associate Professor Dr. Mahmud Ashraf, Deakin University, Australia

Title of Presentation: Additive Manufacturing in Structural Engineering - A Current State-Of-The-Art and Its Future Prospects in Construction.

Biography: Mahmud is an Associate Professor in Structural Engineering at the School of Engineering in Deakin University (Geelong Waurn Ponds Campus) and he holds a visiting Associate Professorial role in UNSW Canberra. Prior to joining Deakin University in 2017, Mahmud held academic positions in the University of New South Wales and the University of Queensland in Australia. His research interests are primarily related to investigating the structural behaviour of thin-walled metallic structures subjected to a variety of loading conditions including cyclic and impact/blast loading. Recently, he is looking into the structural integrity of 3D printed metallic micro-lattice materials. He has published over 100 technical papers in the areas of stainless steel, high strength steel and aluminium structures.

CONFERENCE ORGANISING COMMITTEE

Chair:
Prof. Dr. Ataur Rahman, Western Sydney University, Australia

Co-Chairs:
Prof. Dr. Shibli R U Islam, Dhaka University, Bangladesh
Prof. Dr. Chin Leo, Western Sydney University, Australia
Prof. Dr. Ahsanul Kabir, Bangladesh University of Engineering and Technology (BUET), Bangladesh

General Secretary:
Dr. Amir Ahmed, Daffodil International University, Bangladesh

Co-General Secretaries:
Dr. Hasan Hafizur Rahman, Science, Technology and Management Crest, Sydney, Australia
Assoc. Prof. Dr. Amimul Ahsan, Uttara University, Bangladesh
Dr. Md. Kamrul Hassan, Western Sydney University, Australia

Treasurer:
Dr. Shafiqul Alam, Registrar, Bangladesh Open University

Co-Treasurer:
Dr. Rezaul Bashar, Science, Technology and Management Crest, Sydney, Australia

Marketing:
Engr. A F M Ali Ashraf, GCSTMR, Australia

Hospitality:
Mr. Iftekhar Khalid, Bangladesh Open University, Bangladesh

Executive Members:
Prof. Dr. Andre M N Renzaho, Western Sydney University, Australia
Prof. Dr. Shams Rahman, RMIT University, Australia
Assoc. Prof. Dr. Fidelis Mashiri, Western Sydney University, Australia
Prof. Dr. Raquib Ahsan, Bangladesh University of Engineering and Technology, Bangladesh
Prof. Dr. Mahbuba Begum, Bangladesh University of Engineering and Technology, Bangladesh
Dr. Rafiqul Islam, Solar E.Technology, Australia
Prof. Dr. Rezaul Karim, Islamic University of Technology, Bangladesh
Dr. M Rafiqul Islam, Charles Sturt University, Australia

CONFERENCE ADVISORY COMMITTEE

Chair:

Prof. Dr. M A Mannan, Vice Chancellor, Bangladesh Open University

Co-Chair:

Dr. Md. Sabur Khan, Chairman (Board of Trustee), Daffodil International University, Bangladesh

Members:

Prof. Dr. Atiur Rahman, Professor, Dhaka University

Prof. M A Hannan, Rector, Engineering Staff Collage

Prof. Dr. Saiful Islam, Vice Chancellor, Bangladesh University of Engineering and Technology, Bangladesh

Prof. Dr. Iftekhar Uddin Chowdhury, Vice Chancellor, Chittagong University, Bangladesh

Prof. Dr. Mohammad Rafiqul Alam, Vice Chancellor, Chittagong University of Engineering and Technology, Bangladesh

Prof. Dr. Md. Alauddin, Vice Chancellor, Dhaka University of Engineering and Technology, Bangladesh

Prof. Dr. Omar Jah, Acting Vice Chancellor, Islamic University of Technology, Bangladesh

Prof. Dr. Yusuf Mahbubul Islam, Vice Chancellor, Daffodil International University, Bangladesh

Prof. Dr. S. M. Imamul Huq, Vice Chancellor, University of Barisal, Bangladesh

Prof. Dr. Jahirul Haque, Vice Chancellor, University of Liberal Arts, Bangladesh

Prof. Dr. Gias U Ahsan, Pro Vice Chancellor, North South University, Bangladesh

Prof. Dr. Akhtar Kamal, Victoria University, Australia

Prof. Dr. Vivian Tam, Western Sydney University, Australia

Prof. Dr. Taha B. M. J. Ouarda, National Institute of Scientific Research, INRS, Canada

Prof. Dr. Biswajeet Pradhan, University of Technology Sydney, Australia

Prof. Dr. Abdallah Shanableh, University of Sharjah, United Arab Emirates

Prof. Dr. Henry Wong Kwai Kwan, ENTPE Universite De Lyon, France

Prof. Dr. Chi Zhang, Dalian University of Technology, China

Prof. Dr. Abu Bakr Rafique, Former CEO, International Islamic University of Chittagong, Bangladesh

Prof. Dr. Abdur Rashid, Dean, Uttara University, Bangladesh

Prof. Dr. Shafiul Bari, Bangladesh University of Engineering and Technology, Bangladesh

Prof. Dr. Md. Jahangir Alam, Chittagong University of Engineering and Technology, Bangladesh

Prof. Dr. Md. Saiful Islam, Chittagong University of Engineering and Technology, Bangladesh

Prof. Dr. M. Habibur Rahman, Bangladesh University of Engineering and Technology, Bangladesh

Prof. Dr. Ishtiaque Ahmed, Bangladesh University of Engineering and Technology, Bangladesh

Prof. Dr. Khan Mahmud Amanat, Bangladesh University of Engineering and Technology, Bangladesh

Prof. Dr. Raquib Ahsan, Bangladesh University of Engineering and Technology, Bangladesh

Prof. Dr. Harunur Rashid, Khulna University of Engineering and Technology, Bangladesh

Prof. Dr. Monjur Hossain, Former Professor, Khulna University of Engineering and Technology, Bangladesh

Prof. Dr. Md. Tarek Uddin, Islamic University of Technology, Bangladesh

Prof. Dr. Sharmin Reza Chowdhury, Dhaka University, Bangladesh

Prof. Dr. Mohammad Nazmul Islam, North South University, Bangladesh

Mr. Kazi Nasir, Chief Architect Department of Housing and Public Works, Bangladesh.

Mr. Mukit Majumdar Babu, Chairman, Prokriti O Jibon Foundation and Sponsor Director, Channel I, Bangladesh

CONFERENCE TECHNICAL COMMITTEE

Chair:

Assoc. Prof. Dr. Fidelis Mashiri, Western Sydney University, Australia

Co-Chairs:

Assoc. Prof. Dr. Swapan Saha, Western Sydney University, Australia
Prof. Dr. Raquib Ahsan, Bangladesh University of Engineering and Technology, Bangladesh

General Secretary:

Dr. Md Kamrul Hassan, Western Sydney University, Australia

Co-General Secretary:

Dr. Md. Naimul Haque, East West University, Bangladesh
Dr. Nazrul Islam, Bangladesh University of Engineering and Technology, Bangladesh

Executive Members:

Prof. Dr. Brian Uy, University of Sydney, Australi
Prof. Dr. Zhong Tao, Western Sydney University, Australia
Prof. Dr. Scott Smith, Southern Cross University, Australia
Prof. Dr. Riadh Al-Mahaidi, Swinburne University of Technology, Australia
Prof. Dr. Emad Gad, Swinburne University of Technology, Australia
Prof. Dr. Morgan Dundu, University of Johannesburg, South Africa
Prof. Dr. Yan Zhuge, University of South Australia, Australia
Prof. Dr. Takeshi Mori, Hosei University, Japan
Prof. Dr. Wei Wang, Tongji University, China
Prof. Dr. Huanjun Jiang, Tongji University, China
Prof. Dr. Shafiul Bari, Bangladesh University of Engineering and Technology, Bangladesh
Prof. Dr. Tahsin Reza Hossain, Bangladesh University of Engineering and Technology, Bangladesh
Prof. Dr. Mahbuba Begum, Bangladesh University of Engineering and Technology, Bangladesh
Prof. Dr. Tanvir Manzur, Bangladesh University of Engineering and Technology, Bangladesh
Prof. Dr. Md. Rabiul Alam, East West University, Bangladesh
Prof. Dr. Md. Moinul Islam, Chittagong University of Engineering and Technology, Bangladesh

Prof. Dr. G M Sadiqul Islam, Chittagong University of Engineering and Technology, Bangladesh
Prof. Dr. Md. Nazrul Islam, Dhaka University of Engineering and Technology, Bangladesh
Prof. Dr. Ganesh Chandra Saha, Dhaka University of Engineering and Technology, Bangladesh
Prof. Dr. Abdur Rashid, Daffodil International University, Bangladesh
Prof. Dr. Harunur Rashid, Khulna University of Engineering and Technology, Bangladesh
Prof. Dr. Md. Tarek Uddin, Islamic University of Technology, Bangladesh
Prof. Dr. Sharmin Reza Chowdhury, Ahsanullah University of Science and Technology, Bangladesh
Prof. Dr. Mohammad Nazmul Islam, North South University, Bangladesh
Prof. Dr. N.H.M. Kamrujjaman Serker, Rajshahi University of Engineering and Technology, Bangladesh
Prof. Dr. Ataur Rahman, Khulna University of Engineering and Technology, Bangladesh
Prof. Dr. Muhammad Harunur Rashid, Khulna University of Engineering and Technology, Bangladesh
Prof. Dr. Md. Rezaul Karim, Dhaka University of Engineering and Technology, Bangladesh
Assoc. Prof. Dr. Mohammad Al Amin Siddique, BUET, Bangladesh
Assoc. Prof. Dr. Gokhan Ozdemir, Anadolu University, Turkey
Assoc. Prof. Dr. Neaz Sheikh, University of Wollongong, Australia
Assoc. Prof. Dr. Muhammad Hadi, University of Wollongong, Australia
Assoc. Prof. Dr. Prabir Sarker, Curtin University, Australia
Assoc. Prof. Mahmud Ashraf, Deakin University, Australia
Dr. Shameem Ahmed, Bangladesh University of Engineering and Technology, Bangladesh
Dr. Nazrul Islam, Bangladesh University of Engineering and Technology, Bangladesh
Dr. Rupak Mutsuddy, Bangladesh University of Engineering and Technology, Bangladesh
Dr. Mohamed Ghannam, Mansoura University, Egypt
Dr. Mohammad Masud Rana, University of New South Wales, Australia
Dr. Mohammad Yousuf, Western Sydney University, Australia
Dr. Md Ashraful Alam, University of Asia Pacific, Bangladesh
Dr. Zhu Pan, Western Sydney University, Australia
Dr. Mohammad Shahidul Islam, University of Tabuk, Saudi Arabia
Engr. Syed Faiz Ahmad, Lievense Arabia Consulting Engineers, Saudi Arabia

Table of Contents

Abstract Title/Author Name/Paper ID Page

Invited Papers

Concrete Materials and Concrete Structures

Steel Materials and Steel Structures

Composite Structures and Composite Materials

Structural Rehabilitation, Retrofitting and Strengthening

Earthquake, Wind and Fire Engineering

Theories and Methods of Structural Analysis

Proc. 2nd International Conference on Structural Engineering Research (iCSER2019)
19-22 Jan 2019, Dhaka, Bangladesh
ISBN: 978-0-6482681-2-3

Case Studies in Australian on Work Health and Safety Requirements during the Construction Process of Temporary Structures

Swapan Saha[1], Ben Caushi[2], Ziad Harika[2] and Payam Rahnamayiezekavat[3]

[1]Associate Professor, Western Sydney University, Sydney, Australia
[2]Honours Student, Western Sydney University, Sydney, Australia
[3]Senior Lecturer, Western Sydney University, Sydney, Australia
Corresponding author's E-mail: s.saha@westernsydney.edu.au

Abstract

The aim of this study is to determine whether construction processes involving erection, use and dismantling of temporary structures such as tower cranes and metal scaffolding in Australian high-rise construction sites have been in compliance with the existing Work Health and Safety (WHS) requirements. The research reviewed five case studies in Sydney to investigate the causes of crane and scaffold safety incidents. The results of evaluation of these separate sites have shown that without stringent safety procedures in place to abide by the WHS Act and Regulations, major accidents associated with carne and scaffold with serious injuries including fatalities are inevitable. Results also found that a number of limiting factors including communication skill, regular maintenance, safety checks, safety culture and safety investments contribute to the severity of the incidents. It was evident that a lack of compliance in both tower crane and scaffolding services has impacted the construction industry greatly. In particular, the results highlighted the importance of educating all employees in regard to risks related to crane operation and use of scaffolding. The study recommends that regular maintenance checks must always be conducted to ensure all components of tower cranes and scaffolding are in working condition free from any defects.

Keywords: Construction, Safety, Crane, Scaffolding, Australia.

1. BACKGROUND

According to Safe Work Australia (2012), the Construction industry employed 1.01 million people in 2011–12, or 9% of the Australian workforce. The construction industry has a major impact on Australia's economic growth. Master Builders Australia state that 'the building and construction industry is a key driver of the Australian economy and makes a major contribution to the generation of wealth and the welfare of the community, particularly through the provision of shelter'. To ensure the construction industry stays strong in Australia, it is imperative that strict rules and regulations are set out in regard to workplace health and safety (Safe Work Australia, 2012a). Australia's safety standards are among the most stringent ones in the world, although there are still opportunities for improvement. Over the five-year period from 2008 to 2012, 211 Construction workers died from work-related injuries and there were 13,735 serious injury claims (Safe Work Australia, 2012b). Of these numbers, being hit by moving or falling objects accounted for 29 deaths and nearly 2,200 or 16% of the serious injury claims. This type of incident is often related to the use of cranes and scaffolding in which improper procedures and maintenance can have fatal effects. There is a need to ensure crane and scaffold contractors are following the correct Work Health and Safety procedures that are in place, as well as ensuring plants and equipment are maintained for safe use throughout its operational life. Regulatory issues related to crane and scaffold safety have come under increased scrutiny as a result of recent incidents that occurred in New South Wales, Australia (Safe Work Australia, 2013). The aim of

this research is to determine whether crane operators and laborers working on scaffolding have the necessary skills to comply with the current WHS laws and regulations in Australia. The objectives of the research are the following: i) compare the procedures set out by the WHS Act and Regulations in regard to cranes and scaffold compared to what is actually happening on construction sites in Sydney; ii) investigate the causes of crane and scaffold incidents that have occurred in New South Wales suburbs; and iii) Observe the skills of workers and management operating in and around cranes and scaffolds and their awareness of the required safety standards and the magnitude of the potential consequences of mismanagement.

This study also observed erection of scaffolding and dismantling of tower crane on a separate commercial project to find out the compliance of these operations as per WHS Act 2011.

Previous studies reported the need for safety investments, revised training methods, frequent maintenance, strict certification and the importance of basic communication to ensure a safer working environment for workers by enhancing the safety capabilities of the crane and scaffold contractors (Safe Work Australia, 2013). Without attention to these key factors, workers on a construction site could be exposed to high risk situations which could result in fatality or in serious injury.

For the purpose of this study, a crane is an item of plant intended for raising or lowering a load and moving it horizontally including the supporting structure of the crane and its foundations (Safe Work Australia, 2012b). Cranes are common on construction sites all around the world and are vital to the progression of a project. The main use for cranes on construction sites is to move materials around the site which is much more efficient than manual handling.

The Safe Work Australia's Construction Fact Sheet (2011) identifies that falls from height accounted for 51 fatalities. Of these numbers, 18 involved falls from buildings, 15 involved ladders and 8 involved scaffolding. Statistics on hit by moving or falling objects accounted for 29 deaths (Safe Work Australia, 2012b). These statistics are heavily linked to cranes and scaffolding therefore, further research work on the safety of cranes and scaffold is important to gauge the status of current safety standards. The statistics from other developed countries is similarly alarming. For example, in Spain, about 40% of serious accidents are caused by falls from height, and of these about 30% involve falls from temporary devices on structures assembled to work at height (Rubio-Romero et al., 2013).

The number of "being hit" incidents by moving or falling objects involving use of crane or scaffolding warrants detailed scrutiny of operation of those plants by employers and regulators. Workers should be able to go to work without the risk of death or serious injury.

It is not uncommon for construction contractors to own and operate a fleet of tower cranes. Most of these towers are rented and operated by in-house or contracted personnel. Frequent inspections of crane are essential in order to keep the machinery safe and to ensure that operators of these cranes are obtaining the necessary checks and maintenance procedures, whether on a weekly, monthly or yearly basis. Scaffolding provides access through a construction site as well as being a safety measure. Scaffolding allows workers to work at extreme heights that would otherwise be unsafe to travel without the aid of scaffolding. Scaffolding is designed to prevent falls from heights which can result in either serious injury or death. In the 2010, Safe Work Australia, reported two fatalities caused by fall from scaffolding.

2. RESEARCH SCOPE AND METHODOLGY

In this study three incidents involving crane and scaffold that occurred in and around the Sydney CBD were investigated to find the causes of these accidents. Data and relevant information on the incidents were sourced from media reports as well as Work Cover NSW incident reports. Information was gathered under "Freedom of Information" (FOI) laws. Details about the causes of the three incidents on crane and scaffolding failure are presented in the following section.

3. CASE STUDIES ON CRANE AND SCAFFOLD SAFETY

3.1. Ultimo Crane Collapse

On 27th November 2012, news broke that a tower crane had caught on fire at the outskirts of the Sydney CBD at a construction site at the University of Technology Sydney (UTS). More than 100 workers and 100 bystanders were in surrounding buildings and were evacuated from the area. The crane operator managed to escape the cabin through the crane ladder. The boom of the crane ultimately collapsed and landed on the building structure below it.

A newspaper article reported that safety maintenance was not up to date and the company had failed to undertake regular safety check even though it was pointed out to them through an earlier safety inspection (Australian Financial Review, 2012). After discussion with officers of the WorkCover Authority of NSW and a review of the incident report it was confirmed that the protruding arm of the crane, as depicted in Figure 1, had collapsed on top at the UTS construction site after catching fire.

Figure 1. The tower crane at Ultimo construction site on fire

3.2. Mascot Scaffold Collapse

On 25th February 2014, it was reported in the local media that a scaffolding structure had collapsed on a construction site in Mascot, New South Wales (Yahoo7, 2014). Two men were on the scaffold at the time of collapse and fortunately they escaped with only minor injury. It was also reported that the collapsed scaffold brought down power lines on the street and completely covered two trucks. There was also a concern for leaking fuel from the impacted trucks. As a result of the incident more than 100 people had to be evacuated from the area. The NSW Police and the WorkCover Authority started their investigations immediately after the collapse was reported. After discussion with WorkCover Authority officers and reviewing the information in the Factual Inspection Reports, it was found that the scaffold collapse caused by: i) a number of broken cables which were hanging from the services pole (electricity and telecommunication); and ii) scaffold and building debris which were resting on the services pole. The consequences reported to include: i) scaffold and building debris protruded out from the building site onto the street which blocked one lane of road for traffic; ii) parked trucks were covered with collapsed scaffold, raising concerns of fuel leaks; and iii) damages to the exterior wall of the existing building next to the collapsed scaffolding. The workers' union had inspected the site a few months earlier and had raised concerns about the safety of the scaffold. The aftermath of the incident is displayed in Figure 2.

Figure 2. The collapsed scaffold on the Mascot building site (Photo courtesy: 7 NEWS)

3.3. Barangaroo Crane Fire

On 12th March 2014, a fire broke out in the basement of a building on the Barangaroo development project in Sydney's CBD. A large blaze resulted in dense smoke being omitted from the construction site raising the alarm to existing surrounding high-rise buildings. Residents from all surrounding buildings were evacuated as a safety precaution (Ralston and Patty 2014). Fire persisted for several hours until the fire was brought under control. There was also a concern that the fire could cause damage to the tower cranes substructure and result in a collapse of the crane. Main roads surrounding the construction site were closed off, causing traffic chaos during the afternoon peak hour commuting period. Fire fighters from NSW Fire and Rescue responded until the blaze was controlled. Fire fighters fought the fire over two days with substantial damage to onsite construction material. The crane did not collapse and after the fire was extinguished, engineers were brought in to assess the structural integrity of the crane. WorkCover mentioned in their report that the fire appears to have been caused by a welding accident which set fire to formwork (Ralston and Patty 2014). Approximately 40 to 60 workers were on the lower levels when the blaze broke out and narrowly escaped death or serious injures (Ralston and Patty 2014). After discussion with WorkCover officers and review of the Incident Report, it was confirmed that the large fire originated in the formwork at the basement area. The incident report also confirmed that a structural engineer would assess the area and provide a remediation plan to be followed before construction would re-commence. Figure 3 shows the crane at the centre of the fire.

Figure 3. The crane incident at the Barangaroo development project near CBD

4. OBSERVATIONS: WHS COMPLAINCE

4.1. Scaffolding – Erection

An observation of a scaffolding being erected was conducted at a construction site in New South Wales to benchmark the extent of reinforcement of WHS requirements. As a result of research ethics constrains, the research team was not able to obtain individual insight from people who were directly engaged in the process. However, visualisation techniques were used to understand the requirements of the existing legislations and regulations in order to identify common risks and issues regarding scaffolding safety. A summary of the selected project is provided below:

Location of the construction site	New South Wales
Type of project	Residential (280 Units)
Total levels	18 levels
Project time frame	2 years 9 months
Type of scaffolding used	Standard steel scaffolding
Type of work to be conducted	Design and Erect
No. scaffolding structures to be erected	6
No. of employees to dismantle	32

The following standards were used to produce the checklist that used for assessing the degree of compliance of the onsite oppression with prescribed standards:

- Work health and Safety Act 2011;
- Work Health and Safety Regulation 2011;
- AS1576.1 – Scaffolding General Requirements;
- Safe Work Australia – Guides for scaffolding.

Thirty-two workers, subjectively evaluated to be competent, worked closely to erect 6 scaffold systems shown in Figure 4. The assessment checklist was produced with guidance from the regulations, legislations and codes of practice. It was found that 30% of items within the compliance check list as per WHS Act 2011 were non-compliant. It was identified that all employees involved had the relevant licencing to conduct the works. Although, it was identified that the risks need to be managed efficiently to avoid any accidents from occurring. The items did not comply were PPE equipment, Edge platform, Scaffolding ties, Maintenance Inspection and Scaffolding Procedure Report.

Figure 4. Standard steel scaffolding (Photo courtesy: Coates Hire)

4.2. Tower Crane – Decommissioning and Dismantling

An observation of a tower crane that was decommissioned and dismantled was conducted at a construction site in New South Wales to further assist with this study conducted on the Work Health and Safety issues. All results within this study was noted through witnessing what actually occurred during the stages of dismantling and understanding the requirements. Common risks and factors affecting safety were able to be identified. The key information about the selected project is listed below:

Location of the construction site	New South Wales
Type of project	Mixed Use (180 Units & 2 Retail)
Project time frame	2 years 4 months
Type of tower crane used	Raimondi MRT159 tower crane
Type of work to be conducted	Decommissioning & Dismantling
No. of employees to dismantle	13

The following standards were used to produce the below checklist to measure the standards with what was actually occurring onsite:
- Work health and Safety Act 2011;
- Work Health and Safety Regulation 2011;
- S.14.7 Tower Cranes Code of Practise 2006;

- Safe Work Australia – Guide to Tower Cranes.

Thirteen workers, subjectively evaluated to be competent, worked closely to dismantle the Raimondi MRT159 tower crane from the construction site shown in Figure 5. Access to the site was granted to the member of the research team for the purpose of assessing the WHS performance. Overall safety compliance throughout the dismantling process was sufficient with little issues that were visible. It was noted that all employees had the necessary licencing and requirements to commence dismantling the crane. The crane was dismantled safely with no accidents, injuries or near misses. However, it was notable that documentation that was legally and practically essential for the safe operation needed improvement. Six items which is 29% of 22 checklist items were non-compliant. The areas that did not comply includes inspection report, Safewrok method statement (SWMS), PPE (Personal Protective Equipment), Emergency Evacuation Plan, Harness Inspection and Exclusion zone.

Figure 5. MRT159 Tower Crane (Photo courtesy: Raimondi Cranes).

5. FINDINGS AND CONCLUDING REMARKS

After considering the news reports on these various incidents and then obtaining incident reports through WorkCover, it is evident that there was a breach of WHS requirements on these construction sites. The first incident in Ultimo could have been fatal had the jib of the crane been pointing out towards the road where hundreds of commuters were passing. It seems that the regular safety and maintenance checks were not carried out on this site. Fuel leaks are reported to have initiated the fire which in turn then caused the crane to collapse. If the appropriate maintenance checks were in place then the incident could have been avoided. It was fortunate that there were no injuries or fatalities although the company in question would still likely to receive a heavy fine for an incident of this scale.

The Mascot incident suggests that regular checks of the scaffold were not undertaken and resulted in a collapse in which two workers luckily were only injured and avoided possible death.

The Barangaroo incident was quite an extraordinary case as the events that unfolded were not directly related to the crane. Although the matter is still being investigated and recently reported that a basement fire was lit in close proximity to the base of the crane and was likely to be the initiating event. It was expected that the crane would have collapsed under the heat of the blazing fire. An interview with the Project Manager and Site Manager pointed out that the design of crane should also consider fire safety.

Three case studies of incidents at Ultimo, Mascot and Barangaroo associated with crane and scaffold safety identified the need for improvements in safety protocols and procedures. Non-

compliance with WHS Act and Regulations leads to large scale incidents especially where cranes and scaffold are involved, resulting in property damage, injury or loss of life. It is evident that crane and scaffold incidents not only affect site workers, but also impact on surrounding buildings and bystanders. These largescale incidents can also lead to tarnished reputation and heavy fines for all companies involved in the events. This study has emphasised the importance of regular safety checks and maintenance of high-risk construction activities such as crane operation and use of scaffolding as per WHS Act 2011. Scheduled inspections are important in minimising safety incidents and catastrophic damages. It was evident that poor compliance of both tower crane and scaffolding service sectors would eventually bring the entire construction process to halt as a result of an incident. It is crucial that all employees are educated on the risks involved when undergoing high risk construction works. Regular maintenance checks must always be conducted to ensure all components of tower cranes and scaffolding are in working condition free from any defects.

REFERENCES

Australian Financial Review. (2012). Crane collapses in inner Sydney. Available: http://www.afr.com/p/national/crane_collapses_in_inner_sydney_ZGi5exLXXmzQvc. Last accessed 1st Aug 2014. 52.

Ralston, N and Patty, A. (2014). Investigators explore possible causes of Barangaroo blaze. Available: http://www.smh.com.au/action/printArticle?id=5258622. Last accessed 11th Oct 2014.

Rubio-Romero, J.C (2013). Analysis of the safety conditions of scaffolding on construction sites. *Safety Science*. 55 (1), 160-164.

Safe Work Australia. (2012a). Construction Fact Sheet. Available: http://www.safeworkaustralia.gov.au/sites/SWA/about/Publications/Documents/430/Construction-Fact-Sheet-2011-12.pdf. Last accessed 27th Mar 2014.

Safe Work Australia. (2012b). Cranes Code of Practice. Available: http://www.safeworkaustralia.gov.au/sites/SWA/model-whs-laws/model-COP/Documents/Draft-COP-December-2012/DRAFT-Cranes-COP.pdf. Last accessed 13th May 2014.

Safe Work Australia. (2013). Scaffolding and Scaffolding Work Code of Practice. Available: http://www.safeworkaustralia.gov.au/sites/swa/about/publications/pages/scaffolds-scaffolding-work. Last accessed 14th March 2014.

Yahoo7. (2014). Two men rode collapsing scaffolding. Available: https://au.news.yahoo.com/nsw/a/21689054/three-injured-in-scaffolding-collapse-at-sy/. Last accessed 1st Aug 2014.

Proc. 2nd International Conference on Structural Engineering Research (iCSER2019)
19-22 Jan 2019, Dhaka, Bangladesh
ISBN: 978-0-6482681-2-3

Developing Safety Assessment Procedure for Existing Buildings in Bangladesh

Ahsanul Kabir[1]

[1]Professor & Head, Department of Civil Engineering, Bangladesh University of Engineering and Technology (BUET), Dhaka, Bangladesh
Corresponding author's E-mail: akabir@ce.buet.ac.bd

Abstract

The collapse of 9-storied Ready Made Garment (RMG) building 'Rana Plaza' at Savar in April 2013, killing 1135 garment workers and injuring over 2500 people was a severe blow to the Garment industry in Bangladesh and human conscience all over the world. All the stake holders in the business especially the foreign buyers and labour organisations expressed great concern over the safety of the garment workers in Bangladesh. Immediately, the government formed a committee and International Labour Organisation (ILO) came forward to fund the project to evaluate the condition of the garment industry buildings in Bangladesh. The department of civil engineering of BUET was entrusted with the job to formulate a guideline to assess the safety of existing buildings and help identify the buildings with high risk. Standard procedures stated in different codes of developed countries were studied and a suitable strategy for safety assessment in Bangladesh context was prepared. During site inspection of various buildings, it was noted that compliance to building codes may not be met yet the building can serve the purpose without risk. A quick visual inspection procedure was outlined which may or may not trigger for second tier Detail Engineering Assessment (DEA) of the concerned building. Finally retrofitting and strengthening scheme for some building elements may become necessary if DEA reveals inadequacy or weakness of such member. However, to meet more stringent requirements considering seismic vulnerability, standard procedures of ASCE 31-03 and FEMA 155 was recommended until some local standard procedures are formulated.

Keywords: Safety Assessment, Buildings, Visual Inspection, Retrofitting, Bangladesh

Proc. 2nd International Conference on Structural Engineering Research (iCSER2019)
19-22 Jan 2019, Dhaka, Bangladesh
ISBN: 978-0-6482681-2-3

Behaviour of HSC Columns Reinforced with Glass Fiber-Reinforced Polymer Bars and Helices: Experimental Investigation

M. Neaz Sheikh[1,*], Muhammad N. S. Hadi[2], and Hayder Alaa Hasan[3]

[1]Associate Professor and Deputy Head, School of Civil, Mining and Environmental Engineering, University of Wollongong, Australia
[2]Associate Professor, School of Civil, Mining and Environmental Engineering, University of Wollongong, Australia
[3]Research Fellow, School of Civil, Mining and Environmental Engineering, University of Wollongong, Australia

[*]Corresponding author's E-mail: msheikh@uow.edu.au

Extended Abstract

In the waterfront structures or structures located in the moist and harsh environment, steel reinforcing *bars are vulnerable to corrosion. The corrosion of the steel reinforcing bars causes significant maintenance cost and leads to damages to the concrete structures. Different techniques, although expensive, are adopted to protect the steel reinforcing bars from corrosion such as epoxy or zinc coating and cathodic protection. In the critical cases, stainless or galvanized steel reinforcing bars are used. However, none of these techniques can fully eliminate the problems associated with the corrosion of the steel reinforcing bars. As Fiber-Reinforced Polymer (FRP) bars are noncorrosive, they have the potential to reinforce concrete structures located in the moist and harsh environment.*

The FRP bars possess several advantages over conventional steel reinforcing bars in reinforcing concrete members. The FRP bars have higher tensile strength compared to the steel reinforcing bars. The density of the FRP bars is about 25% of the density of steel reinforcing bars (Hadi et al., 2017). In addition, FRP bars possess several other attractive features including corrosion resistance and nonmagnetic and nonconductive characteristics. Hence, FRP bars are considered a competitive replacement of steel bars in reinforcing concrete structures.

Several recent research studies investigated the structural behavior of FRP bar reinforced concrete members. The shear and the flexural behavior of FRP bar reinforced normal and high strength concrete members were investigated in the past two decades (Barris et al., 2009; El-Nemr et al., 2013). The outcome of these studies contributed significantly in developing design guidelines and design standards for the design of FRP bar reinforced concrete members (flexural members). However, the behavior of FRP bars under compression loads has not been extensively investigated. This is particularly because of the nonhomogeneous and anisotropic characteristics of the FRP bars, which leads to micro-buckling of fibers in the FRP bars under axial compression (Karim et al., 2016)

Current design codes and design guidelines (ACI, 2006; ACI, 2015; CSA, 2017) do not adequately address the design of concrete columns reinforced with FRP bars. Hence, several research studies investigated the behavior of FRP bar reinforced concrete columns (Hadi et al., 2016). However, the previous studies were limited to the FRP bar reinforced normal strength concrete (NSC) columns (Hasan et al., 2017).

In this study, the behavior of Glass Fiber-Reinforced Polymer (GFRP) bar reinforced high strength concrete (HSC) specimens under different loading conditions was investigated. A total of 12 circular

column specimens were cast and tested. All specimens were 210 mm in diameter and 800 mm in height. The axial load carrying capacity, confinement efficiency of the GFRP helices as well as the ductility and post-peak axial load-axial deformation response of the specimens were investigated. The influence of the key parameters including the type of the reinforcement, the pitch of the transverse helices and the loading condition on the performance of the specimens were investigated. It was found that GFRP bar reinforced HSC specimens sustained similar axial load under concentric axial compression compared to HSC specimens reinforced with the same amount of steel reinforcing bars. However, the efficiency of GFRP bar reinforced HSC specimens in sustaining axial loads decreased with an increase in the axial load eccentricity. The direct replacement of steel reinforcing bars by the same amount of GFRP reinforcing bars in HSC specimens resulted in about 30% less ductility under concentric axial load. It was observed that the ductility and post-peak axial load-axial deformation behavior of the GFRP bar reinforced HSC specimens significantly improved with closely spaced helices.

Keyword: High strength concrete (HSC) columns, Glass Fiber-Reinforced Polymer (GFRP) bar, Experimental Investigation

REFERENCES

American Concrete Institution (ACI). 2006. Guide for the design and construction of structural concrete reinforced with FRP bars, ACI 440.1R-06 , Farmington Hills, MI., USA.

American Concrete Institution (ACI). 2015. Guide for the design and construction of structural concrete reinforced with FRP bars, ACI: 440.1R-15, Farmington Hills, MI., USA.

Barris C, Torres L, Turon A, Baena M, Catalan A. 2009. An experimental study of the flexural behaviour of GFRP RC beams and comparison with prediction models, Composite Structures 91(3): 286-295.

Canadian Standards Association (CSA). 2012. Design and construction of building components with fiber reinforced polymers, CAN/CSAS806-12, Rexdale, ON, Canada.

El-Nemr A, Ehab AA, Benmokrane B. 2013. Flexural behavior and serviceability of normal-and high-strength concrete beams reinforced with glass fiber-reinforced polymer bars, ACI Structural Journal 110(6): 1077-1087.

Hadi MNS, Hasan H, Sheikh MN. 2017. Experimental Investigation on High Strength Concrete Columns Reinforced with Glass Fiber-Reinforced Polymer Bars and Helices under Different Loading Conditions. Journal of Composites for Construction. Journal of Composites for Construction, 21(4): 04017005.

Hadi MNS, Karim H, Sheikh MN. 2016. Experimental Investigations on Circular Concrete Columns Reinforced with GFRP Bars and Helices under Different Loading Conditions. Journal of Composites for Construction; 04016009: 1-12

Hasan H, Sheikh MN, Hadi, MNS. 2017. Performance Evaluation of High Strength Concrete and Steel Fiber High Strength Concrete Columns Reinforced with GFRP Bars and Helices. Construction and Building Materials. Construction and Building Materials 134: 297–310.

Karim H, Sheikh MN, Hadi MNS. 2016. Axial Load-Axial Deformation Behaviour of Circular Concrete Columns Reinforced with GFRP Bars and Helices. Construction and Building Materials, 112: 1147–1157

Proc. 2nd International Conference on Structural Engineering Research (iCSER2019)
19-22 Jan 2019, Dhaka, Bangladesh
ISBN: 978-0-6482681-2-3

Additive Manufacturing in Structural Engineering - A Current State-of-the-art and its Future Prospects in Construction

Mahmud Ashraf[1]

[1]Associate Professor, Deakin University, Geelong, Australia
Corresponding author's E-mail: mahmud.ashraf@deakin.edu.au

Abstract

Additive Manufacturing (AM), commonly known as 3D printing, is seemingly offering a wealth of possibilities in the manufacturing industry. This technology is frequently used in aerospace and biomedical engineering but its impact on construction industry is still at a perceived stage. 3D printing technologies bring along the exciting opportunity of producing innovative and efficient structural shapes to suit specific design requirements without requiring complex and time consuming traditional forming and assembly processes. Metallic 3D printing technologies have advanced significantly during the last decade but large-scale structural applications of 3D printed metallic elements are still non-existent; this is largely due to the smaller size of existing printers. This talk will focus on recent advancements and case studies on metallic 3D printed structures with special emphasis on an ongoing project on metallic microlattice structures printed from stainless steel and titanium. Microlattice structures have been manufactured using Powder Bed Fusion (PBF) techniques i.e. Selective Laser Melting (SLM) and Electron Beam Melting (EBM), showing widely varying surface imperfections for struts in different orientations. Presence of micro-pores is also an alarming issue that could affect the overall integrity of a structure. Appropriate inclusion of all significant factors in numerical modelling brings along unique and exciting challenges to be addressed. A critical evaluation on the prospect of using 3D printing in structural engineering will be discussed with some specific challenges identified that would require extensive research to appropriately exploit the beneficial effects of this exciting new technology in construction.

Keywords: Additive manufacturing, 3D printing, Microlattice structures, Stainless steel, Titanium

Proc. 2nd International Conference on Structural Engineering Research (iCSER2019)
19-22 Jan 2019, Dhaka, Bangladesh
ISBN: 978-0-6482681-2-3

A Review of Acceptable Limits for Various Engineering Properties of Aggregates

Md. Ashiqur Rahman[1], Md. Tariqul Islam[2], Ishtiaque Ahmed[3]

[1]Graduate Research Assistant, Department of Civil Engineering, Bangladesh University of Engineering and Technology, Dhaka-1000, Bangladesh
[2]Postgraduate Student, Department of Civil Engineering, Bangladesh University of Engineering and Technology, Dhaka-1000, Bangladesh
[3]Professor, Department of Civil Engineering, Bangladesh University of Engineering and Technology, Dhaka-1000, Bangladesh
Corresponding author's E-mail: ashiq.buetcivil11@gmail.com

Abstract

Aggregate in concrete is viewed as an inert filler material. It is now believed that aggregate properties not only affect the properties of green concrete but also affect the behaviour of hardened concrete. With the rapid growth of construction activities, the construction industry is now facing a scarcity of mineral aggregates. Apart from mineral aggregates the industry has an appetite for synthetic aggregate like slag and fly ash as obtained from industry by-product. In recent times, synthetic aggregates and recycled aggregates obtained from demolished buildings and pavements are also being used as an alternative to mineral aggregates. This paper attempts to assess the range of engineering properties of various kinds of available aggregates and compare their acceptability against code specified allowable limits. The implication of aggregate property limits specified by various codes will also be discussed with a view to make use of alternative synthetic aggregates for particular application. It will also provide confidence to the user to use synthetic aggregates and recycled aggregates based on their engineering properties. Moreover, the various codes specified allowable limits will provide a base line to compare between the mineral aggregates and the alternative aggregates. This paper also focuses on promoting the use of alternative aggregates in lieu of mineral aggregates. The use of these waste materials as aggregates would be beneficial from environment consideration as well as making cost effective sustainable development.

Keywords: *Synthetic Aggregates, Recycled Aggregates, Engineering Properties, Codes and Standards.*

1. INTRODUCTION

Aggregates are inorganic materials that are mainly inert in nature and granular in shape and normally consists of stone or stone like solids. Aggregates are widely used as a filler material in construction industries. Aggregates give body to structures and effect the economy. Aggregates can be used both as isolated material (in road bases) and as composite material (in concrete). Kosmatka et al (2011) suggested that 70%-80% of the volume of concrete is occupied by aggregates. Behavior of concrete (both fresh and hardened) is largely depended on the properties of aggregates used in it as it occupies a great amount of portion of it. Except in location of abundance in its availability, short supply of natural aggregates are observed all over the world due to rapid growth of construction industry as suggested by IS 383(2016). Currently, the world is concentrating in finding alternatives of mineral aggregates for construction purposes. With the growth of environmental awareness, industrial by-products, secondary raw materials, recycled aggregates are being looked forward to be used as construction materials for ensuring environment friendly and sustainable construction practice.

2. CODE PROVISIONS FOR BASIC REQUIREMENTS OF AGGREGATE PROPERTIES

As the use of various types of aggregates has increased, it is necessary to have the knowledge of basic requirements for aggregates which are stated in various codes and provisions to ensure safety and fulfilling code requirement. ACI Manual of Concrete Practice (1994) describes standard test procedures for various aggregate properties which is illustrated in Table 1.

Table 1. Properties of concrete influenced by aggregate properties (ACI Manual of Concrete Practice).

Relevant Aggregate Properties	Standard Tests	Typical Values
Sulphate Soundness	ASTM C88	1% to 10% (Fine Aggregate) 1% to 12% (Coarse Aggregate)
Resistance to Freezing and Thawing	ASTM C666 & CRD - C - 114 Performance of Aggregate in Air Entrained Concrete by Rapid Cycles	Durability Factor of 10% to 95 %
Absorption	ASTM C127 (Coarse Aggregate) ASTM C128 (Fine Aggregate)	0.2% to 4 % (Coarse Aggregate) 0.2% to 2% (Fine Aggregate)
Presence of Clay and Fines	ASTM C117	0.2% to 6 % (Fine Aggregate) 0.2% to 1 % (Coarse Aggregate)
Aggregate Reactivity	ASTM C 227 Mortar Bar Expansion ASTM C 586 Rock Cylinder Method	0.01% to 0.2 % after 6 Months 0.01% to 0.2 % after 6 Months
Co-efficient of Thermal Expansion	CRD - C - 125 Aggregate Particles	1.0×10^6 /F to 9.0×10^6 /F
Tensile Strength	ASTM D 2936 Rock Cores	300 psi - 2300 psi
Compressive Strength	ASTM D 2938 Rock Cores	10000 psi - 40000 psi
Organic Impurities	ASTM C40 ASTM C87	Colour plate No. 3 or less 85 to 105%
Particle Shape	ASTM D3398 Void Content	35% to 50 %
Clay Lumps and Friable Particles	ASTM C 142	0.5 to 2 %
Maximum Size	ASTM C136 Sieve Analysis	0.5 inch to 6 inch
Modulus of Elasticity	ASTM C469	1.0×10^6 psi - 10.0×10^6 psi
Specific Gravity	ASTM C 127 ASTM C 128	1.6 to 3.2 1.6 to 3.3
Fineness of Modulus	ASTM C136 CRD - C - 104	2.2 - 3.1 (Fine Aggregate) 5.5 - 8.5 (Coarse Aggregate)
Density	ASTM C29	75 lb/cft - 110 lb/ cft
Resistance to Degradation	ASTM C131 and C535 Los Angeles Machine	15% to 50 % loss

Indian Standard (IS 383), Coarse and Fine Aggregate for Concrete-Specification (2016) describes the basic requirements of aggregates for concrete which are shown in Table 2

Table 2. Allowable limits of various parameters for aggregates (IS 383)

Parameters of Aggregates	Allowable limits
Aggregate Impact Value (AIV)	Wearing Surface: <30% Concrete Other than Wearing Surface: <45%
Aggregate Crushing Value (ACV)	Wearing Surface: <30% Concrete Other than Wearing Surface: <45%
Ten Percent Fines Value (TFV)	Concrete Other than Wearing Surface: <50kN
Los Angeles Abrasion Value (LA)	Wearing Surface: <30% Concrete Other than Wearing Surface: <50%
Soundness of Aggregate (Tested with Na_2SO_4)	Fine Aggregate: <10% Course Aggregate: <12%
Soundness of Aggregate (Tested with $MgSO_4$)	Fine Aggregate: <15% Course Aggregate: <18%
Sizes of Coarse Aggregates for Mass Concrete (20mm to 4.75mm)	20mm: 90%-100% 4.75mm: 0%-10% 2.36mm: 0%-0.2%
Flakiness Index	<40%
Elongation Index	<40%

British Standard (BS 882), Specification for Aggregates from Natural Sources for Concrete (1992) describes the requirements of aggregates to be used in concrete which are given in Table 3.

Table 3. Quality Requirements of Aggregates (BS 882)

Parameters of Aggregates	Allowable limits
Aggregate Impact Value (AIV)	Heavy Duty Concrete Floor Finishes: <25% Pavement Wearing Surfaces: <30% Others: <45%
Ten Percent Fines Value (TFV)	Heavy Duty Concrete Floor Finishes: >150kN Pavement Wearing Surfaces: >100kN Others: >50kN
Flakiness Index	Crushed Stone: <40% Natural Gravel: <50%
Single Sized Coarse Aggregates for Mass Concrete (20mm to 4.75mm)	20mm: 85%-100% 14mm: 0%-70% 10mm: 0%-25% 5mm: 0%-5%
Fines (% Mass Passing 75µm Sieve)	Crushed Gravel Course Aggregate: 2% Crushed Rock Aggregate: 4% Crushed Gravel Sand: 4% Crushed Rock Sand: 16%

3. COMPARISONS OF VARIOUS TYPES OF COURSE AGGREGATES

In order to establish the suitability of Induction Furnace Slag as coarse aggregate, a series of tests have been conducted on the various aggregates available. Test results of various engineering properties for different types of aggregates are shown in Table 3.

Table 3. Comparison among different coarse aggregates

Test Parameters	Stone Chips (Coarse Aggregate)	Brick Chips (Coarse Aggregate)	Slag (Coarse Aggregate)
Fineness of Modulus (FM)	6.81	6.28	6.52
Bulk Specific Gravity (OD)	2.63	1.73	2.42
Water Abortion Capacity	0.80%	11.40%	2.70%
Unit Weight (Bulk Density)	1530 kg/m^3	1040 kg/m^3	1290 kg/m^3
Voids in Aggregates (Compacted by Rodding)	42%	40%	47%
Aggregate Impact Value (AIV)	32%	37%	44%
Aggregate Crushing Value (ACV)	24%	36%	44%
Ten Percent Fines Value (TFV)	160 kN	90 kN	40 kN
Flakiness Index	24%	23%	8%
Elongation Index	38%	28%	19%
Angularity Number	8	8	12
Los Angeles Abrasion Value (LA)	30%	33%	45%
pH	7.0	6.0	7.2

From the test results, it can be seen that induction furnace slag aggregate (slag aggregate) and brick chips fulfill most (except the ten percent fines value for slag) of the codes as suggested by ACI Manual of Concrete Practice (1994), IS 383 (2016) and BS 882 (1992) required provisions for their use in concrete other than wearing surfaces (like slab). Besides, Mohammed et al (2017) suggested that concrete made of slag coarse aggregate had higher compressive strength and showed better performance compare to concrete made of masonry coarse aggregate in cylinder tests. Considering the environmental effects, slag aggregates can be used in lieu of stone aggregates in such cases.

CONCLUSIONS

Review of various available international codes and standards and their suggested acceptable limits for various engineering properties of aggregates for specific purposes have been presented in this paper. Test results were also presented with a view to compare the engineering properties of different types of aggregates. As an alternative to commonly used stone or masonry chip aggregate, the properties of slag obtained from induction furnace as by-product of steel making has also been determined. From the above discussion, it can be concluded that minimum required engineering properties for aggregates are not same in various codes and provisions for all kinds of construction works. Therefore there lies a scope for using alternative aggregates in cases where the requirements are less. Industrial by-product like slag and recycled aggregates can be used in specific works for reducing the consumption of mineral aggregates like stone chips.

REFERENCES

ACI manual of Concrete Practice, part 1 (1994). Material and general properties of concrete, University of Michigan.

ASTM C88 (2005). Standard test method for soundness of aggregates by use of sodium sulfate or magnesium sulfate, ASTM International, West Conshohocken, PA.

ASTM C666 (2015). Standard test method for resistance of concrete to rapid freezing and thawing, ASTM International, West Conshohocken, PA.

ASTM C127 (2015). Standard test method for relative density (specific gravity) and absorption of coarse aggregate, ASTM International, West Conshohocken, PA.

ASTM C128 (2015). Standard test method for relative density (specific gravity) and absorption of fine aggregate, ASTM International, West Conshohocken, PA.

ASTM C117 (2017). Standard test method for materials finer than 75-μm (no. 200) sieve in mineral aggregates by washing, ASTM International, West Conshohocken, PA.

ASTM C227 (2010). Standard test method for potential alkali reactivity of cement-aggregate combinations (mortar-bar method), ASTM International, West Conshohocken, PA.

ASTM C586 (2011). Standard test method for potential alkali reactivity of carbonate rocks as concrete aggregates (rock-cylinder method), ASTM International, West Conshohocken, PA.

ASTM D2936 (2008). Standard test method for direct tensile strength of intact rock core specimens, ASTM International, West Conshohocken, PA.

ASTM D2938 (2002). Standard test method for unconfined compressive strength of intact rock core specimens, ASTM International, West Conshohocken, PA.

ASTM C40 (2016). Standard test method for organic impurities in fine aggregates for concrete, ASTM International, West Conshohocken, PA.

ASTM C87 (2003). Standard test method for effect of organic impurities in fine aggregate on strength of mortar, ASTM International, West Conshohocken, PA.

ASTM D3398 (2006). Standard test method for index of aggregate particle shape and texture, ASTM International, West Conshohocken, PA.

ASTM C142 (2017). Standard test method for clay lumps and friable particles in aggregates, ASTM International, West Conshohocken, PA.

ASTM C136 (2014). Standard test method for sieve analysis of fine and coarse aggregates, ASTM International, West Conshohocken, PA.

ASTM C469 (2014). Standard test method for static modulus of elasticity and poisson's ratio of concrete in compression, ASTM International, West Conshohocken, PA.

ASTM C29 (2017). Standard test method for bulk density ("unit weight") and voids in aggregate, ASTM International, West Conshohocken, PA.

ASTM C131 (2014). Standard test method for resistance to degradation of small-size coarse aggregate by abrasion and impact in the los angeles machine, ASTM International, West Conshohocken, PA.

ASTM C535 (2016). Standard test method for resistance to degradation of large-size coarse aggregate by abrasion and impact in the los angeles machine, ASTM International, West Conshohocken, PA.

BS 882 (1992). Specification for aggregates from natural sources for concrete, British Standard, UK.

CRD C114 (1997). Test method for soundness of aggregates by freezing and thawing of concrete specimens, Army-COE Standards, National Institute of Building Sciences, Washington, DC.

CRD C125 (1963). Method of test for coefficient of linear thermal expansion of coarse aggregates (strain-gage method), Army-COE Standards, National Institute of Building Sciences, Washington, DC.

CRD C104 (1980). Method of calculation of the fineness modulus of aggregate, Army-COE Standards, National Institute of Building Sciences, Washington, DC.

IS 383 (2016). Coarse and fine aggregate for concrete-specification, Indian Standard, New Delhi.

Mohammed TU, Noor MA, Apurbo SM, Ahmed M, Elahi A, Mazumder MH (2017). Utilization of induction furnace slag in concrete as coarse aggregate, 1st International Conference on Engineering Research and practice, Dhaka, Bangladesh.

Kosmatka SH, Kerhoff B, Panarese WC (2011). Design and control of concrete mixtures, Portland Cement Association.

.

Proc. 2nd International Conference on Structural Engineering Research (iCSER 2019)
19-22 Jan 2019, Dhaka, Bangladesh
ISBN: 978-0-6482681-2-3

Compressive Strength of Concrete made with Gray and White Cements

Md. Zakaria Habib[1], Al-Amin[1*], Syed Ariful Islam[1]

[1] Department of Civil Engineering, Uttara University, Uttara, Dhaka-1230.
Corresponding author's E-mail: al.ce.uu18@gmail.com

Abstract

Cement is one of the most important binding materials in civil engineering field. In construction industry cement is having higher demand day by day. Higher consumption of cement in construction industry leads to higher pollution. That's why engineers recommend such cement which will be environmentally friendly, have aesthetic properties, economical and will be sufficient enough to give the desired strength. Generally there two types of cement available in our local market (gray, white). Recently it is claimed by some of the experts that gray cement concrete gives more strength than white cement concrete. The study mainly aims at justifying the view by comparing the strength of concrete made of white and gray cement. For this purpose 72 cylinders (4" X 8") were cast in total using mix ratios 1:1.25:2.5 and 1:1.5:3, water cement ratios 0.40 and 0.45 and for curing periods 7, 14 and 28 days both for white and gray cement equally. Results show that initial strength gaining rate of white cement concrete is very much higher than gray cement concrete but after 28 days curing period's ultimate compressive strength of gray cement is more by 156 psi (minimum), 205 psi (maximum) and 181 psi on an average.

Keywords: *Compressive Strength, White Cement, Gray Cement, Concrete*.

1. INTRODUCTION (TIMES NEW ROMAN BOLD 14 ALL CAPS)

White Portland cement (WPC) has similar bonding characteristics as gray Portland cement. WPC has also higher performance due to use of high-quality materials and control process in its production. WPC is generally used in the production of non-structural members, which are built for decorative and aesthetical purposes. White concrete produced with WPC has higher compressive strength and reaches its ultimate compressive strength faster than normal gray Portland cement [Temiz et al., 2013].

Practically, white cement concrete can be used to increase safety or energy efficiency. Because it is highly reflective, it can either highlight median barriers or increase the light in the large industrial building. Alternatively, the reflectance can be used to maintain the same level of light in a room with fewer light fixtures or can be used to reduce the costs of heating/cooling [Gillette, 2004].
White cement concrete can be used structurally, in the same manner as gray cement concrete, with the added drama of colour. Unlike the dry shake or exterior cladding, the colour is integral with the structure and less maintenance is required of the surface if there is chipping or cracking exposing the interior concrete [Gillette, 2004].

One significant barrier, which often results in traditional gray concrete, being chosen instead of white concrete, is the perception among decision-makers that white concrete produces less strength and durability than gray concrete. However, the chemical composition of white cement from white Portland cement made in Bangladesh is ideally suited for the production of concrete with high strength and durability [Bye, 1999]. On this background, an experimental program was conducted to determine the compressive strengths of concrete made with white and gray cement.

Table 1: Comparison of gray and white cement compositions [Thomas Telford, 1999]

Cement		Clinker		Cement		Clinker	
	Gray %	**Black %**	**White %**		**Gray %**	**Black %**	**White**
SiO_2	19-23	21.7	23.8	**LSF**	90-98	98.4	97.2
Al_2O_3	3-7.0	5.3	5	**LCF**	-	96.2	93.8
Fe_2O_3	1.5-4.5	2.6	0.2	**S/R**	2-4	2.7	4.6
CaO	63-67	67.7	70.8	**A/F**	1-4	2	25
MgO	0.5-2.5	1.3	0.08	**C_3S**	-	65.4	59.4
K_2O	0.1-1.2	0.5	0.03	**C_2S**	-	12.9	23.5
Na_2O	0.07-0.4	0.2	0.03	**C_3A**	-	9.6	12.9
SO_3	2.5-3.5	0.7	0.06	**C_4AF**	-	7.9	0.6
LOI	1-3.0	-	-				
IR	0.3-1.5	-	-				
Free Lime	0.5-1.5	1.5	2.5				

2. METHODOLOGY

The experimental program was designed to compare the compressive strength of white and gray cement. For this purpose a number of 72(36 for white cement+36 for gray cement) cylinders (4" X 8") were cast and then crushed in UTM for two mix ratios (1: 1.25: 2.5& 1:1.5:3) and two water-cement ratios (0.40 & 0.45) and the curing period of each parameter were 7, 14 and 28 days.

2.1 Variables

The first step done in the experimental study was identifying the control variables. The variables which remain unchanged throughout the experiment are called independent variables. The variables which are changed throughout the experiment are called dependent variables. The independent variables of the experiments are Mix ratio, Water cement ratio and Curing Period. The dependent variable is compressive strength.

2.2 Materials

Locally available white and gray cement, fine (Sylhet sand) and Coarse (Crushed stone) aggregate were used in that study the properties of which are as follows.

Table 2: Properties of cement used in the study

Name of The Test	Gray Cement	White Cement
Normal Consistency	28.5%	28%
Initial Setting Time	85 minutes	65 minutes
Final setting Time	170 minutes	120 minutes

Table 3: Properties of fine and coarse aggregate

Properties	Coarse Aggregate	Fine Aggregate
Fineness Modulus (FM)	5.45	2.95
Specific Gravity	-	2.58
Bulk Specific Gravity (OD)	2.62	-
Apparent Specific Gravity (SSD)	2.64	-
Unit Weight	1541 kg/m^3	1495 kg/m^3
Absorption Capacity	0.4%	1.3 %

2.3 Casting

All batches of cylinders were cast inside the laboratory. The mixing and casting is conformed to ASTM [1945] C192. Each batch was used to cast 12 standard sized cylinders specimens were cast in three layers and each layer was compacted by using a tamping rod of size 16mm in diameter up to 25 blows. After compacting the top of the specimen was finished smoothly with the help of a trowel and was then exposed to an actual environmental condition. All the specimens were unfolded after 24 hours then immersed into water.

3. RESULTS AND DISCUSSION

In this chapter result of the study has been summarized considering the variables stated previously. After curing of all cylinder specimens for desired periods, each was crushed in UTM (Universal Testing Machine). The graphical representations of results are as follows

It is seen in Fig. 3.1 that, the compressive strength gaining rate of white cement concrete is much more than gray cement initially but after 28 days curing period strength obtained by gray cement concrete is more by almost 205 psi than white cement concrete. After 7 and 14 days of Curing period white cement concrete gain almost 82-84 % and 95-97 % strength where for gray cement is 64-66 % and 88-90 % respectively.

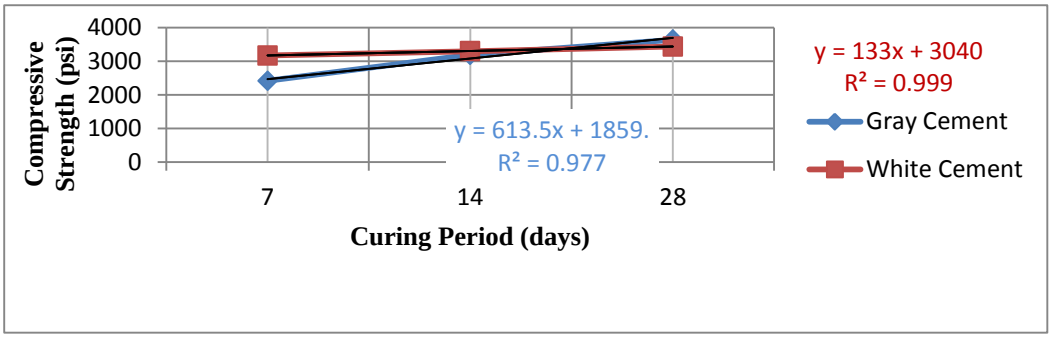

Fig. 3.1: Compressive Strength of Concrete made with gray and white cement.

[W/C: 0.40 and Mix ratio: 1: 1.25: 2.5]

Fig. 3.2 shows that initial strength of white cement concrete is higher than the gray cement concrete but after a certain curing period gray cement concrete possess higher strength than white concrete(Almost 160 psi more strength in gray cement concrete after 28 days curing period). Within 14 days of curing period white concrete gain almost 97% of total strength where for gray it is seen about 90%. Fig. 3.3 shows that initial strength gaining rate of white cement concrete is considerably high in compared with gray cement concrete but after a certain curing period gray concrete possess higher strength than white concrete. After 28 days curing period gray cement concrete obtains almost 190 psi more strength than white cement concrete. Fig. 3.4 shows that initial strength of white cement concrete is higher than the gray cement concrete. Within 15 days of concrete age white concrete gain almost 97% strength where for gray it is seen about 90% of total strength.

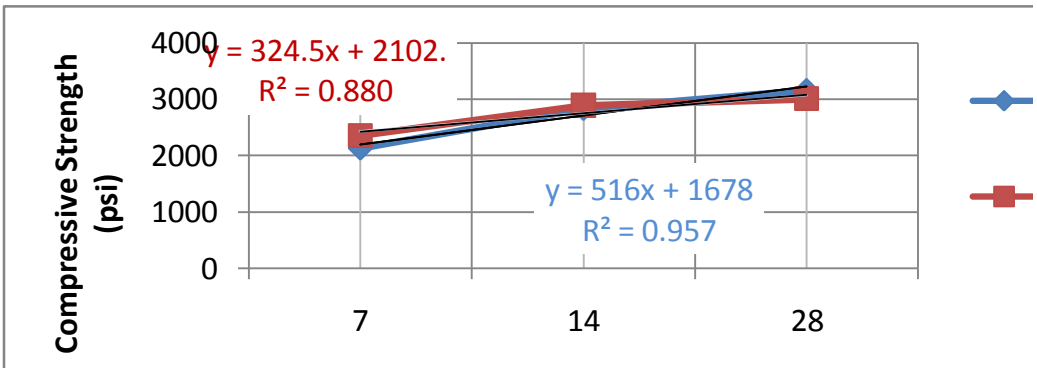

Fig. 3.2: Compressive Strength of concrete made with gray and white cement. [W/C: 0.45 and Mix ratio: 1: 1.25: 2.5]

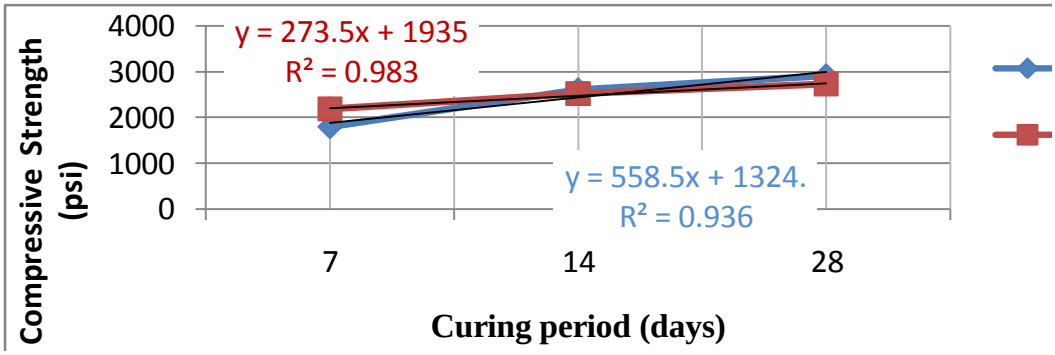

Fig. 3.3: Compressive Strength of concrete made with gray and white cement. [W/C : 0.40 and Mix ratio : 1:1.5:3]

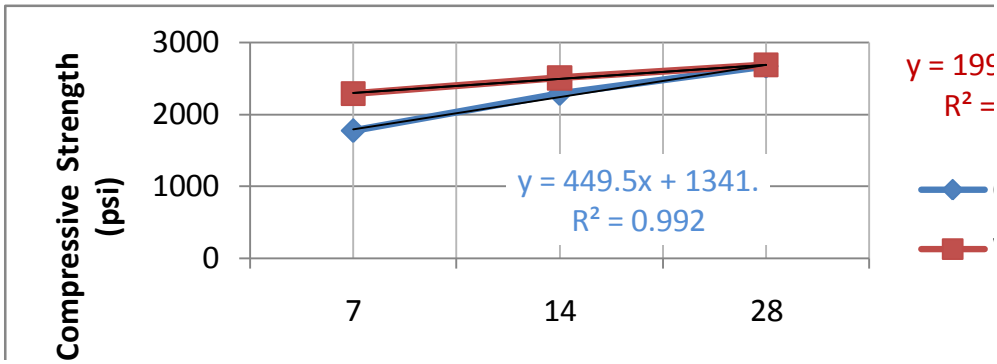

Fig. 3.4: Compressive Strength of Concrete made with gray and white cement. [W/C : 0.45 Mix ratio : 1:1.5:3]

4. CONCLUSIONS

The following conclusions are made for the study:

i. Initial strength gaining rate of white cement concrete is considerably higher than gray cement concrete.
ii. The ultimate compressive strength of gray cement concrete is more by 156 psi (minimum), 205 psi (maximum) and 181 psi on an average than white cement concrete. After 7 days of curing time gray cement concrete gains about 65-70% of its total strength whereas for white cement it is 80-85% which much more than of gray cement.

REFERENCES

Bye. G. C. Portland cement: Composition, production and properties. *Thomas Telford Publishing*, London, Vol. 5, pp. 164-165, 1999.

Camilleri, J. The physical properties of accelerated Portland cement for endodontic use. *International Endodontic Journal,* Vol. 41, pp. 151–157, 2008. doi:10.1111/j.1365-2591.2007.01330.x.

Gillette, M. White cement concrete. University of California, Berkley, 30th March 2004.

Gray Cement. Retrieve from http://www.dyckerhoff.com/online/en/Home/Gray

Hoque, M., F., Gani, M., O. and Hoque, M., N. A Study on Strength Properties of White-Cement. *International Journal of Business, Social and Scientific Research,* Vol. 01, pp. 61-64, 2014. ISSN: 2309-7892.

Sen, S. and Rao, K. B., Effect of Water Cement Ratio on the Workability and Strength of Low Strength Quarry Dust Concrete. *International Journal of Civil Engineering and Technology*,Vol. 8, pp. 1448–1455, 2017.

Temiz, H., Kose, M. M. and Genc, H. M. Mechanical Behavior of White Concrete. *TEM Journal,* Vol. 2, 2013.

Proc. 2nd International Conference on Structural Engineering Research (iCSER2019)
19-22 Jan 2019, Dhaka, Bangladesh
ISBN: 978-0-6482681-2-3

Effect of Saline Water Curing on Properties of Concrete

Md. Tariqul Islam[1], Md. Ashiqur Rahman[2], Ishtiaque Ahmed[3]

[1]Postgraduate Student, Department of Civil Engineering, Bangladesh University of Engineering and Technology, Dhaka-1000, Bangladesh
[2]Graduate Research Assistant, Department of Civil Engineering, Bangladesh University of Engineering and Technology, Dhaka-1000, Bangladesh
[3]Professor, Department of Civil Engineering, Bangladesh University of Engineering and Technology, Dhaka-1000, Bangladesh
Corresponding author's E-mail: tariqulaunto.1993@gmail.com

Abstract

Structural properties of concrete mainly depend on the proper hydration of the cement. Hydration of cement refers to the chemical reaction where water chemically reacts with cement. As the hydration process proceeds, the components of the concrete bond together and create a strong and solid mass. For ensuring proper hydration over time, additional external water is supplied, the process which is known as curing. With the rapid growth of civilization, construction activities are on the rise. In coastal areas, concrete structure is exposed to saline environment where there is scarcity of fresh water for mixing and curing. This paper focuses on evaluating the effects of saline water curing on the structural properties of concrete like compressive strength, tensile strength and modulus of elasticity and compare the results with those under conventional curing process. Compressive strength of concrete on 3rd, 7th, 14th and 28th days, tensile strength of concrete on 7th and 28th days and modulus of elasticity of concrete on 28th day of curing period was evaluated on both saline water cured and conventionally cured specimens. From the test results, it was found that concrete specimens cured in saline water showed better strength performance in compressive behaviour than conventionally cured concrete specimens. These results give a quantitative comparison and provide field engineers an aid for opting a suitable method as per the situation demands.

Keywords: *Compressive Strength, Modulus of Elasticity, Tensile Strength, Saline Water, Curing.*

1. INTRODUCTION

Concrete is the most highly used construction material that has gained widespread acceptance for its many useful properties. Concrete is mainly used for its ability to resist compressive loads. Besides, it is a construction material that can be economically produced and has high durability as suggested by Tiwari et al (2014). Curing plays an important role in the development of its compressive strength and durability properties. Properties of concrete highly depend on hydration process. Proper curing is necessary for ensuring better hydration. Moreover, various constituents present in the curing water may have profound influence on the setting and hardening properties of concrete. Corrosion of the embedded steel is one of the main reasons for the lack of durability of concrete. Presence of chloride ion in the saline environment can cause serious durability problems of concrete by increasing corrosion probabilities of the embedded steel. Chloride ion can penetrate into the concrete through diffusion process and initiate and accelerate the corrosion of embedded steel in concrete as suggested by Wegian (2010). With the rapid growth of civilization, more and more structures are constructed near the coastal areas and in the saline environment where there is scarcity of fresh water. Duff (1924) suggested that sea water has a total salinity of about 3.5% and majority of its dissolved solid is NaCl. As the planet earth is facing a problem of having shortage of fresh water, investigation of the effets of 3.5% NaCl solution on the properties of concrete is necessary for creating durable and long lasting

concrete structures in the near future.

2. METHODOLOGY

The test scheme includes comparing compressive strength, tensile strength and modulus of elasticity of concrete cylinder specimens cured with conventionally used fresh water and cured with 3.5% NaCl solution (by weight) which represents the salinity of sea water by Rashid et al (2013). The mix ratio used for 1 m^3 concrete for all the cylindrical specimens are given below:

Ordinary Portland Cement: 402 kg
Stone chips (3/4 inch downgraded): 1119.8 kg
Coarse Sand: 602.5 kg
Water (Fresh): 160.8 kg

2.1. Compressive Strength Test

Compressive strengths of all test samples were measured as suggested by ASTM C39 (2012).

2.2. Tensile Strength Test

Split tensile strength (Tensile Strength) was measured as suggested by ASTM C496 (2017). Details of the test procedure is described in Figure1.

2.3. Test for Determination of Modulus of Elasticity

Modulus of elasticity was measured as suggested by ASTM C469 (2014). Test procedure is illustrated in Figure2.

Figure 1. Tensile strength test

Figure 2. Modulus of Elasticity Test

3. RESULTS AND DISCUSSIONS

Comparisons of the compressive strength, tensile strength and modulus of elasticity of cylindrical specimens, cured with fresh and saline water are presented in Figure 3 to Figure 6.

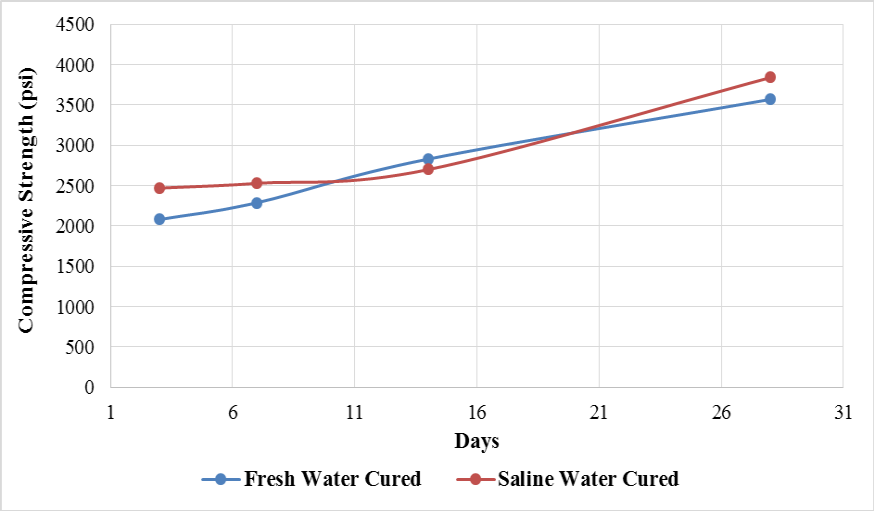

Figure 3. Compressive strength development with time under different curing condition.

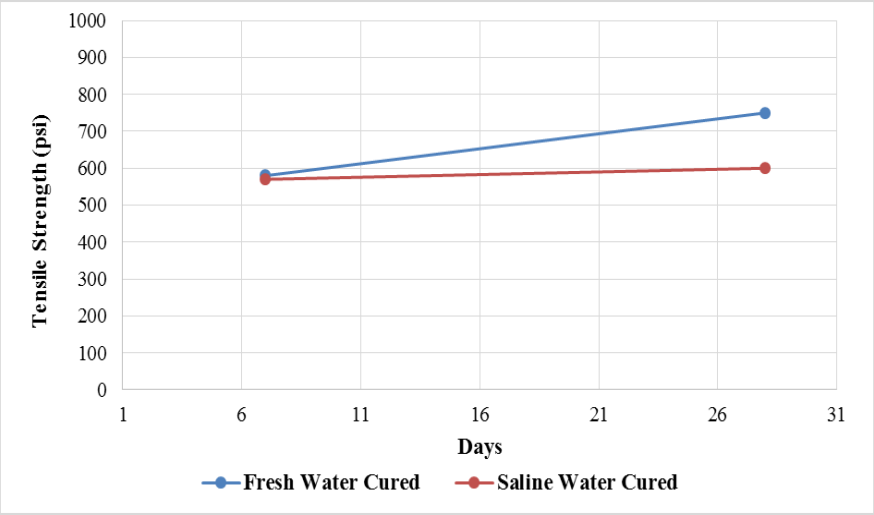

Figure 4. Tensile strength development with time under different curing condition.

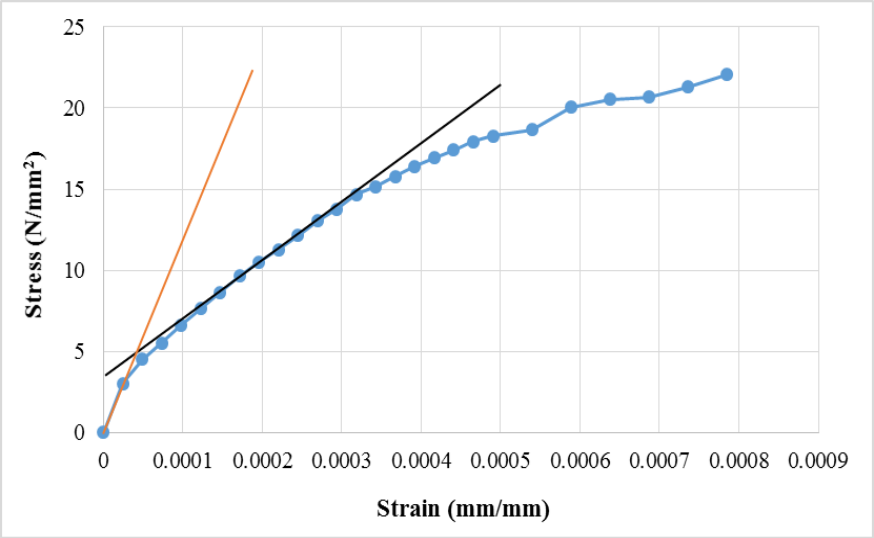

Figure 5. Stress varying with strain under fresh water curing condition.

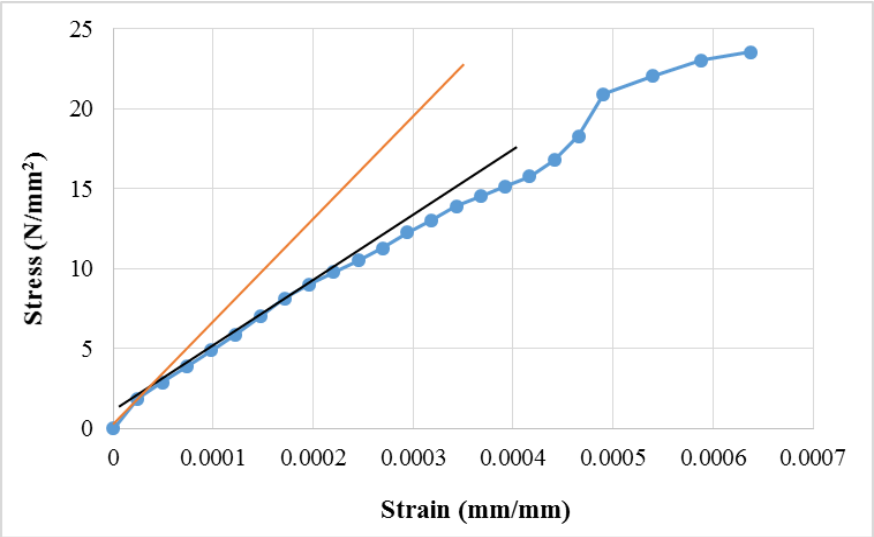

Figure 6. Stress varying with strain under saline water curing condition.

Modulus of Elasticity (Modulus of Elasticity) was determined from the slope of stress-strain curve of Figure 5 and Figure 6. Modulus of Elasticity was determined at both initial-portion (from slope denoted by red line) and straight-line portion (from slope denoted by black line). Obtained results are shown in Table 1.

Table 1. Summary of modulus of elasticity test.

Curing Condition	Modulus of Elasticity (psi)	
	Initial Portion	Straight Line Portion
Fresh Water	16312500	5082673
Saline Water	9666667	4725298

4. CONCLUSIONS

From the test result presented in this paper, it was found that strength development cured in saline water is largely unaffected with a marginal (7.56%) rise in the compressive strength of concrete when it is cured in saline water compared to conventional fresh water curing. The finding is similar to what has been reported by Tiwari et al (2014) and Wegian (2010). Initial strength gain is faster in the case of saline water curing. However, in case of tensile strength, samples cured with saline water has showed lower (20%) less strength than fresh water cured samples. Whereas, in case of modulus of elasticity samples cured with saline water has less (7.03 %) value compared to fresh water cured samples (for the straight-line portion). Less tensile strength increases the probability of concrete cracking and hence, increases the probability of chloride induced corrosion of rebar embedded in the concrete. However, the increased compressive strength can also compensate in the cause. If proper precautions are taken to prevent corrosion of the embedded rebar, curing in saline water may not have adverse effect on the strength development of concrete.

REFERENCES

ASTM C39 / C39M (2012). Standard test method for compressive strength of cylindrical concrete specimens, ASTM International, West Conshohocken, PA.

ASTM C469 / C469M (2014). Standard test method for static modulus of elasticity and poisson's ratio of concrete in compression, ASTM International, West Conshohocken, PA.

ASTM C496 / C496M (2017). Standard test method for splitting tensile strength of cylindrical concrete specimens, ASTM International, West Conshohocken, PA.

Duff A (1924). American Concrete Institute, 20, 422

Osei Ya (2000). Nutralization, new school chemistry, African First Publisher Onitsha Nigeria.

Rashid T, Hoque S, Akter F (2013). Ocean acidification in the bay of bengal. Open Access Scientific Reports.

Tiwari P, Chandak R, Yadav RK (2014). Effect of salt water on compressive strength of concrete, International Journal of Engineering Research and Application, 4, 38-42.

Weigan FM (2010). Effect of seawater for mixing and curing on structural concrete, The IES Journal Part A: Civil & Structural Engineering, 3, 235-243.

Proc. 2nd International Conference on Structural Engineering Research (iCSER2019)
19-22 Jan 2019, Dhaka, Bangladesh
ISBN: 978-0-6482681-2-3

Parametric Study of Thermal Behaviour of Reinforced Concrete Columns in Fire

Imtiar Jalal Niloy[1], Dr. Md. Raquibul Hossain[2] and Md. Abdul Basit[3]
[1]Student, Department of Civil Engineering, Bangladesh University of Engineering & Technology, Dhaka, Bangladesh
[2]Assistant Professor, Department of Civil Engineering, Bangladesh University of Engineering & Technology, Dhaka, Bangladesh
[3]Student, Department of Civil Engineering, Bangladesh University of Engineering & Technology, Dhaka, Bangladesh
Corresponding author's E-mail: raquibulhossain@ce.buet.ac.bd

Abstract

This paper is concerned with parametric analysis of reinforced concrete square columns in a fire environment. Because of concrete's inherent material properties, it is proven to have a high degree of fire resistance than that of steel. So steel reinforcements within the column section must be protected from exposure to fire by providing adequate concrete clear cover. The computer modeling technique adopted illustrates the thermal response of concrete column sections when exposed to fire. Numerical models of column sections of three sizes (12"x12", 16"x16" and 20"x20") with same steel percentage (3%) and with various clear covers (1"~4") were created using general purpose FEM software package ABAQUS to obtain the data for analysis. Temperature-dependent nonlinear material properties were adopted according to Eurocode standards. A finite element heat transfer analysis was used to determine the thermal response of the reinforced concrete columns when exposed to the ISO 834 standard fire environment. The temperature distribution histories obtained were then used to develop an empirical relation between required clear cover for column section and fire resistant time. The necessary thicknesses of the clear cover for protection against fire are different for different exposure times. This empirical relation can be used to calculate the clear cover required for different fire exposure times.

Keywords: Parametric analysis, ISO 834 Fire Environment, Clear Cover, Fire Resistant Time, ABAQUS

1. INTRODUCTION

The high temperatures that result from building fires have a significant effect on the strength and deformation characteristic of structural components such as columns, beams, walls, and slabs. These effects are dependent on the thermal and mechanical properties of the materials comprising the structure. Amongst the various structural elements, columns are the most critical components as the failure of a column in the lower story could lead to a partial or complete collapse of a structure. A good understanding of the structural behavior and the overall response of a column exposed to fire is therefore important in an effort towards eliminating costly damage to the structure and saving human lives. Civil engineering structures are mainly of two types: Steel Structures and Concrete Structures.
One of the advantages of concrete over other building materials is its inherent fire-resistive properties; however, concrete structures must still be designed for fire effects. Structural components still must be able to withstand dead and live loads without collapse even though the rise in temperature causes a decrease in the strength and modulus of elasticity for concrete and steel reinforcement. This research improves the concept obtained from the work of Mohammad Nizam Uddin and Sabbid Ibnul Gafur Shuvo (2017). In their research they created the numerical models of column sections using GiD, conducted the numerical analysis using SAFIR and the post-processing was done using Diamond.

Experimental results from Bikhiet (2014) indicated that concrete begins to lose about 30% of its compressive strength when heated up to 300^{o}C and loses about 70% of its compressive strength when heated up to 600 ^{o}C. Concrete's modulus of elasticity reaches 60% of its original value at 300℃ and reaches 15% of its original value at 600°C. According to Fleischmann and Buchanan (2016), the compressive strength of concrete start to decrease at about 300°C but remains relatively close to original value up to 500°C. Above 500°C, the compressive strength of the siliceous aggregate concrete starts to decrease rapidly and is considered ineffective at temperatures above 650°C, where the compressive strength has been reduced by approximately 50 percent of the value at normal temperatures. So, concrete heated up to 300°C can be considered as damages that need to be repaired.
Fire applied in the simulation was according to ISO 834 fire curve which represents a fully developed fire in a compartment with a constant rate of increase in temperature.

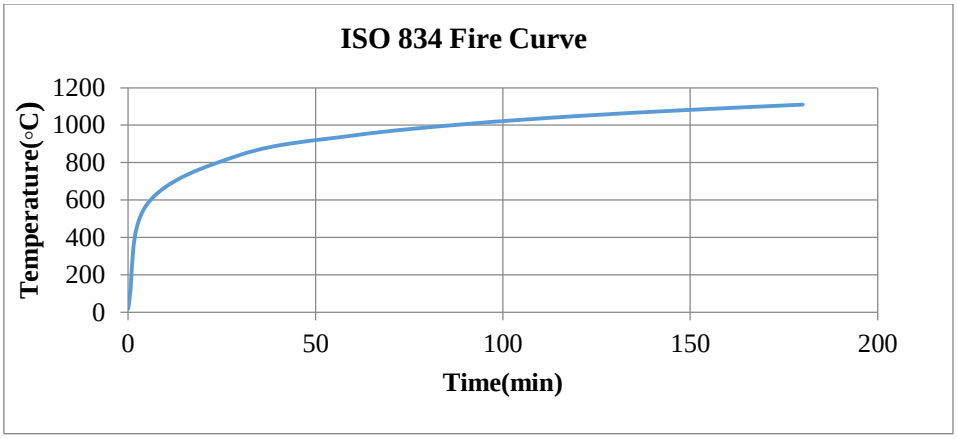

Figure 1: ISO 834 Standard Fire Curve as per Eurocode 1992-1-2 (2004)

2. SIMULATION

Numerical modeling and analysis of square column were done using a general purpose FEM software package ABAQUS. Finite element method in ABAQUS has three stages to perform a numerical analysis:

1) Preprocessing
2) Processing
3) Post-processing

The first step of pre-processing is to draw the column section with proper reinforcement and actual size. This was done using the part module in ABAQUS CAE. Two separate parts were sketched. One was the column and another was the main reinforcement. Two homogenous and solid sections were defined using concrete and steel materials. They were named column section and main reinforcement section respectively. Column section was assigned to the column part and main reinforcement section was assigned to the main reinforcement part. Using the assembly module two instances (column and main reinforcement) were created and assembled in the correct position. Using the step module two steps were defined. One step represented the predefined condition before the application of fire and another step represented the application of fire. A predefined field was included in the initial step to apply room temperature of 25°C to the whole model. An amplitude was defined using values from the ISO-834 fire curve to apply it in the simulation. Fire was applied to the model using the interaction module in ABAQUS. The interactions were defined base on three methods of heat transfer: conduction, convection, and radiation. The conduction property was defined using the interaction module by finding contact pairs in the model which automatically identified the surface-surface contact between the column section and the main reinforcement section. The convection property for the model was defined using surface film condition in the interaction module. The radiation property for the model was defined using surface radiation in the interaction module. Meshing was done using the mesh module of ABAQUS. Partitioning was used in the column section to achieve fine and

undistorted mesh. DC3D8 element was used in meshing which is an 8-noded linear heat transfer brick. Processing was conducted using the job module in ABAQUS. Once all of the tasks involved in defining a model is finished the Job module was used to analyze the model. The visualization module was used for post-processing. The visualization module was also used to obtain time-temperature variation data at the face of reinforcement. This data was then exported to Microsoft Excel to obtain the curves.

2.1. Material Properties

Material behavior may be divided into two categories: thermal and mechanical. Temperature based nonlinear material properties of steel and concrete were used in the simulation. Thermal properties of concrete were used as described in Eurocode 1992-1-2 (2004) and thermal properties of steel were used as described in Eurocode 1993-1-2 (2005). The following material properties were used in the simulation:

Table 1: Material properties of Concrete

Properties	Value
Thermal Conductivity	As per Eurocode 1992-1-2 (2004)
Specific Heat	As per Eurocode 1992-1-2 (2004)
Density	2400 kg/m3
Poisson's Ratio	0.18
Modulus of Elasticity	As per Fleischmann and Buchanan (2016)

Table 2: Material Properties of Steel

Properties	Value
Thermal Conductivity	As per Eurocode 1993-1-2 (2005)
Specific Heat	As per Eurocode 1993-1-2 (2005)
Density	7800 kg/m3
Poisson's Ratio	0.3
Modulus of Elasticity	As Per Fleischmann and Buchanan (2016)

3. RESULT AND DISCUSSION

Simulation has been performed for 3 sets of RCC Column Section (12″X12″, 16″X16″, 20″X20″) of 3% Steel Percentage and 13 different sizes of Clear Cover (from 1″ to 4″ with 0.25″ interval) for variation of the result. The fire has been appointed at concrete reinforcement interface (shown in Figure 2) in two ways (4 sides, 2 Sides) and temperature data has been collected at ten times (from 15 minutes to 1 hour with 5 minutes interval). Simulation result demonstrates different temperature ranges on different points of the column section with the change of time.

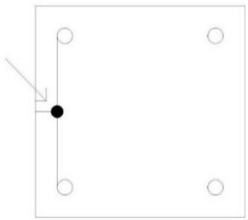

Figure 2: Concrete Reinforcement Interface Sides

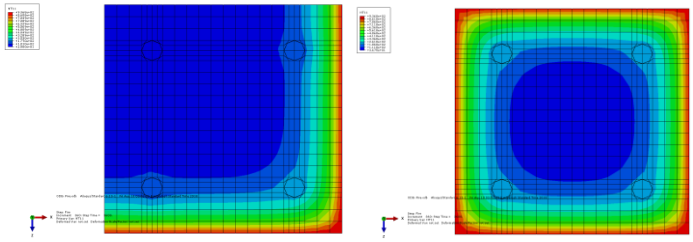

Figure 3: 60 Minutes Fire Application on 2 Sides and 4 Sides

3.1. Time vs. Clear Cover Graph

To understand the impact of temperature at concrete reinforcement interface with the change of temperature, six detailed Clear Cover vs. Temperature curves have been constructed. We already

know that the parts of a concrete structure that is exposed to temperatures above approximately 300 °C should be considered to fix. That's why a straight line has been constructed at 300°C temperature parallel to the X-axis (Clear Cover) in the graph. The 300°C temperature straight line intersects different time curves, and we get some intersection points. Then the corresponding clear cover data of the intersection points have been noted.

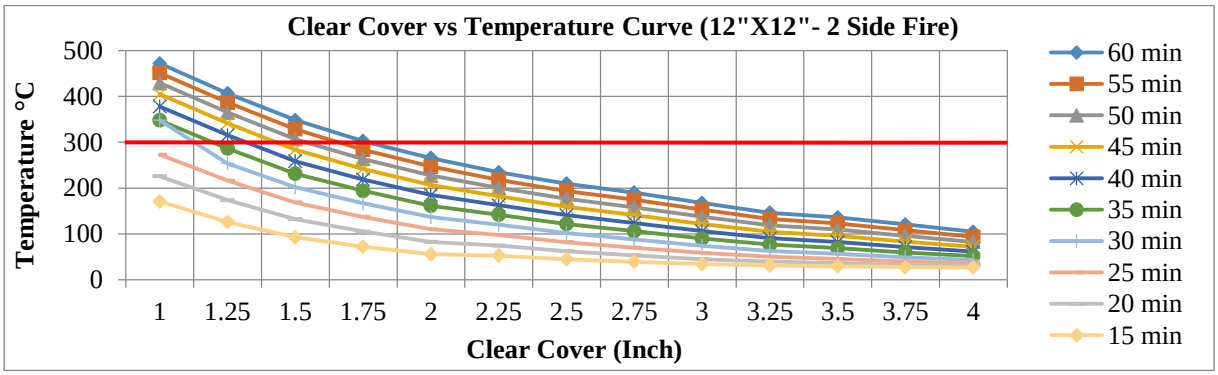

Figure 4: Detailed Clear Cover vs. Temperature Curve at different times (2 side fire at Concrete Reinforcement Interface, Steel percentage 3%)

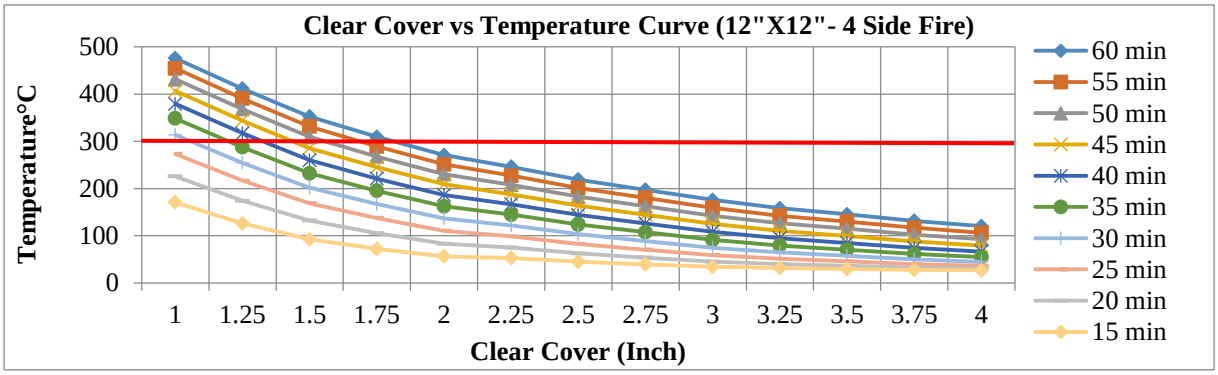

Figure 5: Detailed Clear Cover vs. Temperature Curve at different times (4 side fire at Concrete Reinforcement Interface, Steel percentage 3%)

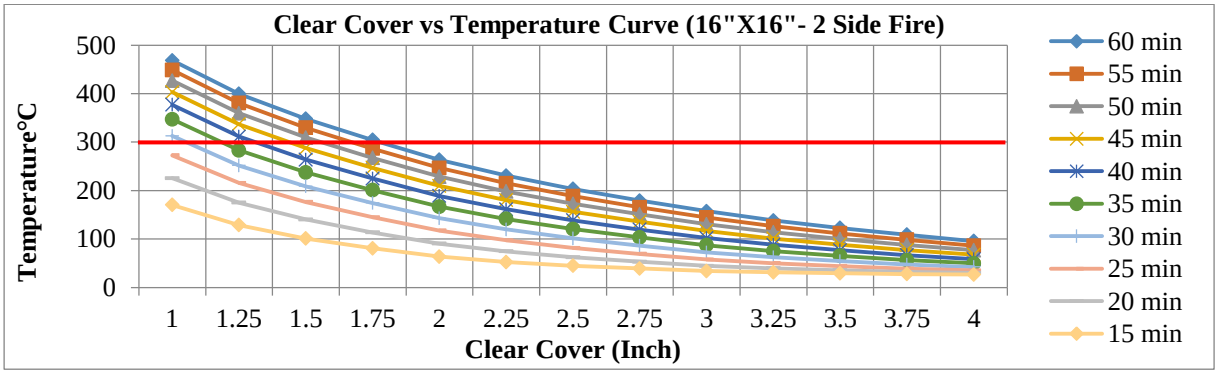

Figure 6: Detailed Clear Cover vs. Temperature Curve at different times (2 side fire at Concrete Reinforcement Interface, Steel percentage 3%)

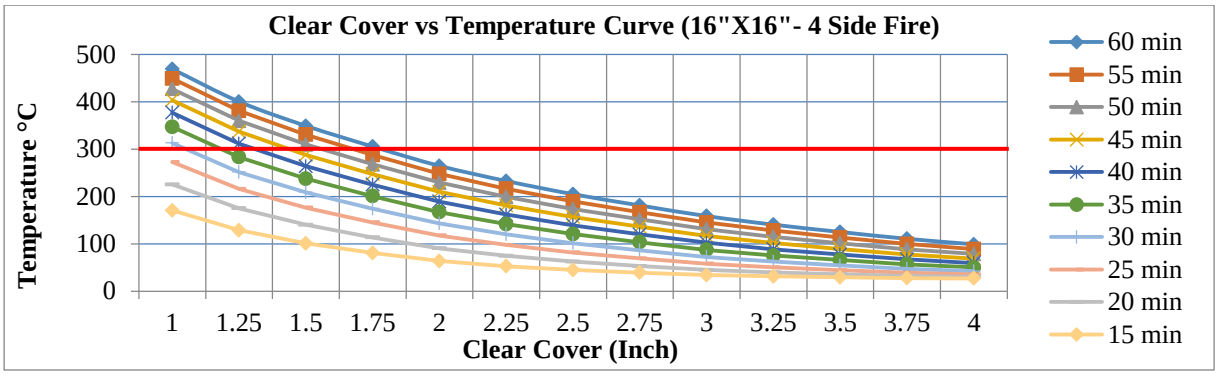

Figure 7: Detailed Clear Cover vs. Temperature Curve at different times (4 side fire at Concrete Reinforcement Interface, Steel percentage 3%)

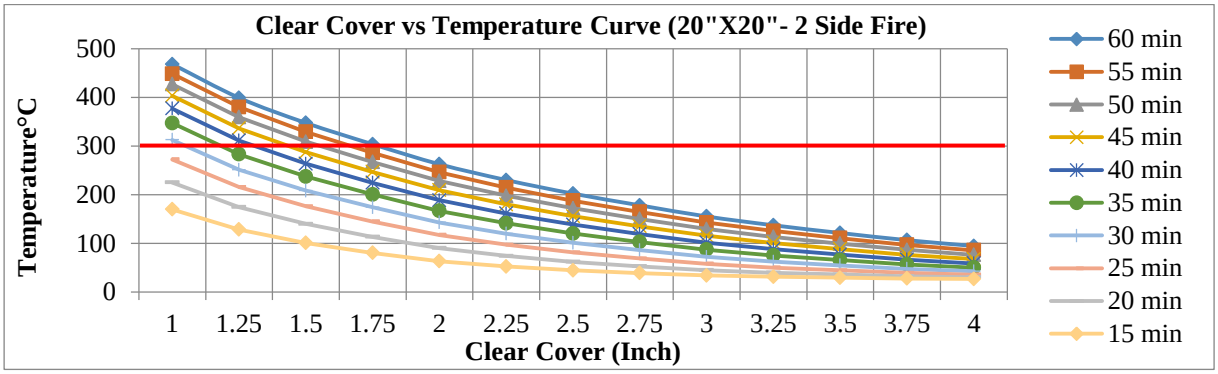

Figure 8: Detailed Clear Cover vs. Temperature Curve at different times (2 side fire at Concrete Reinforcement Interface, Steel percentage 3%)

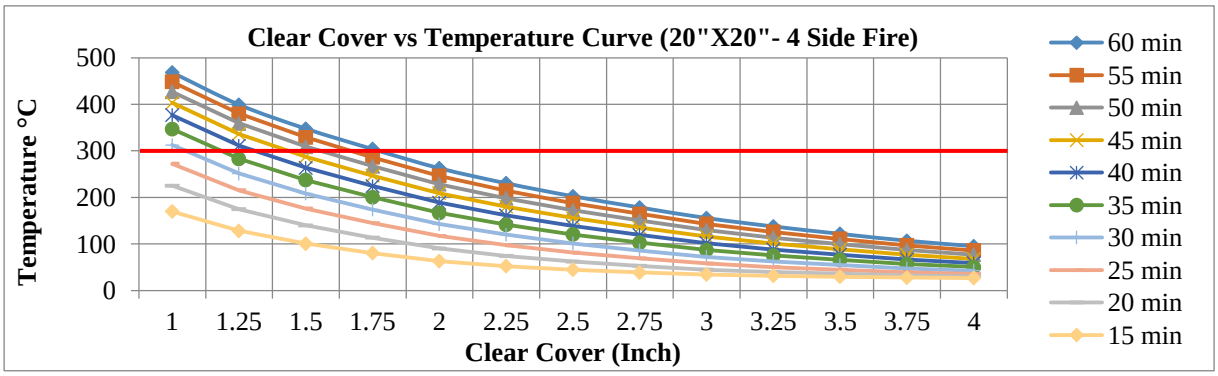

Figure 9: Detailed Clear Cover vs. Temperature Curve at different times (4 side fire at Concrete Reinforcement Interface, Steel percentage 3%)

3.2. Formation of Empirical Relation between Time & Clear Cover

By using corresponding clear cover data of intersection points, a Time vs. Clear Cover graph has been sketched. A best fitted straight line has been constructed to represent the relation between Fire Resistant Time and Clear Cover.

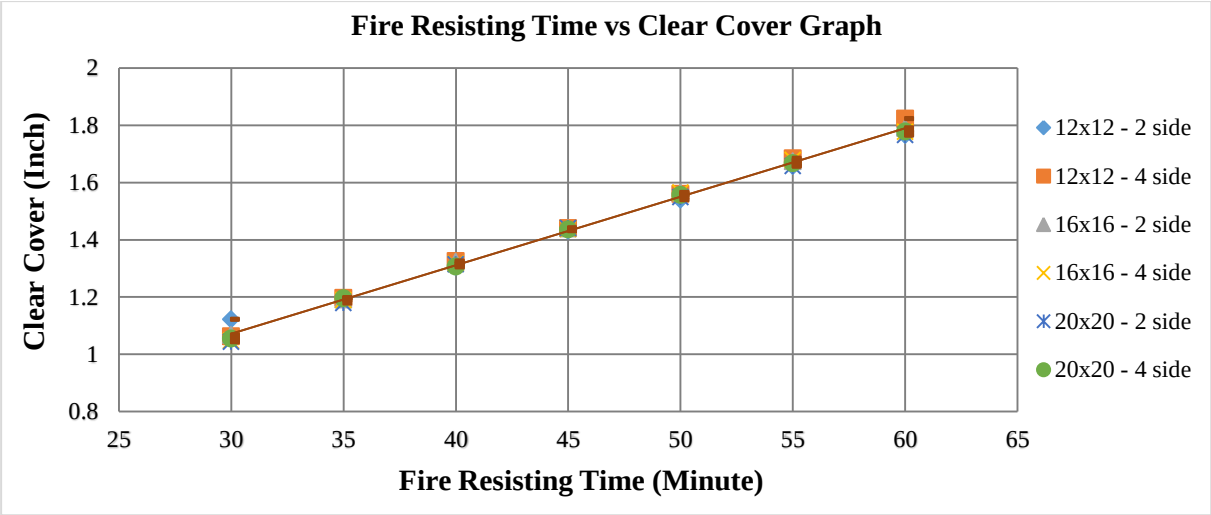

Figure 10: Formation of Empirical Relation between Fire resistance time and Required Clear Cover for 300°C Temperature

The equation we get from the graph is-

$$C = 0.0239T + 0.3551$$

Where, C = Required Clear Cover (Inch)

T = Fire Resisting Time (Minute)

3.3. Implication of the Empirical Relation

This empirical equation has notable significance to build a fire-resistant structure. It gives us clear cover value if we input time in the equation. It demonstrates us what should be the size of the clear cover of a square column if want to protect the column for a certain time from fire damage.

For example: If we want a column of 1-hour fire resistance, then we calculate what should be our clear cover size of the column.

$$C = 0.0239T + 0.3551$$
$$= 0.0239*60 + 0.3551$$
$$= 1.789$$
$$\approx 2.00 \text{ inch}$$

Generally, we use 2.5 inch clear cover in our column. Therefore, for C=2.5

$$C = 0.0239T + 0.3551$$
$$\rightarrow 2.5 = 0.0239T + 0.3551$$
$$\rightarrow T = 89.74 \text{ minute}$$

So, our traditional 2.5 inches clear cover in the column is safe until 89.74 minutes of fire application. After that, the column should be repaired.

4. CONCLUSION

In this study, it was observed that, whether the fire is applied in 2 sides or 4 sides, concrete reinforcement interface point at fire application side shows almost the same temperature. The relation between Fire resistant Time, t (minute) and Clear Cover Size, C (Inch) for the square column has been established as C = 0.0239T + 0.3551.

While performing the study some limitations have arisen. For the feasibility of the simulation, only four reinforcements were placed on the four sides of the column section after providing clear cover in every case. An empirical equation has been evaluated to establish the relation between Fire Exposure Time & Required Clear Cover Size. But the equation won't be acceptable if any material property of

the column is changed. The simulation was time-consuming. So fire was applied for 1 hour. The empirical relation could be different in case of fire application of 2 or more hours.

REFERENCES

M. Mohamed Bikhiet, N. F. El-Shafey, H. M. El-Hashimy (2014). Behavior of reinforced concrete short columns exposed to fire, Alexandria Engineering Journal, vol. 53, 643-653 pp.

Fleischmann C and Buchanan A (2016). Analytical Methods for Determining Fire Resistance of Concrete Members, SEPE Handbook of Fire Protection Engineering, 5th Edition, Section 4, Chapter 10, 4-241 pp.

Mohammad Nizam Uddin and Sabbid Ibnul Gafur Shuvo (2017). Parametric Study of RCC Square Column Under Fire, Bangladesh University of Engineering and Technology.

Proc. 2nd International Conference on Structural Engineering Research (iCSER2019)
19-22 Jan 2019, Dhaka, Bangladesh
ISBN: 978-0-6482681-2-3

Comparative Study of Circular Concrete Column with Different Types of Ferrocement Confinement

Ayesha Binta Ali[1] and Mrittika Hasan Rodela[1]

[1]Lecturer, Department of Civil Engineering, Sonargaon University, Dhaka, Bangladesh
Corresponding author's E-mail: ayesha.binta.ali.25@gmail.com

Abstract

Column is one the predominant structural elements designed to support compressive load as well as transfer load to the foundation. The strengthening of reinforced concrete columns by ferrocement jacketing is a frequently used effective method because of its availability of raw material and low cost. Moreover, the unique properties of ferrocement such as fire resistant, durability, low self-weight, water proof and crack resistant makes it an ideal material for wider applications. Significant amount of work has been carried out on confinement of column with ferrocement considering change in parameter such as types of meshes with different sizes. Basically, ferrocement is a thin wall reinforced concrete made of wire mesh closely bound together, sand and cement which possess unique qualities of strength and serviceability. The use of ferrocement as an external confinement to concrete column is investigated in this study for which a comparative analysis is carried out with circular column jacketed with and without different types of wire mesh in mortar mix. The compressive load, compressive strength, volume fraction and specific ratio are calculated for each member. It is found from the study that ferrocement confinement increase the strength of column and the maximum load is found for column with square wire mesh and the minimum load is found for column with expended wire mesh 2.

Keywords: Ferrocement, Circular column, Confinement, Wire mesh.

1. INTRODUCTION

The word "Ferro" originates from ferrous which means iron. As the name implies, Ferrocement is a type of cement, but it is applied in a very special way, utilizing minimal material and as a result being much less costly than traditional cement construction. Ferrocement is a type of thin wall reinforced concrete. Basically using relatively small size wire meshes, normal cement, potable water and admixture (such as fly ash etc.), we can compositely make this concrete. It is a special form of reinforced concrete which exhibits a behavior differing much from conventional reinforced concrete in strength performance.

Ferrocement is a composite material which is used in construction around the world. It is used to build homes, boats, bridges, and a variety of other structures, and some artists also work with Ferrocement, creating sculptures and architectural features from this very strong, durable, versatile material. In developing countries, the raw materials for Ferrocement construction are easily available, and also it could be constructed in any complicated shape. The skill required is of low level and it has superior strength properties as compared to conventional reinforced concrete. These are the reasons for which the Ferrocement is considered to be an appropriate confinement material in developing countries such as Bangladesh. The development of innovative rehabilitation and strengthening technique is required to extend the life expectancy of many concrete structures. The above mentioned factors have contributed to motivate researchers to unleash the potential of using composite materials to retrofit and strengthen the structures. Procedures that are technically sound and economically feasible are needed to upgrade the deficient structures. The use of Ferrocement as an external confinement to concrete cylinder was investigated in this study.

The American Concrete Institute (ACI) Committee 549 put forward the definition of Ferrocement as follows "Ferro cement is a form of reinforced concrete using closely spaced multiple layers of mesh and/or small diameter rods completely infiltrated with, or encapsulated in mortar. The most common type of reinforcement is steel mesh. Other materials such as selected organic, natural or synthetic fibres may be combined with metallic mesh."
The strength of a Ferrocement structure depends on basically two things:

- The quality of the sand/cement mortar mix. The sand must be clean and sharp. The cement must be fresh, and the mortar mix "dry"-that is: well mixed using a minimum of water. The mortar should be used as soon as possible after mixing, especially in warm weather.
- The quantity of reinforcing material, usually common "chicken wire". More wire results in a stronger structure. A high quality boat hull will require as many layers of wire as can be gotten into the thickness of the hull.

2. METHODOLOGY

The purpose of the study is to compare Ferrocement cylinder and normal cylinder strength, to know the difference between different types of wire mesh and also to investigate the characteristics of their behavior. The work was performed mainly in two ways. Firstly concrete cylinders were made with Ferrocement confinement and then plastered on those. The whole procedure is shown below.

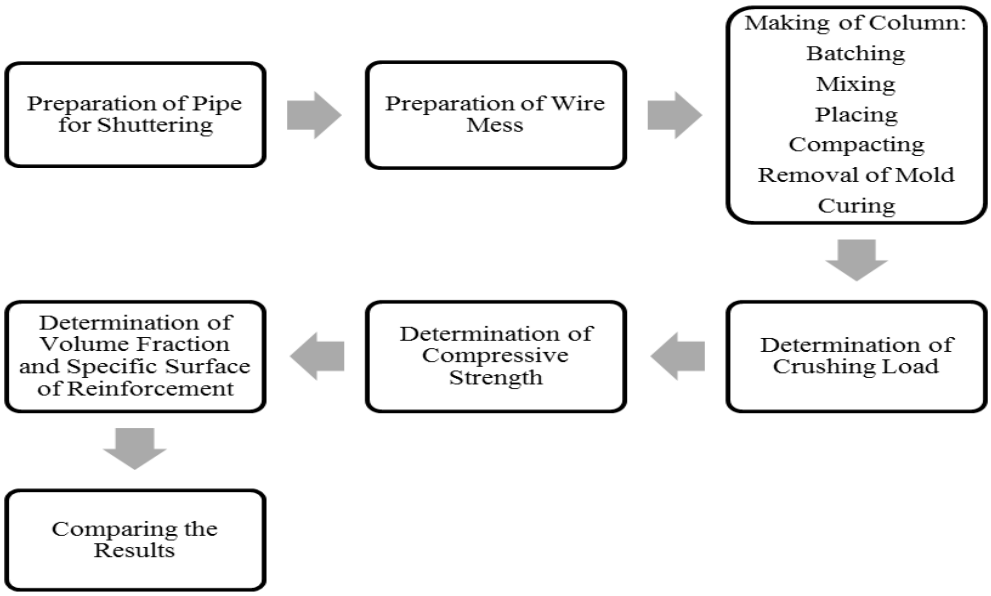

Figure 1. Flow chart of Methodology

For this study the circular cylinders (6 inch dia * 24 inch height) were made. In total 10 cylinders were made for the experiment. Two were without any wire mesh and remaining cylinders were with Ferrocement containing different types of wire mesh.

2.1 Mix Proportion of Concrete Cylinder

The ranges of mix proportions recommended for concrete cylinder applications are:
Cement:Sand:Stone Chips = 1:2:4
Water-Cement Ratio = 0.5
For one cylinder:
Wt. of Cement = 4.00kg
Wt. of Sand = 8.00kg
Wt. of Stone Chips =16.00 kg
Wt. of Water = 2.00 kg

Figure 2. Cement, Sand and Stone Chips

2.2 Mix Proportion of Ferrocement Mortar

The ranges of mix proportions recommended for common Ferrocement applications are:
Cement:Sand = 1.5:2.5 and
Water-Cement ratio = 0.35 to 0.5.
The higher the sand content, the higher the required water content to maintain the same workability. Shrinkage is not a problem in Ferrocement because of the high reinforcement content. Instead, in Ferrocement mortars it is most important to maintain plasticity as a design criterion.

2.3 Preparation of Pipe for Shuttering

PVC pipes of (6 in) 150mm diameter were used for shuttering work. Then 10 pipes of same height (2 feet) were cut.

2.4 Preparation of Wire Mess

Taking proper and accurate measurement of the entire column all wire meshes were resized as same size. In this study all cylinders were of sizes 6 inch diameter * 24 inch height and 4 types of wire mess were used.

Table 1. Different types of wire meshes with sizes

Serial No.	Wire Mess	Size (mm^3)
1	Expanded wire mess 1	8*5*0.6
2	Expanded wire mess 2	20*14*0.6
3	Expanded wire mess 3	20*14*1
4	Square wire mesh	12*12*1.3

2.5 Making of Column

Production of quality concrete requires meticulous care exercised at every stage of manufacture of concrete.

a) Batching
b) Mixing
c) Placing
d) Compacting

2.6 Batching

A proper and accurate measurement of all the materials used in the production of concrete is essential to ensure uniformity of proportions and aggregate grading in successive batches. In this study gravimetric batching were used for measuring the materials.

2.7 Mixing

The objective of mixing is to coat the surface of all aggregate particles with cement paste, and to blend all the ingredients of concrete into a uniform mass. In this study concrete mixing were done by hand mixing. Mixing proportion (1:2:4) and w/c ratio 0.50 of cement mixing were used.

2.8 Placing

The methods used in placing concrete in its final position have an important effect on its homogeneity, density and behavior in service. In this study concrete was poured into the mould with corny by hand.

2.9 Compacting

The process of removal of entrapped air and of uniform placement of concrete to form a homogeneous dense mass is termed as compaction. In this study hand compaction was done according to ACI code.

2.10 Removal of Mold

The hardened cubical concrete specimen was brought out removing the mould after 24 hours of its casting. Then leveling of specimen on its surface by permanent marker pen was gone so that they can be separated without any confusion. Much care was taken while removing the mould so that the specimens do not affected adversely.

2.11 Curing of Concrete

The physical properties of concrete depend largely on the extent of hydration of cement and the resultant microstructure of the hydrate cement. Hydration of cement is activated in the presence of water. For this reason, curing of concrete is obviously required. Test specimens were immersed under normal water in curing tank for 28 days.

Figure 3. Placing of Wire Mess inside the pipes

Figure 4. Curing

3. DATA ANALYSIS

In the laboratory UTM machine was used to impose load. The Volume Fraction of reinforcement (*Vf)* and Specific Surface Ratio of reinforcement *(Sr)* were also calculated. The results obtained are summarized below in a tabular form.

Table 2. Compressive loads of Ferrocement columns

Mesh Size	Cylinder Number	Compressive Load (KN)	Average Compressive Load (KN)
Expanded Wire Mesh 1 Longitudinal Length=5mm Transverse Length= 8mm Thickness=0.6mm	1A	205	198
	1B	190	
Expanded Wire Mesh 2 Longitudinal Length=20mm Transverse Length=14mm Thickness=0.6mm	2A	150	150
	2B	150	
Expanded Wire Mesh 3 Longitudinal Length=20mm Transverse Length= 14mm Thickness=1mm	3A	180	185
	3B	190	
Square Wire Mesh Length=12mm Width=12mm Thickness=1.3mm	4A	225	238
	4B	250	
Without Wire Mesh	5A	150	140
	5B	130	

Table 3. Compressive Strength of all Specimen

Cylinder No.	Wire Mesh Type	Cylinder Diameter (m)	Cylinder Area (m^2)	Compressive Load (KN)	Compressive Stress (MPa)
1	Expanded Wire Mesh 1	0.1905	0.0285	198	6.95
2	Expended Wire Mesh 2	0.1905	0.0285	150	5.26
3	Expended Wire Mesh 3	0.1905	0.0285	185	6.50
4	Square Wire Mesh	0.1905	0.0285	238	8.35
5	Without Wire Mesh	0.1905	0.0285	140	4.91

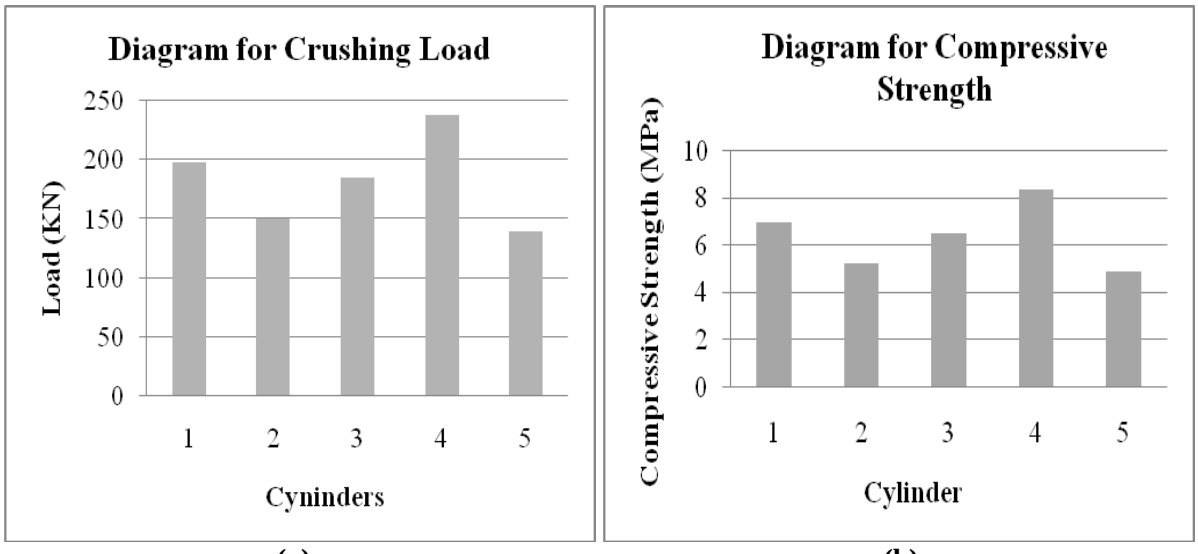

(a) **(b)**

Figure 5. (a) Diagram for Crushing Load and (b) Diagram for Compressive Strength

Table 4. Volume Fraction and Specific Surface of Reinforcement

Cylinder No.	Wire Mess Type	Spacing Long Dl (mm)	Spacing Short Dt (mm)	Thickness of Ferrocemeth (mm)	Diameter of wire Mesh (mm)	$V_f = \frac{N\pi d_b^2}{4h}\left(\frac{1}{Dl}+\frac{1}{D_t}\right)$ (%)	$S_r = \frac{4V_f}{d_b}$ (% per meter)
1	Expanded Wire Mesh 1	5	8	19.05	0.6	0.48	32.16
2	Expended Wire Mesh 2	20	14	19.05	0.6	0.18	12.02
3	Expended Wire Mesh 3	20	14	19.05	1	0.5	20.03
4	Square Wire Mesh	12	12	19.05	1.3	1.2	35.73

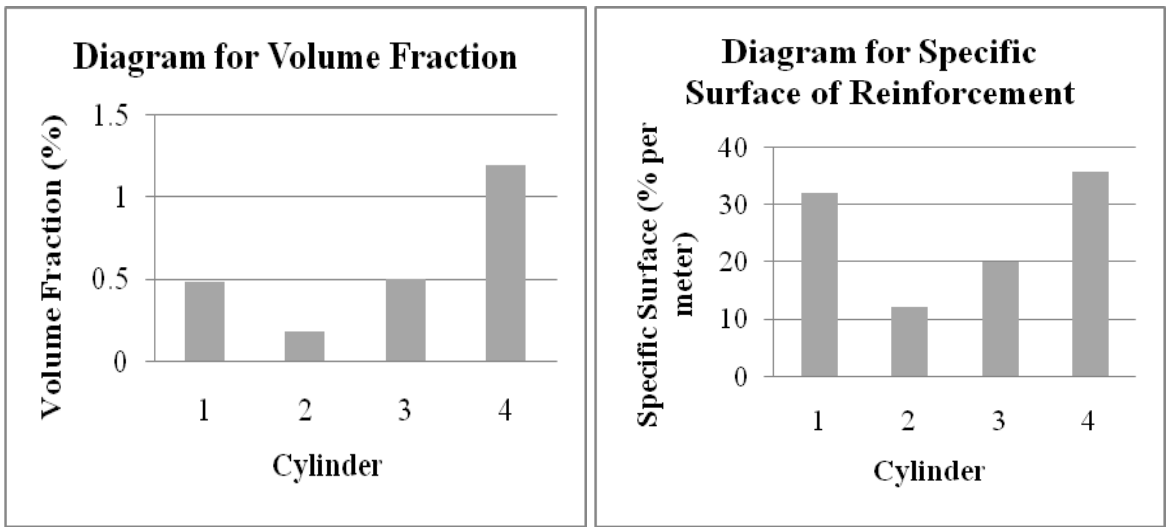

(a) **(b)**

Figure 6. (a) Diagram for Volume Fraction and (b) Diagram for Specific Surface of Reinforcement

4. RESULT AND DISCUSSION

The maximum load was found 238 KN for cylinder with square wire mesh and the minimum load was found 150 KN for cylinder with expended wire meshes 2 whereas for cylinder without wire mesh, the crushing load was 140 KN. Therefore the sequence according to crushing load was Square wire mesh>Expanded wire mesh 1>Expanded wire mesh 3>Expanded wire mesh 2>Without wire mesh. So the maximum and minimum compressive strength was found 8.35 MPa and 5.26 MPa for square wire mesh and expended wire meshes 2 respectively. It was noticed that the crushing load and the compressive strength was directly proportional to the volume fraction as well as the specific surface of reinforcement. With the increase of the crushing load and compressive strength, the volume fraction as well as the specific surface of reinforcement also increases.

5. REFERENCES

G.J. Xiong, X.Y. Wu, F.F. Li, Z. Yan, "Load carrying capacity and ductility of circular concrete columns confined by ferrocement including steel bars" Department of Civil Engineering, Shantou University, Shantou 515063, PR China., Construction and Building Materials 25 (2011) 2263–2268.

Abid A. Shah, "Applications of Ferrocement in Strengthening of Unreinforced Masonry Columns" International Journal of Geology Issue 1, Volume 5, 2011.

Abdullah, Takiguchi. K, "An investigation into the behaviour and strength of reinforced concrete columns strengthened with ferrocement jackets", Cement & Concrete Composites 25 (2003) 233–242.

Proc. 2nd International Conference on Structural Engineering Research (iCSER2019)
19-22 Jan 2019, Dhaka, Bangladesh
ISBN: 978-0-6482681-2-3

Effect of Supplementary Cementitious Material on the Mechanical Properties of Nylon Fiber Reinforced Concrete

Samina Samrose[1], Md. Gulam Kibria Pioul[1], Md. Abu Sayed[1], Israt Zaman Lisa[1], Rupak Mutsuddy[2]

[1] Student, Dept. of Civil Engineering, BUET, Dhaka-1000, Bangladesh
[2]Assistant Professor, Dept. of Civil Engineering, BUET, Dhaka-1000, Bangladesh
Corresponding author's E-mail: samina.samrose@gmail.com

Abstract

Now-a-days, concrete structures reinforced with steel have become an exacting material in Bangladesh. As this kind of structures show inimical effect when they are exposed to deleterious environment, it exacerbates the sustainability and causes serious corrosion of structure with the passage of time. This scenario elucidates the reduction of service life of a structure. For this, resilient performance of structure decreases remarkably. Most often supplementary cementitious materials (fly ash, slag etc.) are used to enhance the durability and strength of concrete. On the other hand, studies showed improved strenuous condition when concrete is reinforced with small fiber (steel, polypropylene, jute, nylon etc). Nylon, a versatile synthetic thermoplastic material, is readily available in Bangladesh. Relatively higher energy absorption is derived from flexural strength test when concrete is reinforced with nylon fiber. This study aims to find a comparison of mechanical properties of concrete mixes prepared with Ordinary Portland Cement (OPC) and Portland Composite Cement (PCC) along with the effect of nylon fiber on those properties.

Keywords: Fiber Reinforced Concrete, Nylon, OPC, PCC, Flexural Strength, Compressive strength, Split Tensile Strength.

1. INTRODUCTION

Concrete has become most versatile material all over the world in building any infrastructure but deterioration can be occurred due to its weak tensile strength coalesced with brittle behaviour. Conventionally, various kind of fiber reinforcements like steel, polypropylene, nylon, jute etc. are being used to control the cracks in tensile area and improve other properties. Fiber reinforced concrete is a composite material consisting of conformist concrete reinforced by random dispersal of short, discontinuous and discrete fine fibers. Previous studies show a significant improvement in concrete properties using steel fiber reinforcement (Behbahani 2011). Maximum increase in mechanical properties of steel fiber reinforced concrete was also defined (Thomas and Ramaswamy 2007). Earlier studies captured the strength contribution of fiber through the combined influence of fiber content and fiber aspect ratio (Hannant 1978). In general, concrete property improves with using steel fiber reinforcement. Typical stress strain curve for steel fiber shows substantial increase in strain at peak (Fanella and Naaman 1985). However, steel fiber shows corrosive behaviour with time and causes vulnerability of structure. This is because of the pozzolanic reaction of fly ash makes denser concrete. Besides, polypropylene fiber significantly controls hazardous situation by ensuring durable structure (Mohod 2015) and improving strenuous condition (Martínez-Barrera et al. 2005).

In recent years, alternative of steel fiber was invented. Mineral admixture such as fly ash, slag, silica fume etc. affects concrete properties substantially. Concrete mixed with fly ash and micro silica construct firm durable structure (Salih 2018). Addition of silica fume increases the early strength of concrete (R. Duval et al, 1998). In the perspective of Bangladesh, nylon is a widely available micro-

synthetic fiber which can be used to intercept cracking of concrete in tensile zone. Having strong, elastic and fast drying property, many researches have already done to investigate the situation where nylon can be utilized. Improved concrete condition with optimum percentage is derived by using nylon (Martínez-Barrera et al. 2006). Moreover, achieving expected characteristics of concrete, numerous chemical admixtures are used whereas small amount of nylon fiber with longer length can simply enhance properties of concrete (Spadea et al. 2015).

Now a day, some cement company of Bangladesh is producing PCC type of cement with fixed proportion of fly ash and slag. In this study, the mechanical properties such as compressive strength, flexural strength and split tensile strength are evaluated using different nylon content for a particular water-cement ratio. Improved strenuous condition of nylon fiber reinforced concrete demonstrates better structural integrity. Also, longer service life is corroborated from flexural strength test and makes structure more durable. Sustainable structural development can be ensured using nylon as fiber reinforcement.

2. MATERIALS AND METHODS

This research was performed with a typical mix ratio of cement, sand and coarse aggregate of 1:2:4 widely used in Bangladesh. As binding material, some mixes were prepared with OPC and some mixes were prepared with PCC. Sylhet sand and stone chips were used for fine aggregate and coarse aggregate respectively. A fixed water-cement ratio of 0.4 was chosen for this study. Nylon was used with three different doses of 0%, 0.25%, 0.50% of volume percentage. Length of the nylon fiber was about 38mm and mixed uniformly in the concrete. To prevent loss of the nylon fiber, each mixes were prepared with manual system instead of using mixer machine. As using fiber reinforcement causes less workability of concrete, superplasticizer admixture was used for this study to increase the workability. Concrete samples were prepared as per ASTM C192 (2002).

Compressive strength test was conducted in accordance with ASTM C39 (2003). 100 mm diameter and 200 mm height cylinder was casted for this test. After 28 days curing period, specimen was placed in the testing machine and load was applied continuously without shocking. A rate of 0.15-0.35MPa/sec loading was set until the specimen failed to observe the failure condition.

Split tensile test was performed as per ASTM C 496 (2004) to evaluate tensile property. For this test, cylinders of 100 mm diameter and 200 mm height was prepared and cured for 28 days. Marking diametric line, diameter and length of specimens were measured and specimen was placed on plywood strips aligning with plywood strip. Within a range of 0.7 to 1.4 MPa/min, continuously load was applied without any shock until failure. Maximum applied load and the type of failure was recorded.

ASTM C78 (2002) was followed in order to carry out flexural strength test. The dimension of the prism was 76mm×76mm×280mm and tested after 28 days curing period. Centring the loading system, load applying blocks were placed in contact with surface of the specimen at the third point loading. Deflection gauge was used for measuring the mid span deflection up to L/150 were L is the span of beam. The load was applied at a constant rate to the breaking point as per ASTM and load was recorded corresponding to the deflection gauge reading.

3. RESULTS AND DISCUSSION

3.1. Compressive Strength Test

Compressive strength was determined for different fiber content using OPC and PCC cement for 0.4 water-cement ratio. Increase in compressive strength behavior was found for PCC with increase in nylon content. For 0.50% nylon, PCC shows 5.76% greater strenuous property than OPC while OPC

exhibits more strength for lower nylon content. This happens due to replacement of fine aggregate with fly ash is attributed to the pozzolanic action of fly ash.

In case of nylon fiber content, 0.25% nylon fiber exhibits maximum compressive strength, 34.72 MPa for OPC and 31.76 MPa for PCC. Though after reaching an optimum content, strength decreases. 0.50% nylon fiber shows lower compressive strength because addition of more nylon fiber causes higher porosity in concrete which causes decrease in compressive strength.

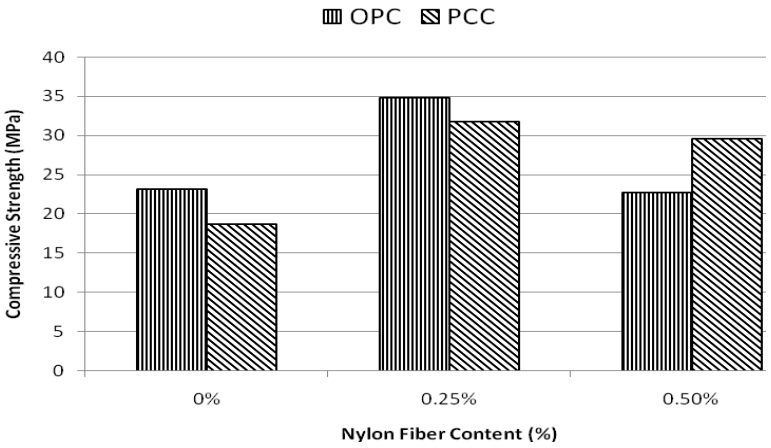

Figure 1. Variation of Compressive strength

3.2. Split Tensile Strength

The split tensile strength was established for different fiber content using OPC and PCC cement. Combined failure type was observed for each type of concrete mix under maximum load. For OPC, tensile strength decreases with higher fiber content but PCC shows significantly improved tensile strength for 0.50% nylon. Split tensile strength of PCC is about 10% greater than OPC value. Being finer particle, fly ash and slag improves the bond between concrete and manifests higher tensile strength.

Considering nylon content, results are antithetical to PCC result. OPC with 0% nylon fiber shows maximum strength while 0.50% nylon fiber proves moderate strength. Intensification in tensile strength was found with increment of nylon fiber content. This is because nylon generates bridge between the cracks under tensile area.

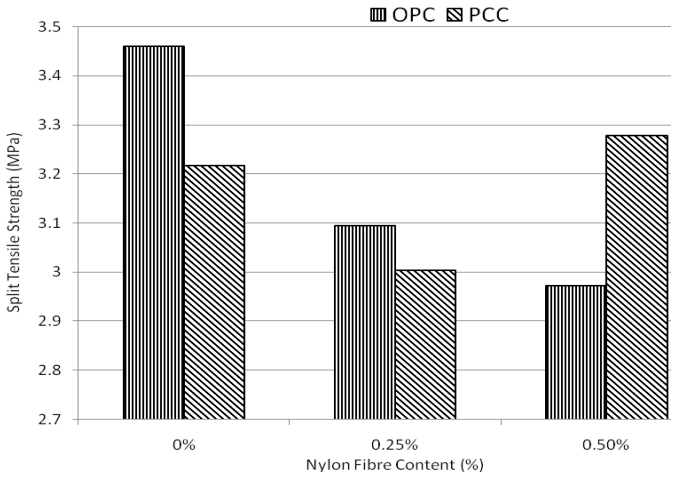

Figure 2: Split tensile strength for OPC and PCC with nylon fiber content

3.3. Flexural Strength

For flexural strength test, OPC shows more stability under loading condition. Representative data illustrates OPC reinforced with 0.25% nylon can undertake 9.14 MPa whereas PCC can carry only 7.65 MPa. It can also be observed that the addition of 0.25% nylon had limited increase about 0.50% in static flexure strength in case of PCC samples.

For a firm and durable structure, higher energy absorption is required before failure. OPC demonstrates more rigid structure than PCC since maximum energy absorption for OPC is 2.84 kN-mm whereas PCC takes 2.54 kN-mm. As supplementary cementitious materials have less intensity to absorb energy, OPC shows better result. Also, OPC with 0.25% nylon provides more rigid and sustainable structure with increased service life.

Evaluating results, maximum modulus of rupture was 3.95 MPa for PCC and 5.59 MPa for OPC which is 41.5% higher modulus of rupture than PCC. For PCC, addition of 0.50% nylon fiber provided remarkable decrease in modulus of rupture of about 5.33%. On the other hand, for OPC, 17.4% increase and 28% decrease are found for modulus of rupture comparing with 0.25% and 0.50% nylon fiber respectively.

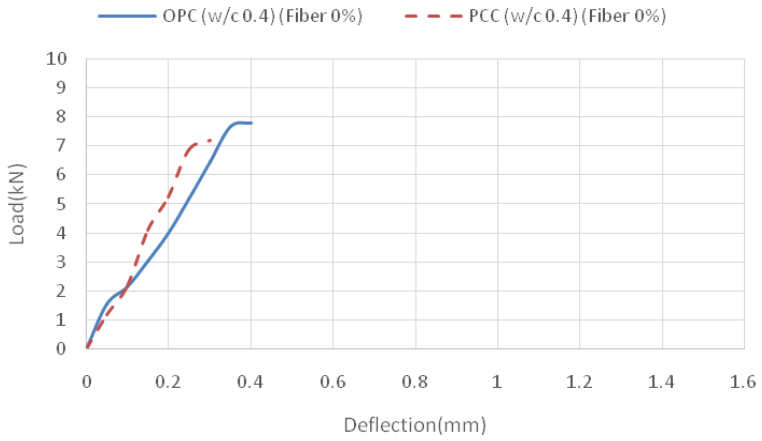

(a)

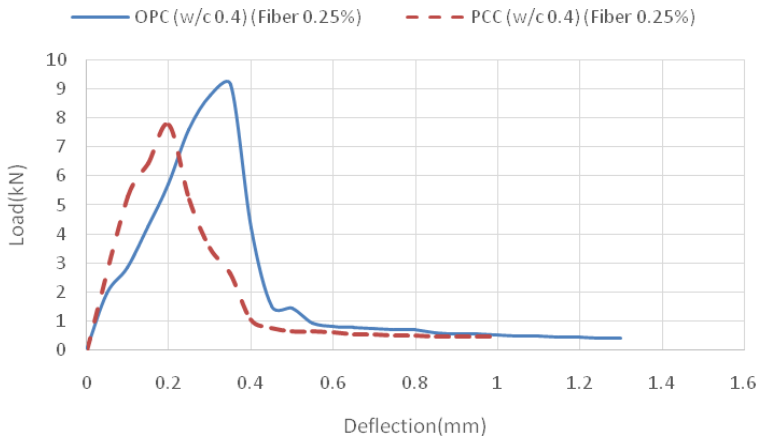

(b)

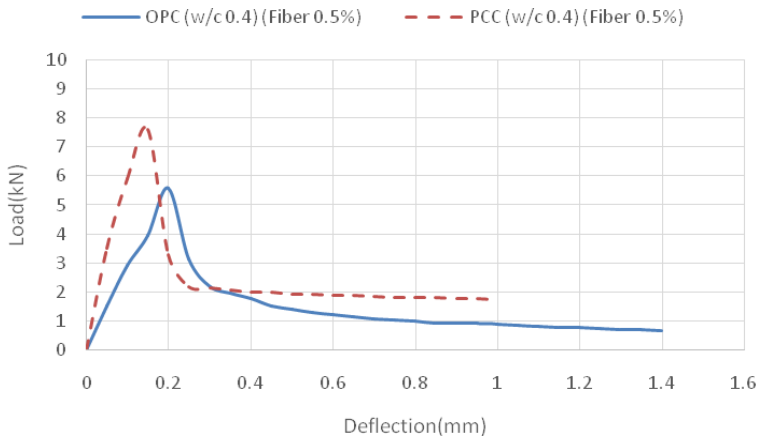

(c)

Figure 3: Representative load-deflection curve (a) for 0% nylon, (b) for 0.25% nylon, (c) for 0.50% nylon

According to ACI Code (ACI-318), empirical value of modulus of rupture was calculated and compared with the experimental value. Figure 4 shows deviation of modulus of rupture of experimental and empirical value of both OPC and PCC with nylon fiber content. Empirical relation was calculated as per equation (1).

$$f_r = 0.62\sqrt{f'_c} \quad (1)$$

Where, f'_c is maximum compressive strength of concrete. For OPC cement type, experimental value deviation is higher than PCC although the deviation pattern is similar. For OPC type of concrete, both empirical and experimental modulus of rupture matches closely but for PCC massive deviation occurred.

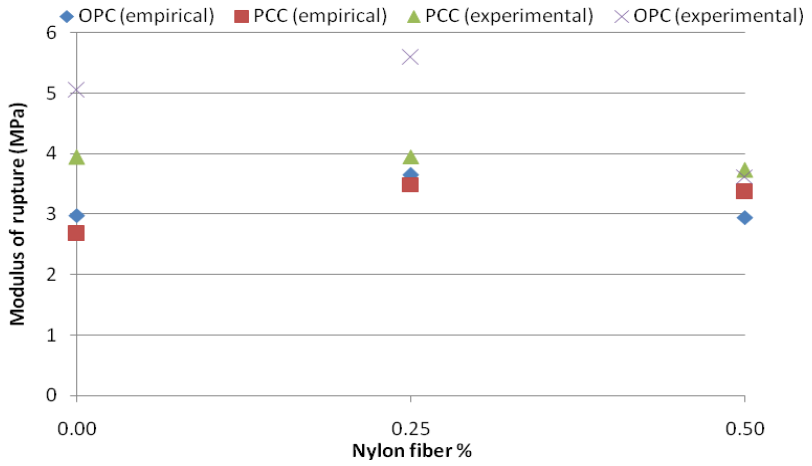

Figure 4: Comparison between experimental and empirical value of modulus of rupture

4. CONCLUSION

This research shows possible effect of various nylon fiber reinforced content on mechanical properties of concrete for water-cement ratio of 0.4. Due to the effect of supplementary cementitious materials, PCC with 0.50% nylon has more strenuous and durable condition than OPC. Among various fibers content, both OPC and PCC sample with 0.25% nylon fiber showed better performance. However, PCC sample with higher nylon content shows better performance on flexural rigidity, it shows anomalous behavior on other properties. Considering overall characteristics, 0.25% nylon fiber illustrates better performance. Also, this outcome of the study necessitates the importance of further research with varied water cement ratio.

ACKNOWLEDGMENTS

Bangladesh University of Engineering and Technology (BUET), Department of Civil Engineering provided financial and technical support for this work. The authors would like to appreciate the generosity of Concrete Laboratory and S.M Laboratory of BUET.

REFERENCES

ASTM C 39/C 39M-03 (2003). Standard Test Method for Compressive Strength of Cylinder Concrete Specimens. West Conshohocken, PA

ASTM C 78-02 (2002). Standard Test Method for Flexural Strength of Concrete (Using Simple Beam with Third-Point Loading), West Conshohocken, PA

ASTM C 192/ C 192M-02(2002). Standard Practice for Making and Curing Concrete Test Specimens in the Laboratory, West Conshohocken, PA

ASTM C 496/C 496M-04 (2004). Standard Test Method for Splitting Tensile Strength of Cylindrical Concrete Specimens, West Conshohocken, PA

Behbahani, Hamid Pesaran. 2011. "Steel Fiber Reinforced Concrete: A Review," 13.

Fanella, D.A., and Naaman, A.E., 1985, Stress-Strain Properties of Fiber Reinforced Concrete in Compression, *ACI Journal Proceedings*, V. 82, No. 4, July-Aug., pp. 475-483.

Martínez-Barrera, Gonzalo, Carmina Menchaca-Campos, Susana Hernández-López, Enrique Vigueras-Santiago, and Witold Brostow. 2006. "Concrete Reinforced with Irradiated Nylon Fibers." *Journal of Materials Research* 21 (02): 484–91. https://doi.org/10.1557/jmr.2006.0058.

Martínez-Barrera, Gonzalo, Enrique Vigueras-Santiago, Susana Hernández-López, Gonzalo Martínez-Barrera, Witold Brostow, and Carmina Menchaca-Campos. 2005. "Mechanical Improvement of Concrete by Irradiated Polypropylene Fibers." *Polymer Engineering & Science* 45 (10): 1426–31. https://doi.org/10.1002/pen.20418.

Mohod, Milind V. 2015. "Performance of Polypropylene Fibre Reinforced Concrete," 10.

R. Duval, E.H.Kadri, "Influence of Silica Fume on the Workability and Compressive Strength of High-performance Concretes, " Cem. Concr. Res. 28 (4) (1998) 533-547.

Salih, Dr Moslih Amer. 2018. "Strength and Durability Of High Performance Concrete Containing Fly Ash And Micro Silica," 12.

Spadea, Saverio, Ilenia Farina, Anna Carrafiello, and Fernando Fraternali. 2015. "Recycled Nylon Fibers as Cement Mortar Reinforcement." *Construction and Building Materials* 80 (April): 200–209. https://doi.org/10.1016/j.conbuildmat.2015.01.075.

Thomas, Job, and Ananth Ramaswamy. 2007. "Mechanical Properties of Steel Fiber-Reinforced Concrete." *Journal of Materials in Civil Engineering* 19 (5): 385–92. https://doi.org/10.1061/(ASCE)0899-1561(2007)19:5(385).

Proc. 2nd International Conference on Structural Engineering Research (iCSER2019)
19-22 Jan 2019, Dhaka, Bangladesh
ISBN: 978-0-6482681-2-3

Monitoring of Corrosion in Fly Ash Concrete Slab Containing Chlorides by Electrochemical Method

Sristi Das Gupta[1] and Mantaka Mahjabin Momo[2]

[1]Lecturer, Ahsanullah University of Science and Technology (AUST), Dhaka, Bangladesh
[2]Lecturer, Ahsanullah University of Science and Technology (AUST), Dhaka, Bangladesh
Corresponding author's E-mail: payelcuet@gmail.com

Abstract

Corrosion of steel reinforcement initiated by chloride contamination has become a common type of deterioration for RC slab used for road bridges in snowy cold regions. Chlorides are present in the RC slabs from the exposure to de-icing road salts. The chloride ion diffuses into RC slab to contact the reinforcements and initiate the corrosion process. So, monitoring of reinforcement conditions in RC slab by non-destructive techniques for the detection of corrosion initiation of reinforcement is a key factor for the maintenance of RC slab. Recently, fly ash concrete has been practically employed to RC slab in snowy cold region so that the durability of the RC slab can be enhanced. This study principally aimed to assess the corrosion development of reinforcing steel within RC slab containing fly ash at two replacements levels of cement 15% and 30% subjected to a sodium chloride solution of 10% in the concentration, through continuous half-cell potential monitoring system using Pb/PbO_2 reference electrode. In addition, a portable corrosion meter was also employed at a periodic interval to obtain the corrosion rate in terms of corrosion current density as well as half-cell potential using Ag/AgCl reference electrode. After corrosion initiation based on ASTM (C 876), Chloride Threshold Level (CTL) was examined and significant drop of chloride threshold level in fly ash concrete was confirmed. Through the examination of the alkalinity in concrete at the vicinity of rebars by Thermo-Gravimetry/Differential Thermal Analyzer (TG/DTA) analysis the CH (Portlandite) content was found less in fly ash concrete compared to normal concrete.

Keywords: Non-destructive test, Fly ash concrete, Half-cell potential, corrosion current density, Chloride Threshold Level (CTL), CH (Portlandite).

1. INTRODUCTION

Iron and plain carbon steels (iron alloyed with small amounts of carbon) are thermodynamically unstable materials. The corrosion of steel reinforcing bars is an electrochemical process that requires a flow of electric current and several chemical reactions (Hammer A T, 2008). The initiation and continuation of the corrosion process are controlled by the environment in the concrete surrounding the steel reinforcing bars. However, corrosion occurs more rapidly under conditions of exposure to chlorides. Using de-icing salt in concrete bridge slab is a common phenomenon for reinforcement corrosion due to chloride attack (Gupta S D, *et.al;* 2017). In a chloride-laden environment the presence of adequate moisture and oxygen causes localized break in alkali protected film and initiate corrosion of rebars in concrete when chloride concentration goes above a critical concentration (Chloride Threshold Level, CTL). Chlorides actually act as a catalyst in this process to facilitate the initiation of corrosion (Yang Z. *et.al*, 2013). Recently, several cementitious materials have been used in RC slab for durability purposes. Pozzolans are materials which when mixed with cement and water form C-S-H whereas latent hydraulic materials require a catalyst to produce C-S-H. The addition of these products to a concrete mix reduces the cement requirement for strength and enhances its durability over time. The most prevalent additions are ground granulated blast furnace slag, fly ash, and silica

fume. The presence of fly ash reduces the heat of hydration as well as the mixing water required for a particular slump. The reduction of the water requirement is extremely important for achieving low w/c mixes **(**i.e., high performance concretes). Chlorides penetrating into hardened concretes with fly ash exhibit lower active corrosion rates (Hansson C.M. *et.al*; 2012). Chloride induce corrosion involves reliable detection of corrosion initiation and accurately estimation of chloride content at the rebar depth. Electrochemical methods such as; a) Half-cell potential monitoring b) Macro-cell current monitoring between an anode and a cathode to detect the onset of corrosion. The former principle is used mainly to detect the corrosion initiation in this study. Half- cell potential monitoring has been used to identify the corrosion initiation widely. Additionally, macro-cell corrosion also causes the half-cell potential to fluctuate due to the polarization. According to Nakamura E. *et.al*, 2008, macro-cell corrosion with two layers of reinforcement sometimes potential of down rebar shifted more negative -350 mV than positive while, the visual inspection of reinforcement showed there was no sign of corrosion in rebar surface. This fluctuation of half-cell potential is due to localized corrosion with high chloride content in up rebar in which potential of down rebar have been shifted by polarization. The corrosion rate could be measured by the polarization technique or AC impedance method. Later is used for corrosion rate measurement in the current research. AC impedance gives probably the most reliable result for corrosion rate.

This research principally aimed to establish a test method to point out the initiation of corrosion of rebars in concrete reliably. A combination of two different systems is proposed to detect the corrosion initiation and its rate estimation. Thereafter, chloride threshold level was determined for three different mixes proportioned Ordinary Portland Concrete (OPC) and Fly Ash (15% & 30%). In connection with this Ca(OH)2 was quantified at the vicinity of rebars using a Thermo Gravimetry/Differential Thermal Analyzer (TG/DTA).

2. EXPERIMENTAL METHODOLOGY

2.1. Specimen Preparation

This research mainly deals with fly ash concrete in RC slab and makes the comparison with ordinary Portland cement (OPC) concrete. Two different replacement levels of fly ash of 15% and 30% for OPC were studied namely, F15and F30. The reinforcing steel used for RC slab was deformed steel bar with a diameter of 19 mm. A total of 30 specimens with 6 groups were prepared. All specimen series were cured in water for 91 days. The details of the mix proportions for N, F15 and F30 are found in Table 1. In this research two different dimensions of RC slabs were studied, namely Type A and Type B. The size and the cross sections of the specimen are shown in Figure 1. Every specimen contains two longitudinal reinforcements one is 30 mm cover distance from top surface named as up rebar and another is 30 mm cover distance from bottom surface named as down rebar. An Acrylic canister (having opening in top and bottom) of 50 x 100 mm in cross section had been set on the middle of the specimen with transparent type glue. After allowing the glue sufficiently drying and hardening, NaCl solution of 10% in concentration was poured in that canister.

Table 1. Mix proportions of concrete

Type	**G_{max} (mm)**	**Slump (cm)**	**Air (%)**	**W/ (C+FA) (%)**	**s/a (%)**	**Unit weight (kg/m³)**					**Strength (N/mm²)**	
						W	C	F A	S	G	28 Days	91 days
N	20	9.5	4.7	63.5	50.0	142	224	0	1,002	995	30.2	33.3
F15	20	9.5	4.8	58.5	48.0	132	192	34	969	1042	28.1	33.9
F30	20	9.5	4.8	49.5	46.0	126	178	76	919	1071	29.6	37.5

2.2. Measurements

Figure 2a, shows the half-cell potential monitoring set up of test specimens. For Non-destructive corrosion test, half-cell potential method and polarization resistance method were used. The measurement of half-cell potential was done by using Lead-Lead oxide electrode (Pb/PbO2). In

addition, the Corrosion meter with double ring counter electrode ($Ag/AgCl_2$ reference electrode) was employed allowing precise polarization resistance and corrosion rate in terms of corrosion current density to be measured.

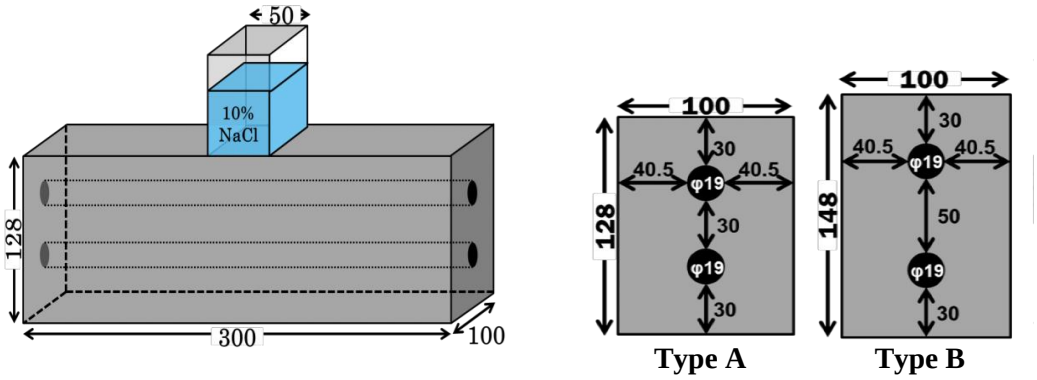

Figure 1. Schematic presentation of concrete specimen used for corrosion test (Unit: mm)

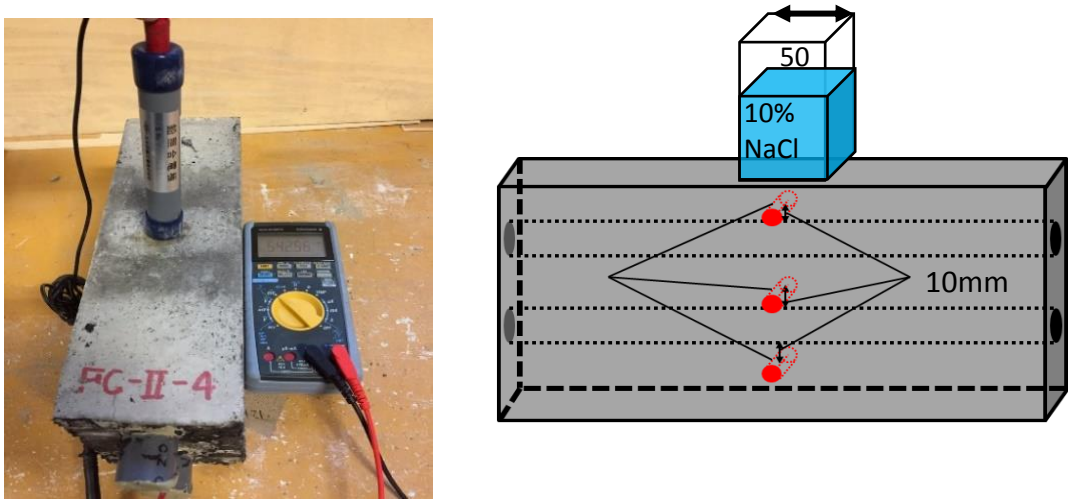

(a) (b)

Figure 2. (a) Half-cell potential monitoring in concrete specimen (b) Schematic presentation of concrete powder taken out for chloride analysis

After successful detection of corrosion according ASTM C-876, chloride analysis was conducted. Approximately, 10 grams of concrete powder was taken out from three points in the near of up rebar and down rebar in each side of the normal and fly ash concrete specimen of the entire chloride application zone (50mm x 100mm) for chloride analysis (Fig.2b). Thereafter, chloride ion concentration in each point of the specimen has been measured using an automatic chloride ion titration device (*GT-100*).

After chloride concentration measurement, the concrete powder that was taken out from the vicinity of rebar was used further to quantify the $Ca(OH)_2$ (*Portlandite*) content in hardened concrete using the Thermo- Gravimetry/ Differential Thermal Analyzer (TG/DTA). The analysis was carried out with the temperature range of 20-1000^oC with an increment rate of 10^oC/min. Nitrogen (N_2) gas was used for the test with a flow rate of 200ml/min. A TG/DTA analysis was carried out in the computer data logger system. The decomposition of $Ca(OH)_2$ occurs in between the temperature range (mostly in between 400-450^oC). From the TG/DTA graph, $Ca(OH)_2$ was estimated from the weight loss measured from the TG curve between the initial and final temperature of the corresponding TG peak by considering the decomposition reaction stated in Equation 1.

$$Ca(OH)_2\ (s) \longrightarrow CaO\ (s) + H_2O\ (g) \qquad (1)$$

3. RESULTS AND DISCUSSIONS

3.1 Electrochemical Data and Corrosion Diagnosis

Since in this research all concrete slab has two layers of reinforcement both polarization resistance method and half-cell potential method were used to measure six different positions for all the specimen. The symbol 'UT', 'DT' and 'JT' indicates when the electrode was placed on top surface and the connected working electrode was Up rebar, down rebar, jointly connected both up and down rebar respectively. Same like, the symbol 'UB', 'DB' and 'JB' demonstrates when the electrode was placed on bottom surface and the connected working electrode was Up rebar, down rebar, jointly connected both up and down rebar respectively (Figure 3c).

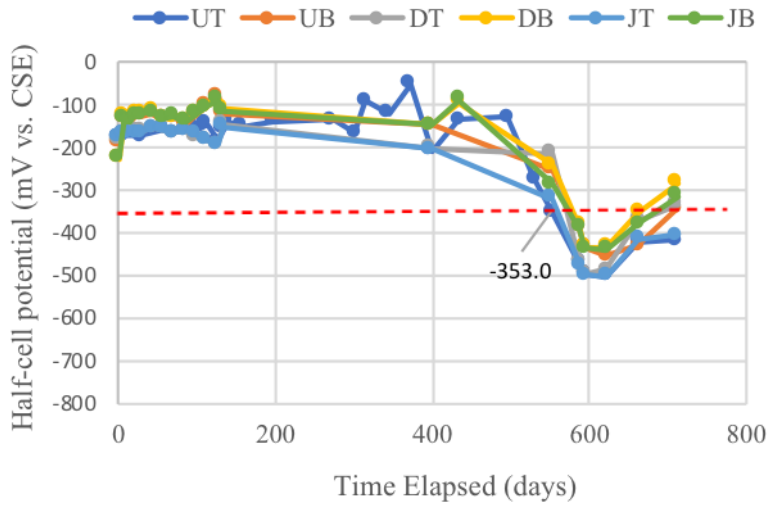

(a)

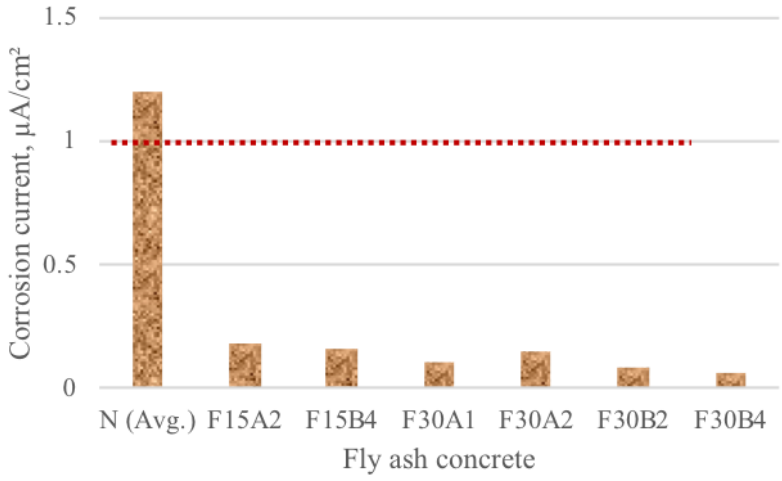

(b)

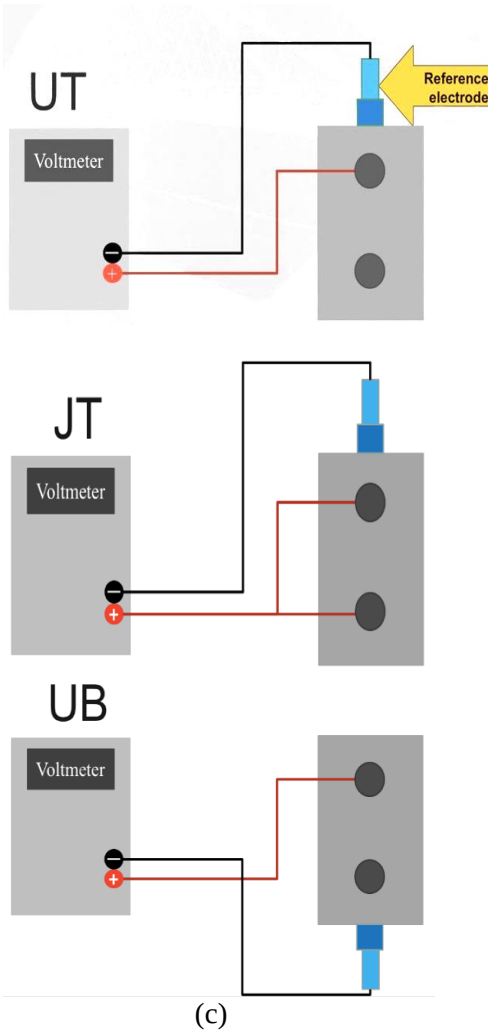

(c)

Figure 3. (a) Half-cell potential monitoring (b) Corrosion current density at the time of corrosion initiation of Up rebar (UT) (c) Corrosion measurements in different positions by portable corrosion meter and half-cell potential method

In Figure 3a and 3b, the threshold half-cell potential (E_{corr} of -350mV vs CSE) and polarization resistance (I_{corr} <1 µA/cm^2) is shown using a continuous dotted line. The corrosion initiation was estimated at the time when half-cell potential value of 'UT' drops more than -350mV. Since the up rebar has lower cover depth than the down rebar it was expected that the down rebar will remain uncorroded while the up rebar initiate corrosion. It has seen that the corrosion initiation in up rebar of

normal concrete was detected comparatively early age than fly ash concrete. The longer period of corrosion initiation in UP rebar in fly ash concrete is due to diffusion of chloride ion in concrete to reach the rebar surface for initiation of corrosion takes longer time than normal concrete. As some of the up rebar of fly ash specimen showed drop in half-cell potential more negative than -350mv by 'UT', the drop of half-cell potential was verified by portable corrosion meter. In all those specimens fly ash concrete whose corrosion was initiated, the corrosion current density rate in both up rebar ('UT') and down rebar ('DB') at the time of corrosion initiation was <0.2 μA/cm^2. The corrosion current density of fly ash concrete at the time of half-cell potential drop in up rebar ('UT') has shown in Figure 3b. Among 10 specimens of normal reinforced concrete corrosion were detected in all specimen and from rest other 20 specimens of fly ash concrete the corrosion detection system diagnosed corrosion initiation in six specimens namely F15A2, F15B4, F30A1, F30A2, F30B2 and F30B4.

3.2 Chloride Threshold Level (CTL)

After the corrosion initiation concrete drilling was conducted for chloride profiling. A nonlinear regression analysis was conducted using computer software to fit the experimental data. Average values of the threshold chloride concentration for corrosion initiation in normal and fly ash concrete has shown in figure 4.

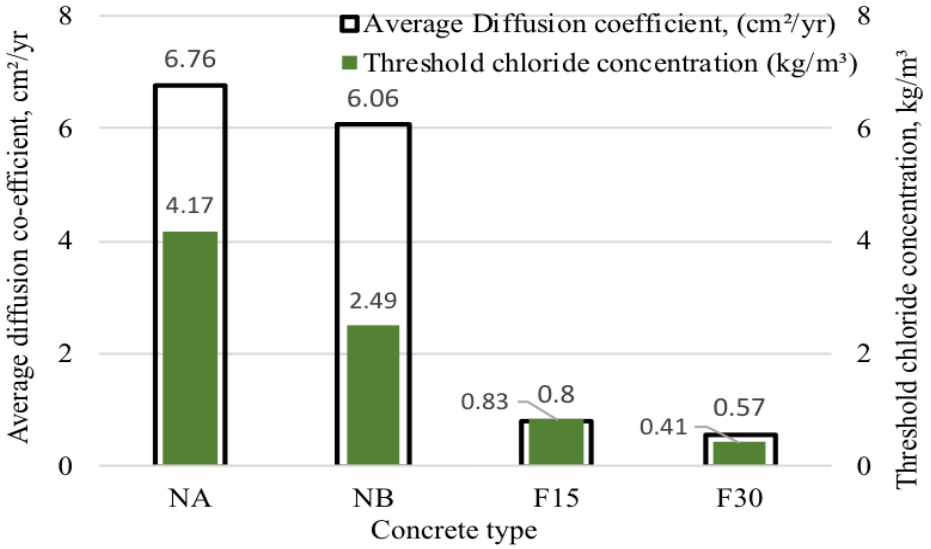

Figure 4. Comparison of Average chloride analysis for normal and fly ash concrete

The average chloride diffusion rate was found 0.57cm^2/yr in F30 concrete which is very low compared to NA and NB category. As the chloride diffusion coefficient of fly ash concrete found very small, the amount of chloride concentration was very low inside the concrete even the experimental chloride analysis did not show evidence of presence of chloride more than 60 mm as well as in fly ash concrete it was observed that only up rebar of fly ash concrete specimen was corroded while in all normal concrete both up rebar and down rebar was corroded. In this study, addition of 30% fly ash as cement replacement the chloride threshold was found 0.41 kg/m^3 while on the contrary, normal concrete highest chloride threshold was found in NA type concrete is 4.17 kg/m^3 (1.86% by mass of cementitious material).

3.2 CH (Portlandite) Content in Normal and Fly Ash Concrete

For analysing the CH (Calcium hydroxide) content in the hardened concrete, the concrete powder which was drilled for chloride analysis was used. The graphical representation of the test results obtained from TG/DTA analysis have shown in Figure 4. The CH content was found lowest in the fly ash concrete than the normal concrete. It is well known that CH content in concrete depends on the amount of cement used.

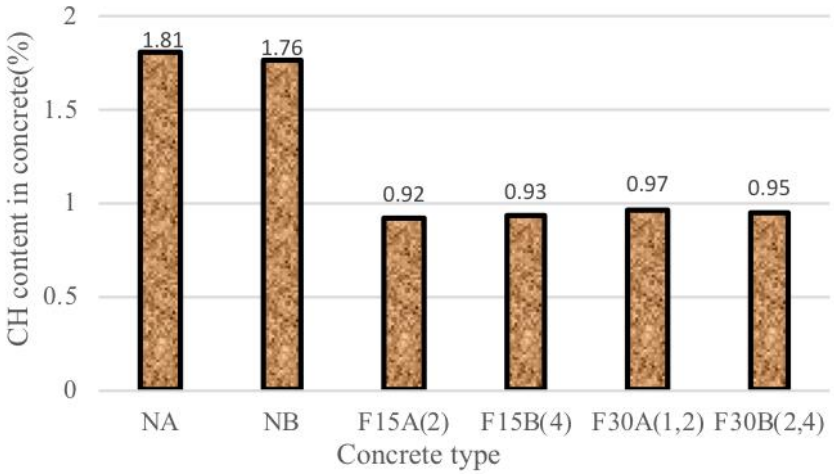

Figure 4. CH content in hardened concrete

The cement content of fly ash concrete was lowest among the other category of concrete. Moreover, the pozzolanic reaction of fly ash with hydrated cement paste consumes some of CH content and finally reduce the CH content in hardened concrete.

4. CONCLUSIONS

- A large number of fly ash concrete hardly exhibits the initiation of the corrosion of the reinforcing steels in the RC slabs after more than two years.
- The average corrosion initiation period of fly ash concrete was more than those of normal concrete.
- The Corrosion current density of fly ash concrete is found <0.2 $\mu A/cm^2$ as opposed to normal concrete, where it was found >1$\mu A/cm^2$.
- The lowest CTL was found 0.41 kg/m^3 in F30 concrete specimen compared to F15 and normal reinforced concrete one.
- It is confirmed that with the increment of fly ash in reinforced concrete slab it reduces the portlandite (CH) content due to the pozzolanic action.

5. ACKNOWLEDGEMENTS

The research support provided by the laboratory of environmental material engineering of Hokkaido University is gratefully acknowledged.

6. REFERENCES

A. T. Hammer, (2008); 'Modelling of reinforcement corrosion in concrete', *state of art,* Olso, Norwoy. ISSN: 1891-1978.

Z. Yang, H. Fischer and R. Polder (2013); Modified hydrotalcites as a new emerging class of smart additive of reinforced concrete for anticorrosion applications: A literature review. *Materials and Corrosion*, DOI: 10.1002/maco.201206915, vol-64.

C. M. Hansson, A. Poursaee and S. J. Jaffer; (2012). 'Corrosion of reinforcing bar in Concrete', www.masterbuilder.co.in

Gupta S D and Sugiyama T (2017); Study on Corrosion of RC Slab with Partial Replacement of Cement as Fly Ash Using Nondestructive Testing Method, *8th Asia and pacific young researchers and Graduates Symposium (YRGS 2017),* September 7-8, University of Tokyo, Japan.

E. Nakamura, H. Watanabe, H. Koga, M. Nakamura and K. Ikawa (2008); Half-cell potential measurements to assess corrosion risk of reinforcement steels in a PC bridge. *International RILEM Conference*, www.sacomatis.org. September1-2, Italy.

Proc. 2nd International Conference on Structural Engineering Research (iCSER2019)
19-22 Jan 2019, Dhaka, Bangladesh
ISBN: 978-0-6482681-2-3

Feasibility Study of Using Stainless Steel Plates in Beam-Column Connection to Improve Seismic Performance

Arifuzzaman Nayeem[1], Shohrat Jahan[1] and Shameem Ahmed[2]

[1]Student, Department of Civil Engineering, BUET, Dhaka, Bangladesh
[2]Assistant Professor, Department of Civil Engineering, BUET, Dhaka-1000, Bangladesh
Corresponding author's E-mail: 3shameemahmed@ce.buet.ac.bd

Abstract

Seismic performance of a structure mainly depends on the flexibility of its joints. Being a nonlinear metallic material with significant strain hardening, stainless steel may be a suitable option to be used in the beam-column joint to improve the seismic performance of steel structures. In this study, performance of beam-column joints using stainless steel was evaluated through numerical analysis. Initially, three dimensional finite element model of a steel beam-column joint was developed and then verified with test results available in literatures. This verified model was used to analyse the behaviour of steel beam-column joint under cyclic loading. After that, the connecting plates of the beam-column joint were replaced by stainless steel plates and the behaviour of that joint was observed for same loading condition. In addition to these, a full stainless steel beam-column joint was also analysed under cyclic loading. The energy absorption capacity of each joint was calculated from the hysteresis diagram. Based on the energy absorption capacity and failure mode, the performance of all the joints was assessed.

Keywords: Cyclic loading, Energy absorption capacity, Hysteresis diagram, Strain Hardening, Seismic Performance, beam-column connection.

Proc. 2nd International Conference on Structural Engineering Research (iCSER2019)
19-22 Jan 2019, Dhaka, Bangladesh
ISBN: 978-0-6482681-2-3

Effect of Jute Fiber on the Mechanical Properties of Concrete Using PCC

Farzana M Nishat[1] and Dr. Rupak Mutsuddy[2]

[1]Student, Bangladesh University of Engineering and Technology, Dhaka, Bangladesh
[2]Assistant Professor, Bangladesh University of Engineering and Technology, Dhaka, Bangladesh
Corresponding author's E-mail: f.mustari03@gmail.com

Abstract

Concrete is a brittle material which is strong in compression but weak in tension. Small discrete fibers are often used in order to improve post tension behaviour of concrete. There are many types of fibers (i.e. steel, glass, polypropylene etc.) already in use in the concrete industry all over the world. However, those fibers aren't available largely in Bangladesh at this moment. Instead, jute fiber has potential of being used as short discrete fiber in concrete due to its abundance. On the other hand, Portland composite cement (PCC), which is a new type of blended cement containing fly ash and blast furnace slag along with regular cement clinker, is gaining popularity as the binding materials in cement composites. In this study, the conventional mixing proportion prevailing in construction sector in Bangladesh was used. The effect of various dosage of jute fiber along with the effect of water-cement ratio on concrete was evaluated. Three strength parameters: compressive strength, split tensile strength and flexural strength were considered in this study. From the experimental results, it can be stated that 0.25% jute fiber along with water-cement ratio of 0.45 improved the compressive strength and split tensile strength. However, flexural strength was higher at 0.5% fiber dosage with 0.55% water-cement ratio.

Keywords: *Fiber Reinforced Concrete (FRC), Jute Fiber, Portland Composite Cement (PCC), Compressive strength, Flexural strength.*

1. INTRODUCTION

Fiber reinforcement cement concrete (FRC) is being used widely around the world to enhance the overall performance of concrete. The design of a durable and low cost fiber reinforced cement concrete for building construction is a technological challenge in developing countries. In order to ensure the safety of structures, many researches had been done so far to measure the mechanical strength of concrete with fiber. There are various works regarding the strength of concrete with steel fiber (Altun et al., 2007; Aydın, 2013; Dahake and Charkha, 2016; Song and Hwang, 2004; Sukumar and John, 2014; Velayutham and Cheah, 2014). Glass fiber was also used in research purpose (Singh and Kumar, 2014). Synthetic fiber like polypropene also got the attention of researchers (Alhozaimy et al., 1996; Aulia, 2002; Balaguru and Khajuria, 1996; Myers, Kang, Ramseyer, 2008). Use of natural fibers were also evaluated in other researches (Codispoti, 2013). It has been observed that natural fibers have the potential to be used as reinforcement to overcome the inherent deficiencies in cementitious materials. Considerable researches are being done for use of reinforcing fibers like jute, bamboo, sisal, coconut husk, sugarcane bagasse in cement composites mostly in case of building materials. Use of natural fibers in a relatively brittle cement matrix has achieved considerable strength, and toughness of the composite (Codispoti, 2013). In the current study the mechanical properties cement composites with PCC and reinforced with short discrete jute fiber. Jute fiber was used as reinforcing fiber as it is locally available in Bangladesh, low cost, easy to handle and process and most of all environment friendly.

2. MATERIALS

2.1. Course Aggregate

The size of coarse aggregate used in this study was 10 mm and the aggregate gradation was well-graded.

2.2. Fine Aggregate

The Sylhet sand used as fine aggregate in this study which was collected from the local market. The fineness modulus of the fine aggregate was 2.47 and the gradation was well-graded.

Table 1. Various properties of Course and Fine aggregate

Aggregate Properties		
Properties	**Course Aggregate**	**Fine Aggregate**
Apparent Specific Gravity, S_a	2.68	2.69
Bulk Specific Gravity (O-D basis), S_d	2.65	2.55
Bulk Specific Gravity (SSD basis), S_s	2.66	2.6
Absorption Capacity (D) in %	0.4	1.94
Unit Weight (kg/m^3)	1522.23	1508.07
Gradation	Open graded	Well graded

2.3. Jute Fiber

Jute fiber was collected from the local market and then prepared into desired length. No chemical treatment was done prior to the use of fiber. The properties jute fiber used are given below:

Table 2. Properties of Jute Fiber

Properties of Jute	Value
Specific Gravity	1.49
Length of Fiber	25 mm

2.4. Cement

Portland Composite Cement (PCC) was used as binding material. The cement was consisted of Fly ash, slag and limestone.

3. METHODOLOGY

3.1. Mix Design

This study intend to use fiber for various structure including typical low rise building, a typical mix ratio of 1:2:4 was used, where 1 part cement, 2 parts fine aggregate and 4 parts course aggregate was used on basis of their volume. In the current experiment three water-cement ratios were used (0.45, 0.5 and 0.55). Three fiber percentages (0%, 0.25% and 0.5%) were used for each water-cement ratio.

3.2. Test Procedures

i. Compressive Strength Test:
The test was done in accordance with the standard test method as issued by ASTM (Designation: C 39/C 39M – 03). The compressive strength of the specimen was calculated by dividing the maximum load carried by the specimen during the test by the average cross-sectional area of specimen. As the specimen length to diameter ratio (8/4=2) was greater than 1.75. So, no correction factor was required. The compressive strength of the specimen was calculated by following equation:

$$C = \frac{P}{\pi d^2/4} \quad (1)$$

Where,
C = Compressive strength, psi [MPa],
P = maximum applied load indicated by the testing machine, lbf [N], and
d = diameter, in. [mm].

ii. Split Tensile Strength Test:
The test was conducted in accordance with the standard test method as issued by ASTM (Designation: C 496/C 496M – 04). The splitting tensile strength of the specimen was calculated by following equation:

$$T = \frac{2P}{\pi ld} \quad (2)$$

Where,
T = splitting tensile strength, psi [MPa],
P = maximum applied load indicated by the testing machine, lbf [N],
l = length, in. [mm], and
d = diameter, in. [mm].

iii. Flexural Strength Test:
The test was done in accordance with the standard test method as issued by ASTM (Designation: C 293– 02). The center point loading method was used in flexure tests of concrete specimen, which ensured that forces applied to the beam, was be perpendicular to the face of the specimen and applied without eccentricity. The modulus of rupture was calculated by following equation:

$$R = \frac{3PL}{2bd^2} \quad (3)$$

Where,
R = modulus of rupture, psi, or MPa,
P = maximum applied load indicated by the testing machine, lbf, or N,
L = span length, in., or mm,

b = average width of specimen, in., or mm, at the fracture, and
d = average depth of specimen, in., or mm, at the fracture.

4. RESULTS AND DISCUSSIONS

Results obtained from the current experiment can be discussed from two points of views, 'Effect of fiber percentage' and 'Water-cement ratio'. The failure pattern was also observed as the failure pattern can also indicate the change in characteristics of concrete with or without fiber.

4.1. Compressive Strength

The results obtained from this experiment showed that the compressive strength increased by more than 37% for various samples upto a fiber percentage of 0.25% and the compressive strength decreased for higher fiber content. With the increment of w/c ratio, strength tended to decrease. Crushing pattern of concrete under compression for various fiber contents did not vary. Though the type was similar kind of cone and split type, the fracture of fiber reinforced concrete was not visible enough like the sample of 0% fiber content.

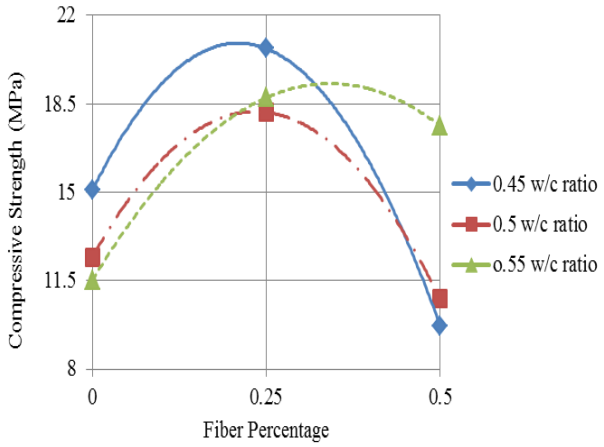

Figure 1. Compressive Strength vs Fiber Percentage

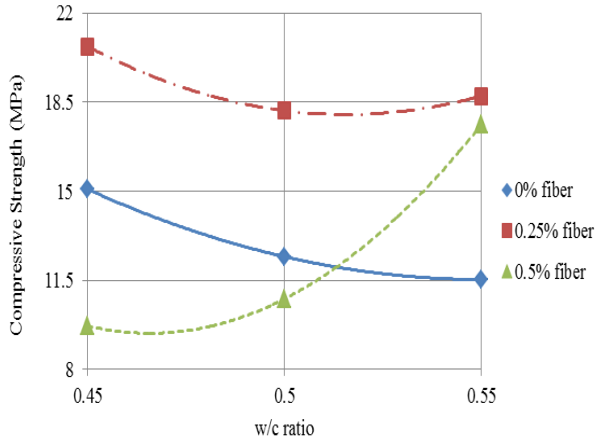

Figure 2. Compressive Strength vs w/c Ratio

4.2. Split Tensile Strength

The split tensile strength also showed similar type of result like the compressive strength. It increased by more than 21% for different samples upto 0.25% fiber content but decreased with additional fiber dosage. With the change in w/c ratio, split tensile strength did not follow the same pattern for various fiber contents. After applying tensile load both specimens, with or without fiber, split into two parts showing columnar fracture. In spite of this similarity, specimen with fiber content showed some resistance due to the pull out effect of fiber.

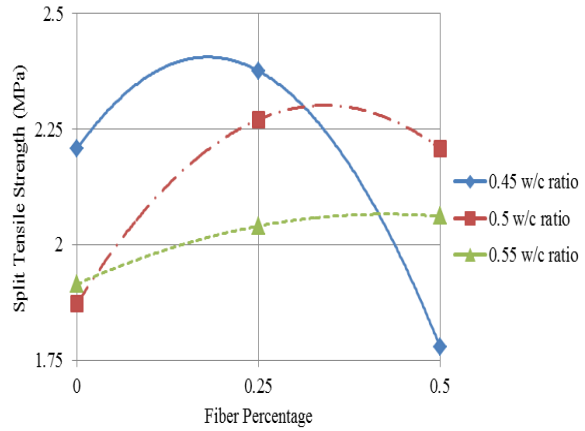

Figure 3. Split Tensile Strength vs Fiber Percentage

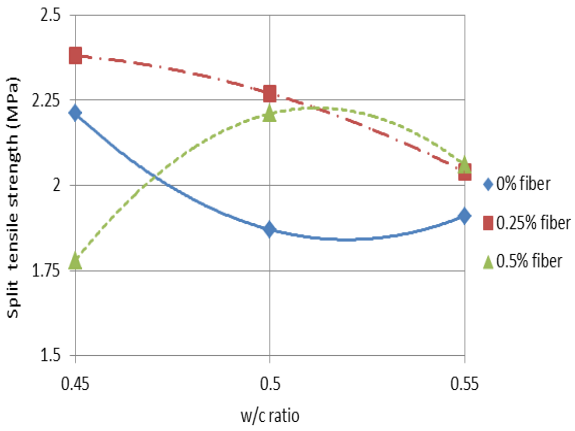

Figure 4. Split Tensile Strength vs w/c Ratio

4.3. Flexural Strength

For different w/c ratios, change in the fiber content produced different type of results. But the flexural strength mainly increased for increment in w/c ratio for a fixed fiber percentage. Under flexural test loading, specimens with or without fiber both broke in tension on the convex tension surface of the concrete beam. Specimen with fiber content showed some resistance due to the pull out effect of fiber.

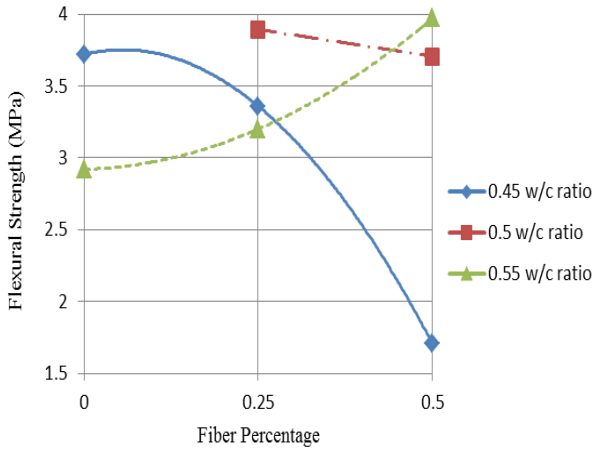

Figure 5. Flexural Strength vs Fiber Percentagegh

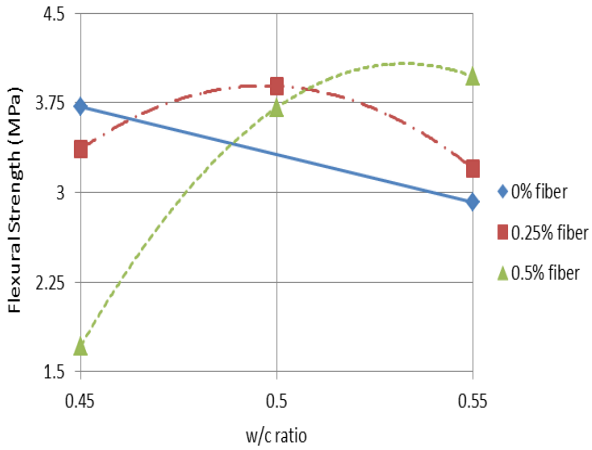

Figure 6. Flexural Strength vs w/c Ratio

5. CONCLUSSION

- With the increase amount of fiber (upto 0.25%), both compressive and tensile strength firstly increased and obtain the maximum value. After that tensile strength started to fall slowly though flexural strength did not change accordingly with the change of fiber content.
- Without any fiber content, compressive and tensile strength rapidly decreased with respect to w/c ratio and then started to climb up with the increase in fiber percentages while flexural strength decreased with the increase in w/c ratio for 0% fiber content.
- 0.25% fiber dosage and 0.45 w/c ratio were found to be optimum for both compressive and split tensile strength. However, additional dosage of fiber with an increase in w/c ratio, improved the flexural strength.

REFERENCES

Alhozaimy, A.M., Soroushian, P., and Mirza, F. (1996). Mechanical properties of polypropylene fiber reinforced concrete and the effects of pozzolanic materials. Cement and Concrete Composites *18*, 85–92.

Altun, F., Haktanir, T., and Ari, K. (2007). Effects of steel fiber addition on mechanical properties of concrete and RC beams. Construction and Building Materials *21*, 654–661.

Aulia, T.B. (2002). Effects of Polypropylene Fibers on the Properties of High-Strength Concretes. 14.

Aydın, S. (2013). Effects of fiber strength on fracture characteristics of normal and high strength concrete. Periodica Polytechnica Civil Engineering *57*, 191.

Balaguru, P., and Khajuria, A. (1996). Properties of Polymeric Fiber-Reinforced Concrete. Transportation Research Record *1532*, 27–35.

Codispoti, R. (2013). PhD Thesis in Materials and Structures Engineering of. 159.

Dahake, A.G., and Charkha, K.S. (2016). Effect of Steel Fibers on Strength of Concrete. *9*, 8.

Myers, Kang, Ramseyer, D., Thomas, Chris (2008). Early-Age Properties of Polymer Fiber-Reinforced Concrete. International Journal of Concrete Structures and Materials *2*, 9–14.

Singh, V.K., and Kumar, D. (2014). EFFECT OF FIBER ON PROPERTIES OF CONCRETE. Mathematical Sciences *3*, 9.

Song, P.., and Hwang, S. (2004). Mechanical properties of high-strength steel fiber-reinforced concrete. Construction and Building Materials *18*, 669–673.

Sukumar, A., and John, E. (2014). FIBER ADDITION AND ITS EFFECT ON CONCRETE STRENGTH. International Journal of Innovative Research in Advanced Engineering *1*, 6.

Velayutham, G., and Cheah, C.B. (2014). The Effects of Steel Fibre on the Mechanical Strength and Durability of Steel Fibre Reinforced High Strength Concrete (SFRHSC) Subjected to Normal and Hygrothermal Curing. MATEC Web of Conferences *10*, 02004.

Proc. 2nd International Conference on Structural Engineering Research (iCSER2019)
19-22 Jan 2019, Dhaka, Bangladesh
ISBN: 978-0-6482681-2-3

Investigating the Properties of Rice Husk Ash (RHA) as a Partial Replacement of Ordinary Portland Cement

Tanvir Hasan Shaon[1], Snahal Roy[1] and Ahsanul Kabir[2]

[1]Undergraduate Student, Dept. of Civil Engineering, Bangladesh University of Engineering and Technology, Dhaka, Bangladesh
[2]Professor, Dept. of Civil Engineering, Bangladesh University of Engineering and Technology, Dhaka, Bangladesh
Corresponding author's Email: tanvirhasanshaon@yahoo.com

Abstract

Cement is the most important binding material used in the construction of building, bridges and other infrastructures. However, in most of the third world countries it is not easily available to be used in rural areas, due to lack of local production and availability at low cost. In south Asian countries, where rice is produced in a large scale, rice husk ash (RHA) — which has high silica content— produced from the burning of rice husk, can be used as a potential material for partially replacing a portion of Portland cement in concrete. This study investigates the use of rice husk ash in small percentages as replacement of Portland cement in mortar, without optimization of the ash with control burning or grinding. The intention of the investigation was to study the effect on strength and durability of mortar made with RHA-cement with a very low tech crushing operation. Since grinding of the ash is a costly procedure, the investigation was done using completely unprocessed rice husk ash (average particle size 297µm) and rice husk ash, sieved through 100 mesh (average particle size 149µm). Compressive and other durability tests like water absorption and soundness test were performed for both the samples of rice husk ash. It was found that 5 and 10% replacement of sieved RHA-cement mortars showed better compressive strength at 28 days than both completely unprocessed RHA-cement mortar and control OPC cement mortar (no RHA). Moreover, other tests also indicated increased durability, due to RHA replacement by 5 and 10% as observed from absorption and soundness tests.

Keywords: Rice Husk Ash, Hydraulic Cement, Mortar Cubes, Compressive Strength, Durability Test

1. INTRODUCTION

Rice Husk Ash (RHA) produced from the effective burning of Rice Husk is widely available in major rice producing countries. The amount of silica in RHA is more than 80-88%. When rice husk is burnt at temperatures lower than 700^{O}C, rice husk ash with cellular microstructure is produced and contains high silica content in the form of noncrystalline or amorphous silica and can be used as supplementary cementitious materials (Mehta 1979). Rice Husk Ash is locally treated as waste material from the residue of burnt Rice Husk. Instead of discarding, the waste can be used in manufacturing process of composite cement production. Cost, pollution and emission of greenhouse gases will decrease in the process of cement production due to the partial replacement by Rice Husk Ash.

The silica in the ash of rice husk possesses pozzolanic characteristics (Yuxia et al. 2015) and (Swaminathen 2013). Different studies have been done on the mechanical, physical and chemical properties of optimized and processed rice husk ash. Alwash and Jawad (2007) used rice husk ash burnt at 500^{o}C and later on crushed in Los Angeles machine to produce finer particle. The compressive test of RHA-cement mortar resulted in increase of 7.5% strength of control Portland

cement mortar in 90 days due to 15% replacement of OPC by RHA. Pande and Makarande (2013) burnt RHA at around 700^{o}C and also followed similar procedure for grinding. Compressive test resulted in compressive strength gain of 11.8% of control Portland cement, for application of 27.5% of RHA. Ambas et al. (2015) used uncontrolled burning procedure and unprocessed RHA-cement and the resulting compressive strength of mortar showed gradual decrease of compressive strength in range of 71-17% due to application of 10 to 40% RHA. Brown (2012) compared the properties of unprocessed RHA and partially grounded RHA. The investigation showed improved mortar strength due to the presence of decreased RHA particle size by partial grounding.

2. CEMENTING MATERIALS

Different cementing materials used for the project are:

2.1 Cement

The cement used for the investigation was collected locally. The collected cement was "FRESH SUPER" brand ordinary Portland cement produced by Meghna Group of Industries conforming to Bangladesh Standard BDS EN 197-1: 2003.

2.2 Rice Husk Ash

The rice husk ash was collected from a local Rice Mill. The Husk was not burnt under control environment. It was greyish white in color. Two types of ash— i) completely unprocessed (not sieved) and ii) sieved through 100 size mesh were used in the research. The unprocessed ash had an average particle size of 297µm and the sieved RHA contained particle sizes less than 150µm. Following table shows the amount of different compounds in percent (by weight) for the selected RHA

Table 1. Chemical Composition of Used RHA

	Compound Composition, wt %	
Elements	**XRF Data**	**Normalized Data**
SiO_2	93.74	92.27
K_2O	2.86	2.82
P_2O_5	0.92	0.91
CaO	0.78	0.78
MgO	0.50	0.49
SO_3	0.46	0.46
Al_2O_3	0.15	0.15
Na_2O	0.07	0.07
Others	0.33	0.30
Loss On Ignition (LOI)	1.57	1.57

Loss on ignition value indicates the amount of unburnt carbon present in the RHA. The presence of unburnt (organic) carbon has several important effects on their concrete applications. The color of concrete and mortar having different quantity of unburnt carbon were found to change black or dark gray (Mohebbi et al. 2015).

3. PREPARATION OF MORTAR SAMPLES

Different percent of rice husk ash (by weight) of cement — (0, 5, 10, 15 and 20%) were mixed with the cement in dry condition. A ratio of 1:2.75 of cement to sand (standard Ottawa sand) was used in the composition of mortar. The samples with 0% RHA i.e. containing no RHA in them are referred as control OPC samples. All the tests were performed following relevant ASTM standard test procedures and are summarized in Table 2

Table 2. ASTM Standards Followed for Different Tests

Tests	ASTM Standards
Normal Consistency	ASTM C187-11
Initial/Final Setting Time	ASTM C191-82
Compressive Strength	ASTM C109 / C109M
Soundness (Mortar Bar Expansion)	ASTM C1038/C1038M

4. CURING

After completion of molding, the test specimens were placed in a moist closet at (25±1)^{o}C for 24 hours. After demolding, the specimens were immersed in saturated lime water until the time of testing.

5. RESULTS AND DISCUSSION

Result obtained from different physical tests performed on mortar samples are presented below

5.1 Compressive Strength Test

Compressive test was performed in stress controlled compressive test machine. Figure 1 presents the compressive strengths achieved in 3, 7 and 28 days due to application of unprocessed RHA as a partial replacement of the Portland cement. Figure 2 shows the compressive strengths reached in 3, 7 and 28 days due to the use of finer RHA (that passed through 100 mesh) with Portland cement.

From Figure 1, it is seen that the strengths of mortar due to application of increasing percent of unprocessed RHA appear to be decreasing. The reduction of mortar strength increases, with increase in percent replacement of OPC by unprocessed RHA. For 20% replacement, the strength reduction is nearly 50% compared to the control sample i.e. with OPC only. A similar result of gradual deterioration of strength on the application of unprocessed RHA was observed by (Ambas et al. 2015).

Figure 2, for the samples with relatively finer RHA particles, the strength reduction is at lower rate. An average deterioration of 0.6, 2.6, 6.6 and 12% in strength for 5, 10, 15 and 20% addition of rice husk ash respectively, with respect to OPC Cement can be observed. The strength reduction range has been reduced considerably compared to the unprocessed RHA. In the case of 5% application of finer RHA a rather improvement of compressive strength with respect to control OPC can be seen. The strength comparison in percent with respect to OPC for both the samples is shown in the Figure 3.
In the earlier stages, the curing water necessary for the reaction in mortar gets diverted to the cement for its hydration and strength gain properties. Once the cement gains considerable strength from the

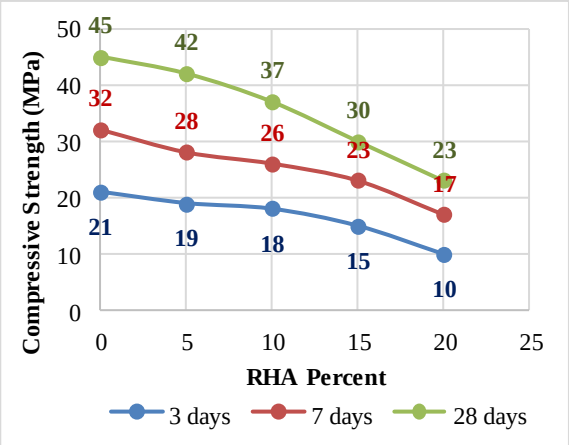

Figure 1. Compressive Strength using Unprocessed RHA

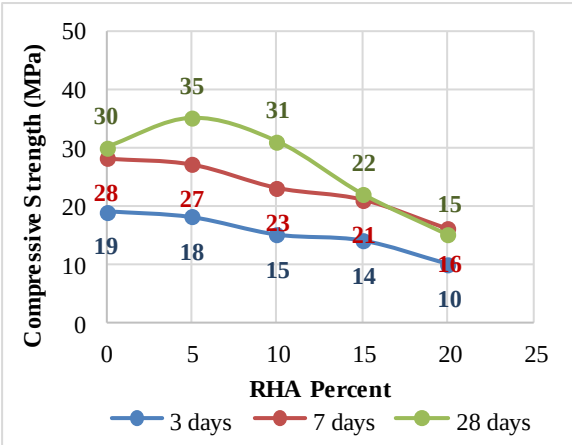

Figure 2. Compressive Strength using sieved RHA (passing 100 mesh)

early reaction and produce majority of calcium silicate hydrate (C-S-H) gel, the pozzolanic reaction takes place. So, further development in the strength will be slower than ordinary Portland cement. That explains the later strength development at 28 days. In other research works, (Alwash and Jawad 2007) and (Rashid et al. 2010) longer time of 90 days were required for attaining higher strength compared to OPC. It is to be noted that, the OPC used in the compressive strength test of unprocessed RHA was fresh (new) and just unwrapped, on the contrary the OPC used in the test of finer RHA (passed through 100 mesh) was 45 days old. Due to the effect of ageing overall deterioration of the strength can be observed. The strength loss for two OPC samples is about 10%. This behavior justifies the effect of ageing on the basis of a literature by (Chacko 2013), where it is stated that up to 20% of strength reduction can be expected as a result of 90 days of ageing of cement. The following Figure 4 shows the strength difference of control OPC due to ageing effect as observed in the study.

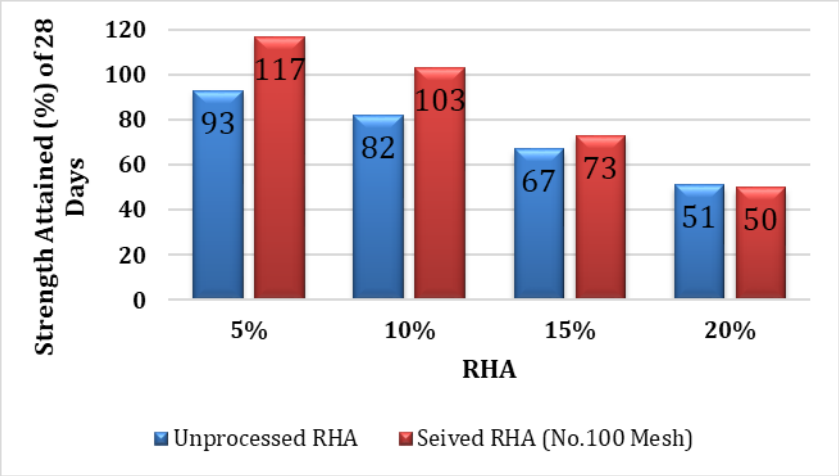

Figure 3. Compressive Strength (28 Days) comparison of Unprocessed and Sieved (No. 100 Mesh) RHA with Respect to OPC

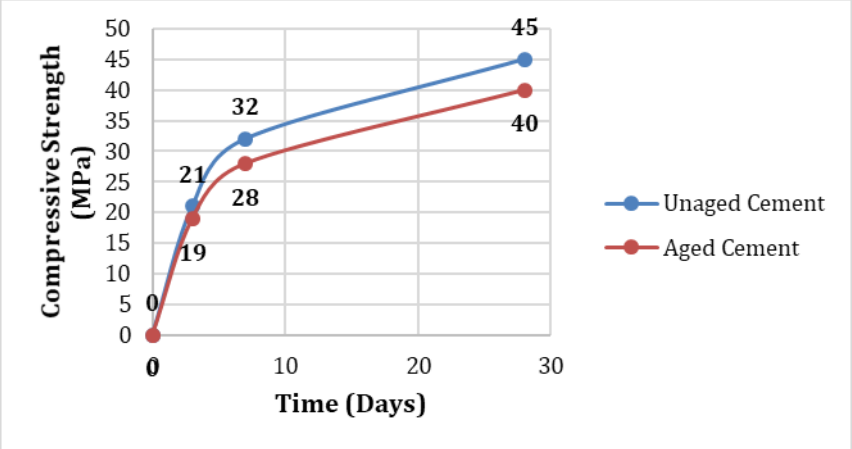

Figure 4. Difference of Strength in OPC for 45 Days Ageing Effect

5.2 Water Absorption Test

For testing of the water absorption of the mortar samples, after curing for 28 days, the surface water was wiped with cloth and the samples were then weighed and oven dried for 24 hours at (105±10)^{o}C. Later the dry specimens were weighed again for calculating amount of water absorbed by weight.

Figure 5 shows the amount of water absorption (by weight %) of mortar made with different percent of unprocessed and sieved RHA. The sieved Rice Husk Ash shows better effectiveness in reducing the absorption capacity of cement mortar. The durability of mortar has also increased significantly

absorbing less water than control Portland cement at 10% application of sieved rice husk ash. However, increased amount of RHA caused water absorption to increase.

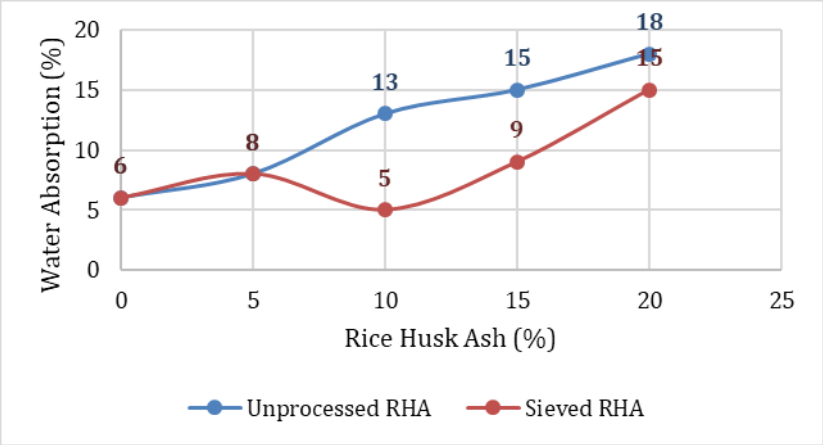

Figure 5. Water absorption (%) by mortar made with different Percent of Unprocessed and Sieved RHA

5.3 Soundness Test of Mortar

The expansion of mortar bar in percent due to the application of different percent of sieved RHA is shown in the Figure 6

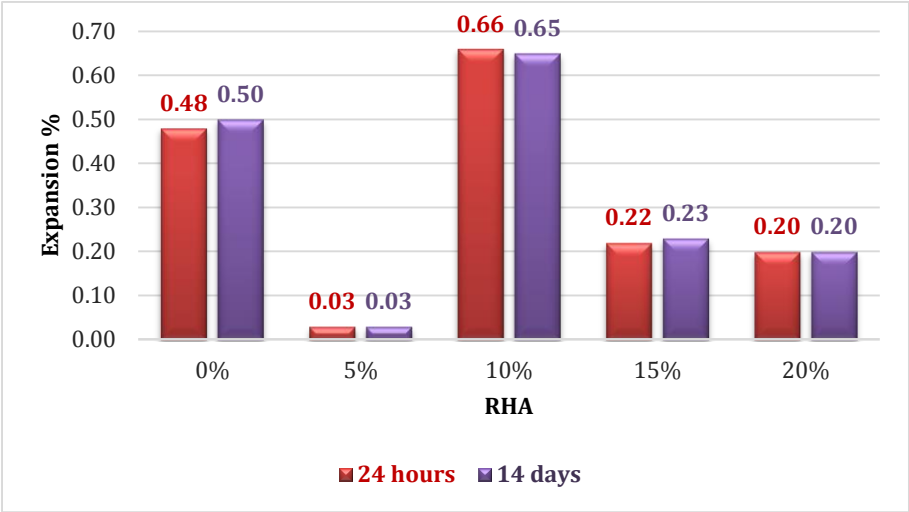

Figure 6. Expansion of Mortar (in % length) due to Application of Different Percent of Sieved RHA (24 Hours and 14 Days)

Difference in expansion of the mortar bars for 24 hours and 14 days is found to be insignificant. It is noticed that for application of 5% RHA, the overall expansion in the mortar bar decreased significantly, indicating the possible increase in durability of the mortar bar.

6. CONCLUSION

The finer (less than 150µm particle size) RHA-cement mortar exhibited better performance in all of the test aspects with respect to unprocessed (average particle size 297µm) raw rice husk ash. Increasing surface area by making particles finer exposes most of the silica to the pozzolanic reaction at later stage.

Use of unprocessed RHA shows steep drop in the value of compressive strength. Improvement of compressive strength is observed due to the application of 5 and 10% of sieved RHA at 28 days.

Strength gain of 17% and 3% were seen for 5% and 10% inclusion of RHA respectively, with respect to control cement mortar samples. An increase in the water absorption was observed due to increase in unprocessed RHA. However, the sample prepared with 10% sieved RHA had shown relatively less absorption. Mortar expansion test showed significant increase in durability due to application of 5% finer RHA compared to control OPC sample. It is suggested that about 8-10% OPC replacement by finer RHA (less than 150μm) can be implemented as partial replacement of cement without overall loss in strength and with improved durability. Further investigation of locally produced RHA is recommended before it can be used as an effective substitute to reduce cement production cost and ensure low cost availability.

ACKNOWLEDGEMENTS

Authors acknowledge the facility provided by the Civil Engineering Department of Bangladesh University of Engineering and Technology for carrying out this research work.

REFERENCE

Alwash, J. J. H. (2013). Use of rice husk ash in cement mortar, Journal of University of Babylon, 21(2), 582-590.

Ambas, D. T., Rosa, G. M. C. D., Esquejo, L. J. A., Gil, J. D., Magtalas, M. L., Rubinas, C. J. D., & Peñas, R. T. L. (2015, December). Effect of Rice Husk Ash as cement replacement in the compressive strength of hydraulic cement mortar cube. In Humanoid, Nanotechnology, Information Technology, Communication and Control, Environment and Management (HNICEM), 2015 International Conference on (pp. 1-3). IEEE.

Brown, D. K. (2012). Unprocessed rice husk ash as a partial replacement of cement for low-cost concrete (Doctoral dissertation, Massachusetts Institute of Technology).

Lovely, K. M., & Anniamma, C. (2013). A study on strength characteristics of ordinary portland cement due to storage. International Journal of Innovative Research in Science, Engineering and Technology, 3, 612-616.

Mehta, P. K. (1979). The chemistry and technology of cements rice husk ash made from rice husk ash. In Proc. UNIDO/Escap Workshop on Rice Husk Ash Cement, Peshawar, Pakistan, 1979.

Mohebbi, M., Rajabipour, F., & Scheetz, B. E. (2015, May). Reliability of loss on ignition (LOI) test for determining the unburned carbon content in fly ash. In World of Coal Ash Conference (WOCA), Nashville, TN, May (pp. 5-7).

Pande, A. M., & Makarande, S. G. Effect of Rice Husk Ash on Mortar.

Harunur Rashid, B. M., Ali, K., Tarif, M. C., & Ahmed, U. (2010). Long Term Effect of Rice Husk Ash on Strength of Mortar.

Swaminathen, A. N. (2013, July). Indian Rice Husk Ash—Improving the strength and durability of concrete: A review. In Current Trends in Engineering and Technology (ICCTET), 2013 International Conference on (pp. 16-17). IEEE.

Yuxia, Z., Xianli, W., Xiangxiu, H., Xiaoyu, C., & Rui, Z. (2014, October). Study on the Effects of Rice Husk Quantity and Particle Size on the Compressive Strength of Concrete Based on Experiment. In Intelligent Computation Technology and Automation (ICICTA), 2014 7th International Conference on (pp. 725-728). IEEE.

Proc. 2nd International Conference on Structural Engineering Research (iCSER2019)
19-22 Jan 2019, Dhaka, Bangladesh
ISBN: 978-0-6482681-2-3

Concrete Compressive Strength Characteristics for Different Proportions of Commonly used Sands in Bangladesh

U.S.M. Dilruba Mahmud[1], Nazia Zerin[1], Farhat Aziz Sheen[1] and SK Sekender Ali[2]

[1] Structural Safety Engineer, Stichting Bangladesh Accord Foundation, Dhaka, Bangladesh
[2] Professor, Department of Civil Engineering, Bangladesh University of Engineering and Technology
Corresponding author's E-mail: dilruba.1417@gmail.com

Abstract

Concrete, a proportionate mixture of cement, water and aggregates (and sometimes admixture), is the most widely used man-made construction material, comparatively economical, easy to prepare, offering continuity and solidity and fast to bind with other materials. An experimental study has been performed to see the effect of different mix proportions of coarse sand (Sylhet sand) and fine sand (local sand) on compressive strength of concrete using burnt clay bricks as coarse aggregate. Ordinary Portland cement was used as a binding agent for three different mix ratios (cement: fine aggregate: coarse aggregate), namely: 1:1:2, 1:1.5:3 and 1:2:4. In each batch, local sand was varied (0%, 25%, 50%, 75% and 100%) with Sylhet sand in concrete mix ratios. In this study, an attempt was made to investigate the effect of the variation of fine aggregates for two sets of brick aggregates (machine broken and manually broken) on compressive strength of concrete. A total of 180 concrete cylinders were cast using a specific water-to-cement ratio of 0.45 and tested under compression as per ASTM standards. The findings of this study revealed that for higher cement content (1:1:2) better compressive strength is attained using a higher percentage of local sand whereas for lower cement content (1:2:4) maximum compressive strength is attained by using an equal mix of local and fine sand. Moreover, for mix ratio 1:1.5:3, higher compressive strength is obtained with machine broken brick chips at 0~25% local sand.

Keywords: Compressive strength, mix ratio, concrete, fine & coarse aggregate.

1. INTRODUCTION

Concrete is obtained by mixing cement, water and aggregates (and sometimes admixture) in required proportions. Aggregates impart higher volume stability and better durability than hydrated cement paste in concrete and provide around 75 percent of the body of concrete [Gambhir, 1993]. The aggregates are usually derived from natural sources but in regions such as Bangladesh and parts of West Bengal, India where natural rock deposits are scarce, burnt-clay bricks are used as an alternative source of coarse aggregate. Here, construction of rigid pavement, small-to medium-span bridges and culverts and buildings up to six stories high using crushed brick (brick aggregate) concrete is quite common [Mansur et al.,1999]. In this study, burnt-clay bricks are used as an alternative source of coarse aggregate as its being cheaper than stone aggregate. And the use of brick aggregate instead of stone aggregate in various components of a building structure can result in a significant reduction of dead load on the column as well as the foundation [Rashid et al., 2008]. Brick chips can be produced in two ways i.e. by crushing in brick chips manufacturing machine or can be crushed manually with the help of a hammer. Aggregates are expected to be angular in shape and strength of concrete is greatly dependent on it. The more is the angularity of aggregates, the more will be the strength of concrete. Brick aggregates that are manually broken are expected to have more compressive strength than that of machine broken one. Fine aggregate (Sand) with comparatively larger particle size is

Sylhet sand (It is named so as it is found in Sylhet, Bangladesh) and sands with comparatively smaller particle size are local sand (found at the river bed). Local sands are available and cheap due to its easy availability in Bangladesh. Strength property of concrete using local sand is considered inferior to Sylhet sand. But a concrete mix requires a good combination of fine and coarse aggregate. This study will give a comprehensive idea about the strength variation due to the use of machine broken and manually broken brick aggregates with an adequate mixture of local and Sylhet sand. It will accommodate a better understanding of structural design planning for construction, especially for ready-mix industries.

A number of studies have been performed in previous years on the strength behavior of concrete using different composition. Those studies are performed using different water-cement ratio, different composition of coarse and fine aggregates etc. Some of the relevant studies are discussed here. Bogas and Gomes [2013] carried out a comprehensive experimental study on structural lightweight aggregate concrete involving more than 50 different compositions of strength classes ranging from LC20/22 to LC60/66 and density classes from D1.4 to D2.0. This study aims to characterize the behavior of structural lightweight aggregate concrete in compression to define the basis for a new simplified method to estimate the SLWAC strength, analyze possible failure modes, evaluated the biphasic model to estimate the strength. Ashraf and Noor [2011] showed a comparative analysis of various tools and methods of aggregate gradation through a number of trial mixes. As aggregate takes up 60% to 90% of the total volume of concrete, its properties are highly affected by physical properties of its aggregate such as aggregate size distribution. Another comparative analysis of the experimental results of the properties of fresh and hardened concrete with different replacement ratios of natural with recycled coarse aggregate is presented by some members of Faculty of Civil Engineering, University of Belgrade, Serbia. Their experiment showed that regardless of the replacement ratio, recycled aggregate concrete (RAC) had a satisfactory performance, which did not differ significantly from the performance of control concrete [Maleˇsev et al., n.d.]. On the other hand, Parashar and Parashar [2012] emphasized bricks as one of the longest lasting and strongest building materials used throughout history. The objective of this study is to observe the variation of compressive strength at different days (7 and 28 days) using different mix ratios, coarse aggregates (mainly brick chips-machine and manually broken) and different percentage of local sand and Sylhet sand.

2. METHODOLOGY

The effect of different mixing ratios of fine aggregate (Sylhet and local sand) on compressive strength of concrete using coarse aggregate (machine broken and manually broken brick aggregate) is investigated. Under ASTM standard specification, some basic properties of concrete ingredients have been investigated in this study.

2.1. Material properties

For this study, the properties of fine and coarse aggregates were determined by performing several tests following ASTM specifications namely C29 [C29/C29M-09, 2009] for determining specific gravity (oven dry and saturated surface dry condition), unit weight & absorption and C136 (ASTM C136/ C136M – 14 2014) is considered for sieve analysis. Los Angeles (L.A.) abrasion value of coarse aggregates is determined by the test method ASTM C131-01.

Cement is the bonding material of concrete which is actually a mixture of paste and aggregates. Through a chemical reaction called hydration, the paste hardens and gains strength to form the rock-like mass known as concrete. This study has been completed using only one type of Portland cement: Ordinary Portland Cement (OPC) of a brand. The basic chemical components of OPC are: Calcium Silica, Alumina Iron.

Table 1. Properties of Aggregates

Aggregate	Bulk Sp. Gr. (O-D Basis)	Bulk Sp. Gr. (SSD Basis)	Apparent Sp. Gr.	Absorption Capacity (%)	Unit weight (kg/ m3)	Fineness modulus	L. A. Abrasion Value
Local Sand	1.454	1.534	1.58	5.485	1387.71	1.28	---
Sylhet Sand	2.531	2.577	2.654	1.833	1534.25	2.63	---
Machine broken brick	1.83066	2.0796	2.4375	15.5995	1000.53	6.80	49.48%
Manually broken brick	1.68455	2.0016	2.4666	18.8213	904.56	7.12	23.44%

2.2. Preparation and mixing of concrete

Steps of mixing of concrete and preparation of concrete cylinders are briefly shown in the flowchart. Total 180 concrete cylinders were cast for two types of coarse aggregates i.e. 90 concrete cylinders for each, machine and manually broken brick aggregates. Among those 90 cylinders, three different mix ratios were adopted and for each mix ratio, 30 cylinders were cast for 7 and 28 days. Finally, 3 cylinders were prepared for each varying proportion (0%, 25%, 50%, 75%, 100%) of local and Sylhet sand. From the data of these three cylinders, average compressive strength of concrete was calculated.

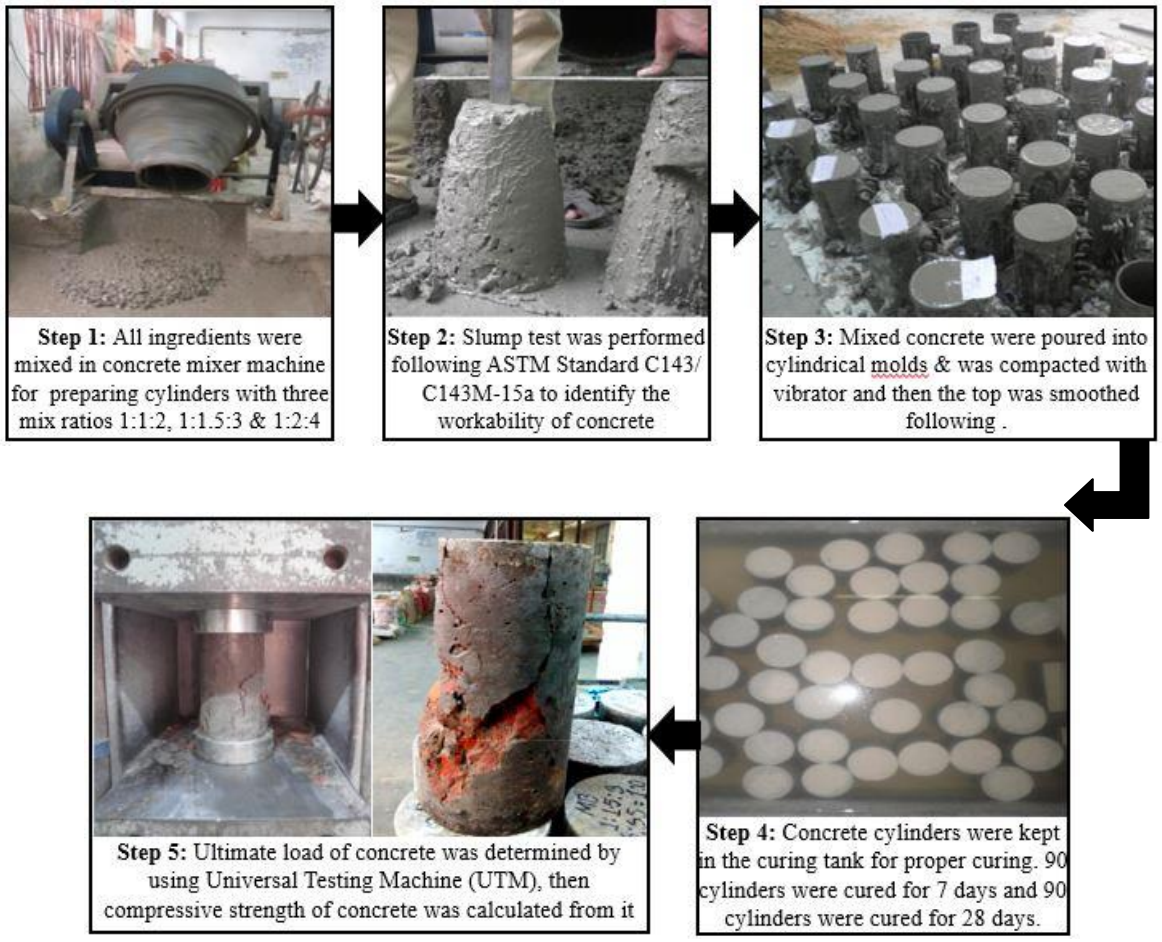

Figure 1. Steps of mixing of concrete and preparation of concrete cylinders

3. RESULTS AND DISCUSSION

For this study following the above-mentioned methodology, total 180 concrete cylinders were cast to evaluate the compressive strength in different parameters for 7 days and 28 days. Two types of coarse aggregates (machine and manually broken brick), three different mix ratios and varying proportions of local and Sylhet sand were used for preparing those cylinders. For each type, three concrete cylinders were tested from which average compressive strength was obtained. Table no.-2 representing the average compressive strength of concrete is given below:

Table 2. Properties of Aggregates

Percentage of Local Sand				0%	25%	50%	75%	100%
Mix Ratio 1:1:2	**Avg. Compressive Strength (MPa)**	7days	Machine Broken Brick	16.48	18.51	15.36	17.98	15.99
			Manual Broken Brick	11.64	13.86	8.71	11.62	8.64
		28days	Machine Broken Brick	21.01	20.43	18.70	30.38	26.39
			Manual Broken Brick	21.01	18.77	12.74	21.98	16.11
Mix Ratio 1:1.5:3	**Avg. Compressive Strength (MPa)**	7 days	Machine Broken Brick	20.59	20.38	15.61	15.61	17.22
			Manual Broken Brick	13.69	14.21	12.61	13.03	10.79
		28days	Machine Broken Brick	29.08	29.71	22.61	22.16	23.99
			Manual Broken Brick	15.19	15.73	12.74	15.52	15.15
Mix Ratio 1:2:4	**Avg. Compressive Strength (MPa)**	7days	Machine Broken Brick	16.14	15.60	17.22	14.01	20.39
			Manual Broken Brick	12.41	8.87	12.49	10.14	10.33
		28days	Machine Broken Brick	25.05	24.31	25.17	25.2	27.18
			Manual Broken Brick	13.84	15.65	15.78	14.17	15.86

Finally, average compressive strength of concrete is plotted against the percentage of local and Sylhet sand. Three different graphs were obtained for three different mix ratios each indicating the variation of compressive strength due to the variation of different parameters at 7 and 28 days.

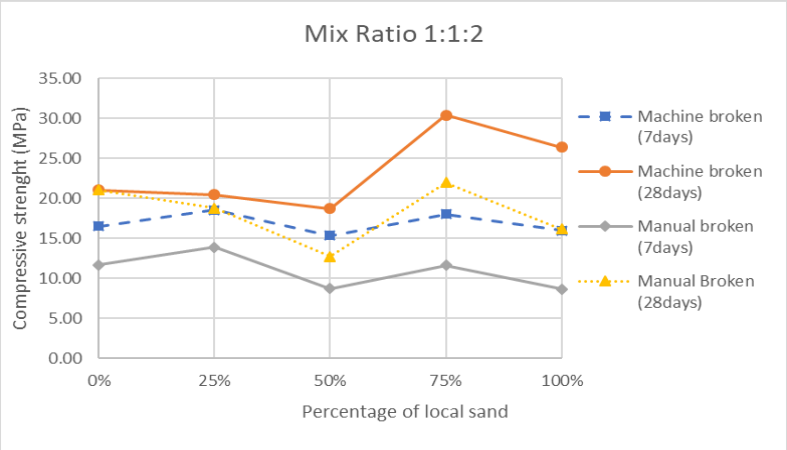

Figure 2. Compressive strength of concrete against different percentage of local sand for mix ratio 1:1:2 with respect to machine and manually broken brick chips for both 7 and 28 days

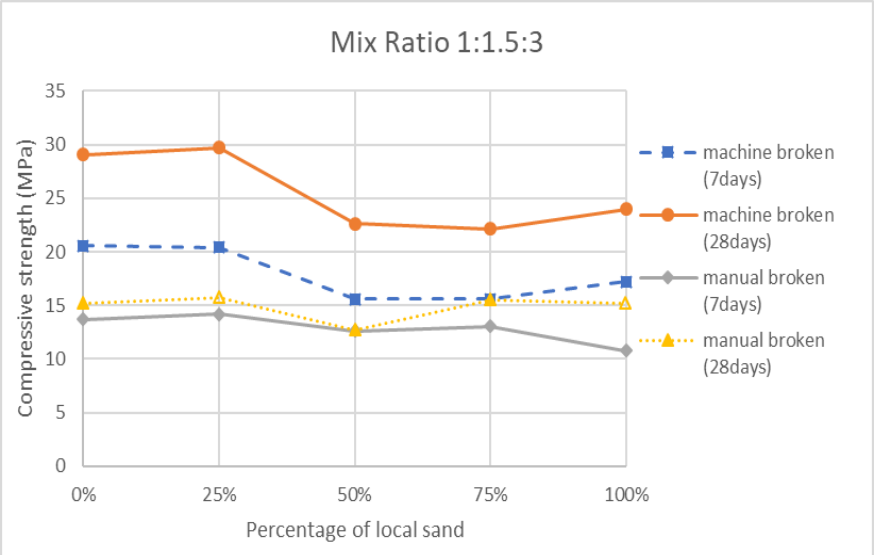

Figure 3. Compressive strength of concrete against different percentage of local sand for mix ratio 1:1.5:3 with respect to machine and manually broken brick chips for both 7 and 28 days

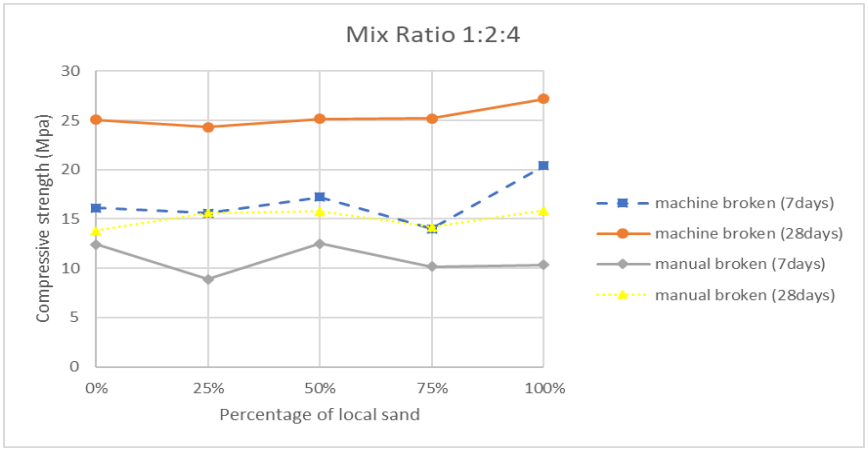

Figure 4. Compressive strength of concrete against different percentage of local sand for mix ratio 1:2:4 with respect to machine and manually broken brick chips for both 7 and 28 days

From Figures. 2 to 4, comparing the test results of 7 day and 28-day strength for different aggregates at different concrete mix ratios a number of inferences can be made. For greater cement content (1:1:2) maximum strength is apparently gained at 75% local sand content. The compressive strength of concrete is highest for 0% Sylhet sand content when cement content is minimum (1:2:4). Comparing all three graphs it is evident that the strength of the concrete is maximized at an optimum cement content (1:1.5:3); neither for maximum nor minimum cement content. The maximum strength of concrete for this optimum cement content (1:1.5:3) is obtained at 25% local sand content in the fine aggregate of concrete. Overall, from all three graphs showed that compressive strength of concrete using machine broken brick aggregate is greater than that of the manually broken brick aggregates.

4. CONCLUSION AND RECOMMENDATION

This study gives a general scenario of strength development characteristics of concrete made with locally available Ordinary Portland Cement (OPC) for different percentage of local and Sylhet sand proportions using two types of brick chips as coarse aggregates that are commonly used in Bangladesh. Material testing, concrete cylinder preparation and compressive strength tests (After 7 and 28 days) were performed as per ASTM standard specification. It can be expected that these

findings will be useful for the design and construction planning of concrete structures. From these studies following conclusions can be drawn:

- The experimental study reveals that the compressive strength of concrete is greatly influenced by the mix ratio of Sylhet and local sand for two types of brick aggregates (machine and manually broken).
- For higher cement content (Mix ratio 1:1:2) maximum strength has been attained at 75% local sand for both types of brick aggregates.
- For lower cement content (Mix ratio 1:2:4) maximum strength has been attained at 50% local sand content for machine broken brick aggregates with an exception of manually broken brick aggregates which attained maximum strength at 25% local sand content.
- For mix ratio 1:1.5:3, maximum strength has been attained at a lower percentage of local sand (0%~25%).

REFERENCES

Ashraf, W. B. and Noor, M. A. [2011]. Performance-Evaluation of Concrete Properties for Different Combined Aggregate Gradation Approaches, Twelfth East Asia-Pacific Conference on Structural Engineering and Construction- EASEC12, Vol. 14, Procedia Engineering, Hong Kong, p. 2627–2634.

Bogas, J. A. and Gomes, A. [2013]. Compressive behavior and failure modes of structural lightweight aggregate concrete, Characterization and strength prediction Materials Design (Formerly known as International Journal of Materials in Engineering Applications) 46: 832–841.

C29/C29M-09, A. S. [2009]. Standard Test Method for Bulk Density (Unit Weight) and Voids in Aggregate, ASTM International, West Conshohocken, PA.

C136/C136M−14, Standard Test Method for Sieve Analysis of Fine and Coarse Aggregates, ASTM International, West Conshohocken, PA.

C131 – 01, Standard Test Method for Resistance to Degradation of Small-Size Coarse Aggregate by Abrasion and Impact in the Los Angeles Machine, ASTM International, West Conshohocken, PA.

Gambhir, M. L. [1993]. Concrete Technology, 4th edition, Tata McGraw-Hill Publishing Company Limited, New Delhi.

Maleˇsev, M., Radonjanin, V. and Marinkovic, S. [n.d.]. Recycled Concrete as Aggregate for Structural Concrete Production, 2: 1204. Sustainability.

Mansur, M. A., Wee, T. H. and Cheran, L. S. [1999]. Crushed Bricks as Coarse Aggregate for Concrete, ACI Materials Journal 96(4): 478–484.

Neville, A. M. and Brooks, J. J. [2010]. Concrete Technology, 4th edition edn, Pearson Education Limited, Harlow, Essex.

Parashar, A. K. and Parashar, R. [2012]. Comparative Study of Compressive Strength of Bricks Made with Various Materials to Clay Bricks, International Journal of Scientific and Research Publications 2(7): 2250–3153.

Rashid, M. A., Hossain, T. and Islam, M. A. [2008]. Higher Strength Concrete Using Crushed Brick as Coarse Aggregate, Indian Concrete Journal.

Wilson, M. L. and Kosmatka, S. H. [2002]. Design and Control of Concrete Mixtures, 15th edn.

Proc. 2nd International Conference on Structural Engineering Research (iCSER2019)
19-22 Jan 2019, Dhaka, Bangladesh
ISBN: 978-0-6482681-2-3

Mechanical Properties of Polypropylene Fiber Reinforced Concrete with Brick Chips

G M Sadiqul Islam[1], Mohammad Imtiaz Uddin[2] and Mohammad Farid Hasan[2]

[1]Professor, Chittagong University of Engineering & Technology, Chattogram, Bangladesh.
[2]UG Student, Chittagong University of Engineering & Technology, Chattogram, Bangladesh.
Corresponding author's E-mail: gmsislam@cuet.ac.bd

Abstract

Concrete is the most widely used construction material throughout the globe. Both stone and brick chips are used as coarse aggregate. In south-east region of Asia brick chips are preferred due to availability, low cost and scarcity of stone. Having porous structure of brick chips the concrete produced with this is a form of light-weight aggregate concrete (LWAC). However, brick chips concrete pose higher brittleness and lower mechanical properties than conventional normal weight stone aggregate concrete. Therefore, improving these aspects of brick chips LWAC is of a great importance. This experimental investigation dealt with the improvement of mechanical properties (e.g. compressive strength, tensile strength, flexural strength and load-deflection behaviour of reinforced beam) of LWAC using 0%, 0.1%, 0.15% & 0.2% by weight polypropylene (PP) fiber. The experimental results show improvement in tensile strength, flexural strength and load-deflection behaviour of the polypropylene fiber reinforced concrete compared to the normal plain concrete. Compared to the control beam, maximum improvement of 20% in tensile strength and 27% in flexural strength was obtained with 0.20% fiber content. In compressive strength test, a slight increase (3.25%) was obtained with 0.1% fiber, but it decreased up to 15% with 0.2% fiber content. Load-deflection behaviour showed that, inclusion of 0.15% fiber increases the load carrying capacity of beam about 20% and increase the deflection about 60% with 0.20% fiber content than control beam. Results of the experiments therefore reveal that polypropylene fiber can be adopted for performance enhancement of brick chips LWAC.

Keywords: Polypropylene fiber, Brick chips, Concrete, flexure.

1. INTRODUCTION

Concrete with a wide range of properties can be obtained by appropriate adjustment of the proportions of the constituent materials. These properties depend on the proportions of the mix, the thoroughness with which the various constituents are intermixed and on the conditions of humidity and temperature in which the mix is maintained from the moment it is placed in the forms until it is fully hardened. The major limitation of concrete is the lack of ductility. The extensive use of brick chips (crushed burnt clay bricks) in a form of light weight coarse aggregate (LWA) in concrete in this south-east region of Asia has posed some additional concerns to ponder; as LWA concrete is expected to have higher brittleness and lower mechanical properties than normal weight concrete (NWC, Hassanpour el al., 2012). Therefore, improving this aspect of brick chips concrete has the prime focus of the Civil Engineers and researchers. Studies have been carried out by incorporating various types of fibers such as steel fiber, glass fiber, fiber polymer, natural fiber, and nanofiber within cement mortar and concrete. Concrete with these fibers could pose improved ductility, better flexural performance and energy absorption capacity (Parveen and Sharma, 2013). Among these, polymer fibers polypropylene (PP) has attracted the most attention among researchers because of its low cost, outstanding toughness, better dispersion and enhanced shrinkage cracking resistance in concrete. The PP fibers have low strength and modulus of elasticity compared to steel fibers (Hassanpour et al., 2012). Kakooei et al.

(2012) reported that PP fiber has the advantages of low specific weight and chemical resistance over the other reinforcing fibers. Akter and Islam (2015) reported insignificant improvement in compressive strength with PP fiber-reinforced concrete, however, improvement in flexural strength was found to be significant. In addition, Islam and Gupta (2016) also suggested that a proper quantity of PP fibers in concrete could be effective in improving the tensile performance of concrete. Flexural strength of plain LWA Concrete is lower than NWC of the same compressive strength. The inclusion of fiber in LWAC could increase its flexural strength. The reason is that, after cracking, the fibers are expected to carry load that the concrete sustained until cracking by the interfacial bond between the fibers and the matrix. Therefore, the fibers resist the propagation of cracks and do not fail suddenly results increase in the load carrying capacity. The increase in flexural strength due to the addition of fiber in LWAC is higher than in NWC (Hassanpour et al., 2012).

Fibers are generally found to provide greater effect on the flexural strength of FRC than on either the compressive or tensile strength, with increases of more than 100% were reported. Commonly, the flexural toughness is defined as the area under the complete load-deflection curve in flexure; this is sometimes referred to as the total energy to fracture. Alternatively, the toughness may be defined as the area under the load-deflection curve out to some particular deflection (Emon et al., 2016). The main aim of this study is to evaluate the mechanical properties i.e. compressive strength, split tensile strength, flexural strength, load-deflection behavior of PFRC beam of PFRC using brick chips. Comparison of the mechanical properties of PFRC with the control concrete is also made.

2. METHODOLOGY

2.1. Materials

Ordinary Portland Cement (OPC) of strength class 42.5 N was used. Two sizes of crushed brick chips was used as coarse aggregate viz. i) 20mm passing and 12.5mm retaining and ii) 12.5mm passing and 4.75mm retaining. Specific gravity, unit weight and absorption capacity of the 20 mm nominal size coarse aggregate was 2.43, 1150 kg/m^3 and 14.5% respectively. Coarse sand with FM of 2.63 was used as fine aggregate. Specific gravity and absorption capacity of the fine aggregate was 2.60, 0.7% respectively. Ø12mm reinforcing steel bars of 60 grade was used as tension reinforcement for RC beam while Ø10mm bar was used as compression and shear reinforcement. Retarding super plasticizer based on poly carboxylic ether (PCE) was used as an admixture. Polypropylene fibers content varied from 0.1% to 0.20% by weight of concrete. Length and diameter of these were 10±2 mm and 20±5 mm with aspect ratio of around 500. The natural white colour fibers had a density of 1.36-1.38 g/cm^3 with tensile strength ≥500 MPa.

2.2. Concrete Mix Proportions

Mix design was conducted as per American Concrete Institute (ACI 211.1-91). Trial mixtures were prepared to obtain a target mean strength of 35MPa at 28 days with target slump value of 75-100 mm. All the aggregates brought to the saturated surface dry (SSD) condition before mixing. The detailed mix proportions of constituent materials (SSD condition where applicable) to produce concretes, used for the study are presented in Table 1.

Table 1. Mix proportions of concrete used in experimental work

Mix	Water (kg/m^3)	Cement (kg/m^3)	Coarse aggregate (kg/m^3)	Fine aggregate (kg/m^3)	Admixture (kg/m^3)	Fiber (kg/m^3)
F1 (0%)	160	374	840	900	3.0	0.00
F2 (0.1%)	162	374	840	900	3.0	2.28
F3 (0.15%)	163	374	840	900	3.2	3.42
F4 (0.2%)	165	374	840	900	3.3	4.56

2.3. Concrete Mixing, Casting and Curing

Initially, coarse aggregate, fine aggregate & cement were dry mixed for a period of 2 minutes. Then fibers were dispersed in the mixture to achieve a uniform distribution throughout the concrete. Super plasticizer was mixed thoroughly with the mixing water and added to the mix. The workability of concrete was determined using slump cone. On achieving required slump value (75-100mm), the concrete was placed in the fabricated mould and compacted using a temping rod. A smooth steel trowel was used to finished fresh concrete. A total of ten plain concrete (9 for compression strength, split tensile strength & flexural strength test, 1 for load deflection of RC beam) and thirty fiber reinforced mixes were prepared. For compressive strength test 150mm × 300mm cylindrical mould, for split tensile test 150mm cube mould and for flexural strength test 100mm × 100mm × 500mm beam mould were used. The RC beam was designed assuming a third point loading of 65 kN each. The dimension of the beam was 1050mm × 200mm × 150mm. No variation was made in longitudinal main reinforcement and shear reinforcements as describe earlier. To avoid shear failure of beam 10mm diameter bar was also used as shear reinforcement at 100mm spacing throughout the beam. Only fiber content was varied from 0.1% to 0.2% on weight basis. Details of the beam are illustrated in Figure 1. All moulds were provided with base plates, having smooth support. The moulds were filled without leakage. For each type of mould compressive, split tensile and flexural test, twelve numbers of cylindrical, cube and beam (prism) sample; for load deflection of RC beam, four samples were prepared from four sets. After 24 hours, the specimens were removed from mould and immediately submerged in clean fresh water for 28 days curing.

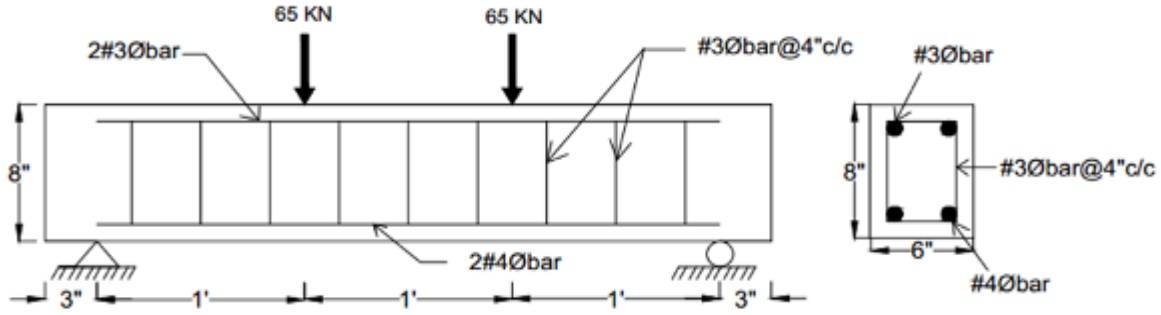

Figure 1. Longitudinal section & cross section of the test beam

2.4. Concrete Strength Testing

Measurement of compressive strength test was carried out according to the standard ASTM C39. After curing, place the cylindrical specimen in the compression testing machine. The load was applied gradually and ultimate load was noted for each specimen. Split tensile strength test was carried out according to the standard ASTM C496. The cube specimen was placed in the compression testing machine. Positioned the bearing strips, test cube & supplementary bearing bar by means of the aligning jig and center the jig so that supplementary bearing bar and center of the specimen are directly beneath the center of thrust of the cube bearing block. The load was applied gradually and ultimate load was noted for each specimen. Flexural strength test of prisms was carried out according to ASTM C293. The beam was cantered in the flexural testing machine with respect to the support blocks. The load applying block was brought in contact with the surface of the specimen at the centre by applying 3-6% of the estimated load and then loaded the specimen continuously at constant rate without shock until failure. Ultimate load was noted for each specimen.

The RC beams were placed in Universal Testing Machine (UTM) and subjected to third point loading. The beams were mounted on a platform and two steel blocks were placed at the bottom at the points of support so that the beam can deflect as a simply supported beam. Loads were applied at each of the third points. Deflection of the beam was monitored by deflection meter at the mid-point and end point of the beam (see Figure 1). Then load versus deflection data was noted continuously until ultimate loading which are the basis of analysis for flexural strength and ductility.

3. RESULT AND DISCUSSION

3.1. Compressive Strength Test

Concrete compressive strength data obtained as per ASTM C39 is given in Figure 2. With addition of up to 0.10% polypropylene fibers the compressive strength was found to be increased and then reduced up to 0.20%. The use of fibers increases the 28 days compressive strength of concrete about 3.25% for polypropylene fiber 0.10%. Compared with control concrete it was found that, 8-15% of 28 days compressive strength was reduced with addition of polypropylene fiber up to 0.20%. With stone chips Islam & Gupta (2016) found the 28 days compressive strength decreased from 2-10% with increase of polypropylene fiber and maximum reduction was 10% with addition of 0.3% fiber. This indicates that compressive strength loss with addition of higher fiber content was lower with brick chips.

Plain concrete – failure

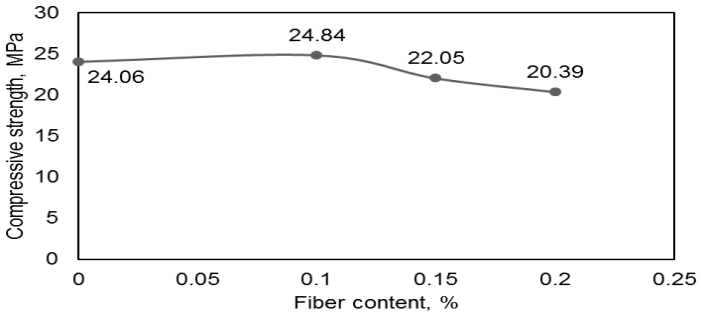

Fibrous concrete - failure

Figure 2. Relationship between compressive strength at 28 days & fiber content

The reduction of compressive strength is due to the interference of fiber with each other and thus the cohesiveness of concrete matrix is affected which produce internal voids in concrete mix and leads to decrease in the total density of mix and thereby decrease the compressive strength of the mix (Parveen and Sharma, 2013). The different compressive failure pattern of plain and fibrous concrete is shown in Figure 2. In case of plain concrete, the concrete is crushing completely while for fibrous concrete the concrete is free from complete crushing due to its crack bridging effect between the concrete matrixes.

3.2. Split Tensile Strength Test

Concrete graphical representation of tensile strength data are given in Figure 3. It was noted that split 28 days tensile strength of concrete was increased (12-20%) from control concrete) linearly with polypropylene fiber content (up to 0.15%). This increase is occurred for holding capacity of fibers which helps in preventing the splitting of concrete.

Plain concrete – failure

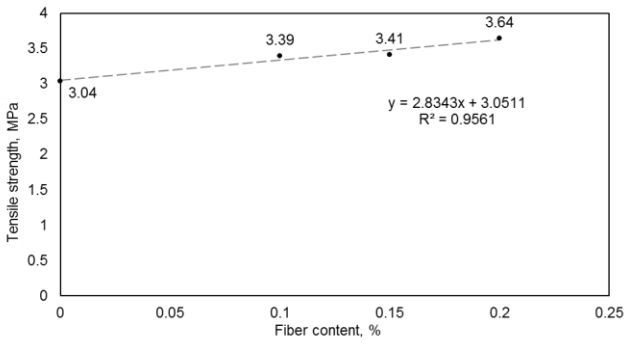

Figure 3. Relationship between split tensile strength at 28 days & fiber content

Fibrous concrete - failure

Islam and Gupta (2016) found that, the 28 days split tensile strength with stone chips concrete increased 1-39% with up to 0.25% fiber content. With 0.3% fiber it was decreased approximately 11%. It was found that beyond 0.10% fiber content, the split tensile strength started to decrease although the strength was higher than control concrete up to 0.25% fiber content. But using brick chips, it was found that tensile strength linearly increased with addition of fiber content than control concrete. The tensile pattern of plain concrete & fibrous concrete is shown in Figure 11. It was noted that the failure pattern is different. In case of plain concrete, the concrete is splitting in two parts and the failure pattern is completely splitting type but in the case of fibrous concrete, the concrete is free from complete splitting due to holding capacity of fiber.

3.3. Flexural Strength Test (with Prism)

Flexural strength test results are given in Figure 4. With addition of polypropylene fiber the 28 days flexural strength of beam was found to be increased linearly 15-27%. According to Akter & Islam, (2015) flexural strength increased 9-21% with addition of up to 0.2% polypropylene fiber in stone chips concrete. As the fibers in the matrix carried some additional load, the flexural strength increased with the increase in percentage of polypropylene fiber (Parveen and Sharma, 2013). Moreover, the failure pattern of control and fibrous concrete in flexural strength test was different; more ductility was achieved with addition of fibers as shown in the bottom of Figure 4. After cracking the matrix, the load was transferred to the fibers at the crack surfaces preventing brittle failure of the composite.

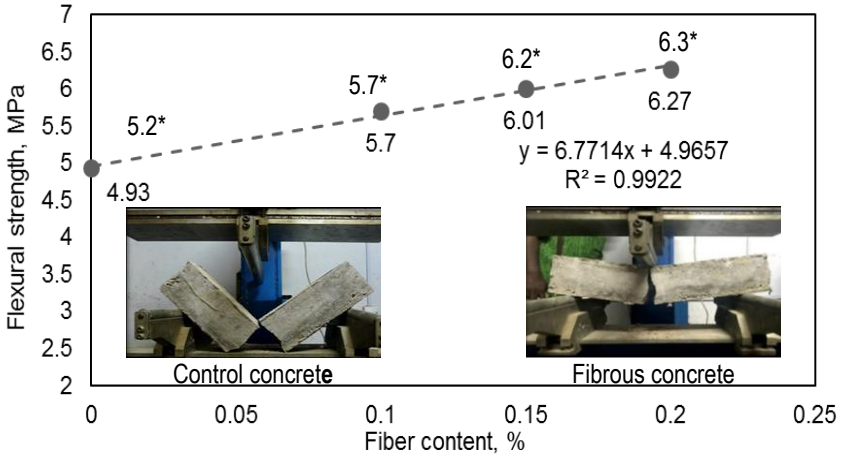

Figure 4. Relationship between flexural strength and fiber content (*Akter and Khatun, 2015)

3.4. Load-Deflection Behaviour of RC Beam

Four beam specimens with different mix proportion containing 0%, 0.1%. 0.15% and 0.2% fiber were prepared. The load-deflection curve under third point loading is given in Figure 5. The control beam was failed at an ultimate load of 138 kN at which the deflection was measured as 4.39 mm. The ultimate failure load and corresponding deflection for 0.1% fiber beam was 148 kN and 4.89mm which is 7% and 11% higher than control beam, respectively. The deflection for control beam and 0.1% fiber beam was almost linear up to 100 kN load. Beyond that, the 0.1% fiber beam is deflected less than the control beam at similar loads. The 0.15% and 0.2% fiber beams failed at an ultimate load of 166 kN and 163 kN with 6.74mm and 7.02 mm midpoint deflection, respectively. The 0.15% and 0.20% fiber beam sustained 20% and 18% higher ultimate load and gave 50% and 60% more deflection than the control beam, respectively. From above results, it is concluded that, the addition of polypropylene fiber in reinforced LWC beams increase its ultimate load capacity and deflection. As with the 0.1% fiber beam the load-deflection was similar for 0.15% and 0.2% beams, however, the fiber beams deflected much than the control at ultimate failure. Jadhav and Koli (2013) reported increase in ultimate load and deflection by 45% and 88% with inclusion of 1.25% hybrid fiber.

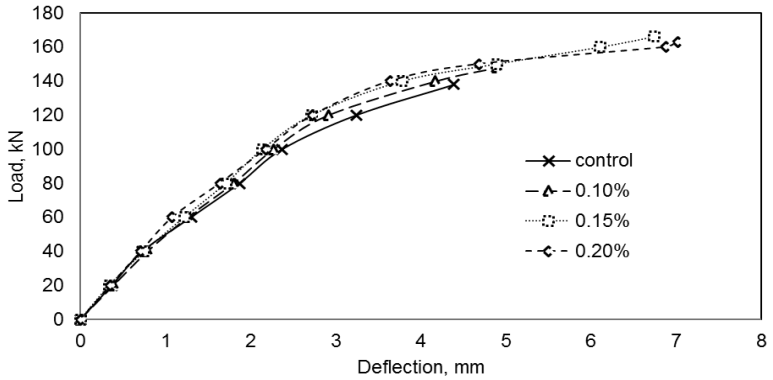

Figure 5. Load-deflection curve of RC beams under third point loading

4. CONCLUSION

- Compressive strength was slightly (3.5%) increased with inclusion of 0.1% fiber; beyond that it decreases. The maximum reduction of compressive strength (15%) was noted with 0.2% fiber.
- Split tensile strength was increased linearly (12-20%) with fiber content. Previous study with stone chips found 17-40% increase in split tensile strength up to 0.2% fiber, however, 0.1% fiber content sample gave maximum strength. The rough surface of brick chips may gave better interlocking and thereby higher tensile strength.
- Flexural strength also increased linearly (15-27%) with the addition of fiber. Flexural test of RC beam showed that PP fiber inclusion increased the ultimate load (7-20%) and deflection (11-60%). Maximum load capacity and deflection was found for 0.15% and 0.20% fiber.
- Opportunities for future researches are numerous. Future research prospects with brick chips and PP fiber with different aspect ratio, other fibers such as steel, glass, asbestos fiber and hybrid fiber concretes can be used to improve the quality of brick chips fiber reinforced concrete.

ACKNOWLEDGMENTS

The authors gratefully acknowledge the laboratory support from Chittagong University of Engineering & Technology. Thanks also extended to industrial partner BASF Bangladesh for material support.

REFERENCES

Akter B, Islam GMS (2015). Mechanical & shrinkage properties of polypropylene fiber concrete. IICSD-2015, Department of Civil Engineering, DUET, Bangladesh (ID: CBM-004).

Emon, MAB, Manzur T, Yazdani N (2016). Improving performance of light weight concrete with brick chips using low cost steel wire fiber. Construction and Building Materials, 106, 575-583.

Hassanpour M, Shafigh P, Mahmud HB (2012). Lightweight aggregate concrete fiber reinforcement – A review. Construction and Building Materials, 37, 452–461.

Islam GMS, Gupta SD (2016). Evaluating plastic shrinkage and permeability of polypropylene fiber reinforced concrete. International Journal of Sustainable Built Environment, 5, 345–354.

Jadhav HS Koli MD (2013). Flexural behavior of hybrid fiber reinforced concrete beams. International Journal of Structural and Civil Engineering Research, 2(3).

Kakooei S, Akil HM, Jamshidi M, Rouhi J (2012). The effects of polypropylene fibers on the properties of reinforced concrete structures. Constr. & Build. Mater., 27, 73-77.

Parveen J, Sharma A (2013). Structural behavior of fibrous concrete using polypropylene fibers. International Journal of Modern Engineering Research, 3(3), 1279-1282, ISSN: 2249-6645.

Sivakumar A, Santhanam M (2007). A quantitative study on the plastic shrinkage cracking in high strength hybrid fibre reinforced concrete. Cement & Concrete Composites, 29, 575–581.

Proc. 2nd International Conference on Structural Engineering Research (iCSER2019)
19-22 Jan 2019, Dhaka, Bangladesh
ISBN: 978-0-6482681-2-3

The Impact of Recycled Pistachio Shells on the Fresh and Hardened Properties of Concrete

Mohammad S Islam[1], Syed Jamal Uddin Ahmed[2], Khaled Alshehri[3] and Mohammad Jobaer Uddin[4]

[1]Assistant Professor, University of Tabuk, Tabuk, Saudi Arabia
[2]Assistant Professor, University of Asia Pacific, Dhaka, Bangladesh
[3]Teaching Assistant, Bisha University, Bisha, Saudi Arabia
[4]Junior consultant, Housing and Building Research Institute, Dhaka, Bangladesh
Corresponding author's E-mail: jshaon@gmail.com

Abstract

Most agricultural (agro) waste materials are not being recycled and reused, thus they end up in landfills and pollute the environment. The present study deals with the use of pistachio shells, an agro waste, as a partial replacement of coarse aggregate in concrete for the purpose of reduction of the natural resource exploitation, waste landfill, and costs. The objective of this study was to investigate the effect of pistachio shells (PS) as a coarse aggregate replacement by volume on the fresh and hardened properties of concrete. Four volume fractions of 0, 1, 2, and 4% of pistachio shells were used to prepare concrete cylinders, and they were tested for the compressive and split tensile strengths at 28 days. The results showed that both the compressive strength and tensile strength of concrete decreased with an increase of the PS. Furthermore, the influence of PS had an adverse effect on the slump of fresh concrete. However, the optimum PS dosage of 1% can be used in concrete with a minor scarifying of the fresh and hardened properties of concrete.

Keywords: Pistachio shells, agricultural (agro) waste materials, concrete slump, compressive strength, tensile strength

1. INTRODUCTION

Concrete, a mixture of cement, water and aggregates, is the most widely construction material in the World. The high demand of concrete is due to the increased residential, commercial and public facilities, which consume a huge amount of natural resources (PCA, 2015). In order to reduce the natural resources and modify the concrete properties, various types of materials have been used in concrete (Prusty et al., 2017, Islam 2018, Islam and Ahmed, 2018, Islam et al., 2018). The use of various agricultural wastes in concrete has become a new trend of research (Prusty et al., 2015). The agricultural (agro) wastes are usually disposed and landfilled thus reducing the lands for the proper uses. In order to minimize the disposal and environmental related problems, the use of agricultural wastes in concrete industries has become one of the top most important factors to reduce the virgin materials and increase land uses (Parvathamma, 2014). Vignesh and Lemessa (2017) stated that agro wastes can be used in concrete to reduce the natural resource exploitation and associated costs, minimization of waste landfill, and modifying the concrete properties.

Over the past decade, a number of agro wastes, such as groundnut shell, periwinkle shell, oyster shell, palm kernel shell, cork, rice husk ash, sawdust, and tobacco wastes, have been used in concrete industries (Prusty et al. 2017). They have been recycled and reused successfully in concrete as replacement alternatives for cement, aggregate, and reinforcing materials. Pistachio nuts are very rich in fiber and healthy fats, antioxidants, magnesium, carotenoids and phenolic compounds, all of which

are beneficial for blood sugar control. The average length, width and thickness of grains ranged from 9.85 to 10.52, 9.15 to 9.63 and 4.94 to 5.51mm. The potential use of pistachio shells, which are solid and strong, for producing nonstructural elements can reduces concrete weight and can produce environmental friendly concrete (Srivastava et al., 2014, Polyphenols, 2016). The size of the shells is very suitable for that of coarse aggregates in concrete (Polyphenols, 2016). Moreover, the pistachio shells is also shown to be stronger than some coarse aggregate groups (Shafigh et al, 2014). Kanagalakshmi et al. (2015) stated that the main advantages of the use of pistachio shells in concrete are to reduce the cost of extraction and ng and breaking aggregates, concrete weight, environmental pollution, and also to improve concrete properties.

2. RESEARCH SIGNIFICANCE

The use of agricultural waste materials in concrete industries to reduce the natural resources has become a new trend due to the high demand of rapid urbanization and disposal problems. Hence, many agricultural waste materials are being used in concrete as a replacement alternative for coarse aggregate, fine aggregate, and even reinforcing materials. The existing studies were limited to the use of groundnut shell, periwinkle shell, oyster shell, palm kernel shell, cork, rice husk ash, sawdust, and tobacco wastes in concrete, and they lacked of the utilization of pistachios shells in concrete. This experimental study evaluates the influence of four rates (0, 1, 2 and 4%) of recycled pistachio shells on the slump, unit weight, ultimate compressive strength and tensile strength of concrete. The findings of the study would surely be an addition to the research on the use of agricultural waste materials in concrete industries.

3. EXPERIMENTAL PROGRAMS

The locally available coarse aggregate, fine aggregate and Saudi produced Portland cement were used in this study. The specific gravity, absorption and moisture content of coarse and fine aggregates were shown to be 2.83, 1.01%, 1.50%, and 2.65, 1.46% and 0.10%, respectively. The pistachio nuts, a member of the cashew family, were bought from the local market, and after consuming their seeds, the pistachio shells were collected. Figure 1 shows the pistachio nuts, seeds and pistachio seeds.

Water-to-cement ratio of 0.50 and the design concrete strength of 30N/mm^2 (3,000 psi) at 28 days were kept constant for all mixtures. Four levels (0, 1, 2, and 4%) of coarse aggregate were replaced by pistachio shell to prepare concrete mixing. For each mixture, the value of slump were mix replacement were as per ASTM, and concrete specimens were prepared. After demolding, the 1-day unit of concrete cylinders were measured followed by water cured at room temperature. The cylindrical specimens were then tested for the ultimate compressive strength at 7, and 28 days.

Figure 1. Pistachio nuts, seeds and shells

4. RESULTS AND DISCUSSIONS

4. 1 Slump of Fresh Concrete

Figure 2 shows the slump of fresh concrete as related to the pistachio shell content. As can be shown, it is clearly revealed that the slump value decreased rapidly with increasing the pistachio shell. When coarse aggregate was replaced by 4% with pistachio shell, the slump value decreased to 0.64cm. This indicates that the fresh concrete nearly lost the fluidity to place in construction.

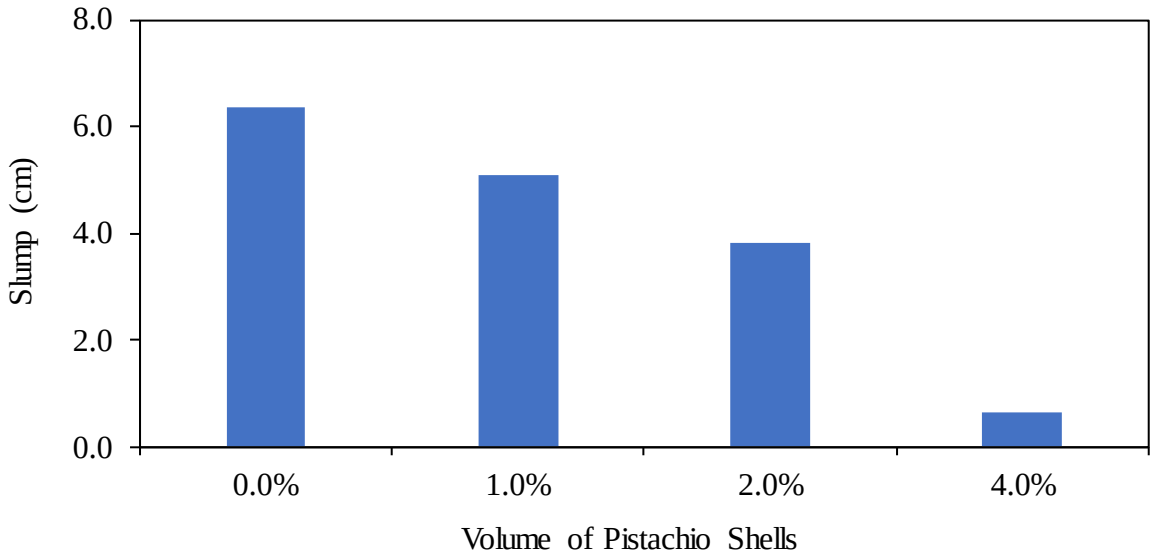

Figure 2. Relationship between pistachio shell and slump of fresh concrete

4.2 Unit weight of concrete

Figure 3 shows the unit of 1-day demolded concrete as related to the volume of pistachio shell added to concrete mixture. As can be shown, the pistachio shell had an insignificant influence on the unit weight of concrete. A nearly 0.6, 1.04 and 2.43% reduction of unit weight was observed when the coarse aggregate was replaced by 1,2 and 4% pistachio shell, respectively.

4.3 Ultimate Compressive Strength of Concrete

Figure 4 represents the ultimate compressive strength of concrete at 7 and 28 days over the pistachio shell replacements. As can be illustrated, the strength increased with an increase in curing age, and decreased with an addition of pistachio shell in concrete. The compressive strength at 28 days increased by nearly 1.35 times of the ultimate compressive strength at the curing age of 7 days. When the coarse aggregate was replaced by 1, 2 and 4% of pistachio shells, the compressive strength decreased by 25%, 36%, and 58% as compared to the ultimate compressive strength of concrete.

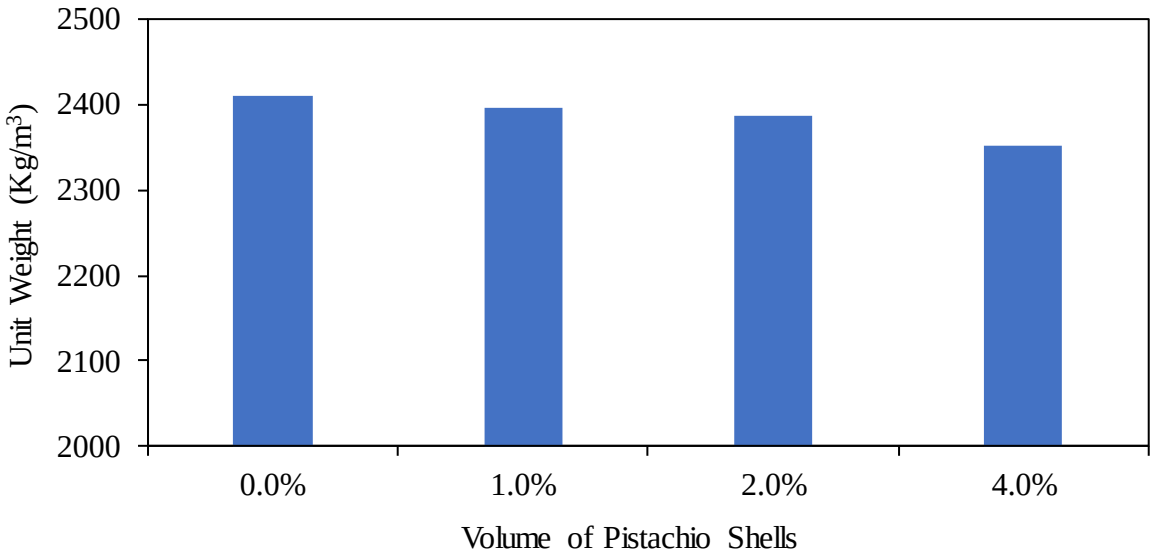

Figure 3. Relationship between pistachio shell and the unit weight of concrete

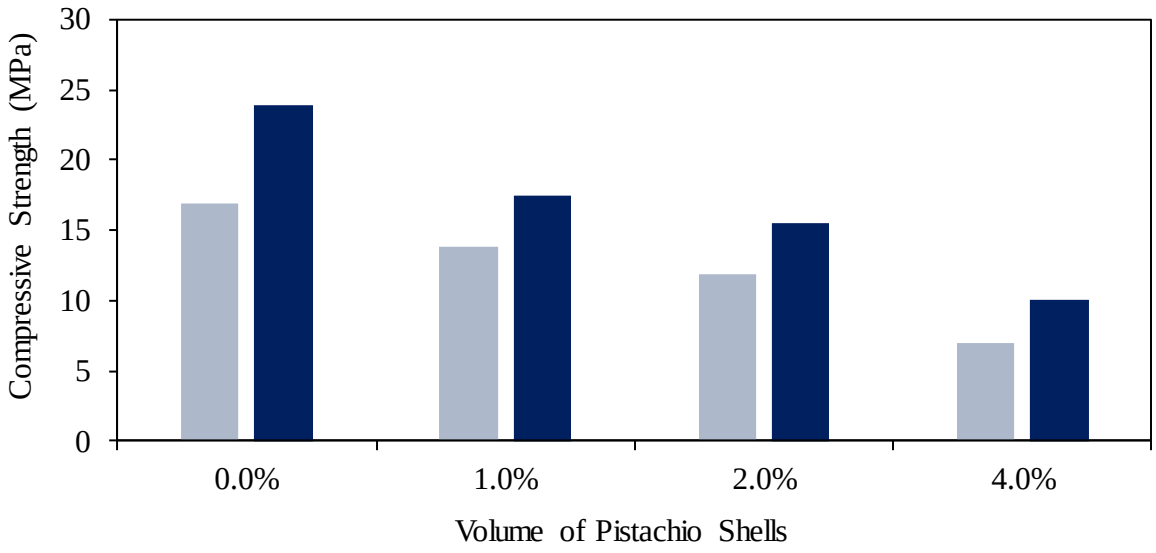

Figure 4. Relationship between the volume of pistachio shell and the compressive strength of concrete

4.4 Split tensile strength

The calculated split tensile strength of concrete cylinders containing various dosages of pistachio shells was measured at age of 28 days, and the results are shown in Figure 5. As can be shown, the tensile strength of concrete showed a decrease trend with the amount of pistachio added to concrete, and similar finding was also observed for the compressive strength of pistachio concrete cylinders, as depicted in Fig. 2.

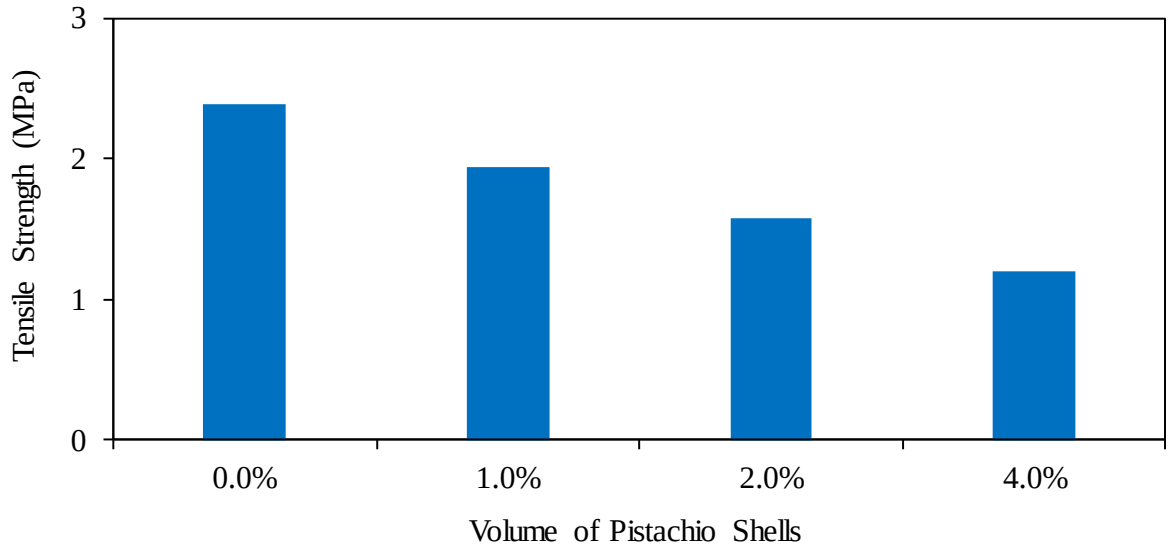

Figure 7. Relationship between the volume of pistachio shell and the compressive strength of concrete

5. CONCLUSIONS

Based on the results of this study, the following conclusions can be drawn.

1. The slump of fresh concrete decreased rapidly with an increase of pistachio shell replacement. When a higher dosage (4%) of pistachio shells was used, the concrete lost its fluidity and can merely utilized in construction purposes.
2. The addition of pistachio shells showed an insignificant influence on the unit weight of concrete.
3. The ultimate compressive strength and split tensile strength decreased with an increase of pistachio shells in concrete.
4. The natural coarse aggregate can be replaced by pistachio shells at a rate of 1.0% to produce a sustainable built environment with the minor scarifying of the fresh and hardened concrete properties.
5. The impact of the higher dosages (2, 4 and 6%) of pistachio shells and the use of various secondary cementitious materials on the concrete properties is highly recommended for future studies.

ACKNOWLEDGMENTS

The authors would like to acknowledge the Faculty of Engineering, University of Tabuk, for providing the financial supports throughout the study. The authors also would like to recognize Engr. Ahmed Morad and Engr. Abdullah Alwated for preparing the materials, mixing concrete, casting the cylinders and performing the tests.

REFERENCES

Islam MS, Uddin MJ, Alshehri K (2018) Plastic waste and carbon footprint generation due to the consumption of bottled waters in Saudi Arabia, Research and Development in Materials Science, 5(1), pp. 1-3.

Islam MS (2018) Simplified Shear Strength Prediction Models for SFRC Beams using Genetic Algorithm,Proceedings of the Institution of Civil Engineering (ICE)-Construction Materials, https://doi.org/10.1680/jcoma.16.00073.

Islam MS and Ahmed SJU (2018) Influence of jute fiber on concrete properties, Journal of Construction and Building Materials, 189(10), pp. 768-776.

Kanagalakshmi A, Velu S, Tamilnathan (2015) Study of peanut shell beams on shear and flexure, International Conference on Engineering Trends and Science and Humanities, pp. 32-45.

Parvathamma GI (2014) An analytical study on problems and policies of solid waste management, India: special reference to Bangalore city, Journal of Environmental Science and Texicology and Food Technology, 8, pp. 6–15.

PCA (Portland Cement Association) (2015) Proportioning concrete mixtures and mixing and placing concrete, Portland Cement Association, Skokie, IL, USA.

Prusty J, Sanjaya KP, Basarkar SS (2016) Concrete using Agro-waste as Fine Aggregate for Sustainable Built Environment-A Review, International Journal of Sustainable Built Environment, 5(2), pp. 484516, DOI:0.1016/j.ijsbe.2016.06.003.

Shafigh P, Mahmuda HB, Zargar M (2014) Agricultural wastes as aggregate in concrete mixture: a review, Journal of Construction and Building Material, 53, pp. 110-117.

Srivastava R, Krishna Vand Sonkar I (2014) Characterization and management of municipal solid waste in India: A review, International Journal of Current Research and Academic Review, 2(8), pp. 10–16.

Vignesh K, Lemessa K (2017) Behavior of concrete with agro and industry waste as a replacement for constitutive materials, American Journal of Engineering Research, 6 (3), pp. 79-85.

Proc. 2nd International Conference on Structural Engineering Research (iCSER2019)
19-22 Jan 2019, Dhaka, Bangladesh
ISBN: 978-0-6482681-2-3

Effect of Recycled PET on the Fresh and Hardened Properties of Concrete

Mohammad Jobaer Uddin[1], Mohammad S Islam[2], Md. Nahidul Islam[3], Mohammad Sohan Hossain[3], Md. Aminul Islam[3] and Ariful Hasnat[4]

[1]Graduate Teaching Assistant University of Asia Pacific, Dhaka, Bangladesh
[2]Assistant Professor, University of Tabuk, Tabuk, Saudi Arabia
[3]Graduate Student, University of Asia Pacific, Dhaka, Bangladesh
[4]Assistant Professor, University of Asia Pacific, Dhaka, Bangladesh
Corresponding author's E-mail: jshaon@gmail.com

Abstract

Polyethylene Terephthalate (PET) is widely used for packaging foods and beverages in all over the World. The ever-rising growth in the application of PET raises a great concern on potential human health and environmental hazards. In order to reduce its impact, researchers have recently conducted studies on the possible use of used PET in many engineering and non-engineering applications. The main objective of this study was to evaluate the influence of PET as coarse aggregate replacement on the fresh and hardened properties of concrete. Concrete cylinders were prepared from 0.0, 2.0, 4.0 and 8.0% of PET as a partial replacement of coarse aggregate quarried from Bholagonj, Bangladesh. The cylinder specimens were tested for compressive strength at 7 and 28; and splitting tensile strength at 28 days. The results showed that the addition of PET to the concrete has increased the slump, whereas a loss in compressive strength and splitting tensile strength were recorded.

Keywords: Polyethylene Terephthalate, Coarse Aggregate Replacement, Fresh Properties and Hardened Properties.

1. INTRODUCTION

Polyethylene Terephthalate, commonly known as PETE or PET, is widely used in textile and food industries in all over the World. Two PET grades are mainly dominated the global industries, i.e. fiber grade PET and bottle grade PET. Since 1980, the bottle grade PET has been traditionally used as storing vessel for beverage. The consumption of PET has been substantially increased over the years due to its lightweight and easiness of handling and storage (Al-Sabagh et al., 2016). Most recently, Laville and Taylor (2017) reported that about 488 billion units of PET bottles were consumed in 2016, which was nearly 200% more than a decade ago. The PET consumption will increase by at least 20% by 2021 (Laville and Taylor, 2017). Though PET is indeed one of the most extensively recycled polymeric materials, less than half of the bottles consumed in 2016 were collected for recycling, of which only about 7% were turned into new bottles (Laville and Taylor, 2017). As such, most of bottles were ended up in landfill or the ocean. Since, PET is considered a non-biodegradable material, it not only remains in nature for a long term, but also it eventually contributes to potential food toxicity and global warming (Islam et al., 2018). To avoid the consequences, researcher from all branch are separately looking forward to increase recycling of PET. Among this one form of recycling process is to encage such waste in concrete (Mohammed, 2017). This recycled management process is comparatively more preferred since it enables recycling of waste in concrete without degradation and more importantly helps to reduce the use of virgin construction materials (Gu and Ozbakkaloglu, 2016). In regards, it can reduce the waste on dump site. PET possesses a high molecular weight, which is an essential criterion for providing good mechanical properties, such as stiffness, toughness and creep resistance, and sufficient flexibility to resist bursting and breaking under pressure (Al-Sabagh et al., 2016). These properties have motivated researcher to use PET in cement concrete to

eliminate brittleness of unreinforced concrete. This study has performed with an idea to encase the plastic waste into concrete as coarse aggregate replacement to reduce both the pressure of dumping plastic waste and the mining of natural coarse aggregate.

2. RESEARCH PROGRAM

2.1. Cement

Blended hydraulic Portland composite cement having the specific gravity of 2.9 and the 28-day compressive strength of 41.3MPa was used in this study.

2.2. Aggregates

Bholagonj stone and Sylhet sand, locally available materials, were used respectively as coarse aggregate (CA) and fine aggregate (FA) in the study. The specific gravity of the coarse aggregate and fine aggregate are respectively 2.44 and 2.84, and unit weight are 1583.51 kg/m3 and 1571.45 kg/m3.

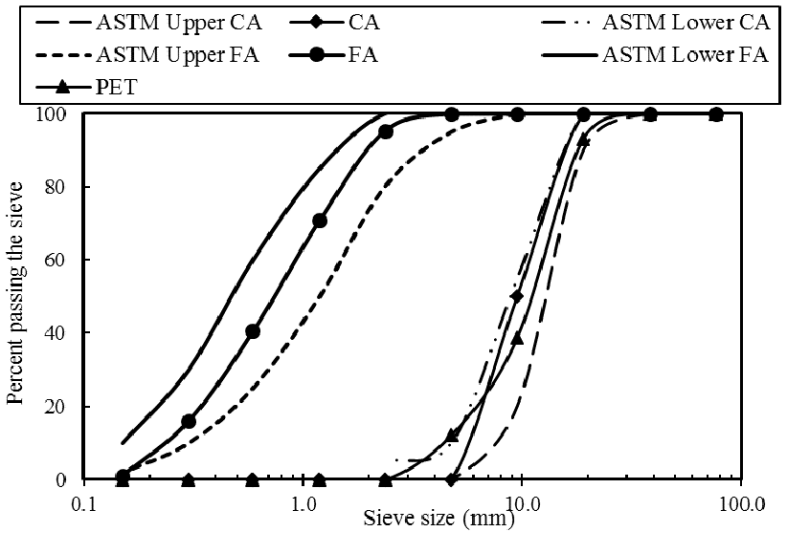

Figure 1. Gradation curves of the aggregates used in this study

2.3. Mix design and test specimens

Coarse aggregates have been replaced volumetrically at different fractions with PET flakes to prepare PET concrete specimens. The coarse aggregate was partially replaced by PET flakes at a rate of 0%, 2%, 4% and 8%, respectively. The water to cement ratio (w/c) of 0.45, and the sand to aggregate ratio (s/a) of 0.42 have been kept constant for all mixes. In addition, the amounts of cement, fine aggregates, and water for all mixes were also kept unchanged. Total four cases of mix proportion were designed by varying the PET replacement to concrete at different fractions to perform the study. The mixture constituents for concrete cylinder are documented in Table 1.

Table 1. Mix proportions for concrete cylinder

Specifications	% PET[a]	Coarse Aggregate (kg/m^3)	PET[a] (kg/m^3)	Fine Aggregate (kg/m^3)	Cement (kg/m^3)	Water (kg/m^3)
Bholagonj Stone (BGS)	0.0	1013.48	0.00	705.67	400	180
	2.0	993.21	20.27			
	4.0	972.94	40.54			
	8.0	932.40	81.08			

a. PET: Polyethylene terephthalate

2.4. The Experimental Methods

For each of the cases shown in Table 1, slump test as per ASTM C143 was performed to determine fresh property of the concrete. Twenty four 10 cm X 20 cm concrete cylinders were prepared to determine the mechanical properties of hardened concrete. Concrete cylinders were tested as per ASTM C39 at 7, 28 and 90 days to determine the compressive strength of concrete and for splitting tensile cylinders test as per ASTM C496 at 28 days. The stress-strain responses of specimens also recorded for compressive strength at 28 days.

3. RESULTS AND DISCUSSIONS

3.1. Slump

Figure 2 shows the effect of the PET replacement on the slump of PET Aggregate concrete. As can be shown, the slump values increase with PET replacement up to 4.0%. This phenomenon might be attributed by smooth surface and almost zero absorption capacity of PET, which restricts formation of adhesion in PET concrete mix. However, a significant loss in Slump is observed for replacement of 8.0%. ACI 211.1-91 states various slump ranges for different types of concrete work. A minimum slump value of 1 inch is recommended for all types of concrete construction work (Dixon et al., 2002). Besides, it has selected a range of 1 inch to 2 inches (2.54 cm to 5.08 cm) for mass concrete work. Such a finding promotes a potential to use PET flake as coarse aggregate replacement for concrete works.

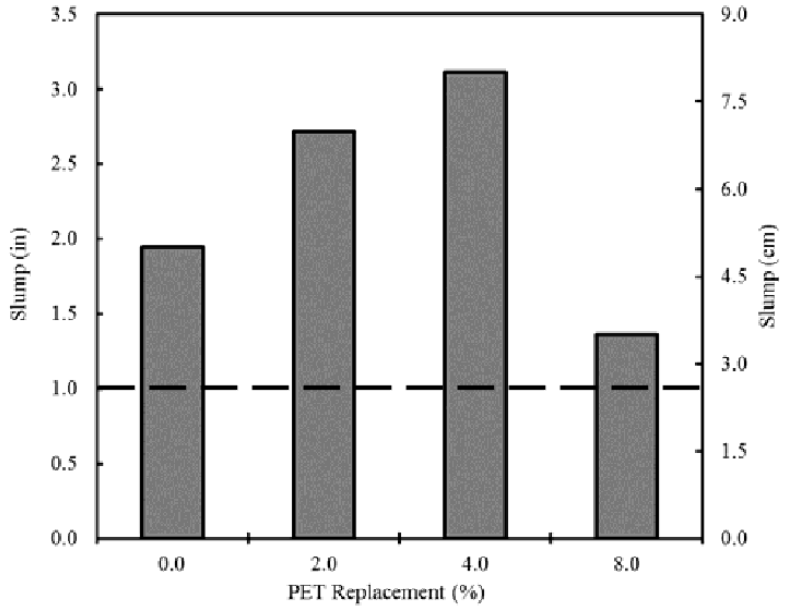

Figure 2. Influence of PET replacement at different PET replacement

3.2. Stress-Strain Responses of PET Concrete Under Compression

Stress-strain responses recorded at 28 days has been illustrated in Figure 3. Although a loss in strength capacities were observed with PET replacement, an increase in strain capacities were recorded with the replacement. Figure 4 shows, a reduction in elastic modulus also with PET replacement. However, it was found that after 4% of aggregate replacement, there is no signification loss in elasticity was recorded.

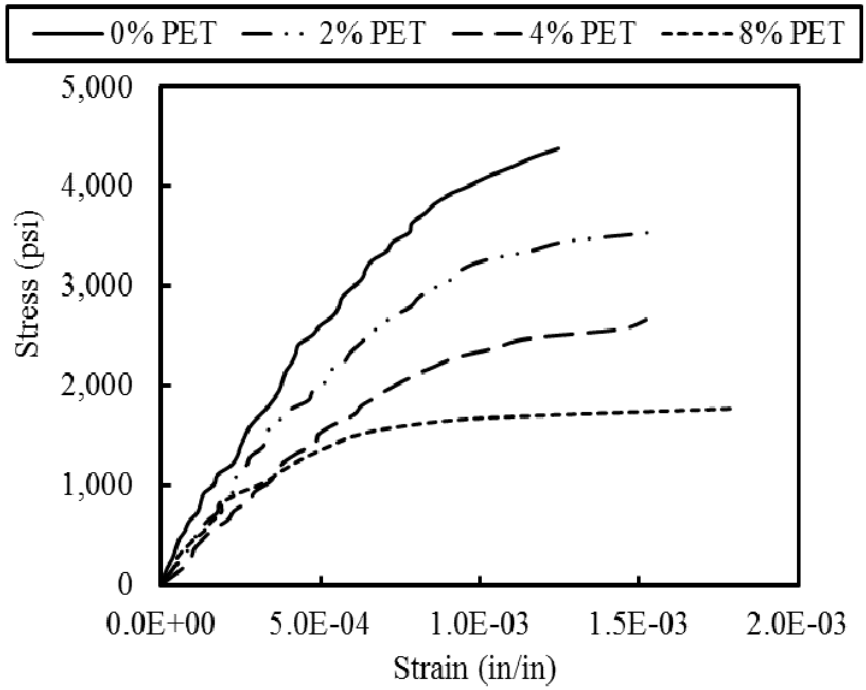

Figure 3. Stress-strain responses at 28 days

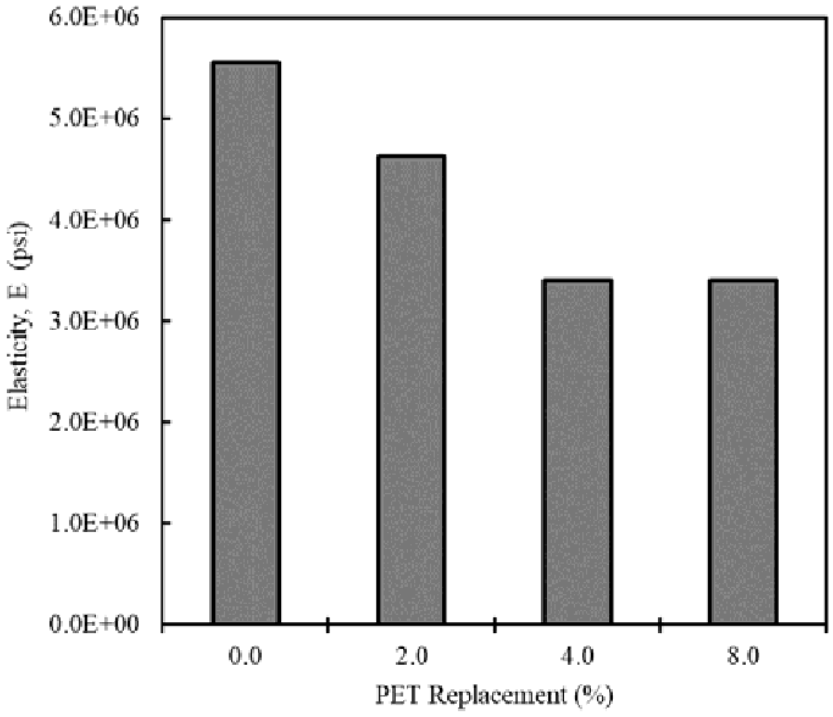

Figure 4. Influence of PET replacement at different PET replacement

3.3. Compressive Strength and Splitting Tensile Strength

Figure 5 illustrates the influence of PET flake replacement on compressive strength of concrete at different curing age. In generally, for both curing ages- 7 days and 28 days, loss in compressive strength were recorded. This phenomenon may be attributed by the hydrophobic nature of PET, which restricts hydration of water and consequently results to poor bond between matrix and fiber (Irwan et al., 2013a). However, the PET substitution of 0.5%, 1.5% and 3% exceeded the minimum compressive strength of normal weight concrete as recommended by ACI 318. The influence of PET

flake replacement on the split tensile strength of concrete has been demonstrated in Figure 6. Overall, as like the compressive strength, a decrease in tensile strength was observed at 28 days. However, it was also noticed that the presence of flake limits the complete split of concrete cylinders by abridging the crack and transferring stress.

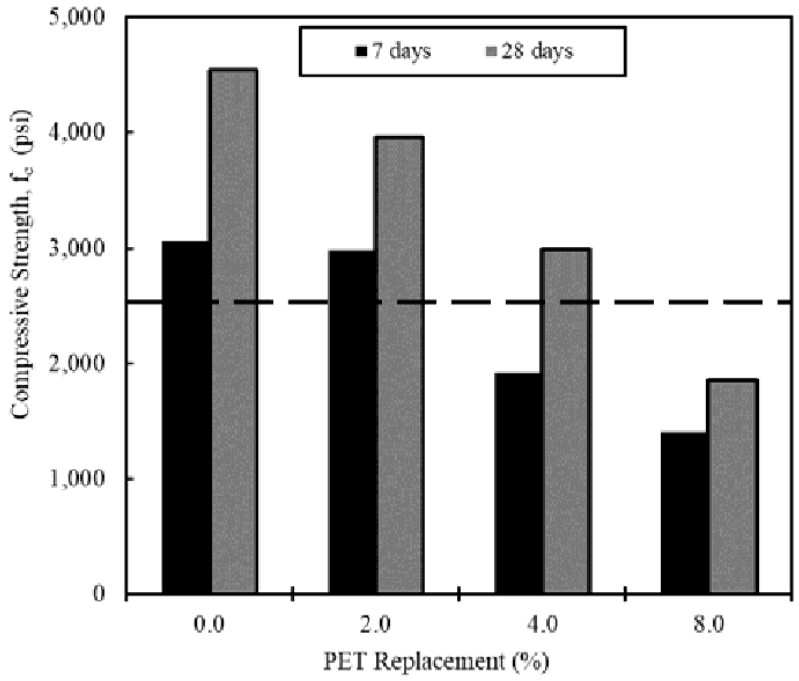

Figure 5. Influence of PET replacement on compressive strength at 7 and 28 days

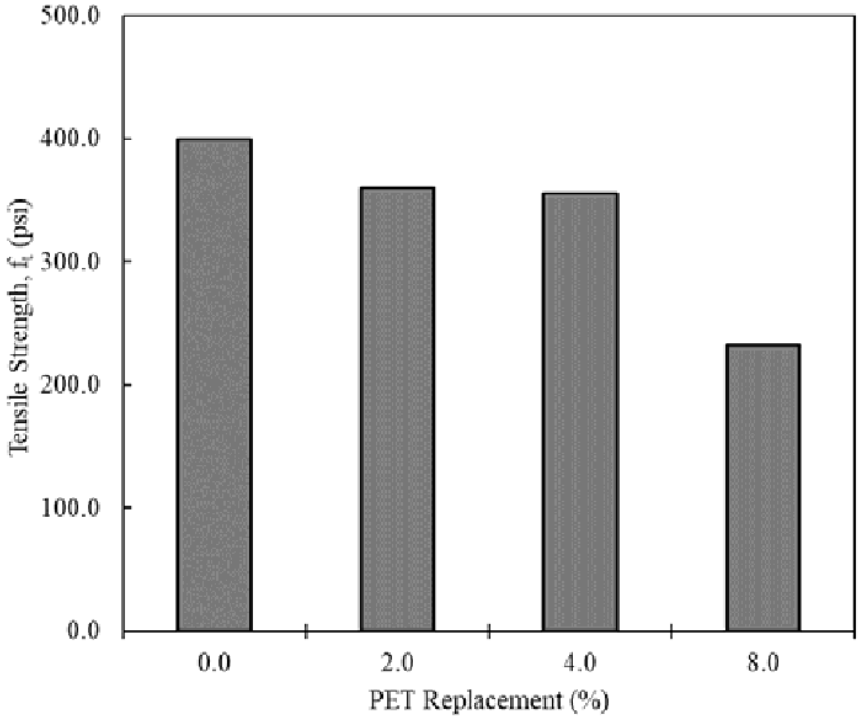

Figure 6. Influence of PET replacement on split tensile strength at 28 days

5. CONCLUSIONS

- With increase in coarse aggregate replacement by PET flakes reduces compressive strength, elastic modulus and split tensile strength of PET aggregate concrete. However, an increase in strain capacities was also found with increase replacement.
- Increase in PET replacement affects positively the fresh properties of concrete.
- It is also found that it is possible to produce mass concrete by replacing virgin coarse aggregate

ACKNOWLEDGMENTS

This research was supported by University of Asia Pacific (UAP), Bangladesh. The authors would like to recognize the contribution of Md. Humayan Kabir and Reazul Islam, lab assistant of Concrete Lab of UAP.

REFERENCES

Al-Sabagh AM, Yehia FZ, Eshaq G, Rabie AM, and ElMetwally, AE (2016). Greener routes for recycling of polyethylene terephthalate, Egyptian Journal of Petroleum, 25(1), 53-64.

Laville S, Taylor M (2017). A million bottles a minute: world's plastic binge 'as dangerous as climate change'. The Guardian, 28.

Islam MS, Uddin MJ, Alshehri A (2018). Plastic Waste and Carbon Footprint Generation Due to the Consumption of Bottled Waters. Research & Development in Material Science, 5 (1).

Gu L and Ozbakkaloglu T (2016). Use of recycled plastics in concrete: A critical review. Waste Management, 51, 19-42.

Irwan JM, Asyraf RM, Othman N, Koh KH, Annas MMK and Faisal SK (2013). The mechanical properties of pet fiber reinforced concrete from recycled bottle wastes, Advanced Materials Research, 795, 347-351.

ACI Committee (1999). Building code requirements for structural concrete: (ACI 318-99); and commentary (ACI 318R-99), American Concrete Institute.

ACI 211.1-91 (2002). Standard Practice for Selecting Proportions for Normal, Heavyweight, and Mass Concrete, American Concrete Institute, Farmington Hills, MI, USA.

Proc. 2nd International Conference on Structural Engineering Research (iCSER2019)
19-22 Jan 2019, Dhaka, Bangladesh
ISBN: 978-0-6482681-2-3

Effect of Thermal Cutting on Structural Steel

SakibReza[1], Mamnun-Ul-Alam[1] and Shameem Ahmed[2]

[1]Student, Bangladesh University of Engineering and Technology, Dhaka, Bangladesh
[2]Assistant Professor, Department of Civil Engineering, BUET, Dhaka-1000, Bangladesh
Email:sakibreza04168@gmail.com,mamnun1404089@gmail.com,shameem.ce@gmail.com

Abstract

Thermal cutting is a popular and economic process of cutting steel in construction industry. Sometimes, test samples are collected by thermal cutting process specially when thickness of the steel plates are larger. Due to heat effect during thermal cutting, mechanical properties of the base material might change and this may lead to erroneous prediction of material behavior. This paper observed the effect of thermal cutting on test specimens of structural steel. In this study, two sets of test specimens were made from steel plates of five different thicknesses. For the first set of test specimens, initially stripes were taken from steel plates by thermal cutting and then tensile coupons and impact test specimens were prepared from those stripes. In the second set, stripes were cut by shear cutter and from those stripes test specimens were prepared. Tensile test and impact test on both sets of specimens were conducted in the laboratory. In addition, hardness test was also performed for all the test specimens. The material properties obtained from the shear cut specimens were considered as the properties of base material. In order to assess the effect of thermal cutting, all the test results obtained from two sets of test specimens were compared to each other. It is observed that, material properties obtained from thermal cut specimens differ from the base material properties. Effect of this variation on steel members design was also evaluated.

Keywords: Heat effect, Thermal cutting , Tensile test , Impact test.

Proc. 2nd International Conference on Structural Engineering Research (iCSER2019)
19-22 Jan 2019, Dhaka, Bangladesh
ISBN: 978-0-6482681-2-3

Comparative Study for Different Bracing Systems of an Irregular Steel Structure.

Farhat Aziz Sheen[1], Dr. Md. Monjur Hossain[2], Asma Ferdous[1] and Arifur Rahman[1]

[1] Structural Safety Engineer, Stichting Bangladesh Accord Foundation, Dhaka, Bangladesh
[2]Senior Structural Engineer, Environment & Infrastructure Management Solution, Dhaka, Bangladesh.
Corresponding author's E-mail: sheen_770@yahoo.com

Abstract

Location of Bangladesh is in an earthquake-prone zone. There is no proper methodology to determine the timing and magnitude of an imminent earthquake, therefore, the infrastructure development is an utmost apprehension. Lateral stability is a major concern in designing a multi-storied structure. Also, the popularity of steel structure is increasing in Bangladesh which carries the importance of our study. This paper represents the comparative study of analyzing different bracing systems in an irregular steel structure of G+7 storied by static and response spectrum method. Indeed, bracing is one of the most indispensable elements to design lateral load resisting frame. Parameters such as section properties, lateral loads, vertical loads, design parameters, support conditions, load combinations were constant and BNBC provisions were followed in this study. Different type of bracings like cross bracing, single diagonal bracing, knee bracing, V bracing and chevron bracing have been used to observe the impacts on different lateral displacements, storey drifts and bracing weights. Additionally, pushover analysis has been carried out to find out seismic response for different structure in the nonlinear zone. Finally, it was observed that cross and chevron bracing are better comparing to other types of bracings within the limitations of this study.

Keywords: Bracing system, displacement, drift, pushover analysis, response spectrum analysis.

1. INTRODUCTION

Steel structures devour less self-weight, less construction time, larger span feasibility & better seismic resistance capability than reinforced concrete structure which are the commonly known facts for what the popularity of steel structure is increasing in Bangladesh. Buildings having irregular configuration both in plan and elevation are seen at various places based on architectural requirement and functional needs of the clients. These asymmetry structures when subjected to lateral forces during earthquakes or any other natural disaster, the oscillatory movement generated from applied lateral forces which can induce a wide range of responses in the high-rise building as well as in the low-rise important structures. However, the major concern in designing irregular multistoried steel structure is to have good lateral load resistance framing system so that the lateral load could be transferred straightforwardly, and the building can sustain during the seismic response. All standard design codes specified the ultimate limit of displacement due to gravity and lateral loads; so, lateral deflection must be limited to prevent P-delta effect. Lateral stability of structures is measured from story drift that is defined as the ratio of maximum displacement at the rooftop of the building to the total height. The value of story-drift of a multi-storied building must be limited to the value specified in codes (ACI, BNBC). One common method that is used to control the lateral stability of the structure is the bracing system. This method is very efficient and economical that widely used to stabilize the structure against lateral loads (seismic and wind loads). Bracings are usually provided to increase the stiffness and stability of the structure under lateral loading and to reduce lateral displacement significantly. There are several types of bracing systems that have been used currently all over the world to stabilize the multistoried structures which are cross (X) bracing, single diagonal bracing, Knee bracing, V-bracing, chevron bracing etc.

In the literature, the effects of these aforesaid bracing systems have been carried out by several researchers. K.K. Sangle, K.M. Bajoria and V. Mhalungkar (2012) carried out the effect of the different pattern of the bracing system and without bracing of a G+40 storied irregular steel structure from the time history analysis for Northridge earthquake. Parameters like natural frequencies, fundamental time period, mode shapes, inter-story drift and base shear are calculated. The study was aimed at to compare the results of seismic analysis of high-rise building with a different pattern of the bracing system and without the bracing system. The analysis result revealed that the bracing element has a significant effect on structural behavior under earthquake loading. The diagonal Brace-B showed a highly effective and economical design of bracing style. Zasiah Tafheem, Shovona Khusru (2013) studied the behavior of a six-storied steel building considering concentric and eccentric bracing patterns in ETABS 9.6.0 software with service and lateral loads. In their study, effects of concentric X bracing and eccentric V type bracings are evaluated using HSS sections. They mentioned that the concentric (X) bracing reduces more lateral displacement and thus significantly contributes greater structural stiffness to the structure. J.S Jagdish and Tejas D. Joshi (2013) studied the bracing system on high rise steel structure. In that study, G+15 storied steel frame was modeled in Staad.pro v8i software having the same section's properties with different bracing patterns of X bracing, double X bracing, Single diagonal, K bracing and V bracings and lateral stability were calculated. In the case of K-bracing and V-bracing, reduction of displacement was higher compared to the un-braced building due to irregularity in the shape of the building. They also mentioned that storey drifts may increase or decrease in braced structure compared to the un-braced structure. Akshay Sonawane et. al. (2016) carried out the effect of the different bracing system on the critical story of a building. In their study, an eleven storied steel frame is modeled considering different bracing pattern like cross bracing, diagonal bracing, inverted V bracing and V bracing and results on storey drift and bending moment in columns and storey displacement were calculated.

In the present study response spectrum analysis and pushover analysis method were selected to evaluate structural performance over static analysis. Response spectrum analysis (RSA) is a linear-dynamic statistical analysis method widely used in the seismic analysis of structures. A response spectrum is a graphical relationship of maximum values of acceleration, velocity, and/or displacement response of an infinite series of elastic single degree of freedom (SDOF) systems subjected to time-dependent dynamic excitation as mentioned by Robert M E (1992). On the other hand, pushover analysis is a non-linear static analysis that has become the preferred analysis procedure for design and seismic performance evaluation purposes, as the procedure considers post-elastic behavior. In this method, the magnitude of the lateral push load is increased progressively according to a predefined loading pattern until either loading or the deflection reaches the specified level.

With the aforementioned background, several researchers had already carried out the effect of several types of bracings in resisting lateral loads by static analysis, but limited models had been carried out by spectrum analysis and push over analysis. The present study will guide the professional engineers, researchers and academicians to understand the variations of behaviors of different bracing systems in resisting lateral loads from the mentioned three methods.

2. METHODOLOGY

In the present study, an attempt was made to compute the structural behavior of a G+7 storied irregular steel building using different bracing patterns. An irregular multi-storied steel building was considered, and five different models were carried out with five kinds of bracings like X, diagonal, knee, V and chevron bracing in two placements along the building height to investigate their seismic behaviors. First, the buildings were designed based on the code (BNBC), and then these models were evaluated by static analysis, response spectrum analysis and pushover analysis to determine different lateral displacement, storey drift, bracing weight & pushover curves. Design configurations were unchanged during the analyses such as section properties, lateral loads, vertical loads, design parameters, support conditions, load combinations etc. following BNBC provisions. Basic data considerations are provided in table 1.

2.1. Data consideration for static analysis (SA)

The following data were considered during the analysis.

Table 1. Modeling data for analysis.

Number of stories	G+7	Live load on slabs	3 KN/m^2
Height of each storey	3.00 m	Basic wind speed	210 kmph
Height of ground floor	4.5m	Zone factor, Z	0.15 for zone II
Plan area	2157.8 m^2	Importance factor, I	1.0
Depth of foundation	3 m	Type of soil	S3
No of bays	8 in x-direction & 9 in z-direction	Response reduction factor, R	6 (static analysis)
Type of building	Industrial	Size of Beam	W 21x73 & W 21x83
Dead load (including slab, floor finish & internal partition wall)	5.4 KN/m^2	Size of column	W24x103 (Corner) W24x131 (Peripheral) W27x161 (Interior)
Wall load on beams	0.73 KN/m	Bracing section	PIPS80

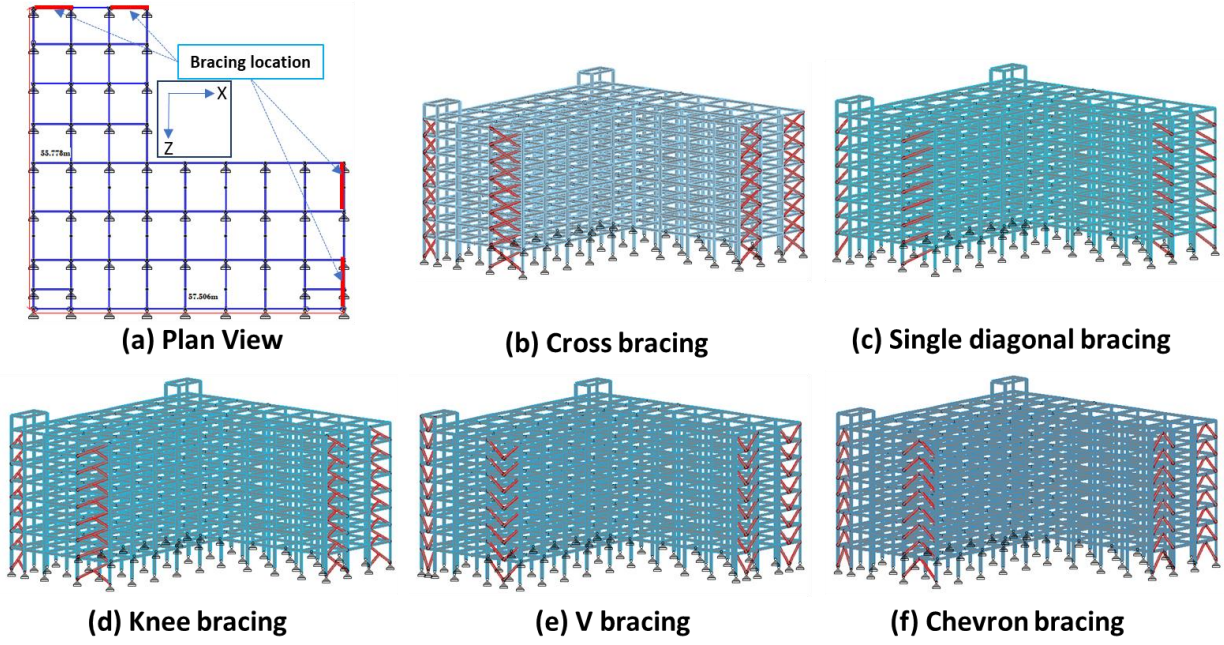

Fig 1. Typical plan and elevation of the different bracing system.

2.2. Response spectrum (RSA) analysis procedure

To differentiate the dynamic response of these different bracing system response spectrum analyses were carried out following BNBC 2017 [Article 2.5.4.3, equation 6.2.34 & 6.2.35]. Among the different methods of response spectrum analysis, CQC method was adopted in the analysis. The data which were considered in this analysis to determine normalized design acceleration response spectrum graph (shown in figure 5) are Seismic Zone co-efficient Z=0.2, Importance co-efficient I=1, Response reduction factor R=3.25, Site co-efficient S=1.35, TB 0.2, TC=0.8, TD=2, ξ %=5, ή=1. The spectral acceleration vs time period data then applied to the FEM. Also, a scale factor has been identified to bring the base shear from response spectrum analysis in an equilibrium form with the base shear from static analysis. The number of modes was selected to obtain combined modal mass participation of at least 90 percent of the actual mass.

2.3. Pushover analysis (PA) procedure

Pushover analyses were carried out after static analysis and response spectrum analysis to investigate the behavior in plastic range for the specific five different bracing systems. To perform the pushover analysis fixed rigid moment frame having geometric nonlinearity is considered. The number of push load step was considered 330 and 550 for X & Z directional analysis. The FEMA specification was selected as hinge properties and the percentage of Critical Damping for the 1st spectrum has a default value of 5% defined in FEMA [article no. 1.6.1.5.3] and site Category of class D as defined in the FEMA [article no 1.6.1.4.1] is selected. The Mapped spectral acceleration at short period (S_s) and one second period (S_1) were evaluated from FEMA [Equation 1-4 and 1-5] as 0.88 and 0.58.

3. RESULTS & DISCUSSION

Following the above procedure static analysis, response spectrum analysis and pushover analysis have been carried out for five different types of braced structure. After that, the analysis results have been taken which is reflected in table 1. The following data are then plotted on a graph to compare the minimum and maximum displacement, drift index, weight for both static and response spectrum analysis. Also, the first point of plastic hinge formation and the nonlinear behavior were determined by conducting pushover analysis. In table 1 the effective values are highlighted.

Table 1. Data variation for the different bracing system.

Subject		Model 1	Model 2	Model 3	Model 4	Model 5
		X brace	Diagonal Brace	Knee brace	V brace	Chevron brace
Displacement (m) (Static analysis)	X Direction	0.087198	0.08829	0.08834	0.087579	**0.086716**
	Z Direction	**0.114884**	0.12352	0.12354	0.120244	0.115011
Drift index	Static analysis	**0.00529**	0.006578	0.00657	0.006024	0.005555
	Response Spectrum	**0.00763**	0.008928	0.00892	0.00833	0.0078125
Weight (KN)	Total bracing only	290.7141	**145.3593**	218.036	190.6736	190.6736
Displacement (m) (Response spectrum)	X Direction	0.099162	0.093015	0.09309	0.095606	**0.097739**
	Z Direction	0.139979	0.150876	0.15090	0.146888	**0.138455**
Pushover 1st plastic hinge (KN)	X Direction	12175.73	9462.124	9473.02	9525.27	**12741.5**
	Z Direction	5928.958	8798.273	**8810.55**	6524.679	8690.85

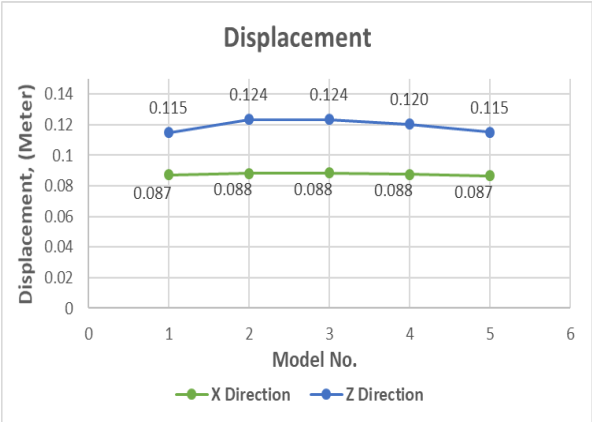

Figure 2. Maximum nodal displacement (SA) for different models in X and Z direction.

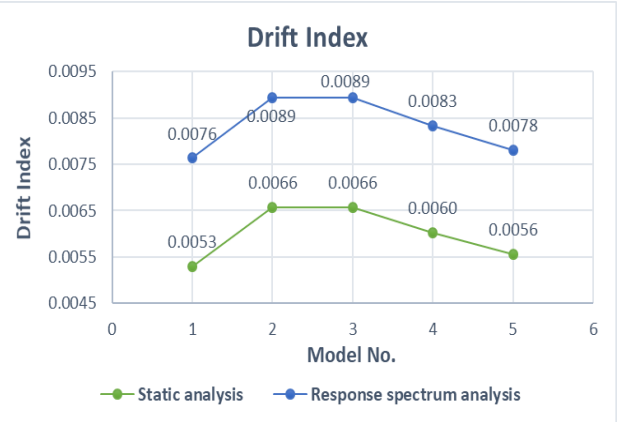

Figure 3. Maximum drift for different models.

From figure 3 it is seen that the drift is relatively lower for X bracing from the other bracing systems where the drift of chevron bracing has increased 3%-5% for static and response spectrum analysis.
The maximum displacement occurs for diagonal and knee bracings and lowest rooftop displacement

values were identified for X and chevron bracing systems. On the other hand, the weight the X bracing systems are maximum, and chevron & diagonal bracing has 65% and 49% weight of X bracing.

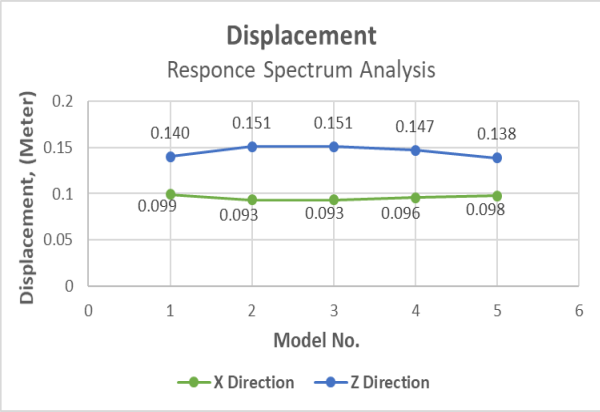

Figure 4. Maximum nodal displacement (RSA) for different models in X and Z direction.

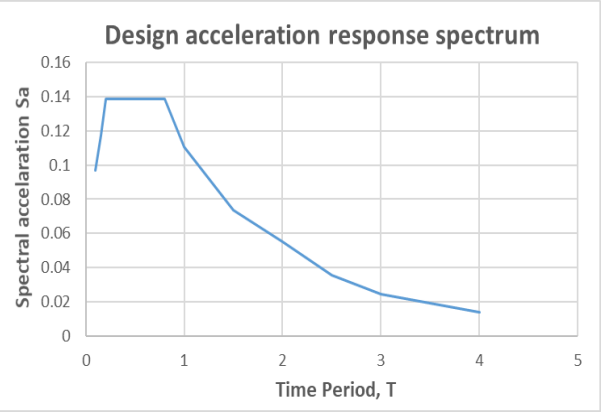

Figure 5. Normalized design acceleration response spectrum.

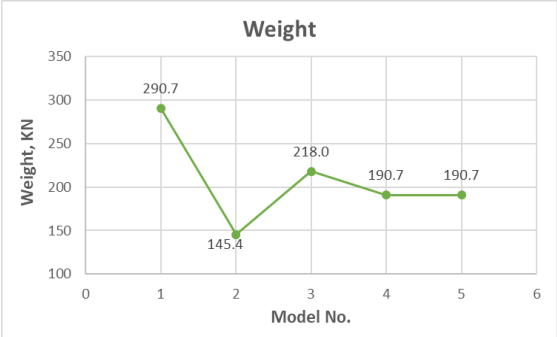

Figure 6. Variation in the quantity of steel for the different bracing arrangement (only).

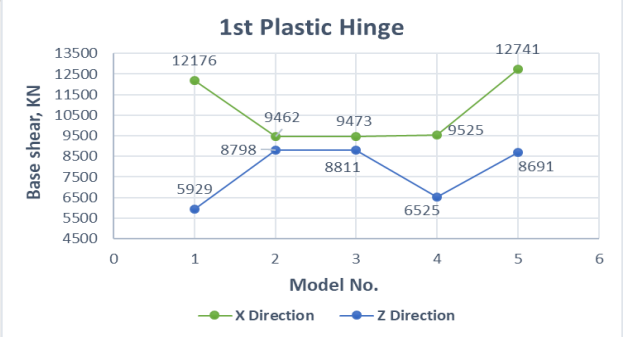

Figure 7. First plastic hinge formation for the different bracing arrangements.

The first point of plastic hinge formation can be seen from figure 7 which shows that chevron bracing systems take more load to create first plastic hinges formation in the structure. Whereas from the figure 8 and 9 it is observed that the chevron bracing structure requires more base-shear in the nonlinear zone to conduct similar displacement compared to the other bracing systems.

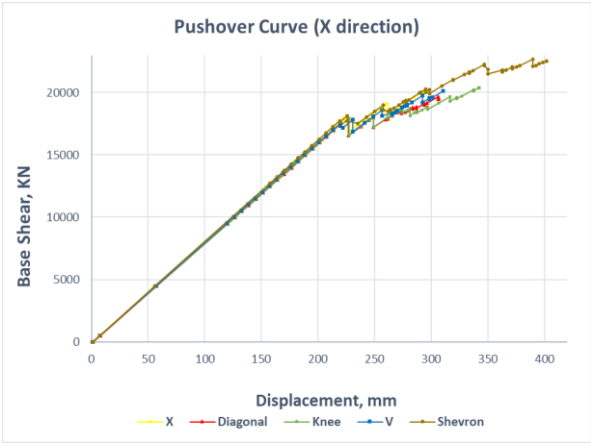

Figure 8. Pushover curve for different bracing arrangement in X direction.

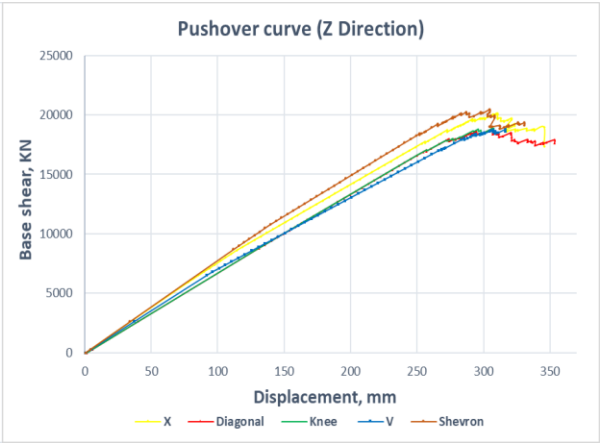

Figure 9. Pushover curve for different bracing arrangement in X direction.

4. CONCLUSION

From the above-mentioned analysis, it is understandable that the bracing systems are highly an effective method to design rigid structures that are subjected to lateral loadings. The following discussion has been made from the present study-

- The maximum nodal displacement for different types of bracing is very close to each other for both the static analysis and response spectrum analysis.
- However, the drift is higher for single diagonal and knee bracing than X and chevron bracing system for the static and response spectrum analysis.
- Considering the weight of the bracings, the chevron bracing system is more economical having 65% weight of X bracing and effective among the five bracings.
- In the nonlinear static analysis, we have determined the first point of plastic hinge formation for the structure which deliberates good results for X and chevron bracings.
- The X and chevron bracing take more lateral loads to displace than other bracings. Also from the pushover curve, it seems that the sustainability of chevron bracing system is better than other bracing systems.

REFERENCES

Akshay Sonawane, Dipak Sonawane, Satish Jadhav, Rajendra Khemnar, Rohit Mahale, Prof. Dumbare Sir "Effect of Bracing on Critical Storey of High-Rise Frame Structure" International Conference on Emerging Trends in Engineering and Management Research (ICETEMR-16)- ISBN:978-81-932074-7-5 Issue 23 March-2016.

American Society of Civil Engineers, Prestandard and Commentary for the Seismic Rehabilitation of Buildings, Federal Emergency Management Agency, Washington D.C., USA, 2000.

Bangladesh National Building Code, House and Building Research Institute.

Dr. M. M. Hossain, F. A. Sheen; M. S. Chowdhury and S.M.R Menon (2015), "Seismic Evaluation of a Simple Steel Structure by Pushover Analysis Procedure" International Conference on Recent Innovation in Civil Engineering for Sustainable Development (IICSD-2015).

Jagadish J. S, Tejas D. Doshi "A Study on Bracing Systems on High Rise Steel Structures" International Journal of Engineering Research & Technology (IJERT) ISSN: 2278-0181 Vol. 2 Issue 7, July - 2013

K. Sangle, K.M. Bajoria and V. Mhalungkar "Seismic analysis of high rise steel frame building with and without bracing" 15WCEE LISBOA 2012

K. S. K. Karthik Reddy, Sai Kala Kondepudi, Harsha Kaviti, "A Comparative Study on Behavior of Multistoried Building with Different Types and Arrangements of Bracing Systems", International Journal of Science Technology & Engineering, ISSN: 2349-784X, Volume 2, Issue 2, August 2015, PP 135-149.

Md. Mahmud Sazzad, Gazi Md. Sharfaraz Imam Azad, Md. Samdani Azad and Niloy Samadder (2018). "Effects of Vertical Irregularity in Steel Braced Frames on Response to Earthquake", Journal of Civil Engineering and Architecture 12 (2018) 106-112.

Robert M. Ebeling "Introduction of Computation of Response Spectrum for Earthquake Loading" Department of the US army corps of engineers, Washington DC 20314-1000. Issue June 1992.

Zasiah Tafheem, Shovona Khusru "Structural behavior of steel building with concentric and eccentric bracing: A comparative study" Volume 4, No 1, 2013 ISSN 0976 – 4399.

Proc. 2nd International Conference on Structural Engineering Research (iCSER2019)
19-22 Jan 2019, Dhaka, Bangladesh
ISBN: 978-0-6482681-2-3

Numerical Simulation on Behaviour of Steel Elliptical Hollow Steel Section Columns under Compression

Radin Md. Mahirul Hoque[1], Khan Mahmud Amanat[2], Rafid Shams Huq[3] and Md. Mahir Asif[4]

[1] Lecturer, Department of Civil Engineering, Bangladesh University of Engineering & Technology, Dhaka, Bangladesh.
[2] Professor, Department of Civil Engineering, Bangladesh University of Engineering & Technology, Dhaka, Bangladesh.
[3] Lecturer, Department of Civil Engineering, Stamford University Bangladesh, Dhaka, Bangladesh.
[4] Post Graduate Student, Department of Civil Engineering, Bangladesh University of Engineering & Technology, Dhaka, Bangladesh.
Corresponding author's E-mail: md.mahirasif92@gmail.com

Abstract

Tubular hollow sections are widely used in the industry for structures because of their significantly reduced dead load and option of installing wires and pipes through the hollow sections. Commonly used sections are rectangular, circular and square but recently elliptical hollow sections are becoming popular day by day. Elliptical sections prove to be more efficient specifically in case of eccentric loads. Furthermore, the sections provide higher torsional stiffness. For having higher moment of inertia, these sections also exhibit higher strength. In order to compare between circular sections and elliptical sections, a numerical finite element investigation has been conducted to study the behaviour of Elliptical Hollow Steel Section (EHSS) under varying thickness and slenderness ratio. Both material and geometric nonlinearities are incorporated in the model. The developed finite element model has been applied to simulate experimental studies done by past researchers and it has been found that good agreement exists between present analysis and past experimental results, which establishes the acceptability and validity of the present finite element model to carry out further investigation. It has been observed that the difference of buckling load carrying capacity between elliptical column and circular column is proportional to the length of the column in case of smaller section whereas the difference remains constant in case of larger section.

Keywords: Elliptical hollow sections, Circular sections, Thickness, Slenderness ratio, Finite element model.

1. INTRODUCTION

In engineering applications, tubular members are very popular and vastly utilized over the world due to their high torsional stiffness, closed nature and structural efficiency. Square, rectangular and circular hollow sections are very frequent and mostly used tubular structures from their commencement. But Elliptical Hollow Steel Section (EHSS) is relatively new shape to the steel construction which opens a new dimension to the field of hollow steel sections because of some of its unique advantages. In the past fifteen years, more attention has been paid to EHSS which have begun to become of more practical interest due to their introduction and availability as hot-finished products as per stated in 'European Committee for Standardization' (2006). Structural properties, technical security, aesthetic view, efficiency in space consumption, economic and architecturally pleasant structure make EHSS an interesting way for engineers to fulfill their vision.

EHSS will be more effective for using in the highly wind exposed structures according to Nithiyaasri

et al (2017). Ruiz-Teran and Gardner (2008), Kempner and Chen (1964), Silvestre and Gardner (2011), Abela and Gardner (2012), Law and Gardner (2013) have found that, in contrast to circular hollow steel tubes, EHS tubes in compression can have stable post-buckling responses and may therefore be able to resist further load beyond the elastic buckling load. Chan et al (2010) have presented that the EHSS exhibits flexural stiffness for having the disparity in major and minor axis in case of higher aspect ratios which is helpful to resist local torsional buckling, but it is not possible for circular hollow section. Elliptical hollow sections have already been used as primary part of some structures like The Royal Albert Bridge, Forth Railway Bridge, Zeeman Building at the University of Warwick, The Society Bridge in Scotland, the main airport terminal buildings in Madrid, London Heathrow etc.

The existing experiments are very useful to predict some of the important behaviors of elliptical hollow sections. More experimental researches are needed to figure out some other important characteristics of such sections. However, such experimental works are quite expense. Therefore, authentic finite element modeling can be an effective solution. The objective of this study is to investigate the behavior of elliptical hollow steel sections numerically with varying slenderness ratios and geometrical cross-sections. Samples have been constructed as three dimensional finite element models and a verification of these finite element models have been conducted with reference to the experiment of Chan and Gardner (2009). The samples have also been compared to equivalent Circular Steel Sections (CSS).

2. METHODOLOGY

Proper modeling is the first step to acquire accurate result. Modeling of the samples was done by following some proper steps. At first end plate of the sample was modeled by scaling circular area according to ratio of the larger diameter and smaller diameter. After that, meshing was done by dividing the end plate along both axes such a way that the individual element was kept square. To make our model as close to the theoretical condition, the EHSS column was divided into five segments since these columns might have slight initial curvature due to manufacturing imperfections in practical condition. Followed by the length of elliptical hollow steel column perpendicular to the axis of the end plate is divided into sufficient number of divisions in such a way that square mesh elements with respect to the end plate elements could be achieved. It may be noted that the number of meshing was tried to keep reasonable for reducing computational time and almost getting accurate result. Eventually, mesh sensitivity was studied. Full isometric view of a model is presented in Figure 1.

Boundary conditions were firmly applied on the model. One end of the column is kept restrained for translation in all the x, y and z direction, while the other end of the column is kept restrained for x and y direction translation only to allow deflection or load along z direction (i.e. length of column). Along xy plane a corner point of column is additionally restrained in y direction translation to prevent twisting of column. Nonlinear analysis could be performed either by applying load or deflection for obtaining the load deflection diagram. The results found from the models were verified with the experiment of Chan and Gardner (2009) as shown in Figure 2 and the model was found to be acceptable.

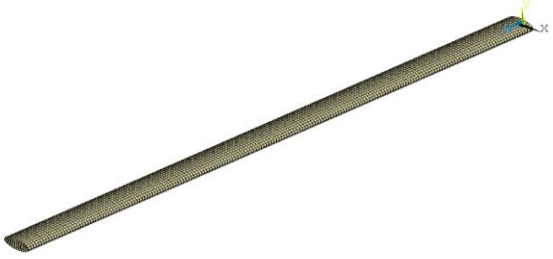

Figure 1: Isometric view of ANSYS model

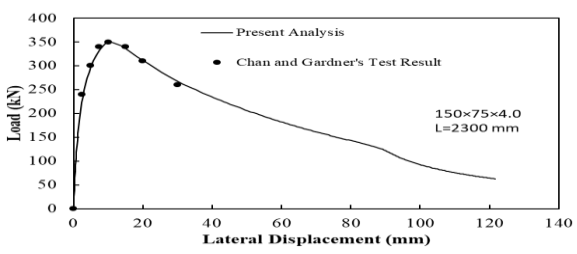

Figure 2: Load-lateral deflection curves

3. RESULTS

After validation of the model with the works of Chan and Gardner (2009), parametric study was conducted. The objective was to compare buckling load capacity and lateral deflection between EHSS and equivalent CSS. The EHSS chosen were of two types as presented in Table 1.

Table 1: EHSS sections Type A and Type B

Section Type A (mm)	Section Type B (mm)
150 × 75 × 4	500 × 250 × 10
150 × 75 × 5	500 × 250 × 12.5
150 × 75 × 6.3	500 × 250 × 14.2
150 × 75 × 7	500 × 250 × 16

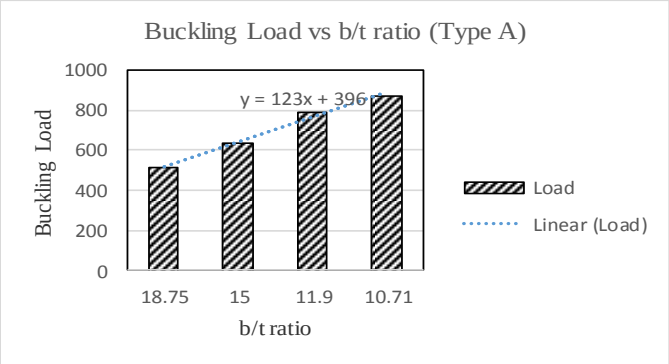

Figure 3: Buckling Load vs. b/t ratio for EHSS section Type A

When the two types of EHSS are compared it is observed that load capacity increases with decrease of b/t ratio in both types. However, the percentage increase is smaller in type B (26%, 11% and 9% with respect to thinnest section) as shown in Figure 3 than that in type A (24%, 25% and 10% with respect to thinnest section) as shown in Figure 4.

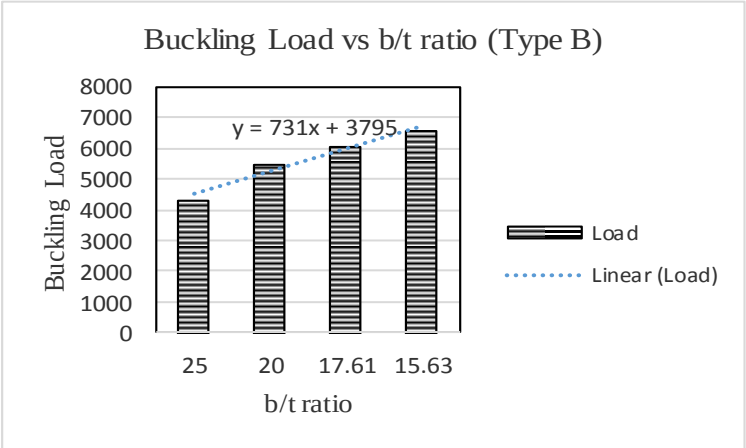

Figure 4: Buckling Load vs. b/t ratio for EHSS section Type B

Therefore, we can conclude that smaller sections like those in type A are effected more by the decreases of b/t ratio than comparatively larger sections like those in type B.

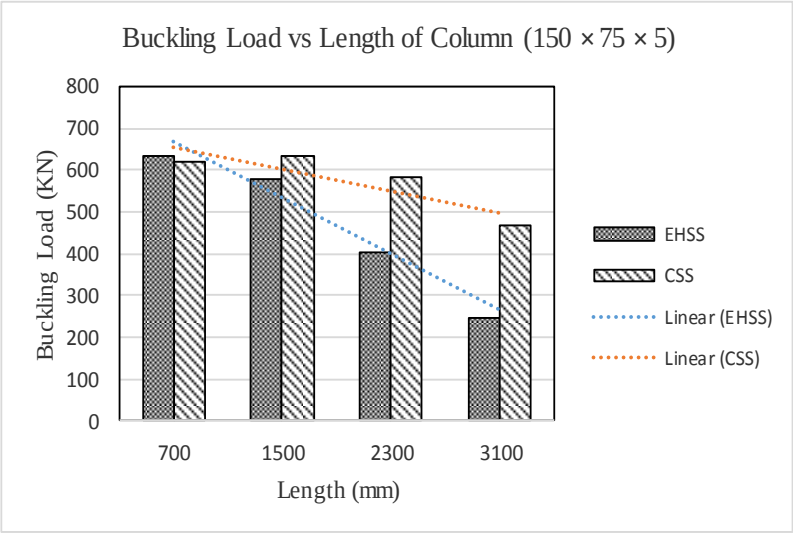

Figure 5: Comparison between small EHSS & CSS Buckling Load vs. Length

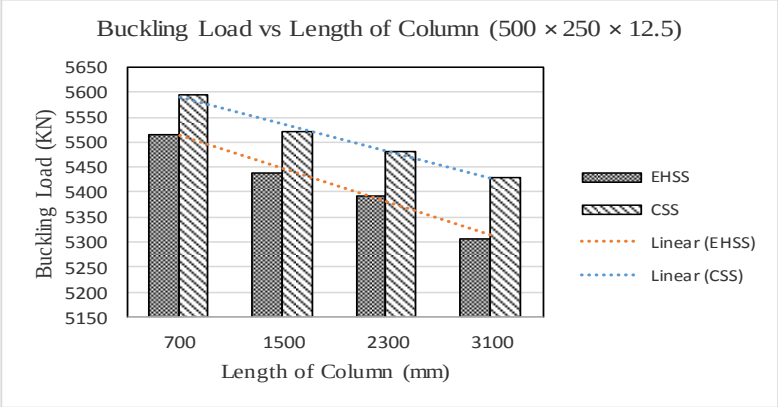

Figure 6: Comparison between large EHSS & CSS Buckling Load vs. Length

Afterwards, one section was selected from both type A and B. 150 × 75 × 5 from type A and 500 × 250 × 12.5 was selected from type B. Then the equivalent circular sections were calculated for each. Length was varied for the sections and corresponding values of buckling load capacity and lateral deflections were recorded. It can be observed in Figure 5 that the buckling load capacity decreases with increase of length for both type A EHSS and equivalent CSS, but the percentage decrease is greater for EHSS as shown by the steeper trend line of EHSS. In comparison, in Figure 6 for type B it is observed that the percentage decrease in capacity is similar in both EHSS and equivalent CSS shown by the parallel trend lines. Hence, it can be concluded that the increase of length (which consequently increases the slenderness ratio) significantly reduces buckling load capacity in type A EHSS which make them less desirable than equivalent CSS. However, the reduction in capacity of type B EHSS and equivalent CSS are similar.

Table 2: Lateral Deflection for Type A EHSS and Equivalent CSS

L (mm)	EHSS	CSS	% Difference
700	0.49	0.07	86
1500	1.63	0.84	48
2300	10.95	2.77	75
3100	32.64	10.57	68

Table 3: Lateral Deflection for Type B EHSS and Equivalent CSS

L (mm)	EHSS	CSS	% Difference
700	0.69	1.89	-174
1500	0.74	0.37	50
2300	0.89	0.63	29
3100	1.2	1.2	0

Table 2 and table 3 present the lateral deflection of columns at the mid-section. If the 700 mm long column is ignored, the trend for difference in lateral deflection between EHSS and CSS is increase with the length of column for type A, but decrease with length of column in type B. 700 mm column is ignored as it is too short for it to deflect significantly enough to consider for making conclusion.

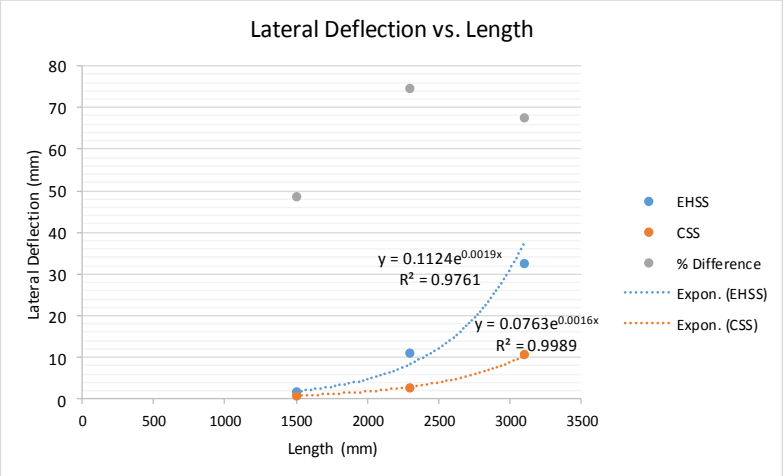

Figure 7: Comparison between Type A EHSS & CSS Lateral Deflection vs. Length

The increase in lateral deflection with increasing length of column in type A EHSS and CSS are shown graphically in Figure 7. The decrease in lateral deflection with increasing length of column in type B EHSS and CSS are shown graphically in Figure 8.

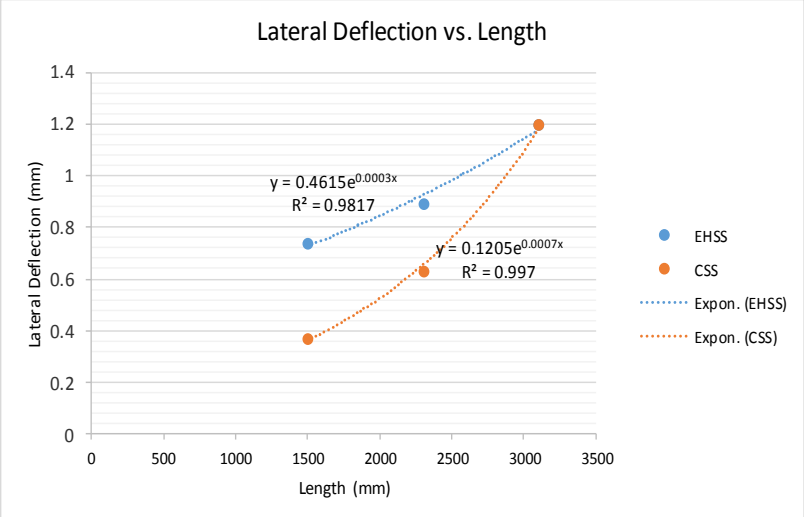

Figure 8: Comparison between Type B EHSS & CSS Lateral Deflection vs. Length

4. CONCLUSION

Buckling Load Capacity and Lateral Deflection are both important parameters for hollow steel sections. Based on the simulations we can draw the conclusion that increasing thickness in smaller EHSS is more effective in increasing buckling load capacity than in larger EHSS section. Also, decrease in buckling load capacity and lateral deflection with increasing slenderness ratio in smaller sections are significantly different in EHSS than those of equivalent CSS. However, these are quite similar in larger sections.

Now that some relationships have been developed between elliptical section size and buckling load capacity, buckling load capacity and column length, lateral deflection and column length a larger sample size should be analyzed in the future to verify the conclusions drawn above.

REFERENCES

Abela JM, Gardner L (2012). Elastic buckling of elliptical tubes subjected to generalised linearly varying stress distributions, Thin-Walled Structures, 58, 40–50.

Chan TM, Gardner L (2009). Flexural Buckling of Elliptical Hollow Section Columns, Journal Of Structural Engineering (ASCE), 135(5), 546-557.

Chan TM, Gardner L, Law KH (2010). Structural design of elliptical hollow sections: a review, Proceedings of the Institution of Civil Engineers - Structures and Buildings, 163(6), 391-402.

Comité Européen de Normalisation, EN 10210-1:2006 (2006). Hot finished structural hollow sections of non-alloy and fine grain steels – Part 1: Technical delivery conditions, British Standards Institution.

Kempner J, Chen YN (1964). Large deflections of an axially compressed oval cylindrical shell, Proceedings of the 11th International Congress of Applied Mechanics, Munich.

Law KH, Gardner L (2013). Buckling of elliptical hollow section members under combined compression and uniaxial bending, Journal of Constructional Steel Research, 86, 1–16.

Nithiyaasri S, Rose AL, Saranya M (2017). Finite element analysis of steel elliptical hollow section column, International Advanced Research Journal in Science, Engineering and Technology, 4(3), 140-146.

Silvestre N, Gardner L. (2011). Elastic local postbuckling of elliptical tubes. Journal of Constructional Steel Research 67(3), 281–292.

Ruiz-Teran AM, Gardner L (2008). Elastic buckling of elliptical tubes, Thin-Walled Structures, 46(11), 1304–1318.

Proc. 2nd International Conference on Structural Engineering Research (iCSER2019)
19-22 Jan 2019, Dhaka, Bangladesh
ISBN: 978-0-6482681-2-3

Load-slip Behaviour of L-shape Rebar Shear Connectors in Steel-Concrete Composite Members

Mohammad Hosainul Kabir[1] and Mahbuba Begum[2]

[1]Graduate Student, Bangladesh University of Engineering and Technology, Dhaka, Bangladesh
[2]Professor, Bangladesh University of Engineering and Technology, Dhaka, Bangladesh
Corresponding author's E-mail: birutkabir@gmail.com

Abstract

In steel-concrete composite beams, at the interface between steel beam and concrete slab shear connectors are provided to resist the horizontal shear between the two components. Shear connectors also prevent the vertical separation or uplift of the concrete slab from the steel beam. In this study, an experimental research on the behaviour of a new type of L–shape rebar shear connector is presented. Eight push-out tests on rebar shear connectors with variable diameter are investigated. The push-out test specimens are designed to study the effect of diameter of connectors and compressive strength of concrete slab on the load-slip behaviour of the shear connector. The experimental results are presented and discussed, focusing on the failure mode and ultimate shear capacity of the connectors.

Keywords: *Steel, concrete, composite, shear connector, push-out, load-slip, ultimate capacity.*

1. INTRODUCTION

In steel-concrete composite beams, at the interface between steel beam and concrete slab shear connectors are provided to resist the horizontal shear between the two components. The shear connectors also prevent the vertical separation or uplift of the concrete slab from the steel beam. The most common type of shear connector used in practice is steel headed stud anchors which are made of cold drawn steel with minimum yield strength of 60 ksi. In case of heavily loaded composite floor beams, C-shape, I-shape or L-shape connectors cut from hot rolled steel profiles are used. Installation of these shear connectors are complex and costly. Deformed rebars cut into L-shape can also be used as shear connectors. This type of shear connectors can be easily prepared at construction site by simply cutting the long deformed rebars. Their installation through welding is also easier as compared to stud connectors. The design strength of shear connectors are determined through experimental push-out test. The design strength and behaviour of C-shape, L-shape & I-shape connectors cut from hot rolled steel profiles and headed stud connectors are studied by several researchers through experimental and numerical investigations [Pashan (2006), Bouchair (2012), Mazoz et al. (2013), Balasubramanian and Rajaram (2016)]. Current design codes such as Eurocode 4 (2005) and AISC (2016) only include the design equations and design values for headed stud and channel shear connectors. However, the shear capacity and behaviour of the L-shape rebar connectors are not available in the literatures as well as in current design standards such as Eurocode 4 (2005), CSA-S16 (2009) and AISC (2016). To this end, an attempt has been made in this study to conduct experimental investigations with a view to determine the shear strength and load-slip behaviour of L-shape rebar connectors in steel-concrete composite beams.

2. EXPERIMENTAL PROGRAM

2.1 Details of push-out test specimen

In present study eight specimens categorized into two push-out test series (series A and series B) are constructed and tested under static loading. Each push-out specimen consists of a short standard (S-shape) compact steel beam section (100 by 200 mm) held in a vertical position by two identical reinforced concrete slabs having dimensions of 250 by 350 mm with a thickness of 130 mm. Details of a typical test specimen is shown in Figure 1. In the test specimen, the concrete slabs are attached to the beam flange by deformed L-shape (100 by 100 mm) rebar shear connectors. These connectors are welded to the flanges of the steel section as shown in Figure 2. In current study, the specimen geometry was kept similar with variation provided in connector size and concrete compressive strength. Concrete strength was varied between the two series of specimens. Specimens in series A are cast with 40 MPa concrete whereas higher strength concrete of 50 MPa is used in series B test specimens. Each test series consists of four push-out test specimens with variable size of rebar connectors. Deformed rebar type of shear connectors are used with diameters varying from 10 mm to 20 mm with two intermediate values of 12 mm and 16 mm. The slabs of all the push-out test specimens are cast vertically according to the procedure adopted by Mazoz (2013). Both slabs are cast from the same batch of concrete to reduce the chance for variation in concrete strength from one slab to another. The push-out test specimens are subjected to downward axial compression applied at the top of the steel beam. The steel section when subjected to a vertical load will produce shear load along the interface between the concrete slab and the steel section through shear connectors.

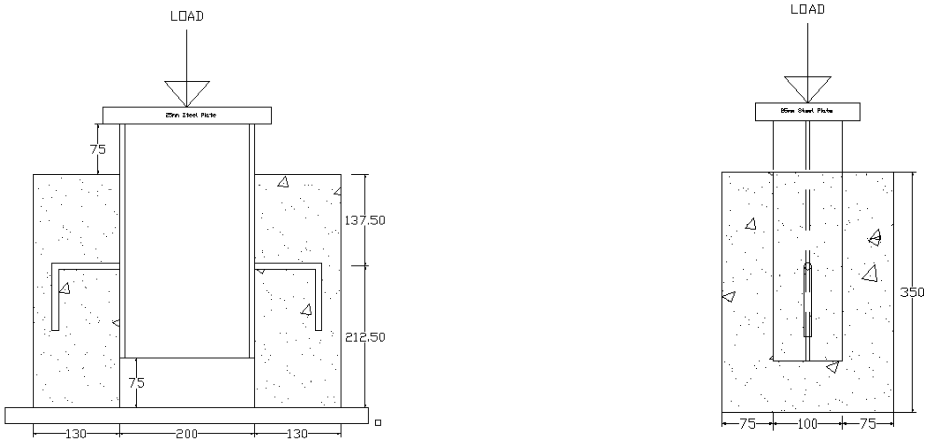

(a) Front view **(b)** Side view

Figure 1. Push-out test specimen with Rebar Connector (units in mm)

2.2 Material properties

The mechanical properties of the materials of steel section, concrete and shear connector are determined using appropriate test procedure. The ultimate compressive strength and modulus of elasticity of concrete obtained from 28-days cylinder test are listed in Table 1. Table 2 presents the mechanical properties the steel section and deformed rebars. These properties are obtained from the tension coupon tests for the steel plate from the steel section and deformed rebars for shear connectors.

Figure 2. Rebar Connectors

Table 1. Mechanical properties of concrete

Series of Specimen	Compressive strength, f'_c (MPa)	Modulus of Elasticity, E_c (MPa)
A	40	34683
B	50	38722

Table 2. Mechanical properties of Steel section and Rebar

Specimen	Yield Strength, f_y (MPa)	Ultimate Strength, f_u (MPa)	Elongation (%)
Steel section	307	424	22
Rebar Connector			
10 mm	382	577	15
12 mm	403	628	16
16 mm	408	638	17
20 mm	500	668	15

2.3 Instrumentation and test setup

All of the push-out specimens were tested under axial compression by a 2000 KN capacity Tinius Olsen Universal Testing Machine (UTM). The specimen was placed over the flat platform of the UTM. The axial compression was then applied at the upper end of steel beam by a hydraulic jack through a rigid steel plate of 25 mm thickness. A rubber pad was placed over the steel plate for uniform contact and proper distribution of the applied load. The slip between reinforced concrete slab and steel beam during loading was measured by two 50 mm capacity dial gauges located at the level of shear connectors. Each dial gauge was attached to the beam by the help of bracket near the connector, one at flange and another to the web. The test setup is shown in Figure 3. The average of these two gauge readings is denoted as the net slip of connector. The load was applied using displacement-controlled method at a rate of 0.5 mm/min. During each load step, the slip between the steel beam and the concrete slab was measured by means of the gauges after the dial had stabilized.

Figure 3. Typical Test Setup & Instrumentation

3. TEST RESULTS

3.1 Failure mechanism

The failure modes observed in the push out tests were shear failure of the rebar connector and concrete cracking followed by crushing. These failure patterns are shown in Figures 4 and 5. Figure 4 shows the shearing of connector. Concrete crushing failure around the connector is illustrated in Figure 5. In the specimens with smaller diameter connectors (i.e., A-1, A-2, B-1 and B-2) failure occurred by direct shear failure of the rebar connectors. No cracking or splitting of concrete was observed in these specimens. On the other hand, in specimens A-3, A-4, B-3 and B-4 failure was initiated by cracking and crushing of concrete followed by shear failure of the connector. Bending of the rebar connector after crushing of concrete was observed in specimen B-4 only. This specimen was cast with 50 MPa concrete and 20 mm diameter connector was used. In this specimen failure was accompanied by a considerable deformation of the connectors.

3.2 Load-slip behaviour

The relation between the push-out load and the slip between the concrete slab and the steel plate is shown in Figures 6 and 7, for specimens in series A and series B respectively. All the specimens in each group are identical except the diameter of connector. Specimens in series A were cast with 40 MPa concrete whereas higher strength concrete of 50 MPa was used in series B specimens. For all specimens slip increased with increasing load until the specimen reached the ultimate point. After the ultimate point the load dropped sharply except in specimen A-4 which exhibits a gradual decline of the peak load at the descending branch of the load-slip curve. In this specimen even after the cracking of concrete in front of the connector, the friction between the cracked concrete surfaces continued to provide shear resistance at larger slips. Load and slip values of eight test specimens are listed in Table 3.

Figure 4. Shearing of connector at failure

Figure 5. Crushing of concrete at failure

3.3 Effect of diameter of rebar connector

In this study four different diameter (10 mm, 12 mm, 16 mm and 20 mm) deformed rebar connectors were used in the push-out specimens. Effect of the rebar diameter on the load-slip curve obtained from the push-out tests are presented in Figures 6 and 7 for series A and series B specimens, respectively. For both series, increasing the diameter of connector results in an increase in push-out load capacity of the specimen without significantly changing the initial stiffness and the overall shape of the load-slip curve. Specimens with smaller diameter connectors exhibited a less ductile behaviour (i.e., smaller slip values at failure) as compared to the specimens with larger diameter of connectors. The ultimate capacity of the test specimen was observed to be affected significantly by the diameter of rebar

connectors as shown in Table 3. For specimens with 40 MPa concrete the increase in ultimate capacity was found to be 69%, 105% and 118% when the rebar dia. is increased from 10 mm to 12 mm, 16 mm

Table 3. Ultimate Load and slip obtained from the Test

Specimen	Compressive strength of Concrete, f'_c (MPa)	Rebar connector dia, d (mm)	Ultimate Load per Rebar connector (KN)	Capacity increment (%)	Slip at ultimate load (mm)	Occurrence of Failure
A-1	40	d10	57.5	-	2.80	Shearing of connector
A-2		d12	97.5	69.6	3.96	Shearing of connector
A-3		d16	118.0	105.2	4.22	Cracking of concrete
A-4		d20	125.5	118.3	4.26	Cracking of concrete
B-1	50	d10	51.0	-	2.18	Shearing of connector
B-2		d12	82.0	60.8	3.96	Shearing of connector
B-3		d16	120.0	135.3	4.31	Cracking of concrete
B-4		d20	145.5	185.3	5.58	Cracking of concrete

and 20 mm, respectively. This increase in capacity for series B specimens were observed to be 60%, 135%, 185% respectively for 12 mm, 16 mm and 20 mm connectors with respect to the capacity for 10 mm connector.

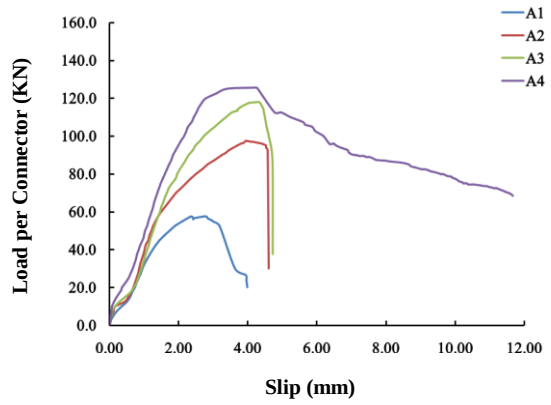

Figure 6. Load vs. Slip Curve for Series A

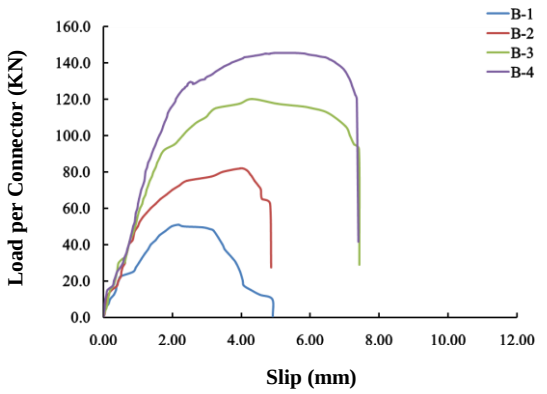

Figure 7. Load vs. Slip Curve for Series B

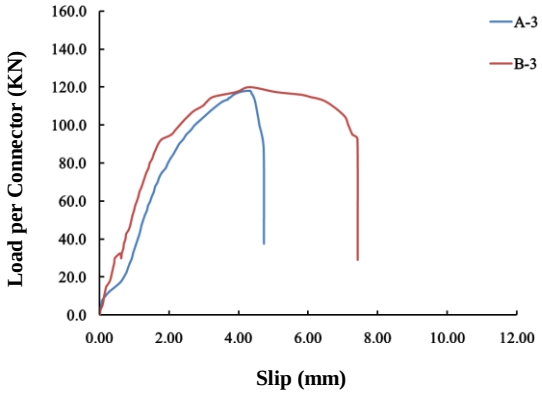

Figure 8. Effect of concrete strength on 16 mm dia. Connector

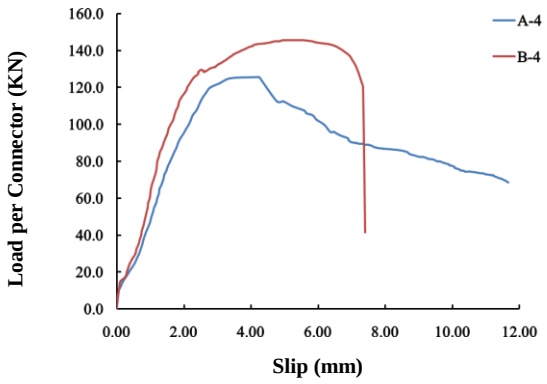

Figure 9. Effect of concrete Strength for 20 mm dia. connector

3.4 Effect of concrete strength

Figures 8 and 9 illustrate the effect of concrete strength on the load-slip behaviour of the push-out test specimens with 16 mm and 20 mm diameter connectors. It is obvious from the figures that as the concrete strength increases the ultimate load carrying capacity of the test specimen increases accompanied by significant enhancement in the slip values near the ultimate point. For 20 mm diameter connectors increasing the concrete strength from 40 MPa to 50 MPa resulted in 16% increase in the ultimate load accompanied by 31% increase in the slip near the ultimate point. However, for 16 mm diameter connectors the capacity was found to be increased only by 1.7% for the similar increase in concrete strength.

4 CONCLUSIONS

Push-out tests were performed to study the behaviour of L-shape rebar connector embedded in a concrete slab subjected to monotonic loading. Eight push-out test specimens were designed with two different strength of concrete and four different diameters of the rebar connectors. The effects of concrete strength and rebar diameter on the load-slip curve and failure behaviour of the test specimens were investigated. The following conclusions are drawn within the limited scope of the study:

- The failure of the push-out specimens with lower diameter connectors (10 mm and 12 mm) occurred by shearing of the rebar connectors followed by separation of concrete block on one or both side(s) of the steel section. No cracking or spalling of concrete was observed.
- For 16 mm and 20 mm dia rebar connectors, failure initiated by cracking of concrete followed by crushing of concrete and separation of the concrete block.
- The ultimate capacity and slip at failure of the push-out specimens were significantly influenced by the diameter of the rebar connectors. Increasing the diameter from 16 mm to 20 mm resulted in 21% increase in the ultimate capacity.
- As the diameter of the connector increases, the slip at the failure load increases resulting in ductile failure behaviour. Increasing the bar dia. from 16 mm to 20 mm resulted in about 30% increase in the average slip value.
- Benefits of increasing the rebar diameter increases with the increase in concrete strength.

REFERENCES

AISC (2016), Specification for structural steel buildings, AISC-360-16, Section I8: Steel Anchors, American Institute of Steel Construction, Chicago, IL.

Balasubramanian, R. and Baskar, R. (2016). Study on Behaviour of Angle Shear Connector in Steel-concrete Composite Structures. International Journal of Steel Structures, 16(3), pp. 807-811.

Bouchair, A., Bujnak, J., Duratna, P. and Lachal, A. (2012). Modeling of the steel-concrete push-out test, Steel Structures and Bridges. Procedia Engineering 40, pp. 102 – 107.

CSA. (2009). CSA S16-09, Limit States Design of Steel Structures, Canadian Standards Association, Toronto, ON.

Eurocode 4 (2005). Eurocode 4: Design of composite steel and concrete structures - Part 1-1: General rules and rules for buildings. EN 1994-1-1, European Committee for Standardization (CEN), Brussels.

Mazoz, A., Benanane, A. and Titoum, M. (2013). Push-out Tests on a new Connector of I-shape, International Journal of Steel Structures, Vol. 13, No. 3, pp. 519-528.

Pashan, A. (2006). Behaviour of channel shear connectors: push-out tests, M.Sc Thesis, Department of Civil Engineering, University of Saskatchewan, Canada.

Proc. 2nd International Conference on Structural Engineering Research (iCSER2019)
19-22 Jan 2019, Dhaka, Bangladesh
ISBN: 978-0-6482681-2-3

Effectiveness of Steel Concrete Composite Beams over RCC Beams

Mehedi Bin Sharif[1], Mahbuba Begum[2], Devabrata Dutta[3]

[1]Consultant Structural Engineer, LGED, Dhaka, Bangladesh. E-mail: smehedibin@gmail.com

[2]Professor, Department of Civil Engineering, Bangladesh University of Engineering and Technology (BUET), Dhaka, Bangladesh. E-mail: mahbuba@ce.buet.ac.bd

[3]Undergraduate Student, Department of Civil Engineering, Bangladesh University of Engineering and Technology (BUET), Dhaka, Bangladesh. E-mail: devabrata.ce.buet@gmail.com

Abstract

Steel Concrete Composite column and beam are structural members in which steel and concrete act together through mechanical interlock, friction and adhesion. Steel concrete composite beams are designed and constructed to work as a single unit. They are constructed by connecting steel members with RCC slab using shear connectors. In this case it is possible to utilize the beneficiary effects of RCC and Steel together. Composite beams have been used for a long time. Initially steel members were designed to carry all the design loads. After development of shear connectors, it was possible to resist the slip between the RCC slab and supporting steel members. So the concept of T beam action in concrete was introduced to steel concrete composite beams. RCC is good in compression and steel is good in tension. The combination of RCC and steel provides an excellent lightweight solution. Experimental and numerical research have been done to investigate the properties and behavior of composite beams and its components. An attempt has been made in this study to compare the behavior of RCC and composite beams especially for long span structures. Analytical Finite Element models were prepared to investigate the results. It was observed that composite beams act better than RCC beams for long span structures. Composite beams are stronger and stiffer than RCC beams. They are most effective for long span structures depth requirement of RCC beams can be a problematic issue. Using composite beams story height can be significantly reduced.

Keywords: Steel-concrete composite members, Shear connector, Finite element modeling.

Proc. 2nd International Conference on Structural Engineering Research (iCSER2019)
19-22 Jan 2019, Dhaka, Bangladesh
ISBN: 978-0-6482681-2-3

Experimental Investigation and Comparison of AISC and EUROCODE for Built-Up CFT Columns under Concentric and Eccentric Loading

Nafisa Tabassum[1], Md. Nurul Islam Nahed[2], Raquib Ahsan[3], A.F.S. Ahad Rahman Khan[4]

[1]Postgraduate Student, Department of Civil Engineering, Bangladesh University of Engineering and Technology, Dhaka, Bangladesh. E-mail: nafisatabassum300@gmail.com
[2] Graduate Student, Department of Civil Engineering, Bangladesh University of Engineering and Technology, Dhaka, Bangladesh. E-mail: nahedp008@gmail.com
[3]Professor, Department of Civil Engineering, Bangladesh University of Engineering and Technology, Dhaka, Bangladesh. E-mail: raquibahsan@gmail.com
[4]Postgraduate Student, Department of Civil Engineering, Bangladesh University of Engineering and Technology, Dhaka, Bangladesh. E-mail: ahadrahman005@gmail.com

Abstract

Due to several advantages over traditional reinforced concrete or steel structures, steel-concrete composite structures are gaining popularity. Among the different type composite columns, concrete filled tube (CFT) has limited study to understand its actual behaviour. For built-up sections, the study is very rare. In the current study, experimental program is conducted to find the effect of concrete strength, cross-sectional size and type of loading on ultimate load capacity for a built-up CFT section. The experimental program consisted of seven specimens with concrete strength varying in 48 MPa and 53 MPa with cross-sections of (100x100) mm, (125x125) mm and (150x150)mm. and was subjected to concentric and eccentric loading. Outer steel portion was made by fabricating steel plates and joining by welding. This experiment shows that due to the use of concrete, strength increases significantly (about 46%) than bare steel column but increase in concrete strength is less significant to increase the overall capacity of the column. If the eccentric load is applied, ultimate load capacity reduces about 50% than concentric loading. Codes for composite structures are not fully developed. This study attempts to find out the safety percentage covered by AISC-2010 and EUROCODE-4, as built-up sections are not specifically detailed in the codes. AISC-2010 code is 14% less conservative than EUROCODE-4 in predicting load capacity for concentrically loaded columns. For eccentrically loaded columns, points of failure from experimental analysis lie within the AISC-2010 code predicted safe zone i.e. this code is not sufficient according to the current study to predict the actual behaviour of built-up CFT column sections. EUROCODE-4 shows better predictions for eccentric load conditions, experimental failure point lies outside code predicted safe zone.

Keywords: Composite structure, Built-up sections, Concrete Filled Tube columns, AISC code, EUROCODE.

1. INTRODUCTION

In a composite column, the concrete and steel are combined in such a fashion that the advantages of both the materials are utilized effectively without having to accept the drawbacks. Composite columns are gaining popularity all over the world and hence, composite construction is becoming more popular. The field of composite construction is not fully developed till now. So, the necessity of research on composite columns is becoming more and more important. This study discusses a specific type of composite column: Concrete filled tube. A CFT member contains two materials with different stress-strain curves and distinctly different behavior which makes its behavior complex. The failure

mechanism depends largely on the shape, length, diameter, steel tube thickness, and concrete and steel strengths. Gardner and Jacobson (1967) conducted a theoretical and experimental investigation into the behavior of concrete filled steel tubes as axially loaded compression members and found that at ultimate load the steel tube was at failure but the concrete core was not. Giakoumelis and Lam(2003)experimented the behavior of circular concrete-filled steel tubes (CFT) with various concrete strengths under axial load and compared with the values predicted by Eurocode 4, Australian Standards and American Codes. They found that all three codes predicted lower values than that measured during the experiments. Eurocode 4 gave the best estimation for both CFT with normal and high-strength concrete. Rahman (2016) discussed briefly about different available design codes for designing composite columns. He presented the design specifications and capacity prediction equations along with the detailing rules for FEC columns in AISC-LRFD (2010), Euro code 4 (2005) and ACI-318. The current study focuses on the analysis of the effect of concrete strength, geometric size of cross-section and effect of loading type and attempt to find out safety margins in AISC-2010 and EUROCODE-4 predictions for built-up square shaped concrete-filled tubes.

2. EXPERIMENTAL PROGRAM

For testing purpose, 7 specimens were prepared with varying concrete strength and cross-section. Five specimens had a cross-section of 100mmx100mm and these are designated as CFT 01 to CFT 05. 1 specimen's cross-section was 125mmx125mm and designated as CFT 06. Another specimen was 150mm x 150 mm which is designated as CFT 07. The height of all test columns was 1000mm. Steel casing was made by steel having cross-section of 100mmx1000mm and thickness of 5mm. Four plates were joined by welding to form the casing. The top was enclosed by the steel of cross-section 100mmx100mm and thickness of 5mm. There was no reinforcement or shear connectors in the test specimens. In CFT 01, no concrete was poured. 1st mix was produced with a ratio of cement, coarse aggregate and fine aggregate 1:1.25:2.5 with w/c ratio 0.4 and poured in CFT 02 and CFT 04. 2nd mix was produced with a ratio of 1:1.64:2.6 with w/c ratio of 0.421 and poured in the rest of the columns except CFT 01. From cylinder test done on the day of column testing, compressive strength of this mixes were found 48 MPa and 53 MPa respectively. From coupon test, yield stress of steel was found 345 MPa and ultimate stress was found 487.25 MPa. All tests were performed using a Universal Testing machine (UTM) and Horizon data acquisition software. Three LVDTs were positioned horizontally in three directions at mid height of the specimen to measure the lateral deformations and two were positioned vertically to measure the axial deformations. For data acquisition DEWESOFT software from DEWETRON was used. CFT 01, CFT 02 and CFT 03 were tested for concentric axial load. CFT 04, CFT 05, CFT 06 and CFT 07 were tested for eccentric loading. To apply eccentric axial load, a steel bar was attached on the top of each column and grooved plates were used to cap the rods and thus ensuring proper application of load with certain eccentricity.

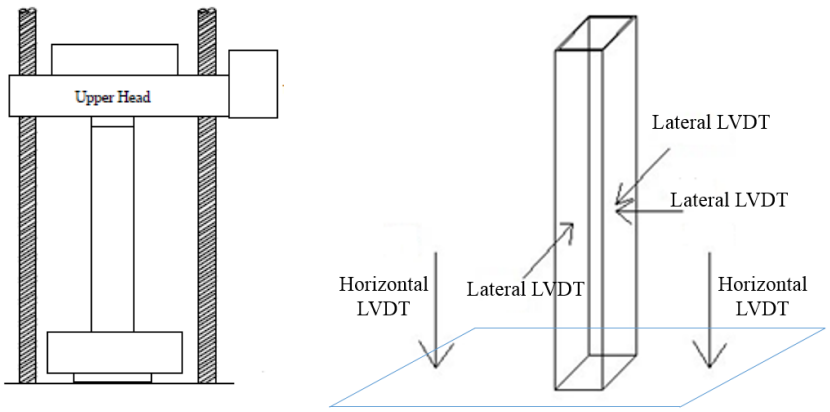

Figure 1: Machinery for testing (schematic drawing)

3. DISCUSSION ON TEST RESULTS

Seven columns were tested under pure compression (concentric) and eccentric loads. Firstly the specimens deformed axially and then failure occurred. Lateral buckling was less than axial deformation, sometimes couldn't be perceived by eyes. As the test specimens were built-up CFT columns, joining portion of steel plates by welding were weak zones and split between them were seen. Figure 2 shows failure mode of CFT 2. Other specimens depicted similar phenomenon.

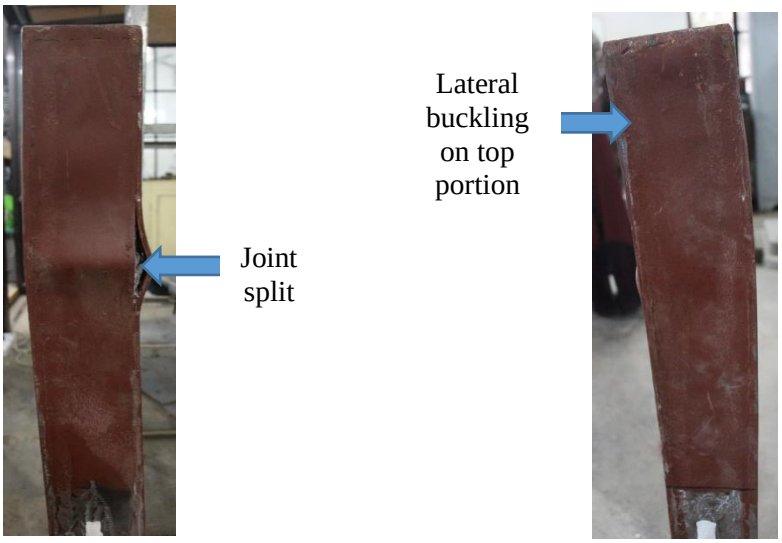

Figure 2: Failure mode of CFT 02

Axial deformation along with their load capacity of different specimens are shown in table 1.

Table 1: Load capacity and deformation for different specimens:

Column Title	Dimension	Infill Concrete Strength	Axial Load	Axial Deformation	Axial Stiffness
	(mm x mm)	(MPa)	(KN)	(mm)	(KN/mm)
CFT 01	100 x 100	No concrete	689.74	8.82	78.20
CFT 02	100 x 100	48	957.54	9.67	99.02
CFT 03	100 x 100	56	1068.3	7.046	151.62
CFT 04	100 x 100	48	510.87	8.12	62.92
CFT 05	100 x 100	56	539.76	7.81	69.12
CFT 06	125 x 125	56	720.07	10.24	70.38
CFT 07	150 x 150	56	669.32	8.85	75.63

3.1. Effect of Variation in Concrete Strength on Axial Capacity

The capacity of hollow steel column under concentric loading was 689.74kN. Capacity of column filled with concrete strength of 48MPa (CFT 02) and 53 MPa (CFT 03) was 957.54 KN and 1068.3 KN under concentric loading. From these data we can find that there is 38% increase in strength than hollow steel tube while using 48 MPa concrete infill. Again, 54% increase in strength is found by using 53 MPa concrete than bare steel column. These values indicate that composite columns are significantly important for carrying more loads without changing the cross-sectional area. Again with the change of 5 MPa concrete strength, overall strength has increased about 10%. Similar type of comparison can be made by applying eccentric loading in test specimens. Eccentrically loaded CFT 04 was infilled with 48 MPa concrete which failed upon reaching 510.87 KN load and CFT 05 was infilled with 53 MPa concrete which failed at 539.76 KN load. For eccentric loading, with increase of

5 MPa strength of concrete, column capacity increases about 5%. These indicates that, increasing the strength of concrete has less significance in increasing the strength of composite columns; especially if the load comes to the structure eccentrically.

3.2. Effect of Loading Type on Axial Capacity

Eccentricity in loading has great impact on capacity of column. A column that is subjected to eccentric loading has lower capacity than loaded by concentric load while keeping the same dimension and concrete strength. CFT 02 and CFT 04 are of 100 mm x 100 mm cross-section and filled with 48 MPa concrete. From table 1 it is found that due to eccentricity in loading, capacity of CFT 04 has reduced about 47%. Similar comparison can be made between the capacity of CFT 03 and CFT 06 which shows about 50% reduction due to eccentric loading. These indicates that if load comes to the structure eccentrically, it will significantly reduce the column capacities.

3.3. Comparative Study of Axial Stiffness for Variation in Test Parameters

Comparing values of CFT 01, CFT 02 and CFT 03, it is found that CFT 02 has 21% and CFT 03 has 48% increased stiffness than hollow steel tube indicating composite columns have significant impact over bare steel column in increasing axial stiffness of the column. Again, comparing CFT 02 and CFT 03, axial stiffness has increased 34% due to increase in concrete strength. This indicates that, though increase in concrete strength had less significance in increasing the capacity of the column, it bears great significance in increasing the stiffness. By comparing CFT 02 with CFT 04, 36% reduction in stiffness is seen due to the application of eccentric loading than concentric loading. Other test parameters were same for these specimen. For CFT 03 and CFT 05, 54% reduction in stiffness is found. This indicates that if load comes to the structure eccentrically, stiffness will be reduced to a great extent. From the comparison of CFT 05, CFT 06 and CFT 07, it is found that though cross-sectional area was increased, stiffness increased slightly. For these specimens, with increase in size, eccentricity was also increased. This might be the reason of less increase in stiffness.

4. ANALYTICAL STUDY USING DESIGN CODES FOR CONCENRICALLY LOADED COLUMNS

AISC-2010 and EUROCODE-4 has provisions for composite column design but there is no special requirements for composite column by built-up sections. For this study, analytical values are found using the existing equations in AISC-210 and EUROCODE-4. Design of composite column is given in chapter I in AISC-2010 guideline. In this study the strength of composite sections is be computed based on the plastic stress distribution method. Formula calculating capacity in pure axial condition is given below for filled compact composite member.

$$P_{no} = F_y A_s + C_2 f_c' (Ac + Asr \frac{Es}{Ec}) \quad (1)$$

Here, A_c and A_s indicates area of concrete (mm^2) and steel section, (mm^2) respectively. P_{no} means nominal axial capacity of CFT column. Using equations (1), axial capacity for concentrically loaded columns were determined as shown in table 2. For finding axial capacities of column using EUROCODE-4, equation (2) is used.

$$N_{pLRd} = A_a f_{yd} + 0.85 A_c f_{cd} + A_s f_{sd} \quad (2)$$

Here, $N_{pl,Rd}$ is design value of the plastic resistance of the composite section to compressive normal force f_{cd} and f_{yd} means design value of the cylinder compressive strength of concrete and design

value of the yield strength of structural steel respectively. Here, $f_{cd} = \frac{fc'}{\gamma c}$ and $f_{yd} = \frac{fy}{\gamma s}$;γ_C is partial reduction factor for concrete which is taken as 1.5 and γ_s is partial reduction factor for steel which is taken as 1.15. Values obtained by using equation (3) is shown in table 2.

Table 2: Ultimate Load Capacity of concentrically Loaded Columns

Specimen Designation	Ultimate Capacity		
	Experimental Program (KN)	Using AISC-2010 (KN)	Using EUROCODE-4 (KN)
CFT 1	689.74	648.17	570
CFT 2	957.54	971.3	829.2
CFT 3	1068.3	1005.6	856.17

Comparing the experimental value with the AISC code predicted values, it is found that the ultimate load capacity for CFT-01 (Hollow Steel Tube) can be predicted by the code with 6% conservative value. For CFT-03, code predicted value is 5.8% conservative than the experimental result. These values indicate that code predicted values are not significantly conservative. Again, value for CFT-02 shows more capacity in the code prediction than the experimental result. The values are about 1.5% higher than the code predicted value. This column had joint split during failure. This can be a probable reason for lower experimental value in this case as the code is not designed for built-up sections. Again, EUROCODE-4 predicts the ultimate load capacity of hollow column 17.4% conservatively. For CFT-02 and CFT-03, the value of ultimate load capacity is predicted on 14% and 19% conservative side for the respective columns in comparison with experimental value. This indicates that EUROCODE-4 is more conservative than AISC-guideline and thus recommended in design where source of uncertainty is greater.

5. ANALYTICAL STUDY USING DESIGN CODES FOR ECCENRICALLY LOADED COLUMNS

CFT-04, CFT-05, CFT-06 and CFT-07 was loaded eccentrically. Eccentricity for CFT-04 and CFT-05 was 25 mm. CFT-06 had 37.5mm eccentricity and CFT-07 had 50 mm eccentricity. For combined effect of axial force and flexure, P-M curves are drawn by following AISC guideline. The zone inside the curved area is considered as safe zone where for different combinations of axial force and flexure, failure should not occur. But for all the eccentrically loaded columns in this test program, failure point is under the curve. Failure point lies in code predicted safe zone. This phenomenon depicts that AISC-2010 is not sufficient to predict the failure point when the load comes eccentrically and thus if this code is to be followed for designing any CFT structure where eccentric load is likely to be occurred, greater safety margin should be kept. The experimental and numerical load capacities of eccentrically loaded CFT columns were compared with the design strength predicted by the EUROCODE-4. Formation of interaction diagram according to this code is done without considering the length effect. For CFT-04, CFT-05, CFT-06 and CFT-07 columns, failure points from both experimental investigations and numerical analysis was outside the P-M curve. The columns didn't fail within the safe region as mentioned by this code. This depicts that EUROCODE-4 is more reliable in predicting the load capacity when eccentric load is supposed to come on the structure. Interaction curve formed using AISC-2010 and EUROCODE-4 for CFT 04 is shown in figure 3. Interaction curves for other eccentrically loaded columns show the same phenomenon.

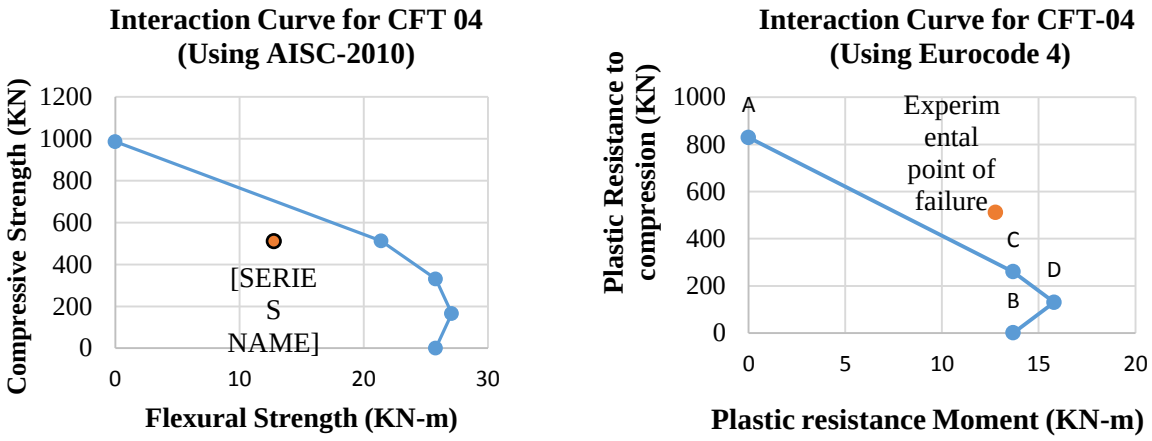

Figure 3: Interaction Curve for CFF-04 using AISC-2010 and EUROCODE-4

6. CONCLUSIONS

Composite columns can carry 45% more loads (on average) for the same cross-sectional area in comparison with bare steel column. For concentrically loaded columns, load capacity increases 10% for 5 MPa increase in strength whether for eccentric loading, load capacity increases only 5%. About 48% reduction (on average) is found for similar type of column due to change in loading type. About 30% more stiffness is found due to composite column than bare steel column. Though increase in concrete strength had less significance in increasing the capacity of the column, it bears great significance in increasing the stiffness. For 5 MPa change in concrete strength, 34% stiffness increased. If load comes to the structure eccentrically, stiffness will be reduced to a great extent. Again, AISC code predicted values are not significantly conservative for concentric loads. For the tests conducted in this study, AISC-2010 is found not sufficient to predict the failure point when the load comes eccentrically, failure point is found within the code predicted safe zone for all the eccentrically loaded columns. If this code is to be followed for designing any CFT structure where eccentric load is likely to occur, a greater safety margin should be kept. EUROCODE-4 is more conservative than AISC-guideline in predicting concentric loads and thus recommended in design where source of uncertainty is greater. EUROCODE-4 is more reliable in predicting the load capacity when eccentric load is supposed to come on the structure. Failure points are found outside the P-M curve for all the eccentrically loaded specimens.

REFERENCES

AISC (American Institute of Steel Construction), (June 22, 2010).Specification for Structural Steel Buildings.

Eurocode 4, (2004). Design of composite steel and concrete structures. BS EN: 1994-1-1:2004

Gardner, N. J., and Jacobson, E. R. (1967). Structural Behavior Of Concrete Filled Steel Tubes. ACI J., 64(7): 404-412.

Giakoumelis, G. and Lam, D., (2003). Axial Capacity of Circular Concrete-Filled Tube Columns. Journal of Constructional Steel Research, 60 (2004):1049–1068

Rahman, M.S., (2016). Behaviour and Strength of Fully Encased Composite Columns. Thesis of doctor of philosophy, Department of Civil Engineering, BUET.

Proc. 2nd International Conference on Structural Engineering Research (iCSER2019)
19-22 Jan 2019, Dhaka, Bangladesh
ISBN: 978-0-6482681-2-3

Experimental Investigation on Concentrically Loaded Square Concrete-Filled Steel Tubular Columns

MD. Mofizul Islam[1], Rubieyat Bin Ali[1], Mahbuba Begum[2] and Md. Soebur Rahman[3]

[1] Graduate Student, Department of Civil Engineering, Bangladesh University of Engineering & Technology (BUET), Dhaka, Bangladesh
[2] Professor, Department of Civil Engineering, Bangladesh University of Engineering &Technology (BUET), Dhaka, Bangladesh
[3]Associate Professor, Military Institute of Science and Technology (MIST), Dhaka, Bangladesh
Corresponding author's E-mail: miltonruet94@gmail.com

Abstract

This paper presents an experimental investigation on the behavior of CFST columns regarding four parameters: concrete compressive strength, tube thickness, cross sectional dimension and column slenderness. Total nine CFST columns with square cross section were tested under concentric loading. The tested columns had cross sectional width (B): 100, 125 and 150 mm; length (L): 1000, 500 and 300 mm; tube thickness (t): 3, 4 and 5mm; and concrete compressive strengths ($f_c^{/}$): 27, 35 and 44 MPa. The influence of these parameters on the failure mode, load-strain response and ductility of the square CFST column is discussed. Finally, the experimental results were compared with the existing codes: AISC-LRFD, EC-4, AS and Canadian Standard Association CSA, which indicates good agreement between experimental and code predicted results.

Keywords: CFST column, local buckling, failure mode, load-strain response, Ductility.

1. INTRODUCTION

Concrete filled steel tube (CFST) column consists of a hollow steel tube filled with concrete. This composite section offers numerous structural benefits over reinforced concrete and steel only sections, including high strength, high ductility and large energy absorption capacities. There is no need for the use of shuttering during concrete construction; hence, the construction cost and time are reduced. In CFST columns the steel tube not only serves as formwork but also provides continuous confinement to concrete core resulting in enhanced strength and ductility of concrete. These advantages have been widely exploited and have led to the extensive use of concrete-filled tubular structures in high rise buildings, bridges and offshore structures (Shanmugam and Lakshmi 2001, Susantha et al. 2001, Sakino et al. 2004).

Extensive experimental and numerical studies have been carried out by several researchers (Han et al. 2014, Zeghiche and Chaoui 2005, Xiamuxi and Hasegawa 2012, Zhu et al. 2010) on concentrically and eccentrically loaded CFST columns with various geometric and material properties. Most of this research work has been performed on CFST columns constructed with available standard tube shapes. However, limited research has been found on CFST columns in built-up steel sections. Current design rules for CFST columns are specified in AISC-LRFD (2010), ACI 318R (2014), EC-4 (1994), British standard BS 5400 (2005) and Canadian Standard Association CSA (2009). CFST column is a new system for the construction industry of Bangladesh. In the upcoming version of Bangladesh National Building Code (BNBC 2016) the design guidelines for CFST columns are included which is adopted from AISC 2005 specifications. The

applicability of these design provisions in the construction environment of Bangladesh needs to be explored. To this end, an attempt has been made in this study to investigate the behaviour and strength of the CFST columns constructed with built-up steel section and locally available materials.

2. EXPERIMENTAL INVESTIGATION

2.1 Test specimens

In the experimental study, nine columns were tested for concentrically applied axial load. The parameters considered in the test were: concrete compressive strength ($f_c^{/}$)**:** 27 Mpa to 44 Mpa; width to thickness ratio (B/t): 25 to 41.6; length to width ratio (L/B): 3 to 10.

Table 1. Properties of CFST test columns

Specimen design	Cross-sectional size	Width to thickness ratio	Length to width ratio	Properties of test concrete			Properties of steel plate			
				Concrete compressive strength	Modulus of elasticity	Ultimate Strain	Yield stress	Ultimate stress	Modulus of elasticity	Yield strain
	B x t x L	B/t	L/B	$f_c^{/}$	E_c	ε_{cu}	f_y	f_u	E_s	ε_y
	(mm x mm x mm)			(MPa)	(MPa)	(με)	(MPa)	(MPa)	(MPa)	(με)
C1	100 x 4 x 1000	25	10	27	24734	1900	350	428	200000	2148
C2	100 x 4 x 1000	25	10	35	28160	1750	350	428	200000	2148
C3	100 x 4 x 1000	25	10	44	31574	1600	350	428	200000	2148
C4	125 x 3 x 1000	41.6	8	35	28160	1750	350	428	200000	2148
C5	125 x 4 x 1000	31.2	8	35	28160	1750	350	428	200000	2148
C6	125 x 5 x 1000	25	8	35	28160	1750	350	428	200000	2148
C7	100 x 4 x 500	25	5	35	28160	1750	350	428	200000	2148
C8	100 x 4 x 300	25	3	35	28160	1750	350	428	200000	2148
C9	150 x 4 x 1000	37.5	6.6	35	28160	1750	350	428	200000	2148

2.2 Material properties

The mechanical properties of steel materials were measured by tension coupon test according to ASTM D638-02a (2003). Typical stress-strain diagram is shown in Figure 1. The results of the steel coupon tests are presented in Table 1.

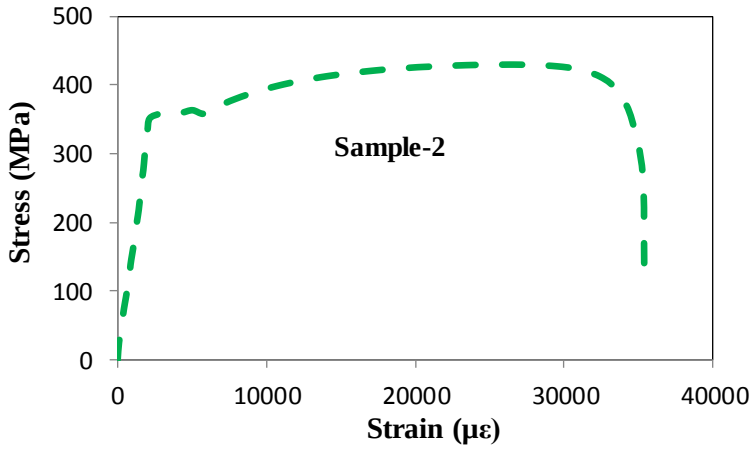

Figure 1. Stress strain diagram from tension coupon test of the steel section

Concrete mixes (M20, M30 and M40) were prepared in the laboratory. For material testing, six concrete cylinders (4inch*8inch) of each batch of concrete were cast at the time of construction of test specimen. Table 1 summerizes the mean compressive strengths of the tested cylinders for the test sepcimens.

2.3 Specimen preparation

In the fabrication of specimens, all the steel tubes were fabricated by joining two channels through continuous welding. Before the placement of concrete, each steel tube was welded to 20mm thick steel bottom plate. Concrete was poured into these hollow tubes and vibrator was used for proper compaction of concrete. After grinding the top surface, another end plate was welded to each of specimen for uniform distribution of the applied load.

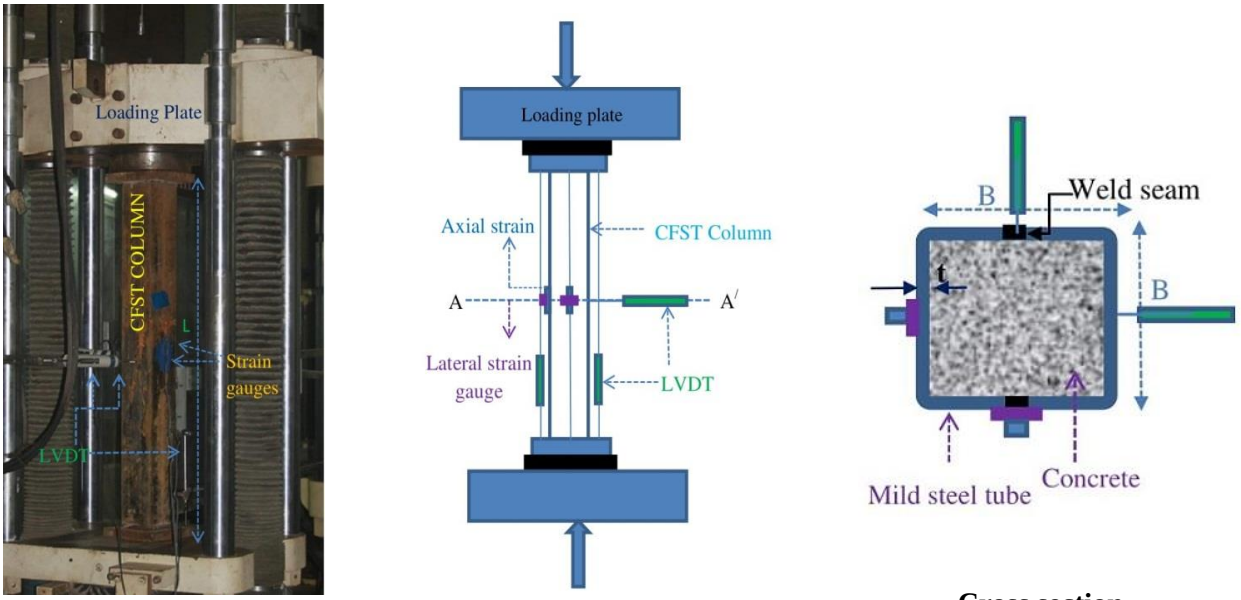

(a) **Elevation (b)** **Cross section (C)**

Figure 2. Test setup for CFST columns

2.4 Test setup

All the tests were performed using a 2000kN loading capacity universal testing machine (UTM). The columns were aligned vertically and centred in the UTM to provide uniform bearing. The experimental setup of the tested specimens is shown in Figure 2. Four strain gauges were used on two faces of steel tube to measure the longitudinal and transverse strains of the tube, where linear variable differential transducers were used to measure out of plane deflection in vertical and lateral direction. Displacement control loading at a rate of 0.5 mm/min was used throughout the loading of the test specimens.

3. RESULTS AND DISCUSSION

3.1 Failure modes

Generally global slenderness ratio (L/D) and plate slenderness ratio (B/t) were found to have a significant effect on the failure mode of the CFST column as shown in Figure 3. Three types of failure modes, as presented in Table 2, were observed in the test columns. For columns with heigher L/D ratio, failure was initiated by global buckling followed by crushing of concrete. Columns with higher B/t ratio failed by

outward local buckling followed by crushing of concrete. The stub column specimens showed local buckling and concrete crushing at failure.

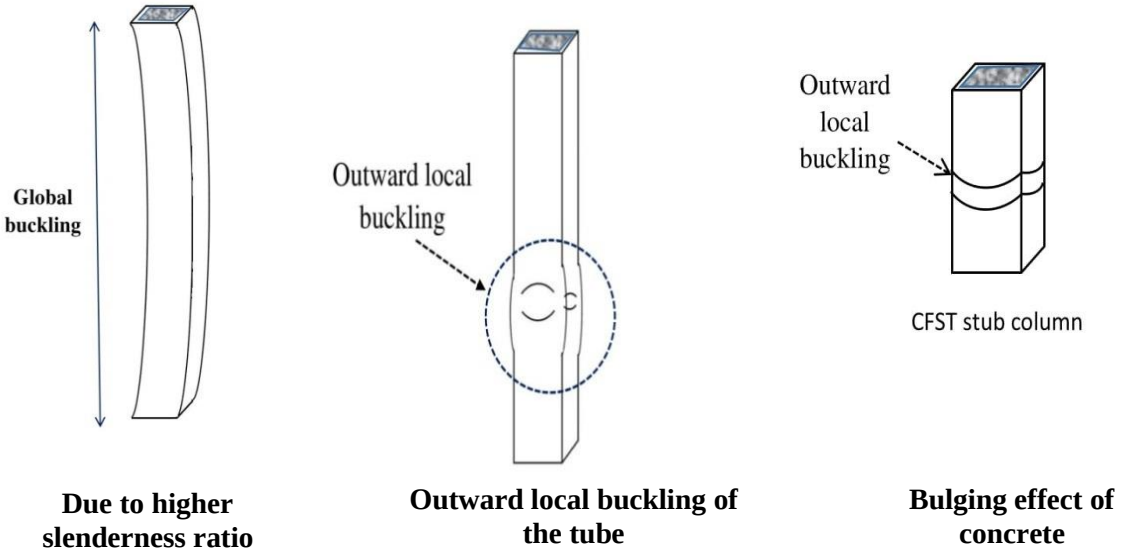

Figure 3. Typical failure modes of test columns

Specimens with higher cross sectional width presented more pronounced outward local buckling of the tube with or without slippage between steel and concrete. Slippage indicates the bulging formation of the specimen without internal work of the concrete infill and in case of proper confinement, failure occurred without slippage by the lateral expansion of the concrete.

Table 2. Test results of the test columns

Specimen design.	Cross-sectional size	Concrete compressive strength	Yield stress	Peak load	Strain at peak load	Failure pattern
	B x t x L	$f_c^{/}$	f_y	P_u	ε_u	
	(mm x mm x mm)	(MPa)	(MPa)	(KN)	(με)	
C1	100 x 4 x 1000	27	350	697	7098	Global buckling
C2	100 x 4 x 1000	35	350	729	5619	Global buckling
C3	100 x 4 x 1000	44	350	804	5571	Global buckling
C4	125 x 3 x 1000	35	350	930	6706	Outward local buckling
C5	125 x 4 x 1000	35	350	1011	7204	Outward local buckling
C6	125 x 5 x 1000	35	350	1269	8143	Outward local buckling
C7	100 x 4 x 500	35	350	770	5956	Outward local buckling
C8	100 x 4 x 300	35	350	810	6359	Welding failure
C9	150 x 4 x 1000	35	350	1340	6500	Outward local buckling

3.2 Axial load versus axial strain relations

The axial load vs. axial strain diagrams are shown in Figure 4. The axial loads were calculated from the testing machine and axial strains were calculated from the average value of strain gauges and LVDTS. To measure the strains: strain gauges were used before tube buckling and after that, displacement readings of the LVDTS were divided by the length of the specimens (Yu et al. 2016).

It can be seen from Figure 4 (a) that, the ascending curves of the specimens become steeper with the increase of concrete strength. It indicates that as the concrete strength increased, the stiffness and peak load of the specimens also increased. This is due to the presence of less micro cracks in higher strength concrete. The descending branch represents gradual decrease of the peak load for normal strength concrete and specimens with higher strength concrete showed sudden drop from the peak load. Therefore, as the concrete strength increases the axial strength of the column increases sacrificing it's ductility.

Figure 4 (b) shows the comparative effect of thickness of the tube on the behavior of CFST columns by changing width to thickness ratio (B/t). The elastic range of the specimens increased with the increase of the tube thickness or the decrease of B/t ratio. This may be attributed due to the higher rigidity and steel contribution of the thicker tube. Specimens with thicker steel tube also exhibited better deformation capacity and peak load due to its greater lateral support to the concrete core.

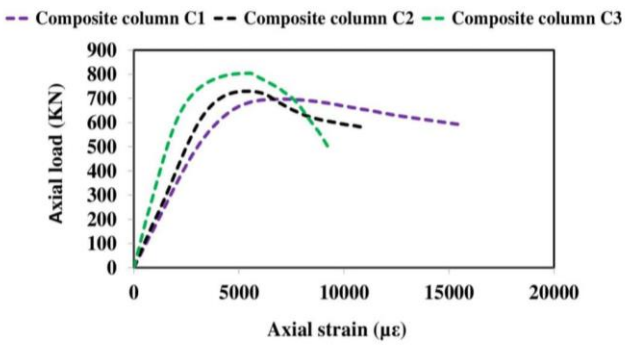

(a) Effect of concrete compressive strength ($f_c^{/}$)

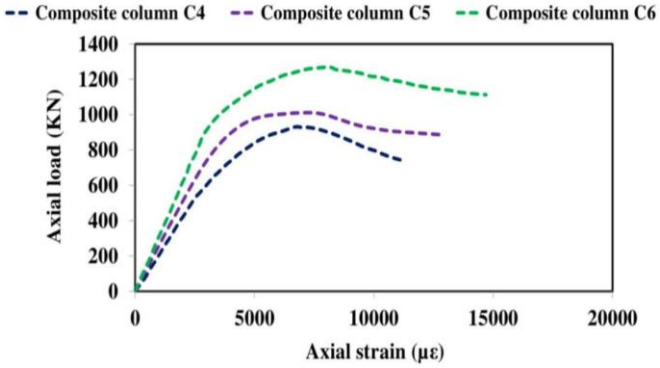

(b) Effect of thickness (t)

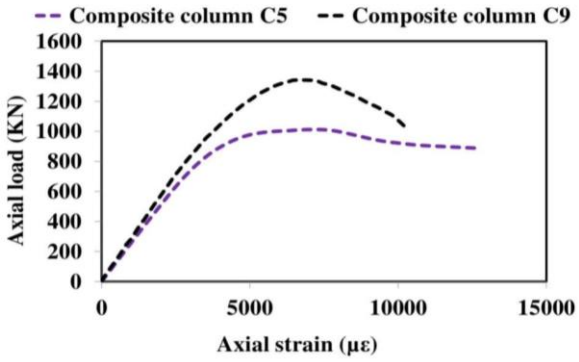

(c) Effect of width (B)

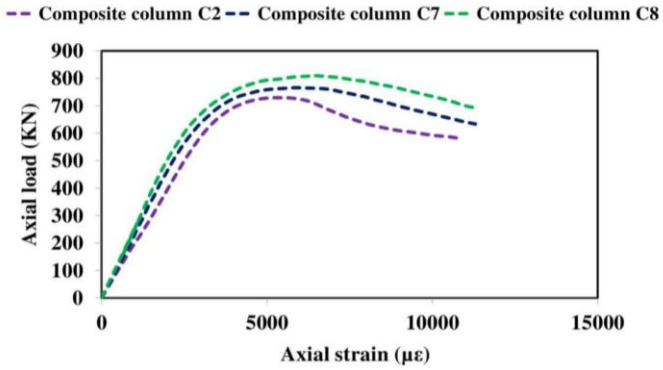

(d) Effect of Column overall slenderness (L/B)

Figure 4. Axial load (P_u) versus axial strain (ε) diagrams

Figure 4 (c) represents the cross sectional effect on the specimens by changing B/t ratio. It can be observed that the load carrying capacity and the deformation capacity increased with the increase of cross sectional width or B/t ratio. This is because of increasing cross sectional width of the specimens resulting greater cross sectional area of the column. It can be concluded that, increasing thickness or cross sectional width can improve the overall quality of the CFST column.

The effect of global slenderness ratio was observed considering different length of the specimens as shown in Figure 4 (d). As the length of the columns increased, the columns with higher slenderness had a lower maximum load than columns with lower slenderness and the load reduced quickly once the ultimate load was reached. This is attributed due to the greater flexibility of columns with higher slenderness ratio.

4. COMPARISON OF EXPERIMENTAL RESULTS WITH STANDARD CODE PREDICTIONS

In this study, four design codes: AISC-LRFD (2010), AS 5100 (Australian Standard) (2004), CSA S16 (Canadian Standards Association) (2009), EC-4 (1994) were applied to predict the ultimate strength of the tested specimens. Afterwards, the predicted capacities were compared with the tested results. Design codes present different expression for predicting ultimate strength. However, these strength predictors express the steel and concrete contribution of the CFST column. In design calculations, reduction factors or material safety factors are set to unity. In order to determine the error of the predicted capacity, the experimental results were divided by the predicted results as shown in Table 3. The results indicate that the codes somewhat overestimated the capacities in a safe range. Among them, AISC presented best prediction with a mean of 1.01 and Standard deviation of 0.03. EC4 and AS predicted the results about 8% higher than the experimental results; whilst CSA predicted 2% higher capacity. In general, all the codes showed good agreement with the experimental results.

Table 3. Code prediction for square CFST columns

Column design.	B x t x L	f_c'	f_y	P_{exp}	P_{AISC}	P_{AISC-L}	P_{EC4}	P_{CSA}	P_{AS}	P_{AISC} / P_{exp}	P_{AISC-L} / P_{exp}	P_{EC4} / P_{exp}	P_{CSA} / P_{exp}	P_{AS} / P_{exp}
	(mm x mm x mm)	(MPa)	(MPa)	(KN)	(KN)	(KN)	(KN)	(KN)	(KN)					
C1	100 x 4 x 1000	27	350	697	724	687	757	722	757	1.04	0.99	1.09	1.04	1.09
C2	100 x 4 x 1000	35	350	729	777	736	821	775	821	1.07	1.01	1.13	1.06	1.13
C3	100 x 4 x 1000	44	350	804	845	798	900	841	900	1.05	0.99	1.12	1.05	1.12
C4	125 x 3 x 1000	35	350	930	924	890	998	921	998	0.99	0.95	1.07	0.99	1.07
C5	125 x 4 x 1000	35	350	1011	1074	1037	1146	1071	1146	1.05	1.02	1.12	1.05	1.12
C6	125 x 5 x 1000	35	350	1269	1201	1160	1269	1198	1269	0.95	0.91	1.00	0.94	1.00
C7	100 x 4 x 500	35	350	770	777	767	821	775	821	1.00	0.99	1.06	1.00	1.06
C8	100 x 4 x 300	35	350	810	777	774	821	775	821	0.95	0.95	1.01	0.95	1.01
C9	150 x 4 x 1000	35	350	1340	1403	1368	1508	1365	1508	1.05	1.02	1.13	1.02	1.13
							Mean			1.01	0.98	1.08	1.02	1.08
							Standard deviation			0.03	0.04	0.05	0.05	0.05

5. CONCLUSIONS

In this study nine square CFST columns with a variety of geometric and material properties were tested under axial compression. Effects of global slenderness ratio (L/B), tube slenderness ratio (B/t) and concrete strength on the load versus axial strain curve and failure behaviour of the test columns were investigated. Comparisons of the test results were also made with several existing design codes. The following conclusions can be drawn within the limited scope of this study:

1. The typical failure mode of the specimen was characterized by local buckling of the steel tube and crushing of concrete, but the failure of the specimens with $L/B \geq 10$ exhibited global buckling. Specimens with higher cross-sectional width showed more pronounced outward buckling.

2. Stiffness and ultimate capacity of the tested column decreased with the decrease of cross-sectional width by tube thickness (B/t) ratio, whilst they increased with the increase of concrete compressive strength and the decrease of the length of the specimen.

3. Axial strain at peak load and ductility of the tested specimen increased with the decrease of cross sectional width, concrete compressive strength and length of the specimen, whilst they decreased with the decrease of tube thickness.

4. The codes somewhat overestimated the ultimate load in a safe range, having lower difference between the predicted and experimental results.

ACKNOWLEDGEMENTS

All assistance including laboratory, computing and financial supports from Bangladesh University of Engineering and Technology (BUET), Dhaka, Bangladesh are gratefully acknowledged. In addition, the authors would like thank McDonalds Steel Building Products Ltd. for the supply of the tubular steel sections for the CFST specimens.

REFERENCES

ACI 318R (2014), "Building Code Requirements for Structural Concrete". American Concrete Institute, ACI, Detroit.

AISC-LRFD (2010), "AISC Manual for Steel Construction". American Institute for Steel Construction, USA.

AS5100 (2004), "Bridge Design-steel and Composite Construction". Australian Standard.

ASTM D638-02a (2003), "Standard test method for tensile properties of plastics". American Society of Testing Materials.

BNBC (2016), "Bangladesh National Building Code". Dhaka, Draft version.

CSA Standard S16 (2009), "Design of steel structures". Published by Canadian Standards Association, A not-for-profit private sector organization 5060 Spectrum Way, Suite 100, Mississauga, Ontario, Canada.

European Committee for Standardization (1994). "Eurocode 4: Design of Composite Steel and Concrete Structures". CEN.

Han, L.H., Li, W. and Bjorhovde, R. (2014). "Developments and advanced applications of concrete-filled steel tubular (CFST) structures: Members." Journal of Constructional Steel Research, 100, 211-228.

Ren, Q.X., Zhou, K., Hou, C., Tao, Z. and Han, L.H. (2018). "Dune sand concrete-filled steel tubular (CFST) stub columns under axial compression: Experiments." Thin-Walled Structures, 124, 291-302.

Sakino, K., Nakahara, H., Morino, S. and Nishiyama, I. (2004). "Behavior of centrally loaded concrete-filled steel-tube short columns." Journal of Structural Engineering, 130(2), 180-188.

Shanmugam, N.E. and Lakshmi, B. (2001). "State of the art report on steel–concrete composite columns." Journal of constructional steel research, 57(10), 1041-1080.

Standard, B. (2005). "Steel, concrete and composite bridges—Part 5: Code of practice for the design of composite bridges." British Standards Institution, BS, 5400-5.

Susantha, K.A.S., Ge, H. and Usami, T. (2001). "A capacity prediction procedure for concrete-filled steel columns." Journal of Earthquake Engineering, 5(04), 483-520.

Xiamuxi, A. and Hasegawa, A. (2012). "A study on axial compressive behaviors of reinforced concrete filled tubular steel columns." Journal of Constructional Steel Research, 76, 144-154.

Yu, X., Tao, Z. and Song, T.Y. (2016). "Effect of different types of aggregates on the performance of concrete-filled steel tubular stub columns." Materials and Structures, 49(9), 3591-3605.

Zeghiche, J. and Chaoui, K. (2005). "An experimental behaviour of concrete-filled steel tubular columns." Journal of Constructional Steel Research, 61(1), 53-66.

Zhu, M., Liu, J., Wang, Q. and Feng, X. (2010). "Experimental research on square steel tubular columns filled with steel-reinforced self-consolidating high-strength concrete under axial load." Engineering Structures, 32(8), 2278-2286.

Proc. 2nd International Conference on Structural Engineering Research (iCSER2019)
19-22 Jan 2019, Dhaka, Bangladesh
ISBN: 978-0-6482681-2-3

Shear Strengthening of Damaged RC Beam Using Externally Bonded Steel Plate with Embedded Connector and Steel Bar

Md Ashraful Alam[1], Nazmul Hossain[2], H.C. Debnath[2], P.K. Ghosh[2] and M.M. Rahman[2]

[1]Associate Professor, Department of Civil Engineering, University of Asia Pacific, Dhaka-1215, Bangladesh
[2]Student, Department of Civil Engineering, University of Asia Pacific, Dhaka-1215, Bangladesh
Corresponding author's E-mail: dr.ashraful@uap-bd.edu

Abstract

Shear strengthening of deficient or damaged reinforced concrete beam using externally bonded plate is the most popular choice. However, premature debonding at concrete-adhesive interface is the main limitation of the bonded plate to obtain ultimate shear strength of retrofitted beam. The main aim of this research was to prevent or delay the debonding of externally bonded steel plate of shear strengthened RC beam using embedded connector and steel bar. Three reinforced concrete beams were completely damaged and shear strengthened to investigate the effects of embedded connector and steel bar. The bond strengths of externally bonded steel plate with embedded connector and steel bar were also experimentally investigated through indirect pull out test of five RC prisms. Results showed that the bond strength of externally bonded steel plate with embedded steel bar was 5.6 MPa which was 66% and 48% higher as compared to those of prisms without and with connectors respectively. Plate with connector showed debonding at concrete-adhesive interface, whereas, plate with embedded steel bar showed concrete cover separation. All damaged shear strengthened beams fully re-stored the capacity of original beams. Embedded connector and steel bar prevented debonding of steel plate at concrete-adhesive interface. As compared to others, shear strengthened beam with embedded steel bar had higher shear capacity and showed more ductile behaviour.

Keywords: Shear strengthening, Externally bonded plate, Debonding, Connector, Embedded bar

1. INTRODUCTION

Steel plate is worldwide popular construction material due to its well know mechanical properties and has been used for shear strengthening of deficient reinforced concrete beams [1-5]. Nevertheless, premature debonding of steel plate has found to be the most common and major drawback of the system [6-10]. Externally bonded steel plate technique would be the most effective method for shear strengthening of RC beam as compared to those of carbon fibre reinforced polymer (CFRP) laminate if the debonding failure is eliminated. Various anchor systems i.e. bolts, U-jacket, U wrap, spike and feng had been proposed by researchers in shear strengthening of RC beam with steel plate, CFRP laminate and fabrics to eliminate debonding failure [11-17]. It was reported that U-jacket and U wrap could enhance the capacity of beam, debonding of laminates and plates yet to be prevented. Furthermore, bolts, feng and spike could be effective to prevent debonding, however, these anchor systems may not be the practical choices because of the usages of hole on the shear strengthening plates. Generally, the plate was debonded at concrete-adhesive interface once the interfacial stresses exceeded the bond strength of concrete or bond strength of adhesive. In most cases, debonding happened at concrete adhesive interface rather than plate adhesive interface. It was because of lower bond strength of concrete as compared to adhesive. Since, weaker bond strength causes debonding of externally bonded plates, research on effective method to enhance bond strength for eliminating debonding of steel plate would be novel.

This study proposed embedded connector and embedded steel bar systems at concrete adhesive interface to enhance the interfacial bond strength of externally bonded steel plate for shear strengthening of damaged reinforced concrete beams. The capacities of connectors to enhance the bond strength of externally bonded steel plates were experimentally predicted. The structural performances of shear strengthened reinforced concrete beams using the proposed methods were also experimentally investigated.

2. EXPERIMENTAL PROGRAMME

2.1. Specimens

Five prisms each with dimension of 300 mm x 150 mm x 150 mm were prepared and tested to investigate bond strength of externally bonded plates. The details of all prism specimens are shown in Table 1. Prism PNC was strengthened with steel plate only without connector and bar and prisms P-1and P-2 were strengthened using steel plate with embedded connectors. Others two prisms PC-1and PC-2 were strengthened using steel plate with embedded steel bar.

A total three reinforced concrete beam specimens each with dimension of 1300mm long, 150 mm width and 250 mm depth were prepared for shear strengthening. Table 2 shows the details of all beam specimens. Beam SB was shear strengthened using steel bar where beams SPC and SPB were shear strengthened using steel plate with embedded connectors and steel plate with steel bar, respectively.

Table 1. Prism specimens

Prism specimens			**Steel plate**		**Steel bar**	**Embedded connector**	
Number	Designation	Dimension (mm x mm x mm)	Width (mm)	Thickness (mm)	Diameter (mm)	Diameter (mm)	No. of connectors
1	PNC	300X150X150	25	2.5	--	--	--
2	P-1	300X150X150	25	2.5	--	12	2
3	P-2	300X150X150	25	2.5	--	12	2
4	PC-1	300X150X150	25	2.5	8	--	--
5	PC-2	300X150X150	25	2.5	8	--	--

Table 2. Beam specimens

Beam specimens			**Steel plate**		**Steel bar**	**Embedded connector**	
Number	Designation	Dimension (mm x mm x mm)	Width (mm)	Thickness (mm)	Diameter (mm)	Diameter (mm)	No. of connectors
1	SB	1300X250X150	--	--	8	--	--
2	SPC	1300X250X150	25	2.5	8	--	--
3	SPB	1300X250X150	25	2.5	--	12	2

2.2. Preparation of Specimens

In each of the reinforcement concrete prisms, two -16 mm diameter high yield strength deformed bar were used. The 16 mm bars were strongly welded at 90^0 angle with 6 mm thickness steel plate of 150 mm x 100 mm as shown in Figure 1. The bars were 150 mm inside the prism and 100 mm outside the prism which were used to pull from both sides during pull out test. Four stirrups with dimension of

100mm x 100mm were used in each prism (Figure 1).

Two -16 mm diameter flexural reinforcement and 6 mm diameter shear reinforcement with the spacing of 130 mm were used to prepare the beam specimens shown in Figure 2. The yield strength of shear reinforcement was 420 MPa. Concrete with strength of 23 MPa was used to cast the prisms and beam specimens. The beam specimens were tasted to damage after 28 days of casting shown in Figure 3 and
4.

Figure 1. Preparation of prism

Figure 2. Preparation of beam

Figure 3. Damaged beam

Figure 4. Damaging the beam

Figure 5. Prepared surface of beam

Figure 6. Embedded connector

Figure 7. Embedded steel bar

Figure 8. Strengthened beam

2.3. Strengthening of prisms and beams

The loose particles on bonding surfaces of prisms and damaged beams were removed using diamond cutter shown in Figures 5. The dust was then cleaned with thinner. The steel plates were fixed with the concrete substrate using Sikadur-31 CFN adhesive. The well-mixed adhesive was spread on the bonding area of the concrete surface to fill the putty and cavity and also from a thin layer of uniform level. The adhesive was applied with a special "dome" shaped spatula onto the bonding face of steel plate. The plate was gently pressed until the adhesive was forced out on both sides of the plate to eliminate entrapped air. The surplus adhesive was then removed. After fixing the plate the beams or prisms were kept aside for proper air curing. The prism specimens were strengthened using steel plate of 250 mm x 25 mm x 2.5 mm dimension without connector, with connector and with steel bar. Steel plates having the same dimension (250 mm x 25 mm x 2.5 mm) were fixed on the shear spans of beams SPC and SPB with the spacing of 110 mm c/c as shown in Figures 6, 7 and 8. Shear connectors

of 8 mm diameter steel bar were used in beam SPC and embedded steel bar of 8 mm diameter bar was used in beam SPB. Beam SB were shear strengthened using 8 mm diameter steel bar only with the same spacing of plate as shown in Figure 7. The prism specimens were tested under pull out test and beams specimens were tested under single point load with shear span of 550 mm shown in Figure 10.

Figure 9. Pull out test of prism

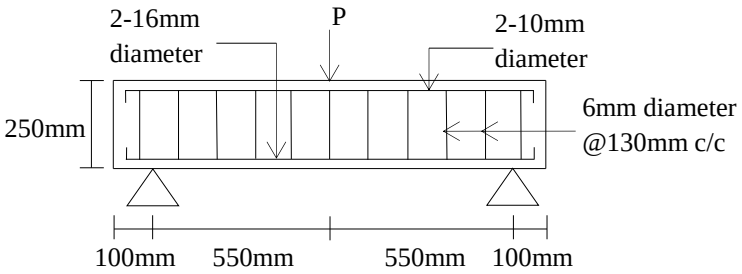

Figure 10. Details of beam

3. RESULTS AND DISCUSSIONS

Table 3 shows details experimental pull out test results of prism specimens. Strengthened prism with steel plate without connector failed by debonding of plate at concrete adhesive interface (Figure 11-a), whereas prisms with embedded connector failed by debonding at plate adhesive interface (Figure 11-b). The strengthened prisms with steel plate and embedded steel bar did not show debonding of plate but had shown cover separation as shown in Figure 11(c). The strengthening technique of plate with embedded steel bar had excellent bond behavior and had average bond strength of 5.54 MPa which was 48% and 66% higher as compared to those of plate with embedded connector and without connector.

Table 3. Experimental results of strengthened prisms

Specimen ID	Concrete strength (MPa)	Cracking Load (kN)	Debonding load (kN)	Failure Load (kN)	Bond strength (MPa)	Failure mode
PNC	23.3	30.9	38.4	41.6	3.328	Debonding at concrete interface
P-1	23.3	38.4	41.5	46.9	3.752	Debonding at plate interface
P-2	23.3	30.9	44.8	46.9	3.752	Debonding at plate interface
PC-1	23.3	57.5	62.9	68.2	5.456	Cover separation
PC-2	23.3	52.2	66.1	70.3	5.624	Cover separation

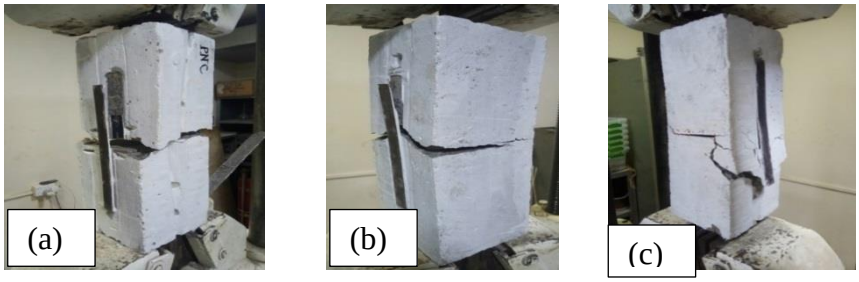

Figure 11. Failure modes of prism specimens

The experimental results of all beam specimens are summarized in Table 4. Results showed that all strengthened beams fully re-stored the capacity of damaged beams and even had shown higher failure loads as compared to control beam. As compared to others, strengthened beam with embedded steel bar had higher shear capacity. It could be due to pure shear failure behavior of strengthened beam by yielding of embedded bar (Figure 12-c). However, strengthened beams with externally bonded steel plates (SPB and SPC) had failed by crushing of concrete near cracks and followed by debonding of plates as shown in Figure 12 (a,b), thus showed lower failure loads. The deflection patterns of all strengthened beams were found to be almost linear elastic pattern, because of shear failure rather than flexural failure of beams (Figure 13).

Table 4. Experimental results of damaged strengthened beam specimens

Specimens ID	Concrete strength (MPa)	Debonding load (kN)	Failure Load (kN)	Mode of failure
CB	23.3		160	Shear
SB	23.3	185.3	190.6	Shear
SPC	23.3	174.7	179.9	Diagonal crushing of concrete
SPB	23.3	158.7	164	Diagonal crushing of concrete

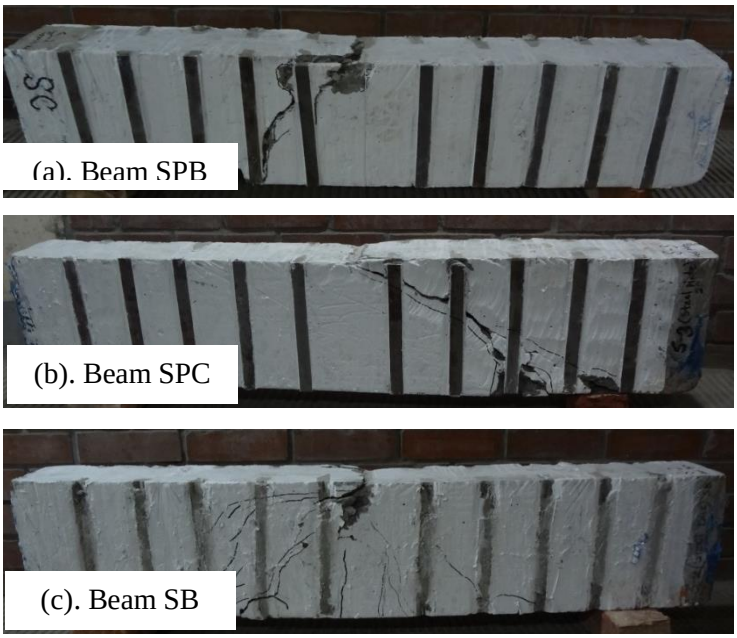

Figure 12. Failure modes of strengthened beams

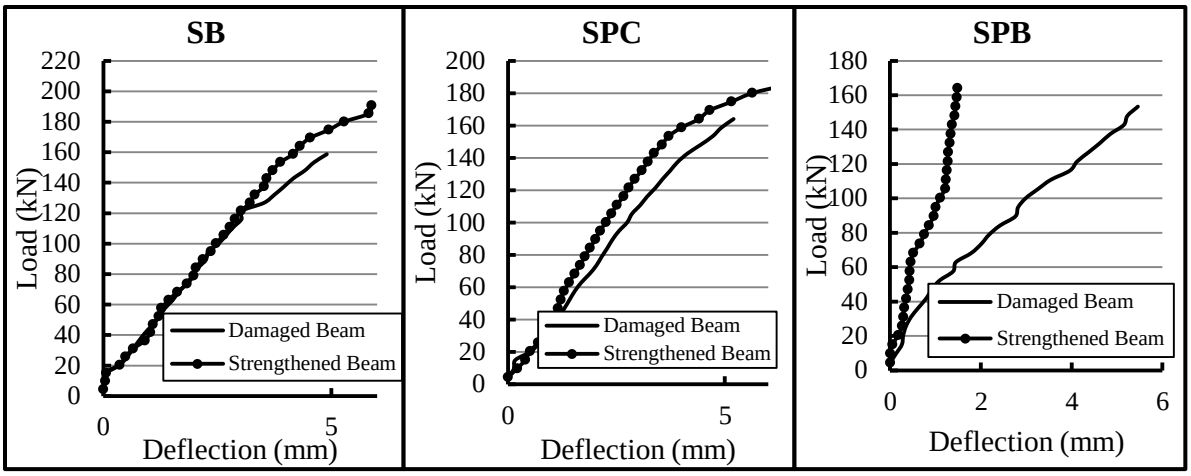

Figure 13. Deflection behaviour of strengthened beams

4. CONCLUSION

The shear strengthening techniques of reinforced concrete beams using externally bonded embedded steel bar, steel plate with embedded connector and steel plate with embedded steel bar were found to be very effective to fully re-store the original capacity of damaged beams. Although externally bonded steel plate with embedded steel bar had shown higher bond strength as compared to others, embedded steel bar system showed better performance in shear strengthening of reinforced concrete beam. Shear strengthened beams using externally bonded plates with connector and bar mostly failed by crushing of concrete followed by debonding of plate.

ACKNOWLEDGMENTS

The authors are very much thankful to IEERD of University of Asia Pacific for issuing the grand under IEERD/AC/19 and the Civil Engineering Department of UAP for facilitating the research.

REFERENCES

[1] Adhikary BB, Mutsuyoshi H, Sano M. Shear strengthening of reinforced concrete beams using steel plates bonded on beam web: experiments and analysis. Constr Build Mater 2000;14(5):237-44.

[2] Ahmed M, Oehlers DJ, Nguyen NT, Bradford MA. Reinforced concrete beams with steel plates bolted to their sides. In: Proceedings of Fifth International Conference on Structural Failure, Durability and Retrofitting. 1997: 362-9.

[3] Barnes RA, Baglin PS, Mays GC, Subedi NK. External steel plate systems for the shear strengthening of reinforced concrete beams. Engineering structures 2001; 23(9): 1162-1176.

[4] Sevuk F, Arslan G. Retrofit of damaged reinforced concrete beams by using steel plate. In: Structures congress, ASCE, New York, USA, 2005, April 21-23.

[5] Swamy RN, Jones R, Bloxham JW. Structural behavior of reinforced concrete beams strengthened by epoxy-bonded steel plates. Struct Engr 1987;65(2):59-68.

[6] Hamoush SH, Ahmad SH. Debonding of steel-plate-strengthened concrete beams. J Struct Eng ASCE 1990;116(2):356-71.

[7] Jumaat MZ, Alam, MA. Optimization of intermediate anchors to eliminate premature shear failure of CFRP laminate flexurally strengthened r.c. beams**.** International journal of physical sciences 2011; 6(2): 182-192.

[8] Mofidi A, Chaallal O. Shear Strengthening of RC Beams with EB FRP: Influencing Factors and Conceptual Debonding Model. J Composites for Construction 2011; 15 (1): 62-74.

[9] Mohamed Ali MS, Oehlers DJ, Bradford MA. Shear peeling of steel plates adhesively bonded to the sides of reinforced concrete beams. Proc Inst Civil Eng Struct Build 2000; 140: 249-59.

[10] Oehlers DJ, Mohamed Ali MS. Debonding of steel plates glued to RC flexural members. Prog Struct Eng Mater 1998;1(2):185-92.

[11] Ahmed M, Oehlers DJ, Bradford MA. Retrofitting reinforced concrete beams by bolting steel plates to their sides. Part 1: behaviour and experiments. Struct Eng Mech 2000;10(3):211-26.

[12] Galal K, Mofidi A. Shear Strengthening of RC T-Beams Using Mechanically Anchored Unbonded Dry Carbon Fiber Sheets. J Composites for Construction 2010; 24 (1): 31-39.

[13] Guan YH, Jiang BS, Jiang YD. Experimental study on RC beams strengthened in shear with the FRP-Bolt Strengthening Technology. Geotechnical Special Publication 2011; 219: 57-64.

[14] Grelle, Stephen V, Lesley HS. Review of anchorage systems for externally bonded FRP laminates. International Journal of Concrete Structures and Materials 2013; 7(1): 17-33.

[15] Mofidi A, Chaallal O, Benmokrane B, Neale K. Performance of End-Anchorage Systems for RC Beams Strengthened in Shear with Epoxy-Bonded FRP. J Composites for Construction 2012; 16 (3): 322-331.

[16] Nguyen NT, Oehlers DJ, Bradford MA. An analytical model for reinforced concrete beams with bolted side plates accounting for longitudinal and transverse partial interaction. Inter J Solids Struct 2001;38: 6985-96.

[17] Oehlers DJ, Ahmed M, Bradford MA, Nguyen NT. Retrofitting reinforced concrete beams by bolting steel plates to their sides. Part 2: transverse interaction and rigid plastic design. Struct Eng Mech 2000;10(3): 227-43.

Proc. 2nd International Conference on Structural Engineering Research (iCSER2019)
19-22 Jan 2019, Dhaka, Bangladesh
ISBN: 978-0-6482681-2-3

Advances in the Study of Aluminum Tubular Members Strengthened by CFRP

S. M. Zahurul Islam[1], Bulbul Ahmed[1] Maisha Tahsin[1], Abu Saleh Md. Nasim[1] and Ben Young[2]

[1]Department of Civil Engineering, Rajshahi University of Engineering and Technology, (RUET), Rajshahi-6204, Bangladesh

[2]Department of Civil Engineering, The University of Hong Kong, Pokfulam Road, Hong Kong, China
Corresponding author's E-mail: zahurul90@gmail.com

Abstract

Web crippling of aluminium alloy tubular structural members may occur due to the highly concentrated loadings. Nonlinear finite element models were developed and verified with test results. Material properties of aluminium alloy, adhesive and carbon fibre reinforcement polymer were taken into consideration. The traction separation law of the cohesive zone model was used to simulate the debonding between CFRP plate and aluminium alloy tubes in the nonlinear analysis process. Geometric and material nonlinearities were also included in the finite element analysis. The finite element results explained the behaviour of the CFRP-strengthened aluminium alloy specimens subjected to web crippling. The finite element results demonstrate that the ultimate load-carrying capacity (web crippling strength), web crippling failure modes, and web deformation curves agree well with the tests. The verified finite element models are then used for an extensive parametric study of different tubular dimensions. A series of test and numerical result are presented and simulated for reliability analysis. It is found that the verified finite element models provide an effective and time efficient means to predict web crippling strengths of CFRP-strengthened aluminium alloy members. Design equations are proposed to predict the web crippling strengths of CFRP-strengthened aluminium alloy tubular sections against web crippling loading.

Keywords: Aluminium, CFRP strengthening, Finite element analysis, Proposed design equations Reliability analysis, Tubular sections, Web crippling.

1. INTRODUCTION

Aluminium alloy tubular members are being used increasingly in structural applications. Web crippling may occur at highly concentrated loadings or reactions in aluminium alloy tubular members. The web crippling failure of aluminum and cold-formed steel thin-walled members is a common failure mode and has been studied extensively Zhou and Young (2008) and Zhou et al. (2009). The web crippling strength can be enhanced by Carbon fibre-reinforced polymer (CFRP) strengthening in the web of the sections. CFRP provides advanced structural properties with their high strength-to-weight ratios and resistance to harsh environmental effects Zhao and Zhang (2007). It is an efficient method for strengthening metallic structural members using CFRP. Islam and Young (2011, 2012, 2018) and Islam (2012), Wu et at. (2011) explored the use of CFRP plates to enhance the load-carrying capacity of aluminium alloy tubular structural members subjected to web crippling. A significant increase in load carrying capacity was obtained by using this strengthening technique. The CFRP strengthening technique was able to increase the web crippling strength approximately

threefold for aluminium alloy sections. Compared with physical experiments, numerical simulation is relatively inexpensive and time efficient. Finite element analyses (FEA) have been carried out by different researchers to investigate CFRP-strengthened metallic structures. The nonlinear finite element method (FEM) has been used widely for analysis of a wide range of structural engineering problems including simulation of CFRP repaired systems. However, to date there have only been limited investigations of finite element analysis of CFRP-strengthened aluminium alloy tubular sections subjected to web crippling. The web crippling design rules can be found in AA (2015) Specification, AS/NZS Standard (1997) and European Code (2000) for aluminium structures. However, these design rules do not cover aluminium alloy sections strengthened by CFRP. Therefore, a more sophisticated and consistent unified design is needed to predict the web crippling strengths of aluminium alloy tubular sections strengthened by CFRP based on a large database.

The first purpose of this study was to develop accurate nonlinear finite element models of CFRP-strengthened aluminium alloy tubular structural members subjected to ETF, ITF, EOF and IOF loading conditions. The finite element method was used for the numerical analysis. The finite element models (FEM) included material and geometric nonlinearities. The developed FE models were verified against the tests results. The finite element analysis (FEA) results agreed well with those from the experiments in terms of ultimate web crippling loads, load-displacement curves and failure modes. Second, the verified finite element models were used for a further extensive parametric study for a wide range of hollow-section dimensions, with the web slenderness (*h/t*) ranging from 4 to 123. The third aim of the study was to propose modified unified web crippling equations by including the strengthening effect and new coefficients for CFRP-strengthened aluminium alloy square and rectangular hollow sections. The numerical results were also compared with the design strengths predicted by the proposed equations for aluminium alloy structural members. Last, a reliability analysis was performed to assess the reliability of these design rules.

2. EXPERIMENTAL OBSERVATIONS

A test program conducted by Islam and Young Islam and Young (2011, 2012) and Islam (2012) provided experimental ultimate loads and failure modes for CFRP strengthened aluminium alloy tubular sections subjected to web crippling. A series of tests was conducted on strengthened aluminium tubular members using CFRP to enhance the web crippling capacity. The test specimens were fabricated by extrusion from 6061-T6 heat-treated aluminium alloy. The tests were performed on eight different sizes of aluminium square and rectangular hollow sections which covered a range of slenderness ratios (flat portion of web depth-to-thickness) from 6.2 to 62.2. The material properties of the aluminium alloy sections obtained from the tensile coupon tests The six different types of fibre–reinforced polymer (FRP) comprise of two wrap sheets including (a) Sika Wrap-300C/60 carbon fibre, and (b) Sika Wrap-430G/25 glass fibre as well as four laminate plates namely (c) Tyfo UC laminate, (d) Sika CarboDur S1214, (e) Sika CarboDur M614, and (f) Sika CarboDur H514 that symbolized as ‘a’ to ‘f’ in alphabetical order. The adhesive and FRP properties have been detailed by Islam and Young (2011, 2012). The high modulus CFRP Sika CarboDur H514 laminate plate and adhesive Araldite 2015 were used for the strengthening of the aluminium alloy tubular sections in this study. The specimen labelling system includes the material type, nominal specimen dimensions, loading conditions and number of CFRP layers Islam and Young (2011, 2012). The web crippling tests were carried out under the four loading conditions specified in the North American Specification (2016) and Australian/New Zealand Standard (1997).

3. DEVELOPENT OF FINITE ELEMENT MODEL

The finite element software package ABAQUS (2009) was used to build CFRP strengthened aluminium alloy tubular sections subjected to web crippling. Five main components, namely the bearing plates, aluminium alloy tubular section, adhesive, CFRP and the interfaces between aluminium and adhesive, and the adhesive and CFRP plate were modeled in the finite element

analysis. The CFRP plates were modelled as linear elastic materials. Adhesive was modelled as a cohesive element that followed the traction separation law. The finite element mesh used in the model was investigated by varying the sizes of the elements in the cross-section to provide both accurate results and less computational time. The finite element mesh sizes ranging from 2x2mm (length by width) to 10x10mm were used for the flanges and webs, depending on the sizes of the sections. The typical finite element mesh of a rectangular hollow section under the ETF loading condition is shown in Fig. 1.

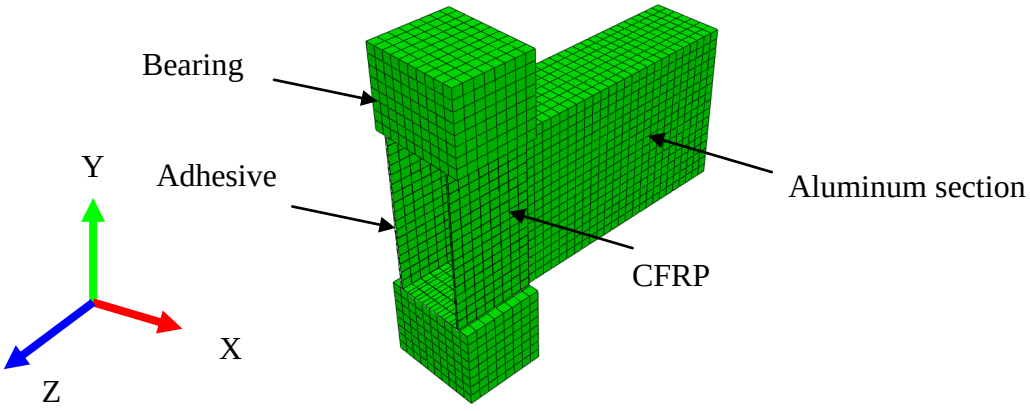

Figure 1. Meshing of aluminium section A100x45x3-ETF-f1 (Islam, 2012)

4. VERIFICATION OF FINITE ELEMENT MODELS

A comparison was made between the experimental results and the finite element results. The main objective of this comparison was to verify and check the accuracy of the FEM. The finite element models were verified against the experimental results in terms of failure modes, web deformation, and ultimate load-carrying capacity. The failure modes of CFRP strengthened aluminium alloy tubular structural members subjected to web crippling depend highly on the loading conditions. It is important to predict the failure modes accurately in the finite element analysis. The failure modes obtained from the tests of CFRP strengthened aluminium alloy sections were compared with the FE predictions for ETF and IOF conditions, as shown in Figs. 2. It can be seen that the failure modes predicted by the FEA were in good agreement with those observed in the laboratory tests.

(a) Experimental

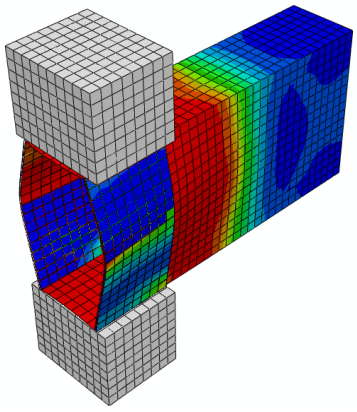

(b) FEA

Figure 2. Failure mode of aluminium alloy section A100x45x3-ETF-f1 (Islam, 2012)

The web deformation curves predicted by the FEA were compared with the experimental curves, as shown in Figs. 3. The comparisons of the test results (P_{Exp}) with the numerical results (P_{FEA}) of the ultimate web crippling strengths per web using the cohesive element and spring element are shown in

Tables 1 for the ETF loading condition. The mean values of the experimental-to-FEA web crippling strength ratio P_{EXP}/P_{FEA} were 1.01 with the corresponding coefficients of variation (COV) of 0.055, for ETF loading conditions. It is clear that the FEA predictions using cohesive element generally agreed well with the test results.

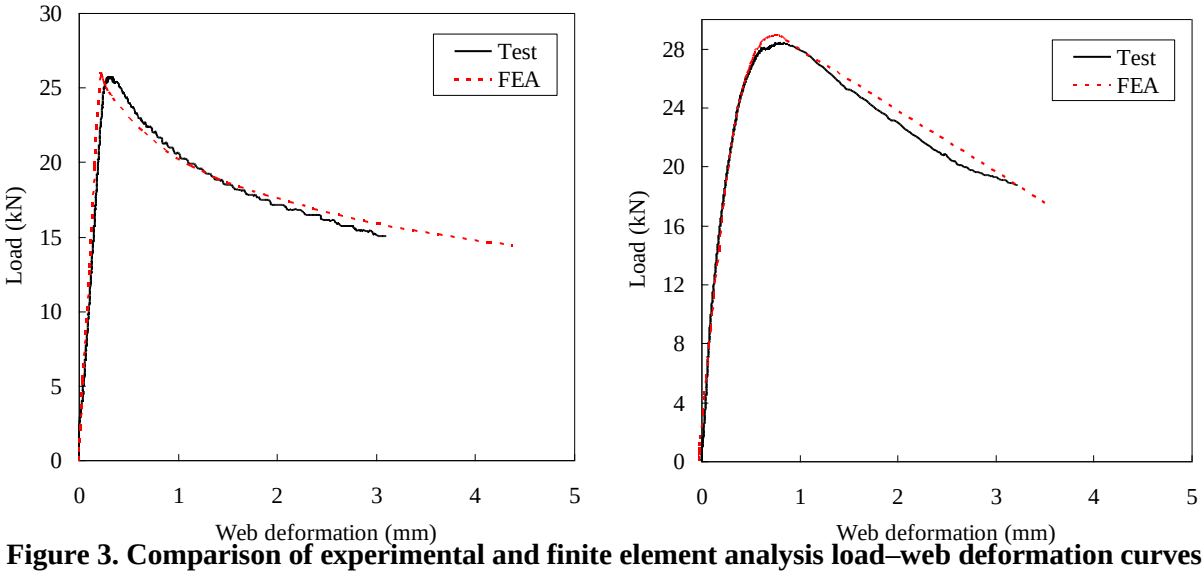

Figure 3. Comparison of experimental and finite element analysis load–web deformation curves for specimen A76x76x3-ETF-0 and A76x76x3-EOF-f1(30) (Islam, 2012)

Table 1 Comparison of experimental results with web crippling strengths predicted from finite element analysis under ETF loading condition using cohesive elements (Islam, 2012)

Specimen	**Web slenderness *h/t***	**Exp. load per web P_{Exp}(kN)**	**FEA load per web P_{FEA}(kN)**	**Comparison P_{Exp}/P_{FEA}**
A40x40x5-ETF-0	6.2	67.1	71.1	0.94
A40x40x5-ETF-f1	6.2	69.7	72.4	0.96
A50x50x3-ETF-0	14.1	24.0	24.5	0.98
A50x50x3-ETF-f1	14.2	26.3	27.3	0.96
A64x64x3-ETF-0	18.8	30.2	29.1	1.04
A64x64x3-ETF-f1	19.2	34.1	34.8	0.98
A76x76x3-ETF-0	22.5	25.7	26.3	0.98
A76x76x3-ETF-f1	22.5	31.5	32.4	0.97
A100x45x3-ETF-0	32.0	25.1	26.0	0.97
A100x45x3-ETF-f1	32.0	33.6	31.4	1.07
A100x100x2.3-ETF-0	42.0	12.5	12.5	1.00
A100x100x2.3-ETF-f1	42.1	25.1	22.8	1.10
A152x152x3.2-ETF-0	43.4	21.3	19.6	1.09
A152x152x3.2-ETF-f1	43.6	30.5	28.5	1.07
A100x45x1.6-ETF-0	60.8	5.9	5.9	1.00
A100x45x1.6-ETF-f1	61.1	16.9	15.3	1.10
Mean				1.01
COV				0.055

Table 4: Comparison of experimental results [12] with web crippling strengths predicted from finite element analysis under ETF loading condition using cohesive elements

5. PARAMATRIC STUDY

A parametric study was carried out to study the effects of the web slenderness ratio (*h/t*), different loading conditions and cross-section sizes on the web crippling strengths of aluminium alloy tubular sections subjected to web crippling. A total of 108 web crippling specimens was analysed in the parametric study and the cross-section dimensions under the ETF, ITF, EOF and the IOF loading conditions, respectively. Fifteen different section sizes were designed in the parametric study, having nominal thicknesses ranging from 1.2 to 5 mm. The nominal depth of the webs ranged from 30 to 200 mm, the nominal flange widths ranged from 30 to 150 mm and the aspect ratio *d/b* ratio ranged from 1 to 4. The dimensions of the specimens ranged from 30x30x5 to 200x50x1.6, including 7 square hollow sections (SHS) and 8 rectangular hollow sections (RHS). This parametric study focused mainly on the effects of the web slenderness ratio of aluminium alloy tubular sections on CFRP-strengthening against web crippling. The web slenderness values of the tubular sections ranged from comparatively stocky webs of 4 to relatively slender ones of 123. The reliability of the web crippling design rules was evaluated using reliability analysis. The reliability index (β) is a relative measure of the safety of the design. A target reliability index of 2.5 for aluminium alloy structural members was used in this study.

6. PROPOSED DESIGN EQUATIONS

For CFRP-strengthened specimens, design models are proposed to include the effect of adhesive mechanical properties, debonding of interface between the CFRP and aluminium surface and the bonded area of the CFRP. The new coefficients were determined based on the test data and FEA results obtained in this study. It should be noted that the aluminium alloy square and rectangular hollow sections have small corner radii as the specimens were fabricated by extrusion. The proposed design equation is based on test data and the FEA results obtained from the parametric study.

The proposed design equation (P_{p1}) is as follows:

$$P_{p1} = Ct^2 f_y \sin\theta \left(1 - C_R \sqrt{\frac{r_i}{t}}\right)\left(1 + C_N \sqrt{\frac{N}{t}}\right)\left(1 - C_h \sqrt{\frac{h}{t}}\right) + [\sigma_{u-ad} . A_{bonding}] . C_{ad-FRP} \quad (1)$$

7. CONCLUSIONS

This paper has presented the results of a nonlinear finite element analysis and practical design equations for CFRP-strengthened aluminium alloy tubular structural members subjected to web crippling. Finite element models that incorporated the geometric and material nonlinearities were developed and verified against experimental results in terms of the failure modes, web deformation curves, and web crippling strengths under ETF, ITF, EOF and IOF loading conditions. Cohesive elements were used to simulate the debonding between CFRP plates and aluminium alloy tubes. The finite element models are able to simulate the web crippling behaviour of the aluminium alloy rectangular and square hollow sections strengthened by the CFRP. Hence, the verified finite element models were used for an extensive parametric study for a wide range of aluminium alloy cross-section dimensions having web slenderness ranging from 4 to 123. Web crippling design equations for CFRP-strengthened aluminium alloy tubular sections under the ETF, ITF, EOF and the ITF loading conditions are proposed from this study. The web crippling strengths obtained from the finite element analyses and experiments were compared with the design strengths calculated using the proposed equations. A reliability analysis was also carried out. It was demonstrated that web crippling strengths calculated using the proposed design equations provide a safe and reliable design for CFRP-strengthened aluminium alloy rectangular and square hollow sections.

ACKNOWLEDGMENTS

The authors gratefully acknowledge the Asia Aluminium Manufacturing Company for supplying the test specimens. The research work described in this paper was supported by a grant from The University of Hong Kong under the seed funding program for basic research.

REFERENCES

AA. (2015). Aluminum design manual. Washington, DC: The Aluminum Association; 2015.

ABAQUS (2009). Analysis user's manual, version 6.9-1. ABAQUS Inc., 2009.

AISI S100 (2016). North American Specification for the design of cold-formed steel structural members. North American Cold-formed Steel Specification, American Iron and Steel Institute, AISI S100-16, Washington, D.C., 2016.

AS/NZS (1997). Aluminium structures—Part 1: limit state design, Australian/New Zealand Standard AS/NZS 1664.1:1997. Sydney, Australia: Standards Australia, 1997.

EC9 (2000). Eurocode 9: Design of aluminum structures—Part 1.1: General rules—General rules and rules for buildings, DD ENV 1999-1-1:2000, Final draft October 2000. European Committee for Standardization, 2000.

Islam S M Z (2012). Strengthening of Aluminium and Stainless Steel Tubular Sections with Fibre-Reinforced Polymer. PhD Thesis, Department of Civil Engineering, The University of Hong Kong. Hong Kong, China.

Islam S M Z, Young B (2018). Design of CFRP-Strengthened Aluminium Tubular Sections subjected to Web Crippling. Thin-Walled Structures, 2018, 124: 605-621.

Islam SMZ and Young B(2011). FRP strengthened aluminium tubular sections subjected to web crippling, Thin-Walled Structures, 49(11),1392-1403.

Islam SMZ, Young B(2012). Web crippling of aluminium tubular structural members strengthened by CFRP, Thin-Walled Structures, 59,58-69.

Wu C., Zhao X.L., and Duan W.H. (2011). "Design rules for web crippling of CFRP strengthened aluminium rectangular hollow sections." Thin-Walled Structures, 49(10):1195–1207.

Zhao XL, and Zhang L (2007). State-of-the-art review on FRP strengthened steel structures. Engineering Structures, 29(8),1808–1823.

Zhou F, Young B (2008) Aluminum tubular sections subjected to web crippling—Part II: Proposed design equations. Thin-Walled Structures, 46(4), 352-361.

Proc. 2nd International Conference on Structural Engineering Research (iCSER2019)
19-22 Jan 2019, Dhaka, Bangladesh
ISBN: 978-0-6482681-2-3

Self-Centering and Overturning Ratio Effect on Self-Centering Steel Rocking Frames

Radin Md Mahirul Hoque[1], Khan Mahmud Amanat[2], Devabrata Dutta[3], Md. Zakir Hossain[4]

1Lecturer, Department of Civil Engineering, Bangladesh University of Engineering and Technology (BUET), Dhaka 1000, Bangladesh. E-mail: mahir@ce.buet.ac.bd
2Professor, Department of Civil Engineering, Bangladesh University of Engineering and Technology (BUET), Dhaka 1000, Bangladesh.
3Undergraduate Student, Department of Civil Engineering, Bangladesh University of Engineering and Technology (BUET), Dhaka 1000, Bangladesh. E-mail: devabrata.ce.buet@gmail.com
4Graduate Student, Department of Civil Engineering, Bangladesh University of Engineering and Technology (BUET), Dhaka 1000, Bangladesh.

Abstract

Self-centering rocking frame is a seismic lateral force resisting system that is developed for earthquake resilient structures. This system has the ability to minimize earthquake induced residual drift and structural damages with its self-centering property. The system is made up of braced steel frame, post tensioning strands and replaceable structural fuses. In this frame system, post tensioning strands provide the overturning resistance as well as the self-centering property against the seismic force and the structural fuses dissipate the seismic energy. The frame is designed to rock on its foundation during earthquakes while frame members and post tensioning strands remain in their elastic limit. The self-centering ratio and overturning ratio of the steel rocking frames for different structural fuse geometry and post tensioning configuration are examined numerically in this study. The self-centering and overturning properties of the frame are evaluated using a finite element model. The performance of the system is evaluated in terms roof drift and uplift for different self-centering and overturning ratio of the frame with the simplified fuse and post tensioning strands model. In depth parametric study has been done with the results obtained from the FE model, which has been validated using the past experimental program. Results from the numerical study show that the drift and uplift of the frame increases with the increase of self-centering ratio and decrease of overturning ratio. From this observations a regression analysis has been conducted and an equation is suggested to find the required self-centering ratio and overturning ratio for the desired design drift and uplift.

Keywords: Self-centering, Seismic force, Rocking frame, Overturning, Finite element model.

1. INTRODUCTION

Code based and conventional seismic design of structures mainly focuses on preventing failure of structures on seismic events. But, after large earthquakes, due to inelastic deformation, structures often have permanent residual drift. Large amount of drift cause architectural and structural damage. As a result, the buildings may not collapse after shock but suffer severe damages which lead to great economical losses.

Self-centering system is designed to make structures safe in the event of earthquake as well as removing permanent residual drift by controlling inelastic deformations. The system works in a controlled rocking mechanism. In the event of earthquake, the frame rocks on its foundation, as the base is not fixed. A prestresing tendon pulls the frame to come back to its original position by providing self-centering force. There is also a sacrificial steel fuse, which dissipates the seismic energy. Others frame members as well as the prestressing tendons remain in their elastic limit. As a

result structure have minimum amount of plastic deformation and residual drift. The procedure of eliminating drift of the structure can be explained with hysteresis as shown in Figure 1.
The behavior of rocking system has been studied extensively in the recent years by many researchers. [Roke et al. (2010), Eatherton and Hajjar (2010), Ma et al. (2011), Wiebe and Christopoulos (2014), Steele and Wiebe (2016)]. However, this paper investigates the performance of the rocking system in terms of roof drift and frame uplift while considering the self-centering and over turning ratio of the frame. The performance of the frame in the event of earthquake has been examined using a numerical model. The model has been subjected to ground acceleration (Northridge, Canoga park, 1994) for this purpose. The obtained results are evaluated in terms of overturning ratio and self-centering ratio.

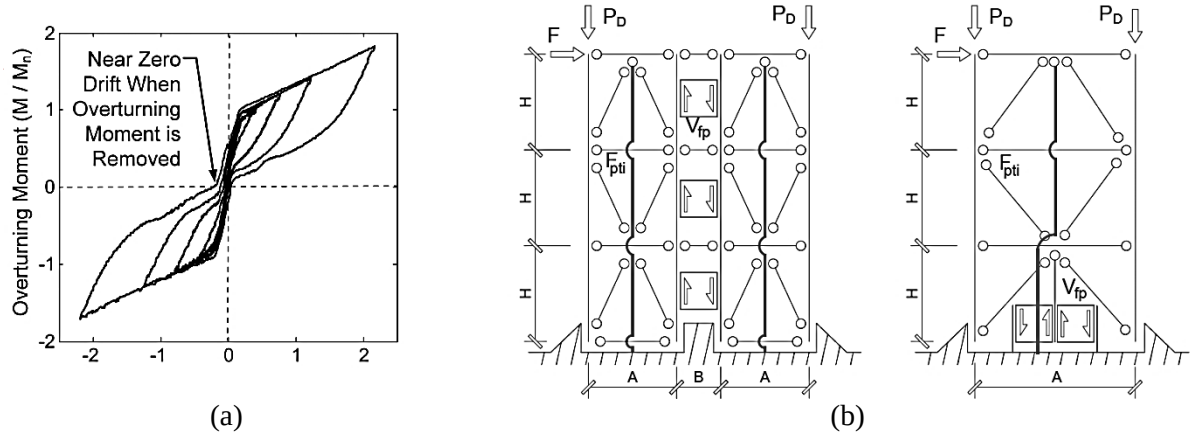

Figure 1. (**a) Experimental load deformation behavior; (b) Idealized frame configuration (dual & single frame)**

The numerical study of this paper is based on experimental program of Ma et al. (2010). The overall performance of the frame examined using the roof drift. The parametric study has been conducted for different fuse forces to vary the overturning and self-centering ratio and the fuse strength has been varied by using different geometry. In this study a particular configuration of a 3 story rocking frame is used which has post-tensioned strand at the center of the rocking frame and fuses are connected with the columns (single frame configuration).

The overturning (OT) ratio and self-centering (SC) ratio are two terms frequently used in this paper. OT ratio quantifies the total resisting moment of the fuses and post-tensioning compared to the overturning moment obtained from the design code. The overturning moment is calculated from the ASCE 7-05 equivalent lateral loads using Equation 1.

$$M_y = \sum F_{pti} X_{PT} + \sum P_{De} X_D + \sum V_{fp} X_{fs} \tag{1}$$

$$OT = \frac{M_{resist}}{M_{OVT}} = \frac{AF_{PT} + V_p(A+B)}{M_{OVT}} \tag{2}$$

$$SC = \frac{AF_{PT}}{V_P(A+B)} \tag{3}$$

Where, A = Center-to-center distance of the columns in each individual frame
B = Center-to-center distance between the columns on each side of the fuse
F_{PT} = Initial axial tension force in the PT
V_P = Shear strength of the fuse
M_{OVT} = Overturning moment due to static code loading

Fuse and PT force are calculated by solving Equation 2 and 3. All other parameters are calculated using the respective equations from Ma et al. (2011).

The values of SC and OT ratio used in this study are selected from the range suggested by Hall, Eatherton and Hajjar (2010).

2. NUMERICAL MODELING OF THE FRAME

Numerical model for the case study are modeled in ANSYS 16.2. To develop the model of rocking system different types of elements are selected from elements library of ANSYS according to their application (Figure 2).

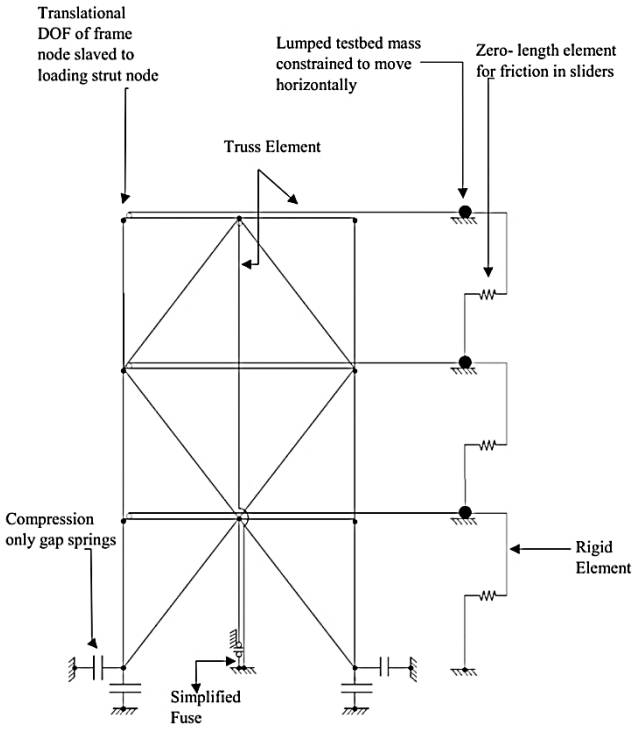

Figure 2. Rocking frame model for simulation of experiment of (Ma et al. 2011)

A three-story model has been used for the parametric study. Leaning columns are positioned to coincide with the adjacent gravity columns on each side of the rocking frame, assuming the rocking frame is not placed at the corner of a building. Mass nodes represent the gravity load which is applied prior to applying ground motion input. The simplified fuse is used in the model by truss element.

The dynamic response of the frame system has been studied using two dimensional finite element model. Only material nonlinearity is considered for simulating the frame assembly. To simulate the shaking table experiment braced frame, testbed mass and post tensioning (PT) strands are included in the numerical model.

It is expected that the frame members and PT strands will remain elastic in the event of earthquake. So, the frame members and PT strands are simulated using material linearity. However, the frame members and PT strands are modeled using beam and truss element respectively from the ANSYS library. The cross sectional characteristics of frame members are employed as described in Ma et al. (2011). Also, spring elements from the library have been used at the column bases of the numerical model to capture the rocking behavior.

The loads from different story as well as the self-weight of the frame are simulated using Mass element as lumped mass. Half of the mass of each story of the frame is applied to the right column nodes and mass of half of the frame plus the connection block is applied to the left column nodes.
The rocking frame consists of a sacrificial energy dissipating fuse. To model the fuse, a single truss element with calibrated force-deformation relationship has been used. The fuse is modeled as

simplified fuse as described in Ma et al. (2011). Also, the strength of the fuse (F_{fuseP}) is calculated using the design formula from Ma et al. (2011).

A time history analysis of the simulated model has been done following the shaking table experiment of Ma et al. (2011). The analysis result also has been used for validation of the numerical study. The system hysteresis has been compared for both experimental program and numerical study using 65% Kobe Earthquake at MCE (Maximum Considered Earthquake) level. The simulation has shown good agreement with the experimental result. The comparison used for validating the numerical model is shown in Figure 3.

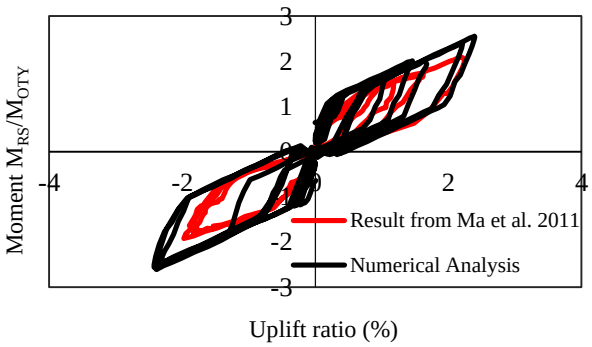

Figure 3. System hysteresis comparison: fuse (65% Kobe)

3. PARAMETRIC STUDY

In this paper focus has been given to find the effect of self-centering and over turning ratio on the rocking frame and their relation with roof drift and uplift. So, the parametric study has been conducted to determine the significance of overturning factor (OT), and self-centering factor (SC) on a three-story prototype controlled rocking system. A time history analysis has been done using ground acceleration of (Northridge, Canoga Park, 1994) at MCE (Maximum Considered Earthquake) level. The ground acceleration record and its response spectrums were acquired from the PEER strong motion database (2000).

Table 1. Test Matrix 1

OT ratio	SC ratio	RDR (%)	ULR (%)	F_{fuse} (N)	F_{pto} (N)	No. of PT strands
1	0.34	1.16	1.07	2066524	1412884	18
1	0.61	1.40	1.3	1712872	2120188	27
1	0.89	1.58	1.48	1465458	2615016	33
1	1.20	1.70	1.59	1256107	3033718	39

Table 2. Test Matrix 2

SC ratio	OT ratio	RDR (%)	ULR (%)	F_{fuse} (N)	F_{pto} (N)	No. of PT strands
1.5	1.13	1.72	1.61	1256107	3768320	48
1.5	1.32	1.66	1.53	1465458	4396373	56
1.5	1.55	1.50	1.35	1712872	5138616	66
1.5	1.86	1.19	1.05	2066524	6199572	79

At first, the effect of self-centering has been observed by making OT ratio constant. Similarly, to evaluate the effect of overturning, self-centering has been kept fixed. To increase OT but hold SC constant, the fuse and PT strengths are increased proportionally. To increase SC and hold OT constant, the fuse strength is reduced while the PT is increased. To change the SC and OT ratio fuse force and post-tensioning force are frequently changed. Fuse strengths are varied by changing the fuse

geometry. The post tensioning forces are also varied similarly due to the change in fuse strength as all other parameters remained same. The different parameters considered for the analyses and to find the effect of SC and OT ratio are summarized in the test matrices. In this study the considered range of OT ratio was from 0.75 to 2 and SC ratio was from 0.5 to 2 as suggested by Hall, Eatherton and Hajjar (2010).

In the test matrix 1, the effect of increasing SC ratio for the constant OT ratio (1) is tabulated. From the result it is evident that roof drift and the column uplift both are increasing with the increasing self-centering ratio. But with the increasing OT ratio, roof drift and uplift are decreasing (test matrix 2) for a constant self-centering ratio of 1. This results are represented graphically in Figure 4. The change in roof drift is quite similar to the change in column uplift with a constant variation. Actually according to the theory, due to the rigid body behavior of the frame the numerical values of RDR and ULR should be the same. But, in the time history analysis of the frame, there induces some flexibilities in the frame members as well as in the fuse, which brings slight variations in the values of drift and uplift ratio.

One of the objectives of using rocking frame is to reduce the structural drift. From the graph (Figure 4) it is evident that we need to choice lower self-centering and higher over turning ratio to minimize the drift. The desired drift during earthquakes is attainable by changing the SC and OT ratio. The change of SC and OT can be done by changing the fuse geometry, post tensioning etc.

A regression analysis has been done for the obtained graph to form an equation. The graphs are best fitted using 2nd and 3rd order polynomial function for the SC ratios and OT ratios respectively. The value of R^2 is found equal to 1 in both cases. Using these graphs and the equations the required amount of SC ratio and OT ratio can be found for allowable drift of the frame. So, during the design of rocking frame one can predict the amount of self-centering and over turning required for limiting the drift within permissible limit. This will also help to find the optimum fuse geometry and the requirements in post tensioning while designing the rocking frame.

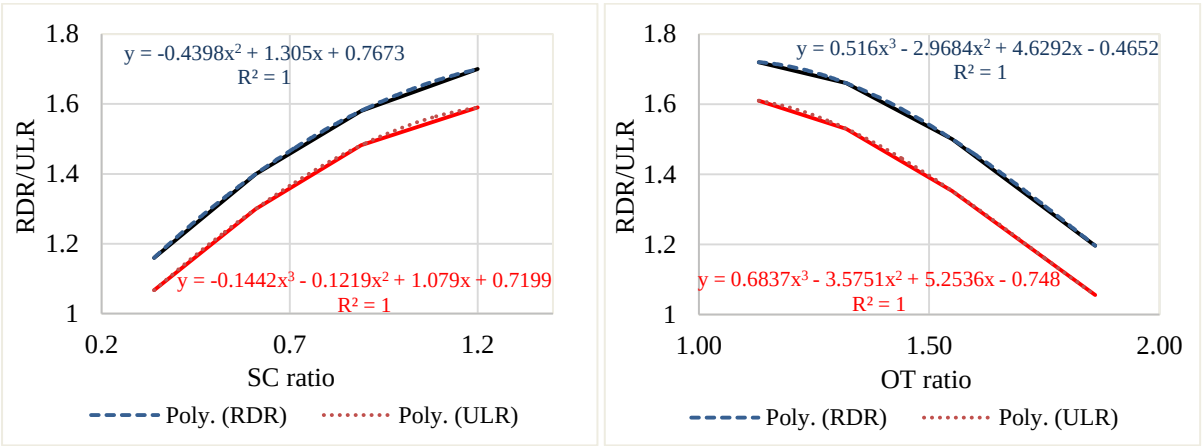

(a) (b)

Figure 4. (a) Relationship between RDR/ULR and SC ratio; (b) Relationship between RDR/ULR and OT ratio

Now using these equations the required SC and OT can be found for the design drift values. Besides, these equations will help to design the rocking frame for the allowable uplift of column. Here, Equation 4 and 5 relates roof drift with SC and OT ratio. In the same way, Equation 6 and 7 relates the frame column uplift with the two ratio.

$$y = -0.4398x^2 + 1.305x + 0.7673 \quad (4)$$

$$y = 0.516x^3 - 2.9684x^2 + 4.6292x - 0.4652 \quad (5)$$

Here, the y values of Equation 4 and 5 represent the amount of roof drift ratio and the x values represent required SC ratio and OT ratio respectively. Similarly, Equation 6 and 7 have been formed for finding the two ratio at the desired column uplift of the frame.

$$y = -0.1442x^3 - 0.1219x^2 + 1.079x + 0.7199 \quad (6)$$

$$y = 0.6837x^3 - 3.5751x^2 + 5.2536x - 0.748 \quad (7)$$

4. CONCLUSIONS

The self - centering rocking frame is designed to prevent structural failure as well as control the drifts during earthquakes. The capacity of the frame to control the drift and prevent failures largely depends on the SC and OT ratio. In this study a relation between the drift and these two ratios are formed, using a regression equation. The equation relating RDR and SC ratio is formed considering the constant ratio of OT equal to 1. Similarly, an equation relating RDR and OT ratio is formed considering SC ratio of 1.5. Knowing the value of allowable drift from code, design can be carried out by finding the SC and OT ratio by using these equations. Also, finding the SC and OT ratios from this equation will also help to proportionate the fuse geometry and post-tensioning parameters. In this study, the SC and OT ratio has been derived only for a 3 story-single frame configuration considering one ground motion (Northridge, Canoga Park, 1994) and a constant value of OT and SC. It is recommended to carry out further study in future for other values of SC and OT ratio and for different story/configuration of frames considering more ground motions.

REFERENCES

FEMA P695 (2009). Quantification of building seismic performance factors 2009, Federal Emergency Management Agency.

K Hall, Eatherton, M H, Hajjar (2010). Nonlinear Behavior of Controlled Rocking Steel-Framed Building Systems with Replaceable Energy Dissipating Fuses, NSEL Report Series Report No. NSEL-026, Stanford University.

Ma X, Borchers E, Peña A, Krawinkler H, and Deierlein G (March, 2010b). Design and behavior of steel shear plates with openings as energy-dissipating fuses, John A. Blume Earthquake Engineering Center Technical Report No 173, Stanford University.

Ma X, Deierlein G, Eatherton M, Krawinkler H, Hajjar J, Takeuchi T, Kasai K, Midorikawa M, and Hikino T (2010a). Large-scale shaking table test of steel braced frame with controlled rocking and energy dissipating fuses, Proceedings of the 9th US and 10th Canadian Conference on Earthquake Engineering, Toronto, ON.

Ma X, Krawinkler H, and Deierlein G.G (March, 2011). Seismic Design and Behavior of Self-Centering Braced Frame with Controlled Rocking and Energy Dissipating Fuses, John A. Blume Earthquake Engineering Center Technical Report No 174, Stanford University.

Proc. 2nd International Conference on Structural Engineering Research (iCSER2019)
19-22 Jan 2019, Dhaka, Bangladesh
ISBN: 978-0-6482681-2-3

Minimizing Drift of Steel Structures by YSPDs

Isteak Mahmud[1], Shuvasish Biswas[2], Md. Imtiaz Sarwar[3] and Md. Raquibul Hossain[4]

[1]Student, Department of Civil Engineering, Bangladesh University of Engineering & Technology, Dhaka, Bangladesh
[2]Student, Department of Civil Engineering, Bangladesh University of Engineering & Technology, Dhaka, Bangladesh
[3]B.Sc. in Civil Engineering, Bangladesh University of Engineering & Technology, Dhaka, Bangladesh
[4]Assistant Professor, Department of Civil Engineering, Bangladesh University of Engineering & Technology, Dhaka, Bangladesh
Corresponding author's E-mail: raquibulhossain@ce.buet.ac.bd

Abstract

Excessive drift in steel structures during earthquake can make irreversible damage. The drift can be reduced significantly by the use of Yielding Shear Panel Devices (YSPDs). YSPD is a low cost device that acts like a fuse for buildings, absorbing much of the exerted energy itself and reducing the energy upon the main structure in the event of an earthquake, thus minimizing the drift. YSPDs though damaged after such an event, can be reinstalled with minimal hassle. But the installation of YSPDs of different sizes in different positions in different combinations can have a huge difference on the expected behaviour of the structure during an earthquake. Modelling the whole system using the finite element analysis software OpenSees and making different combination of YSPDs via other programming languages like C++ and Python can produce all the expected scenarios, thus availing the designer to choose the exact configuration which proves to be the most effective one in reducing the drift of the building. While research had been conducted with YSPDs in the past, the use of other coding languages in our research has made it possible for us to generate more data than ever before to predict the behaviour of the structure in Static Pushover analysis for almost every possible combination of YSPDs. Pushover of different magnitudes too can be simulated in Opensees very easily. That means the combination of OpenSees and other coding languages enables researchers to predict almost every scenario and the implementation of the research would save billions worth of properties and human lives.

Keywords: Finite Element Modelling and Analysis, YSPD, Earthquake, OpenSees, Static Pushover.

1. INTRODUCTION

Earthquake is one of the major catastrophic natural hazards which causes massive damage to lives and properties. This life threatening natural hazard destroys basically the cities and its inhabitants because it affects high rise buildings. The most dangerous part of earthquake is its strength which is beyond control. As it is not controllable, the purpose of this research is to mitigate the losses due to earthquake using passive energy dissipating device YSPD. YSPDs may be installed in the lateral load-bearing frame to dissipate seismic energy in the event of an earthquake. Yielding shear panel device (YSPD) is an energy dissipating device that utilizes yielding of metals. The in-plane shear deformation of a steel plate is exploited to dissipate seismic energy (Chan, 2008). This device can be fabricated using mild steel standard structural sections and can easily be installed on the inverted V braces of structural frames. YSPD is inexpensive, simple to manufacture and its installation process is easy in a seismic force resisting system. YSPD helps reduce storey drift. YSPD has been used in the models for this research. The moment resisting frame of the Los Angeles three storied SAC model structure, designed for the SAC Phase 2 Steel Project has been used to evaluate the performance of YSPD. The structure

has been modelled and analyzed through finite element software OpenSees for its versatility in defining new devices unlike conventional softwares like Etabs. Besides, OpenSees requires the model to be done via writing codes. It means the input can be a simple text file. The text code can be modified and multiplied via other coding mechanisms like C++ thus making the researcher able to perform several models at ease.

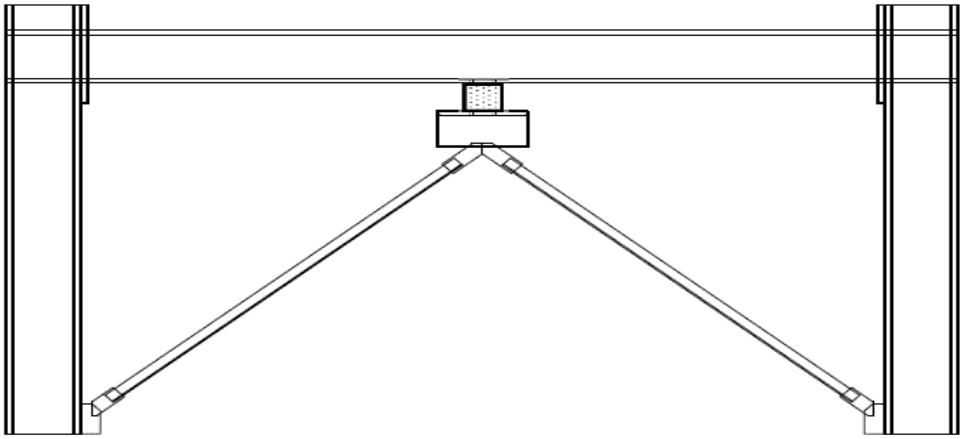

Figure 1. YSPD-brace assembly in a frame

2. METHODOLOGY

In our structure we had 9 nodes where YSPD could be installed. A node is usually the middle point of a beam as shown in Figure 1. Models have been created resembling different number of YSPDs installed in different nodes. If a single YSPD is to be installed it can be installed in 9 nodes, for two YSPDs it can be installed in two nodes in 9C2 or 36 configurations. Considering all the possible configurations with three types of YSPDs the total number of configurations in this research is 1534. Displacement controlled static pushover analysis has been done for all these configurations. The maximum roof displacement was allowed to be 2% of the height of the building. Total 200 steps of pushover analyses are done for each configuration of YSPDs. The name of the configurations is defined in a process where the presence of a YSPD in a node is represented by a 1 and absence is represented by a 0. So a configuration where two YSPDs are installed in node number 4 and 7 looks like config_000100100.

First, a master code was prepared which itself is not a valid model for running in OpenSees but after the modification of it through C++ code, it produces valid models. The output of modification through C++ generates different configurations of YSPDs of a single type in one text file, thus minimizing the trouble of running 1534 different codes in OpenSees manually. That single text file is then inputted into OpenSees and run. In this way the result for all 1534 configurations is produced. The produced data was then sorted. Use of C++ can prove to be most efficient once again for sorting huge amount of data. This huge amount of data was then plotted into graphs through Python. If someone does not have enough knowledge on Python, he can simply use C++ to write the code of Python and run the output in Python! This necessarily does not represent good coding practice or can even be described “sloppy” but in reality it gets the job done.

2.1 Material Properties

Three types of YSPDs are considered for the evaluation of seismic performance. Table 1 summarizes the BWBN model parameters calculated from the closed form equations proposed by Matteis, Landolfo and Mazzolani (2003).

Table 1. BWBN model parameters for the YSPDs

YDPD (D × T × t)	f_y(MPa)	k_t(kN/mm)	F_i(kN)	A	B	γ	n	q	ζ_{1o}	P	ψ_0	δ_ψ	Λ
100 × 4 × 2	250	0.33	26.76	1.0	0.5	0.5	1.213	0.52	0.96	0.018	0.41	0.00001	0.0300
110 × 5 × 3	300	0.42	54.22	1.0	0.5	0.5	0.544	0.38	0.95	0.015	0.27	0.00001	0.0014
120 × 6 × 4	350	0.49	93.51	1.0	0.5	0.5	0.300	0.30	0.95	0.012	0.22	0.00001	0.0002

D is the Size of YSPD (mm), T is the thickness of Square Hollow Section plate (mm), t is the thickness of diaphragm plate (mm), f_y is the yield strength of SHS and diaphragm plates (MPa), k_t is the tangential stiffness of YSPD after tension field formation (kN/mm),F_i, A, β, γ, n are hysteretic parameters and q, ζ_{1o}, p, ψ_0, δ_ψ, λ are pinching parameters.

3. RESULT AND DISCUSSION

Total 1534 configurations were modelled and analyzed. From the analyzed data, two types of graph were plotted. First type was Base Shear vs Roof Displacement and the second type was Inter story Drift ratio for every floor. Huge amount of data were generated which needed to be plotted. The use of Excel for plotting these graphs was inefficient. So, Python was used to plot the data.

3.1 Base Shear vs Roof Displacement Graphs

From the plotted graph we understood basically two things. The first thing we understood from the Base Shear vs Roof Displacement graphs was for which combination, more energy could be absorbed for the same amount of displacement. It can be compared with the dotted line which represents the structure without any YSPD installed. But lower roof displacement for higher base shear does not necessarily mean that the configuration has the least amount of Inter storey drift ratio. The inter storey drift ratio was obtained from the second set of graphs which is more important. Only a few of all graphs are shown here.

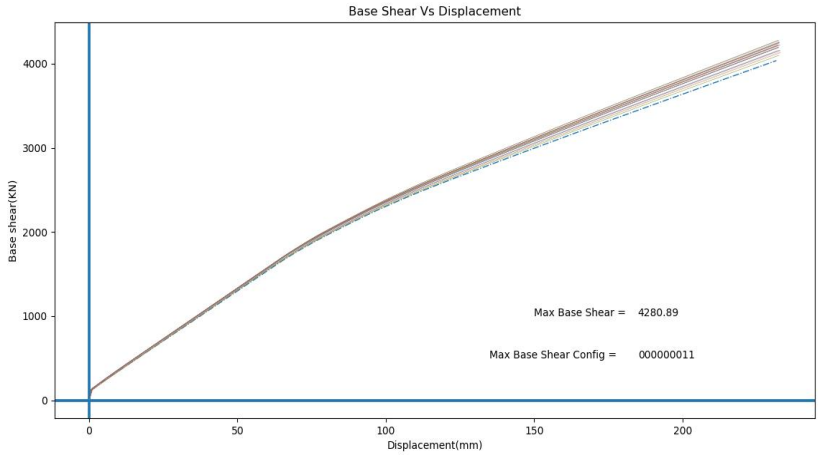

Figure 2. Base Shear vs Roof Displacement for double YSPD configurations (9C2=36 curves) using YSPD type 1
(Max Base Shear is 4280.89 kN for roof displacement 232.825 mm)

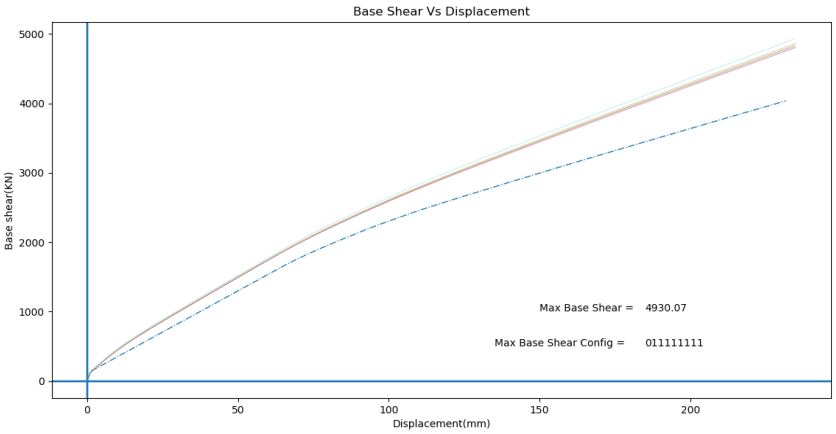

Figure 3. Base Shear vs Roof Displacement for eight YSPD configurations (9C8=9 curves) using YSPD type 2
(Max Base Shear is 4930.07 kN for roof displacement 234.674 mm)

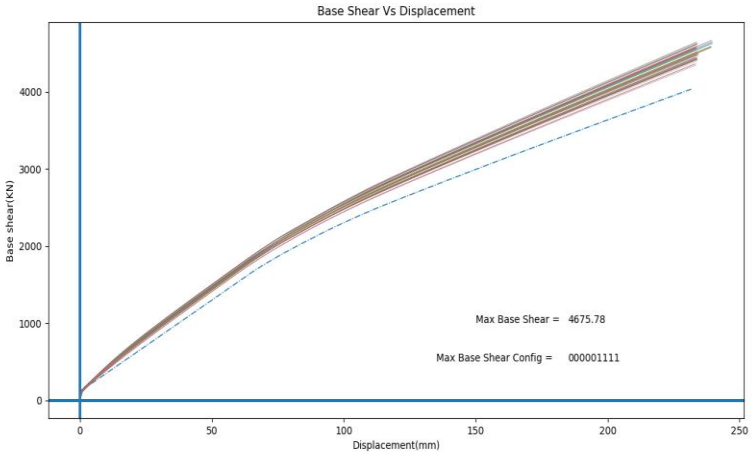

Figure 4. Base Shear vs Roof Displacement for four YSPD configurations (9C4=126 curves) using YSPD type 3
(Max Base Shear is 4675.78 kN for roof displacement 234.071 mm)

3.2 Inter Storey Drift Graphs

The above figures show the comparison between the results for different configuration of YSPDs. Our goal is to find the best result and the associated configuration for that result. FEMA-273 code sets some allowable limits by for Inter storey drift ratio. Those values were represented in the graphs as OP, IO, DC, LS and CP.

Finding the best configuration from the graphs above is not an easy task. It is observed from the graphs that maximum inter storey drift is usually found in floor 1. But we have 1534 values for the inter sorey drift for floor 1. The lowest of these 1534 values gives the best configuration. For exact determination of the configuration, these 1534 values need to be compared. It can be done manually one by one by the process of elimination. It can also be done by writing some codes and sorting the values.

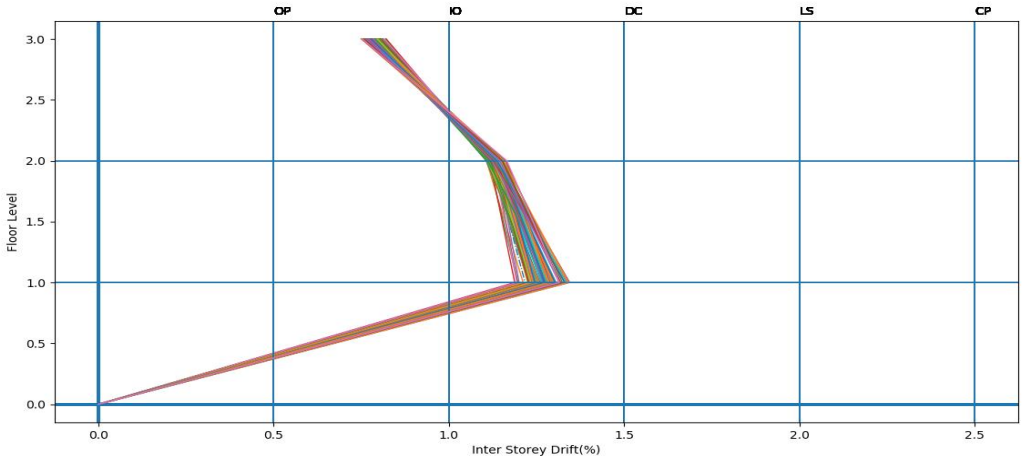

Figure 5. Inter Storey Drift for Four YSPD configurations (9C4=126 curves) using YSPD type 1

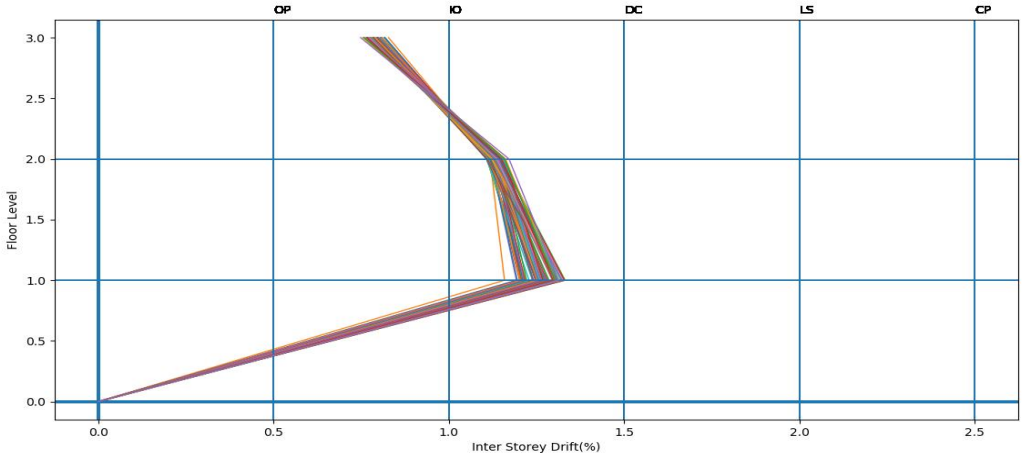

Figure 6. Inter Storey Drift for Triple YSPD configurations (9C3=84 curves) using YSPD type 2

Table 2. Limit states and allowable limit (%)

Limit State	Allowable Limit (%)
Operational	0.5
Immediate Occupancy	1
Damage Control	1.5
Life Safety	2
Collapse Prevention	2.5

4. CONCLUSION

From the graphs we found that config_011111111 of YSPD type 3 can take the highest Base Shear which is 5160.04 kN but the Inter storey Drift ratio for that configuration is higher.
So we used our judgment to balance both and chose config_111001000 to be the best configuration using YSPD type 3. For YSPD type 2, the best configuration seems to be using 3 YSPDs and 4 YSPDs for YSPD type 1.
In our research we had to deal with only 9 nodes and we did not consider mixing of separate types of YSPD in a single model, so we had only 1534 configurations. If the structure were supposed to be bigger and different types of YSPD were used in different nodes in a single model, the number would go way up. But the process we described can handle any number, however big it is.

REFERENCES

Hossain MR, Ashraf M, Padgett JE (2012). "Risk-based seismic performance assessment of Yielding Shear Panel Device." Engineering Structures

Hossain MR, Ashraf M, Albermani F (2009). "Numerical evaluation of yielding shear panel device: a sustainable technique to minimise structural damages due to earthquakes"

Matteis GD, Landolfo R, Mazzolani FM (2003). "Seismic response of MR steel frames with low-yield steel shear panels"

Proc. 2nd International Conference on Structural Engineering Research (iCSER2019)
19-22 Jan 2019, Dhaka, Bangladesh
ISBN: 978-0-6482681-2-3

Seismic Performance of Steel Concrete Composite Frames for Buildings

Naeem Kamal[1] and Mahbuba Begum [2]

[1]Post Graduate student, Bangladesh University of Engineering and Technology (BUET), Dhaka, Bangladesh
[2]Professor, Bangladesh University of Engineering and Technology (BUET), Department of Civil Engineering, Dhaka, Bangladesh
Corresponding author's E-mail: naeem.buet09@gmail.com

Abstract

Steel-concrete composite system has several advantages over traditional reinforced concrete or steel structures: these include high strength-to-weight ratios, structural integrity, durable finishes, dimensional stability and improved toughness. These advantages have led to a substantial increase in the use of composite construction all over the world. However, in a developing country like Bangladesh this innovative technology is not practiced widely. Reinforced concrete members are mostly used in the framing system for most of the buildings since this is the most convenient & economic system for low-rise buildings. In addition, composite structures have higher ductility and toughness compared to reinforced concrete structures making them a better choice for situations where seismic loading is a design consideration. An attempt has been made in this study to evaluate the seismic performance of steel concrete composite framing system in comparison to reinforced concrete buildings in the context of Bangladesh. Nonlinear static analysis using push over method is carried out on a typical commercial building designed with steel concrete composite framing system as well as with RC framing system. Finite element based software ETABS is used to perform the analysis. Capacity curves obtained from pushover analysis show higher load carrying capacity for composite framed building as compared to RC framed building. Larger base shear and greater deflection are observed at the performance point for serviceability, design and maximum earthquake for composite structure during the application of lateral load. Composite structure shows linear behavior and gradual failure pattern indicating higher ductility than reinforced concrete structure.

Keywords: Composite structure, concrete, ductile behaviour, pushover analysis, seismic performance.

1. INTRODUCTION

Steel concrete composite framing system comprises of composite column and steel concrete composite deck floor system. Composite deck floor system consists of steel beams, metal decking, shear studs and concrete. All these materials are combined in a way so that the properties of each element can be used efficiently and economically in the construction of buildings and bridges. Steel concrete composite structure is most suited for medium to high rise buildings. This system has several advantages over traditional RC and steel structure such as higher structural integrity, high strength to weight ratio, limited cross sectional dimension, higher available floor area, sound absorption etc. These advantages have made composite construction more popular and widely acceptable construction system throughout the world. Extensive experimental and numerical research works have been conducted by several researchers e.g. Florides and Cashell (2017), Baran and Topkaya (2014), Ellobodya and Young (2011), Tokgoz and Dundar (2008), Chen and Lin (2006), Shanmugam and Lakshmi (2001) on composite column and floor system for various conditions of loading. Design guidelines for composite frame structures have already been included in various design codes e.g.

AISC (2010), ACI 318 (2005), CISC (2009) and Eurocode 4(2005). However, the behaviour of a composite beam-column frame system under seismic loading is not yet addressed widely. This study intends to investigate the performance of a low rise steel concrete composite frame under seismic loading. Nonlinear pushover analysis is used to evaluate the response of a six storied composite framed building. The behaviour of the composite frame is than compared to a similar reinforced concrete frame.

2. METHODOLOGY

In this research a six storied commercial building with a floor layout plan, as shown in Figure 1, is selected. The basic features of this building including geometry, material properties and loading considerations are provided in Table 1. Two types of framing system are considered for this building – (i) reinforced concrete beam column frame and (ii) steel-concrete composite beam column frame. Typical floor plans for the buildings are shown in Figure 1 and Figure 2. In both cases, the building is kept identically same with the same plan area and floor height. In X- direction, 4 bays of 6.1 m each are considered whereas 2 bays of same length are considered in Y-direction. The analysis and design of the two different building frames are conducted using the finite element based software, ETABS.

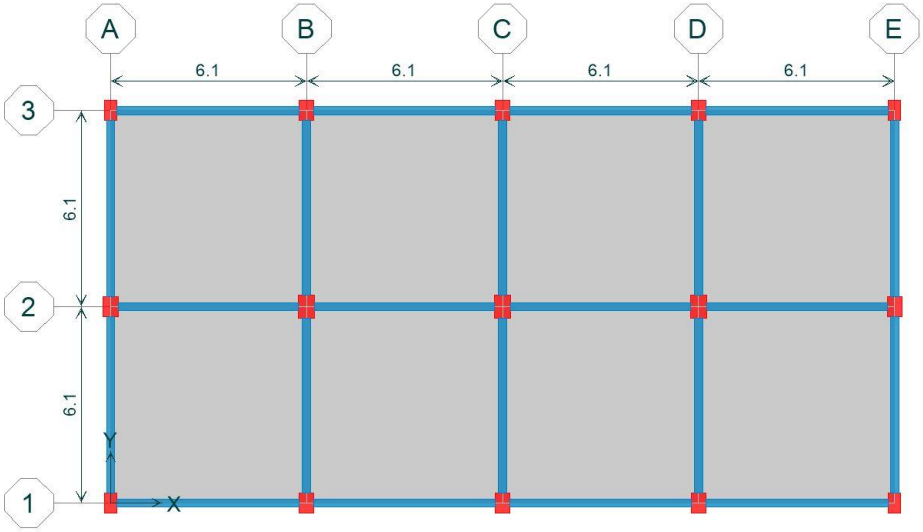

Figure 1. Typical floor plan of reinforced concrete building

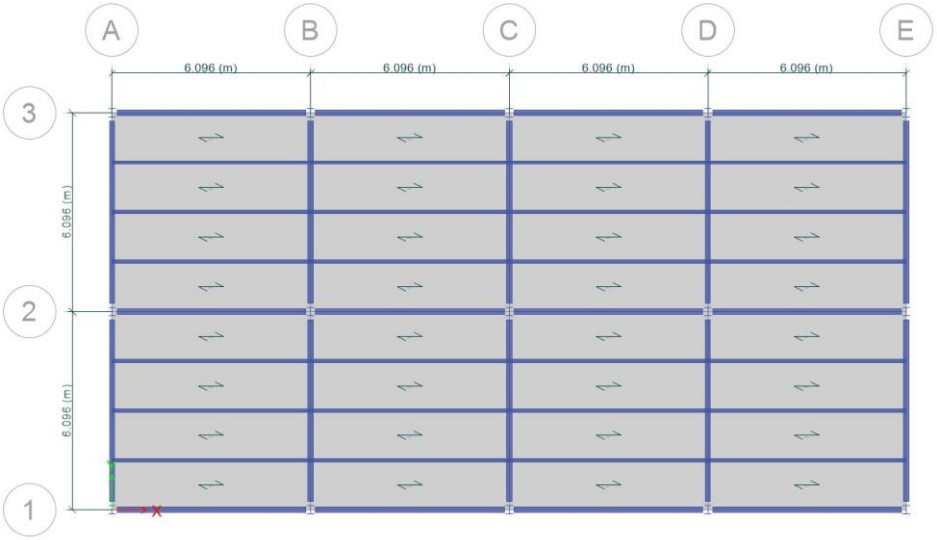

Figure 2. Typical floor plan of steel concrete composite building

Table 1. Basic features of the building

Geometric property	
Type of building	Commercial
No. of storey	6
Height of the building	18.3 m
Typical storey height	3.05 m
Length of the building	24.4 m
Width of the building	12.2 m
Material property	
Concrete strength	28 MPa
Yield strength of steel section	415 MPa
Yield strength of reinforcement	415 MPa
Loading Condition	
Live load	3 KN/m^2
Floor finish	1.5 KN/m^2
Partition wall	4 KN/m^2
Brick wall	7.3 KN/m (exterior beams) and 5.11 KN/m (interior beams)
Wind load (as per BNBC 2006)	
Site location	Dhaka
Basic wind speed	210 km/hr
Exposure	A
Structure importance coefficient	1.0
Earthquake load (as per BNBC 2006)	
Seismic modification factor, R	8 (concrete) and 6 (composite)
Seismic zone coefficient, Z	0.15 for zone 2 (Dhaka)
Structure importance coefficient, I	1.00
Site coefficient, S	1.5

The 6-storied reinforced concrete building is designed according to BNBC (2006) and ACI 318 (2005). In this building a two way beam supported slab is considered for gravity load resisting system. The lateral load is transferred through reinforced concrete beam column frames. In the 6-storied composite building, columns are designed as fully encased composite sections and slabs as composite deck slab resting on steel beams. Steel concrete composite beam-floor system as shown in Figure 3 is used to transfer the gravity load and beam column frame is used as the lateral load resisting system. The columns and beam sections used in the composite frame is shown in Figure 4. No shear wall is used for both types of structures. AISC-LRFD (2010) code is implemented for designing the steel concrete composite frame system.

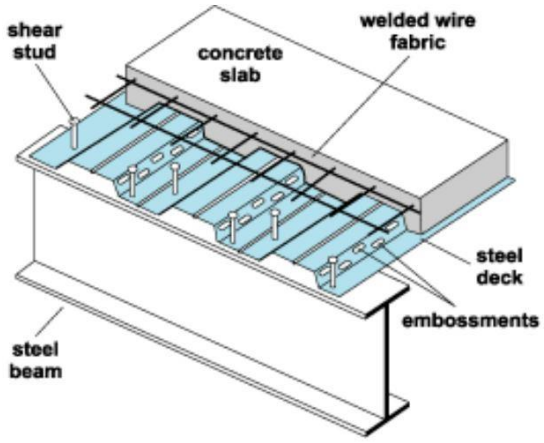

Figure 3. Steel concrete composite beam-floor system

Nonlinear static pushover analysis is used for seismic evaluation of RC and composite structure. In this process, a series of static analysis is conducted to develop a capacity curve for the structure. Capacity spectrum method is used to obtain and compare the performance of RC and composite structure during seismic loading in Y direction.

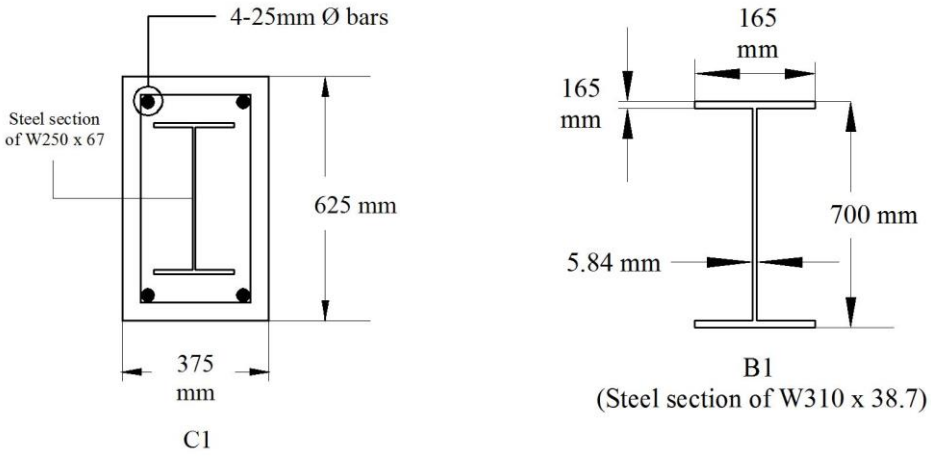

Figure 4. Column and beam Sections for composite building

3. RESULTS AND DISCUSSION

Capacity curves are obtained in Y direction for both reinforced concrete structure and composite structure. These curves are shown in Figure 5 and it is observed that both the curves show similar behaviour of initial linearity and then start to deviate from the linearity as the buildings components such as beams and columns experience inelastic action. Composite structure shows more linear behaviour then RC structures since RC structures behaves linearly up to base shear/ weight (V/W) ratio of 6.85% with a displacement/ height percentage of 0.22 whereas these values are 12.81 and 0.94 respectively for composite structure. Failure pattern of composite structure is gradual whereas sudden

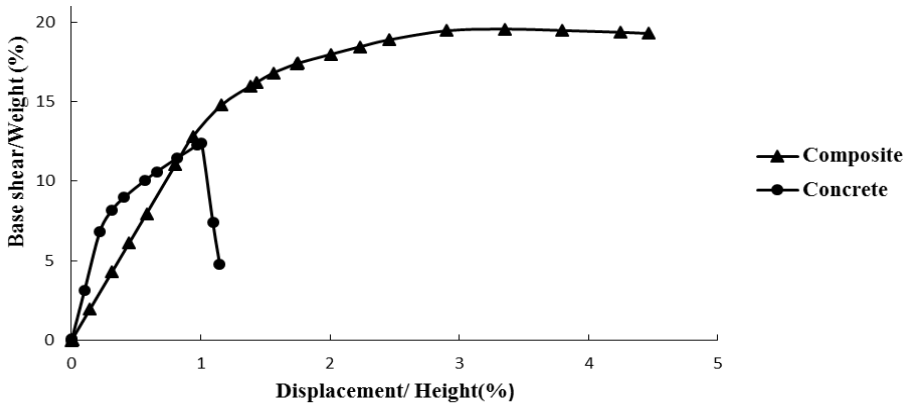

Figure 5. Capacity curve for composite and RC structure

failure pattern is obtained in the RC structure. This indicates improved ductile behaviour of composite structure. As, composite structure exhibits improved ductility, its performance on seismic loading is better than RC structure. Performance point for serviceability, design and maximum earthquake are determined in Y-direction through capacity spectrum for both composite and RC structure. Graphs for design earthquake are shown in Figures 6 and Figure 7. Base shear and displacement at performance points for all three types of earthquakes are presented in Table 2. It is seen from the table that

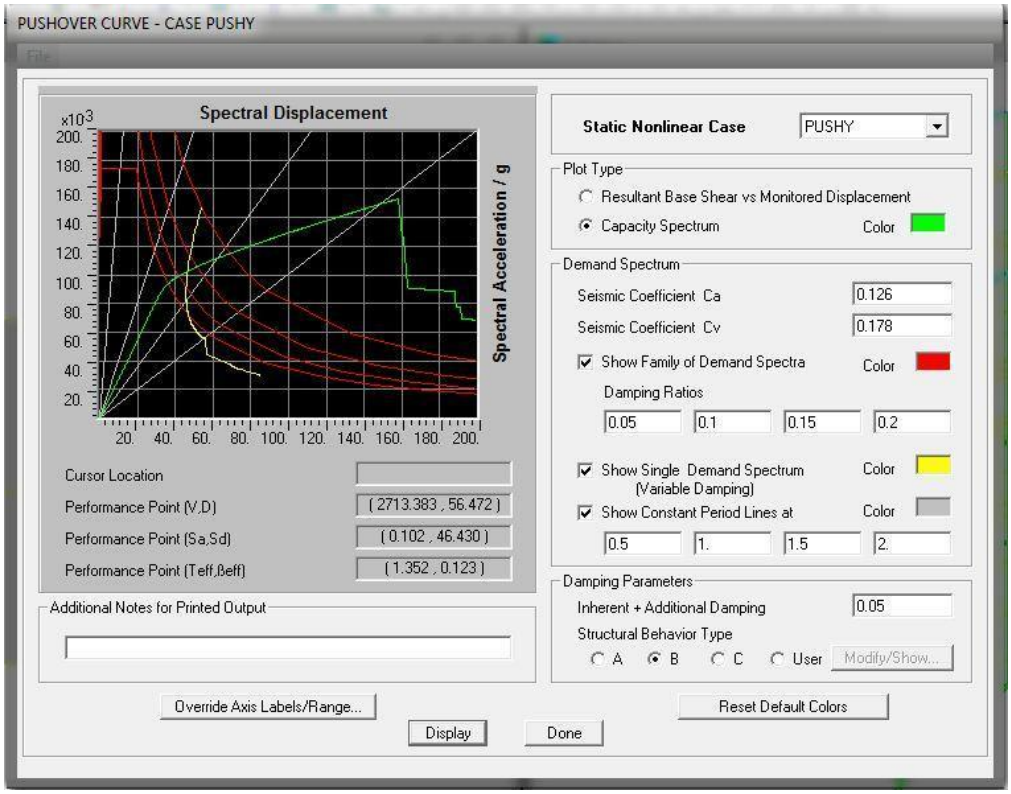

Figure 6. Capacity spectrum for reinforced concrete structure in Y-direction (design earthquake)

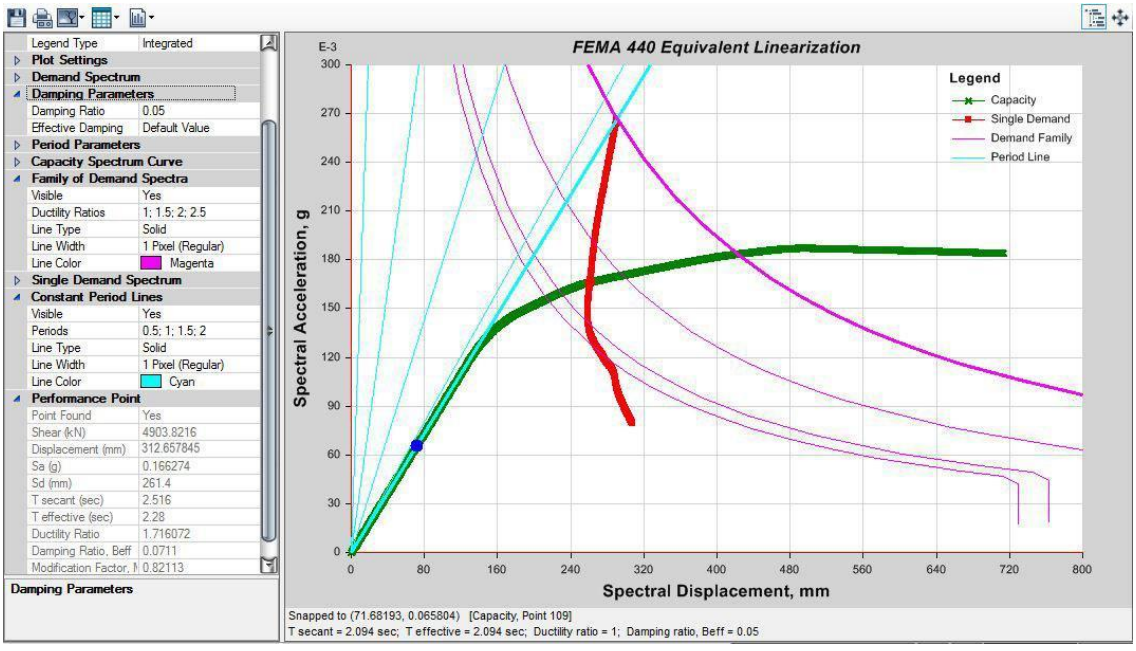

Figure 7. Capacity spectrum for steel concrete composite structure in Y-direction (design earthquake)

composite structure has larger base shear at performance point than RC structures for all three types of earthquake. Again, composite structure shows higher deflection than RC structure at performance point. All these indicates better seismic performance of composite structure than reinforced concrete structure.

Table 2. Base shear and displacement at performance point in Y-direction

Type of earthquake	Base shear (KN)		Displacement (mm)	
	RCC, V_R	Composite, V_C	RCC, D_R	Composite, D_C
Serviceability earthquake	2456	4400	45	237
Design earthquake	2714	4907	56	312
Maximum earthquake	3377	5040	106	351

4. CONCLUSIONS

Nonlinear push over analysis was conducted on a 6-storeid building to evaluate the seismic performance of steel concrete composite frame system. The results were compared with a similar RC frame structure. The capacity curve and performance point for each structure was determined for serviceability, design and maximum level of earthquake. From the capacity curves, it was observed that the ultimate load carrying capacity of composite structure is about 60% higher than RC structure. However, RC structure shows higher initial stiffness as compared to composite structure. Performance points obtained from capacity spectrum show higher (80% higher as compared to RC frame) base shear and displacements of composite structure. Moreover, composite structure showed ductile failure with large displacement as compared to sudden failure of RC structure when subjected to lateral load. All these imply that composite structure exhibits improved performance under seismic loading than RC structure. However, further research on various types of buildings is required to establish the findings of current research.

REFERENCES

ACI 318-05 (2005). Building Code Requirements for Structural Concrete, American Concrete Institute, ACI.

AISC-LRFD (2010). AISC Manual for Steel Construction, American Institute for Steel Construction, USA.

Baran E, Topkaya C (2014). Behavior of Steel–Concrete Partially Composite Beams with Channel Type Shear Connectors, Journal of Constructional Steel Research, Elsevier, 97, 69-78 pp.

BNBC (2006). Bangladesh National Building Code, Dhaka, Bangladesh.

Chen CC, Lin NJ (2006). Analytical model for predicting axial capacity and behavior of concrete encased steel composite stub columns, Journal of Constructional Steel Research, 62,424–433 pp.

CISC (2009), Handbook of Steel Construction, Canadian Institute of Steel Construction, Toronto, Ontario.

Ellobody E, Young B (2011). Numerical simulation of concrete encased steel composite columns, Journal of Constructional Steel Research, 67, 211–222 pp.

EUROCODE 4 (2005). Design of Composite Steel and Concrete Structures, EN, Euro code 4, UK.

Florides MM, Cashell KA (2017). Numerical Modelling of Composite Floor Slabs Subject to Large Deflections, Institution of Structural Engineers, Elsevier, 9, 112-122 pp.

Shanmugam NE, Lakshmi B (2001). State of art report on steel composite columns, Journal of constructional steel research, l57, 1041-80 pp.

Tokgoz S, Dundar C (2008). Experimental tests on biaxial loaded concrete encased composite columns", Journal on Steel and Composite Structure, 8(5), 423-438 pp.

Proc. 2nd International Conference on Structural Engineering Research (iCSER2019)
19-22 Jan 2019, Dhaka, Bangladesh
ISBN: 978-0-6482681-2-3

Feasibility Study of Using Stainless Steel Plates in Beam-Column Connection to Improve Seismic Performance

Arifuzzaman Nayeem[1], Shohrat Jahan[1] and Shameem Ahmed[2]

[1]Student, Department of Civil Engineering, BUET, Dhaka, Bangladesh
[2]Assistant Professor, Department of Civil Engineering, BUET, Dhaka-1000, Bangladesh
Corresponding author's E-mail: 3shameemahmed@ce.buet.ac.bd

Abstract

Seismic performance of a structure mainly depends on the flexibility of its joints. Being a nonlinear metallic material with significant strain hardening, stainless steel may be a suitable option to be used in the beam-column joint to improve the seismic performance of steel structures. In this study, performance of beam-column joints using stainless steel was evaluated through numerical analysis. Initially, three dimensional finite element model of a steel beam-column joint was developed and then verified with test results available in literatures. This verified model was used to analyse the behaviour of steel beam-column joint under cyclic loading. After that, the connecting plates of the beam-column joint were replaced by stainless steel plates and the behaviour of that joint was observed for same loading condition. In addition to these, a full stainless steel beam-column joint was also analysed under cyclic loading. The energy absorption capacity of each joint was calculated from the hysteresis diagram. Based on the energy absorption capacity and failure mode, the performance of all the joints was assessed.

Keywords: Cyclic loading, Energy absorption capacity, Hysteresis diagram, Strain Hardening, Seismic Performance, beam-column connection.

Proc. 2nd International Conference on Structural Engineering Research (iCSER2019)
19-22 Jan 2019, Dhaka, Bangladesh
ISBN: 978-0-6482681-2-3

Dynamic Behavior of a Tied-Arch Bridge to Seismic Excitation

Md. Rakib Hossain[1], Md. Faizur Rahman[1], Shohel Rana[2]

[1]Undergraduate Students, Department of Civil Engineering, BUET, Bangladesh
[2]Associate Professor, Department of Civil Engineering, BUET, Bangladesh
Corresponding author's email: rakibhossainbuetce31@gmail.com

Abstract

This paper represents dynamic behavior and seismic design of a tied arch bridge. A finite element model of the bridge is performed to observe the dynamic behavior of the bridge. El Centro'1940s earthquakes are used as input for the seismic excitation and dynamic time history analysis is performed to observe the various responses of the bridge. From the seismic responses, seismic loading or base shear for the design of the bridge is determined and compared against available standards.

Keywords: Seismic Design, Dynamic Response, Tied-Arch Bridge, Base Shear

1. INTRODUCTION

Bridge engineering is an important part of traffic lifeline engineering. Collapse of the bridge structure due to earthquake may cut off the lifeline of the quake zone. It can cause great inconvenience for the earthquake region when the quake occurs. Hence, earthquake effects are one of the major consideration for the design of bridges. To improve the seismic performance of the bridge, it is very important to analyze seismic response of the bridge. Traditionally, static method is considered for seismic design of the bridges. But earthquake is a dynamic phenomenon. Dynamic behavior of the bridge with real earthquake data is required to be analyzed and to be utilized for design. Dusseau and Wen (1989) studied the seismic responses of deck type arch bridges. Wen (1993) studied seismic response of a tied-arch bridge and proposed design aids for that bridge. Yunping and Dejin (2016) performed seismic response analysis of tied-arch Bridge. Mohseni et. al. (2018) studied and assessed the structural performance of reinforced concrete (RC) arch bridges under strong ground motion. This paper presents dynamic responses of a tied-arch bridge using El-Centro earthquake excitation. Dynamic time-history analysis is performed and responses to earthquake motions are obtained based on direct integration method. The responses are compared with that of available seismic loading calculated using seismic data and procedure of Dhaka city.

2. BRIDGE MODELING AND PARAMETERS

Fig. 1 shows the analyzed arch bridge. It is a highway bridge with four lanes (20.0 m wide), and has a span length of 35 m and an arch rise of 18.0 m. The vertical hanger members are rigidly connected to the arch ribs and the deck. Seismic design was originally conducted in accordance with the AASHTO LRFD Design Specifications of Highway Bridges. The seismic coefficient of 0.20 was assumed in both longitudinal and transverse directions for Dhaka city.

3. GROUND MOTION INPUT AND SEISMIC BASE SHEAR

The North-South component of the El Centro'1940s earthquake is used as the input of ground motion. However, acceleration values are calibrated for Dhaka (Zone 2) (see Fig. 2) such that it has the maximum Peak Ground Acceleration (PGA) of 0.2g as of Bangladesh National Building Code

(BNBC). BNBC has limited the maximum PGA = 0.2g for Dhaka. The seismic response coefficient, C_{sm} according to AASHTO LRFD 2012 is determined as follows:

PGA = 0.2 [Zone 2]

For site class D according to AASHTO LRFD, Horizontal response acceleration coefficient at 0.2s period on loose-to-medium cohesionless soil, $S_s = 0.5$

Horizontal response spectral coefficient at 1.0s period on loose-to-medium cohesionless soil, $S_1 = 0.2$

Determination of Seismic coefficient F_a and F_v for site class D,

For $S_s = 0.5$, $F_a = 1.4$. [AASHTO LRFD Table 3.10.3.2-2]

For $S_1 = 0.2$, $F_v = 2.0$ [AASHTO LRFD Table 3.10.3.2-3]

Natural period of the bridge, $T_m = 0.476$ s (from Finite Element Analysis)

$S_{D1} = F_v S_1 = 2.0 \times 0.2 = 0.4$,

$S_{DS} = F_a S_S = 1.4 \times 0.5 = 0.70$

Now, $T_s = S_{D1}/S_{DS} = 0.4/0.7 = 0.571$ s

$T_o = 0.2\ T_S = 0.2 \times 0.571 = 0.114$ s

For periods greater than or equal to T_o and less than or equal to T_S ($T_o \leq T_m \leq T_S$), the elastic response coefficient C_{sm} for the m-th mode of vibration is given by Equation

$C_{sm} = S_{DS} = 0.7$ [AASHTO LRFD Equation 3.10.4.4-4]

Now, the base shear for the arch is given by the following equation

$$V = \frac{2}{3}\frac{I}{R} C_{sm} W, \qquad \textbf{(Eq. 1)}$$

where I = Structural Importance = 1,
R = Response Modification Factor = 3 [AASHTO Table 3.10.7.1-1],
W = Total weight of the Bridge.

Thus, V = 15.56% W.

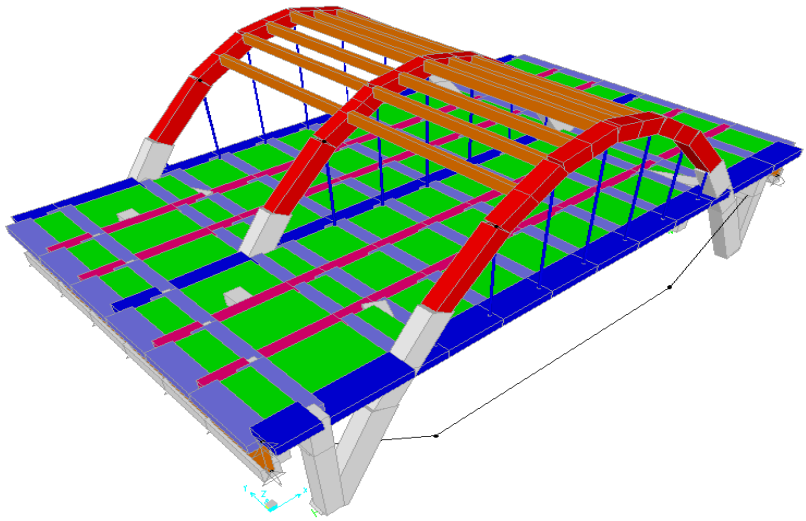

Figure 1. 3-D View of the analyzed Arch Bridge

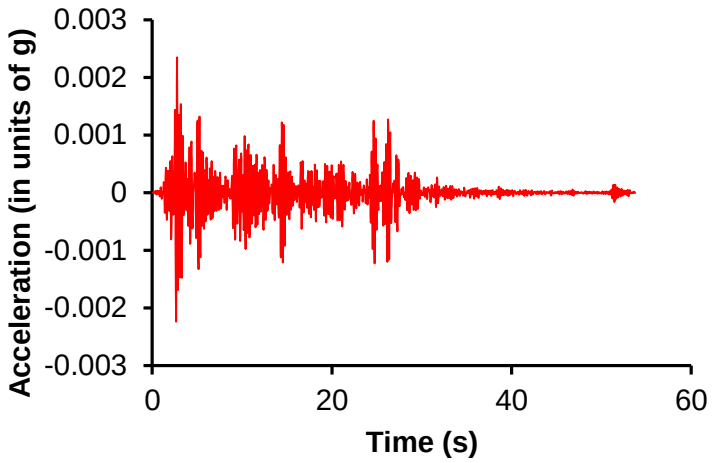

Figure 2. Calibrated Acceleration versus Time Graph (for Dhaka)

4. METHOD OF ANALYSIS

The Time history analysis are performed by using a finite element software. Two types of analysis are executed:

(1) Linear Modal Time History Analysis
(2) Linear Direct Integration Time History Analysis

In the linear modal time history analysis, a constant damping of 5% is maintained. Whereas, in direct integration time history analysis, Hilber-Hughes-Taylor (HHT) time integration method is used. In which $\gamma = 0.5$, $\beta = 0.25$, $\alpha = 0$ and mass and stiffness proportional damping is specified by 5%.

5. COMPARISON OF STATIC AND TIME HISTORY ANALYSIS

A typical response of the bridge at the peak point of the arch is shown in Fig. 3. The seismic base shear calculated according to standard (see Eq. 1) is applied to the bridge and static analysis is performed. The static analysis is compared against dynamic analysis and shown in Table 1. The results indicates that dynamic response is significantly higher for the bridge studied here. The base shear in case of dynamic analysis are both directions are significantly higher and around 2% and 16.5 % higher in x and y direction of the bridge respectively. The x direction is along the bridge and y direction is across the bridge.

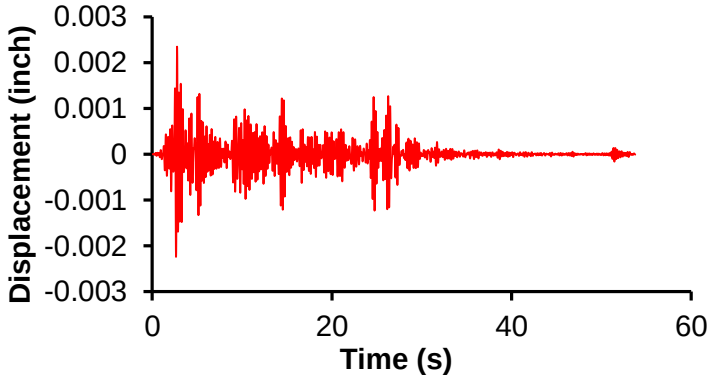

Figure 3. Displacement behavior at the Peak of the Arch with time

Table 1. Static analysis and Time History Analysis Result

Analysis Method	Direction	Base Reaction (Kip)	Seismic Dead Load (Kip)	% of Dead Load
Static Analysis With seismic base shear	Earthquake in X Direction	-854.507	5512	15.50%
	Earthquake in Y Direction	-854.507		15.50%
Time History Analysis (Linear Direct Integration)	Earthquake in X Direction	958.074		17.38%
	Earthquake in Y Direction	-1762.848		31.98%

6. CONCLUSION

This paper studies the seismic response of a tied-arch bridge located at Dhaka excited by earthquake ground motion. The dynamic effects of earthquake excitations, and local site effect on the responses of the tied-arch bridge are investigated. The dynamic response of the bridge due to seismic excitation is significantly different than that of static response. The percentage of base shear in case of dynamic analysis is found almost twice the static analysis in across the bridge direction. It should be noted that the structural responses are determined by the structure itself and the characteristics of earthquake excitations. However, results from this study demonstrate the importance of considering dynamic effect on the seismic design of the tied-arch bridge.

REFERANCES

Dusseau RA., and Wen RK. (1989). Seismic responses of deck-type arch bridges, Earthquake Engineering and Structural Dynamics, 18(5): 701-715.

Mohseni I, Lashkariani HA, Kang J, and Kang THK. (2018). Dynamic Response Evaluation of Long-Span Reinforced Arch Bridges Subjected to Near- and Far-Field Ground Motions, Applied Science, 8-1243; doi: 10.3390/app8081243.

Wen RK. (1993). Seismic response of and design aids for arch bridges. Journal of Structural Engineering, ASCE, 119(10)-2969.

Yunping W, Dejin T. (2016). Seismic response analysis of tied arch bridge, International Conference on Civil, Structure, Environmental Engineering (I3CSEE 2016), March 12-13, 2016 in Guangzhou, China.

AASHTO LRFD Bridge Design Specifications (standard 2010)

Proc. 2nd International Conference on Structural Engineering Research (iCSER2019)
19-22 Jan 2019, Dhaka, Bangladesh
ISBN: 978-0-6482681-2-3

A Comparative Study OF BNBC 1993 and 2017 Provisions for the Design of Multistoried Steel Buildings in High Wind and High Seismic Zone

Md. Shadman Sakib[1] Samia Zakir Sarothi[2] Md. Abir Hasan[3] Arifa Akther[4] and Tanvir Rabbi[5]
Dr.Khan Mahmud Amanat[6]

[1-5]B.Sc. in Civil Engineering, BUET, Dhaka, Bangladesh
[6]Professor, Civil Engineering Department, BUET, Dhaka, Bangladesh
Corresponding author's E-mail: saadmansakib01@gmail.com

Abstract
In order to incorporate knowledge and advancement in structural engineering over the last two decades, significant changes were introduced in BNBC 2017. Modification regarding design parameters and analysis methodology were proposed which primarily pivoted around analysis of wind and seismic loads. In case of wind load, change were introduced by modifying method of analysis and load projection, basic wind speed, gust response factor, external and internal pressure co-efficient, topographic effect, exposure and enclosure classification. For seismic load, design spectral acceleration had been reformulated. Seismic zoning was subjected to re-calibration of PGA values. Response reduction factor for structural system, structural importance factor and soil factor was diversified. In order to get a clear understanding of the modifications, an initiative was taken to conduct a controlled parametric study of steel structures based on the previous (BNBC 1993) and proposed new (BNBC 2017) codes using finite element analysis. Research was carried out by analysis of 8 and 16 story steel structures in Chattrogram city. As per research, the basic difference between the codes are in wind and seismic base shear, maximum lateral displacement. For steel building, variation in steel requirement for structural element such as beam, columns and bracing was prominent. In light of this study, a clear vision of changes in structural detailing, cost effectiveness and safety in between the two BNBC codes has been established.

Keywords: BNBC, Wind load Analysis, Earthquake load analysis, Comparative study

1. INTRODUCTION

Bangladesh National Building Code 2017 has been developed for the further advancement of more rational design of structures to ensure improved serviceability and safety. The primary differences between BNBC 1993 and 2017 are based on the analysis of seismic and wind loads which are relatively more complicated than static dead load. In terms of analysis, significant changes have been introduced to wind and seismic loads. The sole purpose of this study is to investigate this changes from structural and economic point of view. So, a standardized structural analysis of 8 and 16 storied steel frame was conducted in accordance with both sets of code.

2. LITERATURE REVIEW

The proposed changes to BNBC 1993 was first brought up by the research team of Al-hussaini, T.M. et al (2012).They conducted a thorough study on Peak ground acceleration (PGA), spectral acceleration, soil classification system, site-dependent response spectrum and worked extensively in defining seismic design category. They showed that BNBC 1993 needs a major update in term of provision for design and structural analysis. Atique F and Wadud Z (2001) presented Comparison of BNBC-93 with other

building codes with respect to Earthquake and Wind analysis. Research conducted by Bari M.S., Das T (2014) had been one of the most compressive studies where a detailed parametric comparison was put forth based on BNBC-2017, BNBC-1993, and code of India 2005 (NBC-India 2005).

3. MODELING AND ANALYSIS

To study the changes in analysis and design of high rise and low rise steel building in high seismic and high wind zone of Bangladesh (Chattogram), a typical multi-storeyed commercial steel building plan is selected. It was considered as concentric braced frame and special steel concentrically braced frame in BNBC 1993 and BNBC 2017 respectively. The soil condition of the concerned zone is mainly soft to medium stiff clay. The floor-to-floor height has been set to 3.60m. A 3-span by 3-bay plan (16.5 m x 24 m) was considered for both building. The structural analysis and design is carried out using finite element analysis. Structures are analysed and designed for gravity loads (e.g. dead loads and live loads) as well as lateral loads (e.g. wind and earthquake loads). Dead loads include self-weight of building frame and shell elements, floor finish, partition wall and other super imposed loads. Live loads include all temporary loads applied after construction of the building.

Dimensions of the steel structure was determined by following pre-set conditions-

a. To maintain minimum clear distance of 7300mm for 2 parallel set of car parking, column width in long direction is kept to a maximum of 700mm.
b. For air-conditioning ducts between the false ceiling and beam bottom, depth of 150mm to 200mm is required and clear height between floor and false ceiling are generally kept at 2600mm. To satisfy this requirement beam depths were limited to 750mm as the floor to floor height is 3600mm.

Table 1. Analysis parameter - seismic load analysis

Parameter	BNBC 1993	BNBC 2017
Seismic Zone Coefficient - Z	0.15	0.28
Site Classification	S3	SD
Site Coefficient - S	1.5	1.5
Importance Factor - I	1.00	1.00
Time Period - T	$T = C_t h_n^m$; $C_t = 0.035$	$T = C_t h_n^m$
Frame System	Concentric Braced Frame	Special Concentric Braced Frame
Reduction Factor - R	R=8 (Concentric Braced Frame)	R=6 (Special CBF)
ETABS Analysis Algorithm	UBC 94	User Coefficient
SDC	N/A	D (Severe)

Table 2. Analysis parameter – wind load analysis

Parameter	BNBC 1993	BNBC 2017
Analysis Method	Surface Area Method	Analytical Procedure
Basic Wind Speed – V_S	Fastest mile speed: 260 km/hr	3 sec Gust wind: 288 km/hr
Exposure Category	A (Urban – Sub urban area)	A (Urban – Sub urban area)
Standard Occupancy Structure IF	1.00	1.00
Max Deflection Limit	$\frac{n}{500}$ for 100% Wind effect	$\frac{n}{500}$ for 70% Wind effect
Other factors	Combined height and exposure coefficient C_z	Topographical Factor K_{zt} -1.00 Directionality Factor K_d - 0.85 Velocity exposure coefficient K_z
ETABS Analysis Algorithm	UBC 94	ASCE 7-05

Table 3. Design parameter – Steel Frame design

Parameter	BNBC 1993	BNBC 2017
Design code	AISC-LRFD 93	AISC 360-05
Frame type	Braced frame	SCBF
Deflection check type	both	both
Seismic design category	N/A	D
System R	8	6
Design provision	LRFD	LRFD
Stress ratio limit	0.99	0.99
Effective length factor K major and minor Axis	1	1

Structures are analysed and designed for gravity loads (e.g. dead loads and live loads). Dead loads include self-weight of building frame and shell elements, floor finish, partition wall and other super- imposed loads. Live loads include all temporary loads applied after construction of building super imposed dead and live loads that were used for the analysis, are as followed-

Live load= 3 KN/m²
Floor Finish= 1.5 KN/m²
Partition wall= 2.5 KN/m²
Live load due to lift machine= 4.79 KN/m²
Live load due to water tank= 17.24 KN/m²

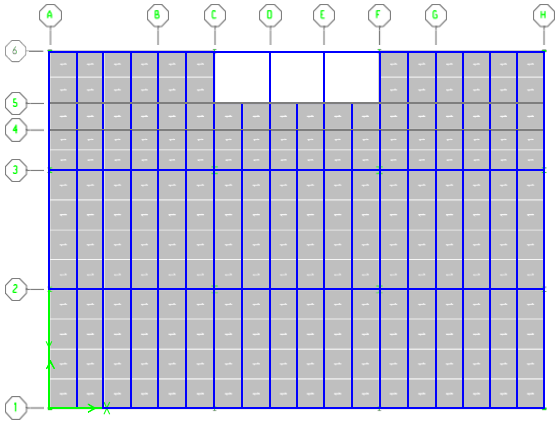

Figure 1. Plan Layout

The building frame system consists of beam, columns and bracing. Concentric K bracing system was used as the main lateral deflection resisting system along with other structural elements. Steel profiled decking supported by floor beams was considered. Floor beams are assigned to be simply supported using frame release command. The deck lies perpendicular to floor beams. Floor beams of all floor are kept same except roof and designed for gravity loads only.

Hot rolled steel sections are most common structural steel for steel building construction. This prefabricated sections are in general 12m long. To keep the design practical and simplify construction procedure, consecutive 3 levels columns are grouped together so that a single steel section can be used, minimizing cut off cost and wastage. Likewise, beams and bracing were subjected to grouping of 4 consecutive levels.

Cross sectional dimension for beam, floor beam, bracing and column were derived by iterative analysis of assigned auto sections to specific structural elements. Dimensions were selected by keeping stress ratio limit 0.99 and maintaining deflection limit for maximum lateral sway and serviceability criteria.

Discarded sections:

a. All special sections having superscript c, f, h (AISC manual) and seismically non compact sections are intentionally removed from auto sections.
b. BNBC 2017 introduces seismically compact section. Sections to become seismically compact need to satisfy the criteria $\frac{b}{t} \leq 0.3\sqrt{\frac{E}{F_y}}$ which yields thicker sections than that required to prevent local buckling. The general local buckling criteria being $\frac{b}{t} \leq 0.38\sqrt{\frac{}{F_y}}$

4. RESULT AND DISCUSSION

Comparison of wind force and design seismic base shear is the main concern of this section. Change in design parameters, methods and load combinations have significant impact on lateral force calculation.

4.1. Effect on Wind Load

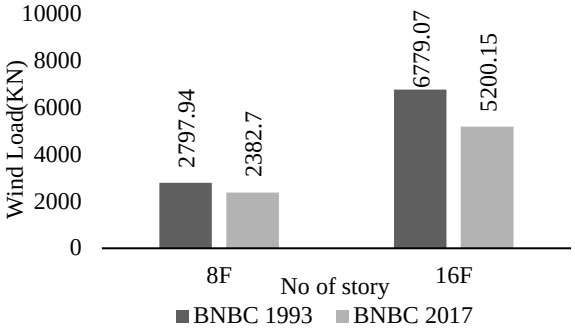

Figure 2. Wind load vs. No of story

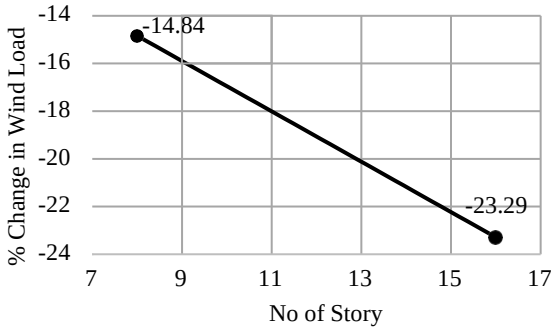

Figure 3. % change in Wind load w.r.t BNBC 93

Figure. 2 indicates, structures designed in accordance with BNBC 17 is subjected to lower wind base shear than BNBC 1993. Figure. 3 indicates percent reduction of wind force decreases with the increase of building height. These are due to differences in analytical procedure and parameters between both codes (Table 1) and significant reduction in wind pressure coefficient $C_{P.}$

Table 4. Wind Pressure Coefficient, C_P

Wind Direction	BNBC 1993			BNBC 2017			C_P decreased w.r.t 93
	Windward	Leeward	Unified C_p	Windward	Leeward	Unified C_P	
X - Axis	1.286	N/A	1.286	0.8	0.41	1.210	6%
Y - Axis	1.534	N/A	1.534	0.8	0.5	1.30	15%

As change in base shear pattern is identical for both axis, only change in longer span is showed here.

4.2. Effect on Seismic Base Shear

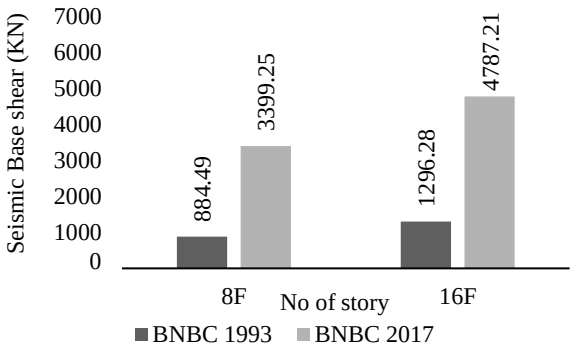

Figure 4. Seismic base shear (KN) vs. no of story

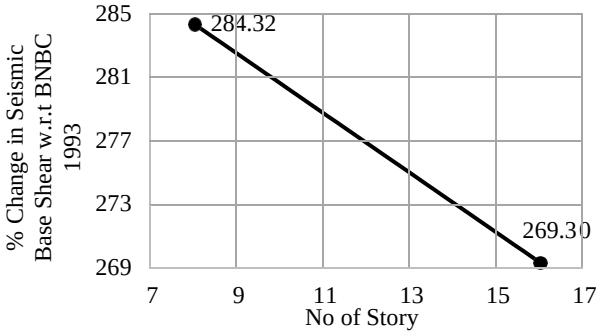

Figure 5. % change in seismic base shear

Figure. 4 indicates seismic base shear values in BNBC 17 has increased by approximately 4 times and Figure. 5 shows that the percent increase in base shear decrease with building height. The reasons behind this are discussed below-

a. The new seismic zoning map in BNBC 2017 has a higher Z value of 0.28 for Chattogram, contrary to a value of 0.15 in 93's code.
b. According to BNBC 1993 CBF system was considered while in BNBC 2017 implementation of Special CBF system was made mandatory due to consideration of seismic design category (SDC) - D, which consequently decreases value of reduction factor R (Table 5). Also introduction of C_s (normalized acceleration response spectrum) in BNBC 2017 contributes in increasing base shear. Table 5 shows variation in base shear due to these changes in parameter. Lower value of R in BNBC 17 generated a higher spectral acceleration (S_a), which results in increased seismic base shear.

Table 5. *C/R* (BNBC 1993) vs. C_s/R (BNBC 2017)

No of story	BNBC 1993				BNBC 2017				Comment On *Cs/R* w.r.t 93
	Base Shear Equation	*C*	*R*	*C/R*	Base Shear Equation	*Cs*	*R*	*Cs/R*	
8F	$V = \frac{ZIC}{R}W$	2.33	8	0.291	$V = \frac{2}{3}\frac{ZIC_s}{R}W$	3.38	6	0.563	93% (↑)
16F		1.69	8	0.211		2.33	6	0.388	84 %(↑)

Cs/R value increases by 93% and 84% respectively for 8F and 16F.

In BNBC 17, although design basis earthquake (DBE) is considered 2/3 of Maximum Considered Earthquake (MCE) total seismic base shear increases due to addition of 25% of live load as seismic dead weight. This a new provision in contrast with the older version of the code. These 2 factors increases the net spectral acceleration (S_a) by a significant margin, causing seismic base shear to increase.

5. DESIGN OUTCOMES

Column design in BNBC 93 and BNBC 17 are governed respectively by wind loading and biaxial seismic loading (BNBC 2017 seismic provision Sec. 2.5.13).The structural steel requirement of ground floor column for both 8 story and 16 story building are illustrated below:

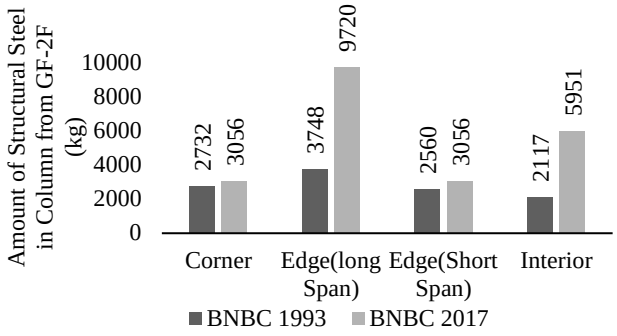

Figure 6. Structural steel 8F structure GF-2F

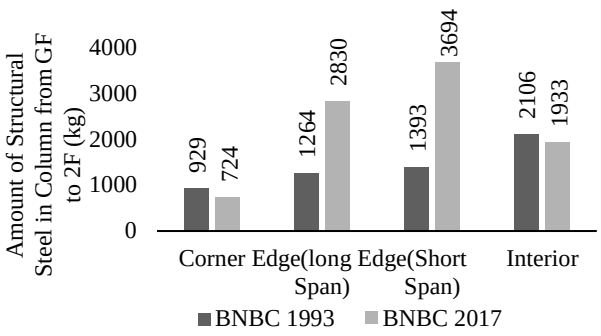

Figure 7. Structural steel 16F structure GF-2F

Table 6. Column sections GF - 2F

Column sections (mm x kg/m)		Corner column	Edge Column		Internal column
			long direction	Short direction	
8F	BNBC 93	W-310x86	W-310x117	W-310x129	W-610x195
	BNBC 17	W-310x67 ↓	W-360x262 ↑	W-310x342 ↑	W-310x179 ↓
16F	BNBC 93	W-310x253	W-360x347	W-360x237	W-360x196
	BNBC 17	W-310x283 ↑	W-360x900 ↑	W-310x283 ↑	W-360x551 ↑

*↑ indicates increase and ↓ indicates decrease in section weight w.r.t sections in BNBC 93 design.

Figure.6 shows that slightly lighter sections governed for corner and internal columns in 8F, even though higher load factor multiplier in BNBC 17 suggests otherwise. Reason for anomaly is directly related to P-M-M interaction ratio and grouping of those particular columns. In short, columns in BNBC 2017 was able to achieve an overall higher PM ratio and better fit using lighter section for all 3 consecutive columns. If we are to discard this anomaly, then all other column sections both in 8 and 16 storey building follow a similar trend. Heavier sections govern in design for BNBC 17 as shown in Figure 6-7 and Table 6. Reasons being –

a. Primarily due to higher load factor multiplier in BNBC 17 w.r.t BNBC 93. (Table 7 and 8)
b. Implementing lighter bracing system in BNBC 17 w.r.t BNBC 93, as the newer code permits larger lateral sway. Lightly braced system causes lateral stiffness of the total structure to decreases and to compensate for that, heavier section governs in vertical members to resist lateral force and excessive bending.

Table 7. Governing load combination and percent change in load factor multiplier for 8 story

Column section	Governing load combination		% Change in load factor w.r.t 93		
	BNBC 1993	BNBC 2017	DL	LL	W/EQ
Corner	1.2DL+0.5LL-1.3WY	1.326DL+LL-EX-0.3EY	↑ 11%	↑ 100%	Biaxial seismic load in 17 > Uniaxial Wind force in 93
Edge short	1.2DL+1.6LL-0.8WY	1.326DL+LL-EY-0.3EX	↑ 11%	↓ 38%	
Edge long	1.2DL+1.6LL-0.8WX	1.326DL+LL-EX-0.3EY	↑ 11%	↓ 38%	
Interior	1.2DL+1.6LL+0.8WX	1.326DL+LL-EY+0.3EX	↑ 11%	↓ 38%	

Table 8.Governing load combination and percent change in load factor multiplier for 16 story

Column section	Governing load combination		% Change - load factor w.r.t 93		
	BNBC 1993	BNBC 2017	DL	LL	W/EQ
Corner	1.2DL+0.5LL-1.3WY	1.326DL+LL-EY+0.3EX	↑ 11%	↑ 100%	Biaxial seismic load in 17 > Uniaxial Wind force in 93
Edge long	1.2DL+1.6LL-0.8WY	1.326DL+LL-EY-0.3EX	↑ 11%	↓ 38%	
Edge short	1.2DL+1.6LL-0.8WX	1.326DL+LL-EY-0.3EX	↑ 11%	↓ 38%	
Interior	1.2DL+1.6LL+0.8WY	1.326DL+LL+EY+0.3EX	↑ 11%	↓ 38%	

6. OBSERVATIONS

Seismic base shear is significantly higher for BNBC 2017 compared to BNBC 1993 due to higher seismic zone coefficient (*Z*), lower response reduction factor (*R*), increased normalized acceleration response spectrum (*Cs*). But base shear due to wind load is slightly lower for BNBC 2017 than BNBC 1993, due to reduction in wind pressure coefficient C_P. Percent change in base shear decreases with building height due to both seismic and wind loads. Heavier W section governs in vertical member design for BNBC 17, primarily due to higher load factor and modified load combinations.

7. CONCLUSION

This case study is conducted for Chattrogram city only. Similar study can be conducted for other cities of Bangladesh with varying wind and earthquake intensities.

8. ACKNOWLEDGMENTS

We highly acknowledge Dr. Khan Mahmud Amanat, Professor, Department of Civil Engineering, BUET for his kind supervision and guidance throughout the research.

9. REFERENCES

Al-hussaini, T.M., Hossain T.R., Al-Noman MN (2012). Proposed changes to the geotechnical earthquake engineering provisions of the Bangladesh National Building Code, Geotechnical Engineering Journal of the SEAGS & AGSSEA, Vol.43, No.2.

Atique F, Wadud Z (2001). A comparison of BNBC-93 with other building codes with respect to earthquake and wind analysis, The Eighth East Asia-Pacific Conference on Structural Engineering and Construction, Nanyang Technological University, Singapore.

Bari M.S., Das T (2014). A Comparative Study on Seismic Analysis of Bangladesh National Building Code (BNBC) with Other Building Codes, Journal of the Institution of Engineers (India).

Proc. 2nd International Conference on Structural Engineering Research (iCSER2019)
19-22 Jan 2019, Dhaka, Bangladesh
ISBN: 978-0-6482681-2-3

Seismic Response and Vulnerability Assessment of Buildings in Patna, India

Avik Samanta[1] and Arabinda Swain[2]

1Assistant Professor, Indian Institute of Technology Patna, Bihta, India
2Masters Student, Indian Institute of Technology Patna, Bihta, India
Corresponding author's E-mail: asamanta@iitp.ac.in

Abstract

In present day scenario, it is inevitable to build structures on soft and deformable soils due to unavailability of space. The behaviour of structures built on soft soil can be significantly different from the structures built on rocky soil. It is necessary to know the response of structures build on such soft soil conditions. Moreover, in the past few decades, a significant amount of losses have been caused by natural disasters like damaging earthquakes around the world. Thus it may be necessary to assess vulnerability of structures founded on soft soil deposits. In this work, response and seismic vulnerability of representative reinforced concrete buildings in Patna, India are assessed. To obtain the seismic response of structures, representative reinforced concrete buildings with masonry infill walls are studied with and without Soil Structure Interaction (SSI). SSI is modelled using direct method using SAP2000. It is found that consideration of SSI may provide underestimation of structural responses and vulnerability for the structures and site considered in this study.

Keywords: Ground motions, seismic vulnerability, soil-structure interaction.

Proc. 2nd International Conference on Structural Engineering Research (iCSER2019)
19-22 Jan 2019, Dhaka, Bangladesh
ISBN: 978-0-6482681-2-3

Comparative Study between Manual Analysis and Computer Software Analysis (ETABS) of a Residential Building in Dhaka City

Mrittika Hasan Rodela[1] and Ayesha Binta Ali[1]

[1]Lecturer, Department of Civil Engineering, Sonargaon University, Dhaka, Bangladesh
Corresponding author's E-mail: rodelamrittika@gmail.com

Abstract

Structural development in Bangladesh has rapidly increased as there are many construction projects has being carried out. Structural analysis is the fundamental part of the engineering design of structures. The foremost basic in structural engineering is the design of simple basic components and members of a building such as slabs, beams, columns and footing. In this paper, first of all, a manual analysis is done for a 6 storied residential building in Dhaka city using Bangladesh National Building Code (BNBC) and then a computer software analysis is done using extended three-Dimensional analysis of building system (ETABS) for the same structure. After that a comparative study between manual analysis and computer software analysis is executed and dissimilarities are found between them. It is recommended that the study can be performed for a high rise building for further studies and comparison can be done by using other structural analysis and design software. Moreover, selection of materials and their properties should meet the requirement of building codes properly otherwise integrity of the structure would fall in risk. Besides, proper supervision and monitoring during reinforcement arrangement and fabrication in the site should maintain because reinforcement bars and tie/stirrups arrangements, splicing of bars etc. in beams and columns need careful attention.

Keywords: Structural analysis and design, Bangladesh National Building Code, Ultimate Strength Design, ETABS.

1. INTRODUCTION

Structural analysis is the determination of the effects of loads on physical structures and their components. The results of the analysis are used to verify a structure's fitness for use, often precluding physical tests. Structural analysis is thus a key part of the engineering design of structures. ETABS is an engineering software product that caters to multi-story building analysis and design. It is a sophisticated, yet easy to use, special purpose analysis and design program developed specially for bending systems. ETABS provides an initiative and powerful graphical interface coupled with unmatched modelling, analytical and design procedures; all integrated using a common database. Although quick and easy for simple structures, ETABS can also handle the largest and most complex building models, including a wide range of nonlinear behaviour, makes it the tool of choice for structural engineers in the building industry. Now-a-day ETABS computer analysis has become popular for designing different types of structures. Through this study it was tried to compare the results of manual analysis and computer software analysis (ETABS) for different structural sections and provide utmost safety for residential structures.

2. METHODOLOGY

First of all a site was selected for a residential building in Dhaka city. Then a manual structural analysis was done from the architectural drawing using BNBC 1993 and ACI Codes. After that the same structural design was executed with extended three-Dimensional analysis of building system

(ETABS). Then the results from manual analysis were compared with the results found from the computer software analysis. A flow chart containing the whole procedures is shown below.

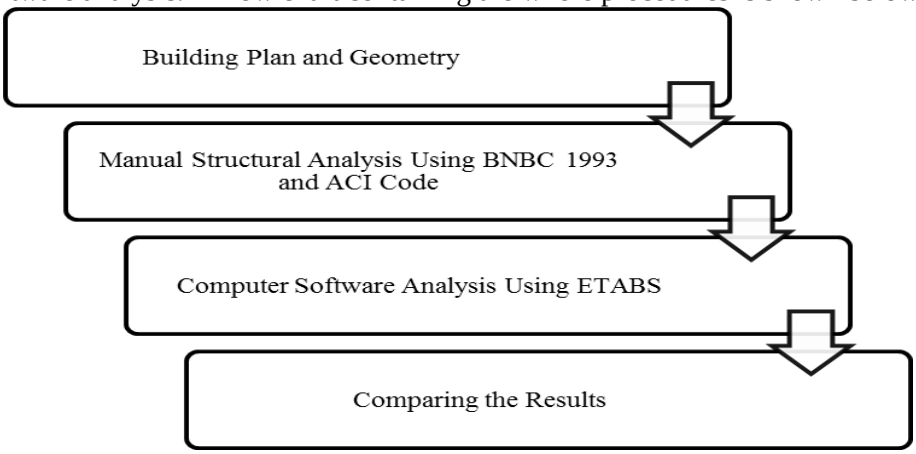

Figure 1. Flow Chart of Methodology

3. BUILDING GEOMETRY AND DIMENSIONS

The main features of the building:

Height of the building : 60 *ft*
Length of the building : 52*ft*
Width of the building : 40 *ft*
Total floors : 06 nos.
Types of floors : Beam-Column floor system
Modern amenities : One stair, generator facilities for emergency electricity supply, car and bike parking facilities at the GF floor, underground reservoir for fulfilling huge water supply demand and septic tank for waste water management of all users and one meeting hall.
Security system : There are automatic fire and security alarming systems in the building.
Safety of the Structure : Designed as per BNBC and ACI codes and specifications. Capable for resisting 210 *Km/h* wind speed and high Richter scale earthquake affects. 3.5 *ksi* concrete (w_c= 150 *pcf*) and 60-grade deformed bars are used.

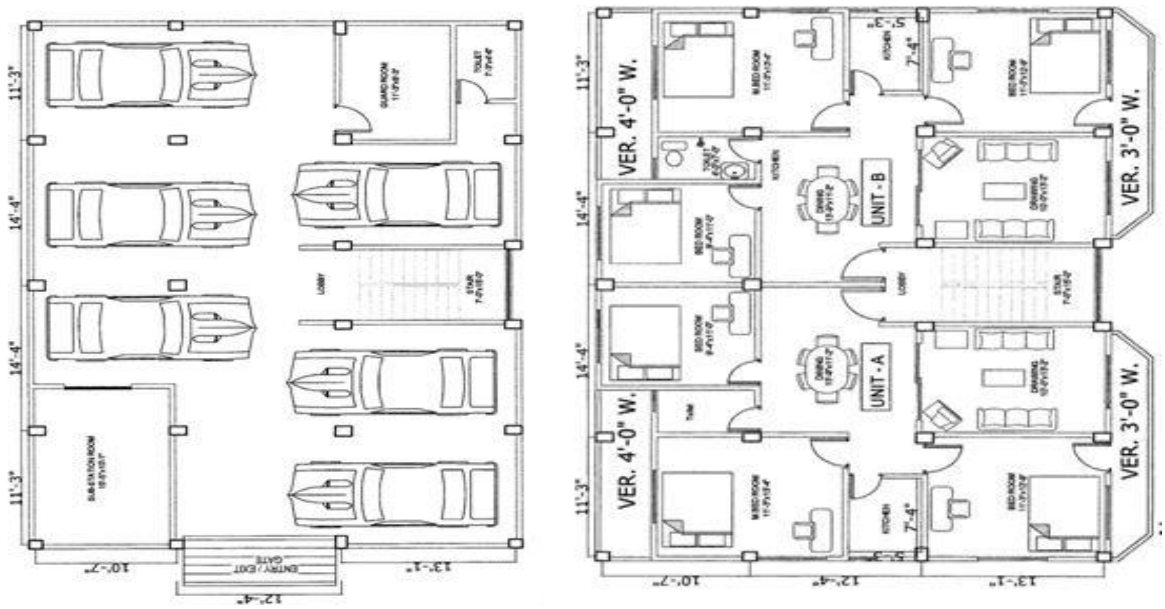

(a) **(b)**

Figure 2. Ground Floor Plan (a), Typical Floor Plan (b)

4. MANUAL ANALYSIS AND DESIGN

This part of paper provides complete design of the residential building using BNBC and ACI codes by improvising the effects of the lateral loads on 06 storied structure having edge supported floor system. Moment Coefficient method was used for analysis.

4.1 Slab Design

There were 6 slabs in the building. The moment and reinforcement calculations for the 6 slabs in both short and long directions found from manual calculation are given below in Table 1.

Specifications: fy= 72.5 ksi PW= 35 psf
f'c= 3.5 ksi FF= 25 psf LL= 40 psf

Table 1. Slab Design

Category	Slab 1	Slab 2	Slab 3	Slab 4	Slab 5	Slab 6
Thickness (in)	4.5	4.5	4.5	4.5	4.5	4.5
DL (psf)	121.25	116.25	116.25	116.25	116.25	116.25
LL (psf)	40	40	40	40	40	40
Total Factored Load (psf)	209.5	203.5	203.5	203.5	203.5	203.5
Moment (Short Direction) +MA (kip-ft)	1.1407	0.7214	0.6219	0.7559	0.6376	0.8441
Moment (Short Direction) -MA (kip-ft)	1.7924	1.5438	0.9500	1.6148	1.4231	1.4583
Moment (Long Direction) +MB (kip-ft)	1.1684	0.2902	0.5537	0.5267	0.3307	1.1666
Moment (Long Direction) -MB (kip-ft)	0.2502	0.4525	1.3995	1.1497	0.4825	1.0383
Provided "d" (in)	3	3	3	3	3	3
Main Reinforcement (Short Direction) For +MA	#3 bar @ 10"c/c alt ckd.	#3 bar @ 10"c/c alt ckd.	#3 bar @ 10"c/c alt ckd.	#3 bar @ 10"c/c alt ckd.	#3 bar @ 10"c/c alt ckd.	#3 bar @ 10"c/c alt ckd.
Main Reinforcement (Short Direction) For -MA	#3 bar @ 20" c/c Extra top in bet^{n} ckd. bars.	#3 bar @ 20" c/c Extra top in bet^{n} ckd. bars.	#3 bar @ 20" c/c Extra top in bet^{n} ckd. bars.	#3 bar @ 20" c/c Extra top in bet^{n} ckd. bars.	#3 bar @ 20" c/c Extra top in bet^{n} ckd. bars.	#3 bar @ 20" c/c Extra top in bet^{n} ckd. bars.
Main Reinforcement (Long Direction) For +MB	#3 bar @ 12"c/c alt ckd.	#3 bar @ 12"c/c alt ckd.	#3 bar @ 12"c/c alt ckd.	#3 bar @ 12"c/c alt ckd.	#3 bar @ 12"c/c alt ckd.	#3 bar @ 12"c/c alt ckd.
Main Reinforcement (Long Direction) For -MB	#3 bar @ 22" c/c Extra top in bet^{n} ckd. bars.	#3 bar @ 22" c/c Extra top in bet^{n} ckd. bars.	#3 bar @ 22" c/c Extra top in bet^{n} ckd. bars.	#3 bar @ 22" c/c Extra top in bet^{n} ckd. bars.	#3 bar @ 22" c/c Extra top in bet^{n} ckd. bars.	#3 bar @ 22" c/c Extra top in bet^{n} ckd. bars.

4.2 Beam Design

There were 2 sizes of beams in the building. The moment, reinforcement and stirrup calculations for the beams found from manual calculation are given below in Table 2.

Specifications:
f'c = 3.5 ksi
fy = 72.5 ksi
Unit weight of concrete = 150 pcf
Unit weight of brick = 120 pcf
Wall thickness = 5 in
Beam length = 11 ft 3 in
Effective depth = 17 in - 2.5 in = 14.5 in

Table 2. Beam Design

	Beam Size 10 in * 15 in	**Beam Size 10 in * 17 in**
DL (kip/ft)	0.8873	0.9551
LL (kip/ft)	0.1058	0.1126
Total Factored Load (kip/ft)	1.2346	1.3200
Moment +M (kip-ft)	9.877	11.93
Moment -M (kip-ft)	11.523	13.92
Check for T-beam	Rectangular beam	Rectangular beam
Reinforcement for +M	2#4 bar (12 mm)	2#4 bar (12 mm)
Reinforcement for -M	2#4 bar (12 mm)	2#4 bar (12 mm)
Stirrup Design	Stirrup is not required.	Stirrup is not required.

4.3 Column Design

There were 3 types of columns in the building. The load and reinforcement calculations for the 3 columns found from manual calculation are given below in Table 3.

Specification:
Column height = 10" c/c
Column type = Tied
Clear cover = 1.5" c/c
α = 0.80 for tied column
ρ_g = 0.02
$\emptyset$ = 0.65
fy= 72.5 ksi
f'c = 3.5 ksi

Table 3. Column Design

Category	**Exterior**	**Interior**	**Corner**
Total Factored Load (kip)	95.30	245.7	110.16
Size of Column	12 in * 16 in	12 in * 18 in	12 in * 14 in
Main Reinforcement	6#9	8#5	8#8
Tie Bar	# 3 bar (10 mm) @ 12" c/c	# 3 bar (10 mm) @ 12" c/c	# 3 bar (10 mm) @ 9" c/c
Check for Lateral Tie	No additional lateral ties are required	No additional lateral ties are required	No additional lateral ties are required

The reinforcement detailing for slabs, beams and columns found from manual analysis are shown in the Figure no. 3(a), 3(b) and 3(c) respectively.

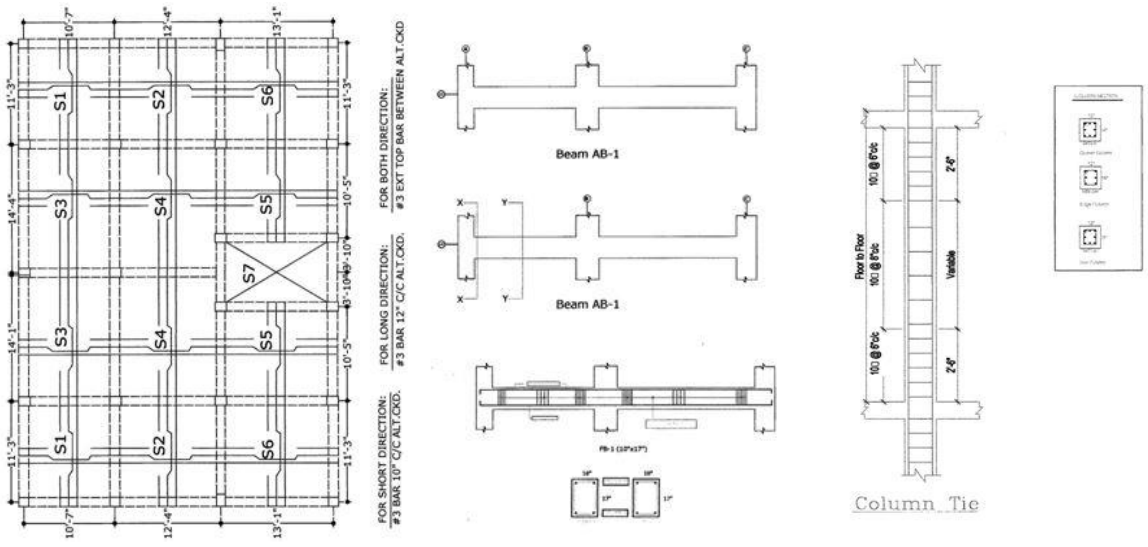

(a) **(b)** **(c)**

Figure 3. (a) Slab Reinforcement Detail (b) Beam Reinforcement Detail and (c) Column Reinforcement Detail

5. COMPUTER SOFTWARE ANALYSIS AND DESIGN (ETABS)

The building plan and elevation of the building found from ETABS are shown in the following Figure no. 4.

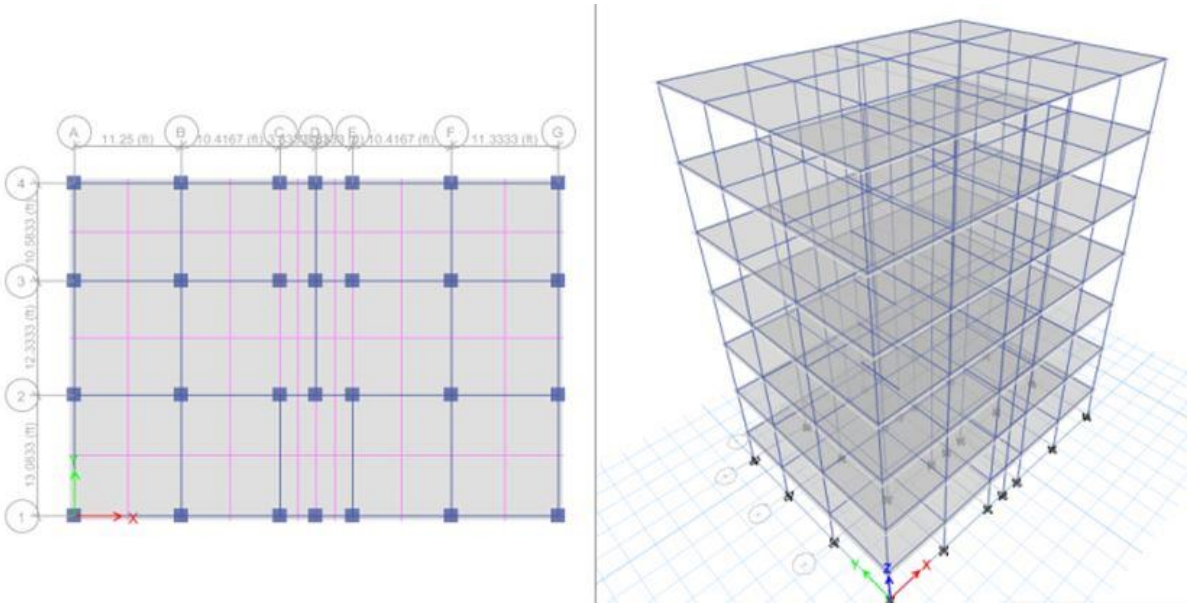

Figure 4. Building Plan and Elevation (ETABS)

The moment and reinforcement calculations for the 6 slabs in both short and long directions found from computer software analysis (ETABS) are given below in Table 4.

Table 4. Slab Design

Category	Slab 1	Slab 2	Slab 3	Slab 4	Slab 5	Slab 6
Main Reinforcement (Short Direction) For +MA	#3 bar @ 12”c/c alt ckd.	#3 bar @ 12”c/c alt ckd.	#3 bar @ 12”c/c alt ckd.	#3 bar @ 12”c/c alt ckd.	#3 bar @ 12”c/c alt ckd.	#3 bar @ 12”c/c alt ckd.
Main Reinforcement (Short Direction) For -MA	#3 bar @ 22” c/c Extra top in bet^{n} ckd. bars.	#3 bar @ 22” c/c Extra top in bet^{n} ckd. bars.	#3 bar @ 22” c/c Extra top in bet^{n} ckd. bars.	#3 bar @ 22” c/c Extra top in bet^{n} ckd. bars.	#3 bar @ 22” c/c Extra top in bet^{n} ckd. bars.	#3 bar @ 22” c/c Extra top in bet^{n} ckd. bars.
Main Reinforcement (Long Direction) For +MB	#3 bar @ 12”c/c alt ckd.	#3 bar @ 12”c/c alt ckd.	#3 bar @ 12”c/c alt ckd.	#3 bar @ 12”c/c alt ckd.	#3 bar @ 12”c/c alt ckd.	#3 bar @ 12”c/c alt ckd.
Main Reinforcement (Long Direction) For -MB	#3 bar @ 22” c/c Extra top in bet^{n} ckd. bars.	#3 bar @ 22” c/c Extra top in bet^{n} ckd. bars.	#3 bar @ 22” c/c Extra top in bet^{n} ckd. bars.	#3 bar @ 22” c/c Extra top in bet^{n} ckd. bars.	#3 bar @ 22” c/c Extra top in bet^{n} ckd. bars.	#3 bar @ 22” c/c Extra top in bet^{n} ckd. bars.

The moment, reinforcement and stirrup calculations for the beams found from computer software analysis (ETABS) are given below in Table 5.

Table 5. Beam Design

Category	Beam Size 10 in * 15 in	Beam Size 10 in * 17 in
Reinforcement for +M	2#3 bar (12 mm)	2#4 bar (12 mm)
Reinforcement for -M	2#3 bar (12 mm)	2#4 bar (12 mm)
Stirrup Design	Stirrup is not required.	Stirrup is not required.

The load and reinforcement calculations for the 3 columns found from computer software analysis (ETABS) are given below in Table 6.

Table 6. Column Design

Category	Exterior	Interior	Corner
Size of Column	12 in * 16 in	12 in * 18 in	12 in * 14 in
Main Reinforcement	8#8	8#6	6#6
Tie Bar	# 3 bar (10 mm) @ 12” c/c	# 3 bar (10 mm) @ 12” c/c	# 3 bar (10 mm) @ 12” c/c

The moment diagram of slabs, reinforcement detailing of beams and columns found from computer software analysis (ETABS) are shown in the Figure no. 5(a), 5(b) and 5(c) respectively.

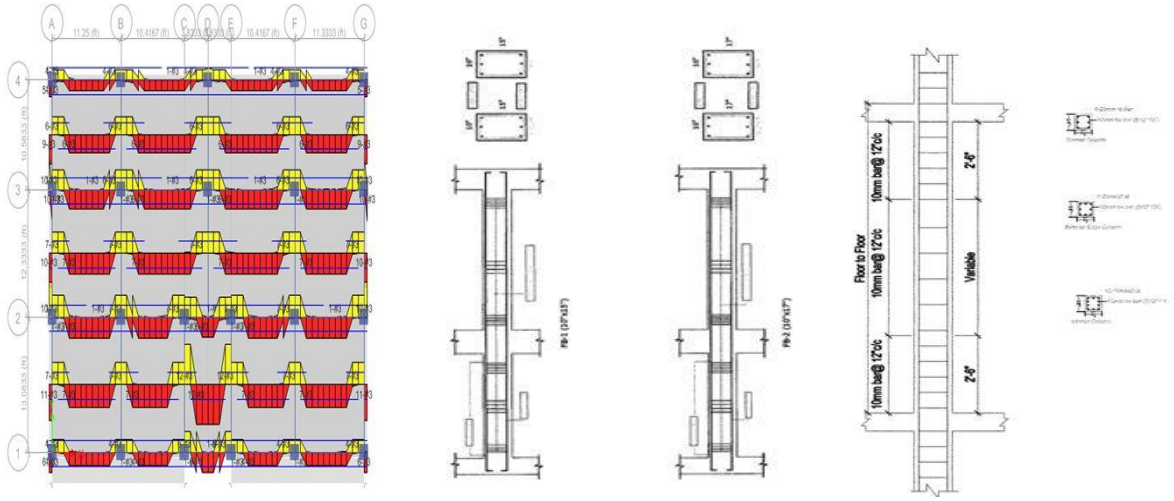

(a) (b) (c)

Figure 5. (a) Moment Diagram of Slab (b) Beam Reinforcement Detail and (c) Column Reinforcement Detail

6. RESULT

The results found from manual analysis and computer software analysis for slabs, beams and columns are summarized below in Table 7, 8 and 9 respectively.

Table 7. Comparison of Slab Design

Category	Manual Analysis	ETABS
Main Reinforcement (Short Direction) For +MA	#3 bar @ 10"c/c alt ckd.	#3 bar @ 12"c/c alt ckd.
Main Reinforcement (Short Direction) For -MA	#3 bar @ 20" c/c Extra top in bet^{n} ckd. bars.	#3 bar @ 22" c/c Extra top in bet^{n} ckd. bars.
Main Reinforcement (Long Direction) For +MB	#3 bar @ 12"c/c alt ckd.	#3 bar @ 12"c/c alt ckd.
Main Reinforcement (Long Direction) For -MB	#3 bar @ 22" c/c Extra top in bet^{n} ckd. bars.	#3 bar @ 22" c/c Extra top in bet^{n} ckd. bars.

Table 8. Comparison of Beam Design

Category	Manual Analysis		ETABS	
Beam Size	10 in * 15 in	10 in * 17 in	10 in * 15 in	10 in * 17 in
Reinforcement for +M	2#4 bar (12 mm)	2#4 bar (12 mm)	2#3 bar (12 mm)	2#4 bar (12 mm)
Reinforcement for -M	2#4 bar (12 mm)	2#4 bar (12 mm)	2#3 bar (12 mm)	2#4 bar (12 mm)

Table 9. Comparison of Column Design

Category	**Manual Analysis**			**ETABS**		
Column	Exterior	Interior	Corner	Exterior	Interior	Corner
Size of Column	12 in*16 in	12 in*18 in	12 in*14 in	12 in* 6 in	12 in*18 in	12 in*14 in
Main Reinforcement	6#9	8#5	8#8	8#8	8#6	6#6
Tie Bar	# 3 bar (10 mm) @ 12" c/c	# 3 bar (10 mm) @ 12" c/c	# 3 bar (10 mm) @ 9" c/c	# 3 bar (10 mm) @ 12" c/c	# 3 bar (10 mm) @ 12" c/c	# 3 bar (10 mm) @ 12" c/c

7. REFERENCES

"Bangladesh National Building Code" (2006). Housing and Building Research Institute (1993) and Bangladesh Standard and testing Institute, pp. 6-68.

Nilson, Arthur.H, Darwin David and Dolan Charles W. (2010-2011). "Design of Concrete Structures" (13th Ed.) McGraw-Hill book Co. Singapore.

"Building code Requirements for Reinforced Concrete" ACI publication 318-63, American Concrete Institute, Farmington Hills, MI, 1963.

Dinesh J. S, Pajgade P.S., "Seismic Evaluation Of Existing Reinforced Concrete Building" (June-2012).

Bungale, S.T.(1988). "Structure Analysis & Design of Tall Buildings". McGraw- HillBook Co:-Singapore, P.P. 8-11, 45-46, 65-78.

Parker, H. (1986). "Simplified Design of Reinforced Concrete" (3rd Ed.) M.S. Seawall for Wiley Eastern Limited, New Delhi, p.p. 142-145.

Proc. 2nd International Conference on Structural Engineering Research (iCSER2019)
19-22 Jan 2019, Dhaka, Bangladesh
ISBN: 978-0-6482681-2-3

A Comparative Analysis of the Sensitivity of Optimum Design Parameters of Post-tensioned Pre-stressed I-girder Bridge at Varied Steel Cost

Tahsin Afroz Hoque Nishat[1] and Raquib Ahsan[2]

[1]Student of Civil Engineering Department, Bangladesh University of Engineering and Technology (BUET), Dhaka, Bangladesh
[2]Professor of Civil Engineering Department, Bangladesh University of Engineering and Technology (BUET), Dhaka, Bangladesh
Corresponding author's E-mail: tahsinbuet13@gmail.com

Abstract

An approach is presented for comparative sensitivity analysis of cost optimum design parameter of post-tensioned PC I-girder bridge system at varied cost of steel. The main objectives of the study are to analyze the sensitivity of each design parameter of the bridge for predicting structural safety and cost of bridge and to compare the sensitivity at different cost regimes. Optimum values of the parameters were obtained using Evolutionary Operation (EVOP), a global optimization technique, for three different cost data. 14 design parameters along with 14 explicit constraints and 46 implicit constraints were considered in the cost optimum design problem. After obtaining the optimum solution, sensitivity analyses were conducted. Deviations of each of the parameters on both the upper and lower sides of the solution were considered. Ranges of the deviation for the parameters from optimum values reflect their realistic possible ranges of deviation during construction procedure. While analysing for one cost data, one parameter was deviated at a time keeping remaining parameters at their optimum values. Repeating the process for remaining design parameters, compliance with the constraints were examined and total cost variations were estimated. The similar procedure was applied for remaining two cost data. It has been observed that, for cost data with increased steel cost, sudden increase in total cost occurs for variations in girder spacing, top flange width, top flange thickness, top flange transition thickness and bottom flange width. And for increased steel cost, slab thickness can be decreased up to 3mm.On the other hand at lower steel cost slab thickness can be decreased only 0.1mm. Therefore, the obtained results suggest that, for the purpose of realistic design, sensitivity analysis at varied cost data should be an integral part of any optimum design methodology of a bridge system.

Keywords: Comparative sensitivity analysis, optimum design, evolutionary operations, PC girder bridge.

1. INTRODUCTION

During any design procedure structural safety and economy are two major concerns. Optimum design methodology can play a significant role in this problem which produces a cost effective solution ensuring structural adequacy. Ghani (1989) developed a global algorithm named EVOP (Evolutionary Operations) which can locate the global minima. Using this algorithm, cost optimization for a post tensioned prestressed I-girder bridge system was done with 14 design parameters (Rana and Ahsan, 2010; Ahsan et al. 2012). However, the optimum parameter values derived from this method are subject to change due to constructional ease. Deviations in these parameters can affect structural adequacy. Therefore, sensitivity analyses should be combined with design methodology to determine the impact of design parameters.

Sensitivity analysis (SA) of any structure is the investigation of the potential changes of design parameters and their impacts on the structure. It allows the designers to assess the effects on structure due to deviations in design parameters and facilitates structural modifications. Over the years, sensitivity analysis is done for optimization problem in various discipline areas. Yue et al. (2008) presented a sensitivity analysis and robust experimental design of a signal transduction pathway system. Becker et al. (2011) presented a Bayesian sensitivity analysis of a model of the aortic valve. Chen and Yang (2017) presented a sensitivity analysis and optimization of a typical passively designed residential building with hybrid ventilation in hot and humid climates. Nishat and Ahsan (2018) presented an analysis of sensitivity of design parameters for 30m span pre-stressed post-tensioned I-girder bridge. It can be recognized that there is limited research on sensitivity analysis for optimization technique in civil engineering field.

The main objectives of the study are to analyze the sensitivity of 14 design parameters of pre-tensioned PC I-girder 30m span optimized bridge in terms of structural safety and cost of bridge and to compare the sensitivity for different cost regimes.

2. METHODOLOGY

In the present study a simply supported post-tensioned PC I-girder bridge system of 30m span is considered. The bridge system consists of only cast-in place reinforced concrete deck with precast girders. A typical I-girder arrangement in the bridge is shown in Figure 1.

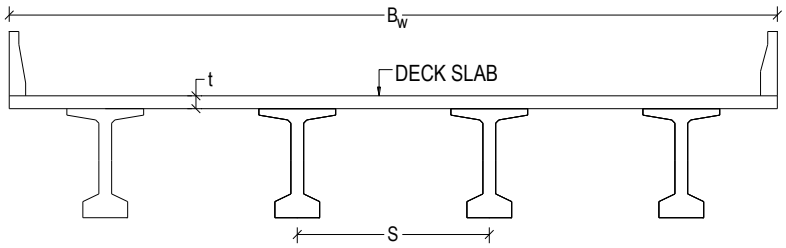

Figure 1 I-Girder arrangement in the bridge

The bridge system was initially optimized for three cost data using the computer program in C++ developed for post-tensioned PC 30m span I-girder bridge system (Rana and Ahsan 2010). The optimization problem consists of 14 design parameters along with 14 explicit and 46 implicit constraints. The cost data used for these analyses are tabulated in Table 1.

After the optimization process sensitivity analyses were conducted for these three cost data based on sensitivity analyses of post-tensioned 30m span PC I-girder bridge (Nishat and Ahsan 2018). The design data used for sensitivity analyses were kept same as that were used for optimization.

The deviation ranges of values of optimum design parameters were selected based on realistic possible ranges of variations during construction procedure. The ranges were then modified so as not to violate any constraint. The ranges of deviations considered are listed in Table 2.

Table 1 Relative cost parameters used for cost minimum design

Item	Unit	Cost1 (BDT)	Cost2 (BDT)	Cost3 (BDT)
Precast girder concrete-including equipment and labor (UP_{GC})	per m^3	12,500	12,500	12,500
Girder formwork (UP_{GF})	per m^2	400	400	400
Cast-in-place deck concrete(UP_{DC})	per m^3	6,000	6,000	6,000
Deck formwork-equipment and labor(UP_{DF})	per m^2	415	415	415
Girder posttensioning-tendon, equipment and labor(UP_{PS})	per ton	90,000	180,000	270,000
Anchorage set(UP_{ANC})	per set	4,500	9,000	13,500
Metal sheath for duct(UP_{SH})	per lin. meter	90	180	270
Mild steel reinforcement for deck and web in girder(UP_{OS})	per ton	45,000	90,000	135,000

Table 2 Deviation ranges of optimum design parameters for sensitivity analyses

Input Design parameters	Range of Deviation for Cost1	Range of Deviation for Cost2	Range of Deviation for Cost3
1. Girder spacing, S (mm)	±25	±25	±25
2. Top flange width, TF_w (mm)	±25	±25	±25
3. Bottom flange width, BF_w (mm)	±25	±25	±25
4. Bottom flange thickness, BF_t (mm)	±23	±21	±22
5. Girder depth G_d (mm)	±25	±25	±2
6. Number of strands per tendon, N_s	±1	±1	±1
7. Number of tendon per girder, N_T	±1	±1	±1
8. Lowermost tendon position, y_t (mm)	±5	±5	±9
9. Initial stage prestress, η (%)	±6	±3	±3
10. Slab thickness, t (mm)	±1	±1	±3
11. Slab main reinforcement ratio, ρ (%)	±0.05	±0.05	±0.05
12. Top flange thickness, TF_t (mm)	±25	±25	±25
13. Top flange transition thickness, TFS_t (mm)	±25	±25	±25
14. Web thickness, W_w (mm)	±25	±25	±6

3. RESULTS AND DISCUSSIONS

3.1. Sensitivity analysis in terms of constraints

In this part sensitivity analyses are done in terms of constraint values. Change in number of tendon and number of strand per tendon violate the constraint range. Hence further analyses are done for remaining 12 parameters. Among these parameters, slab thickness is found to be the most sensitive parameter. However, comparative analysis shows that, slab thickness becomes less sensitive for increased steel cost regime. Variations in implicit constraint parameters that are bottom fiber stress (σ_{b1}) and effective depth ($d_{provided}$) due to variations in slab thickness are given in Table 3, Table 4 and Table 5 for Cost1, Cost2 and Cost3 respectively.

Table 3 Variation of implicit constraints for slab thickness at Cost1

Slab Thickness, t (mm)	σ_{b1}	$\sigma_{b1(min)}$	$\sigma_{b1(max)}$	$d_{required}$	d_{min}	$d_{provided}$	Comments
249.8	3.15197	-24	3.16228	192.842	109.898	192.8	Not Ok
249.9	3.15543	-24	3.16228	192.847	109.901	192.9	Ok
250	3.1589	-24	3.16228	192.852	109.904	193	Ok
250.1	3.16237	-24	3.16228	192.857	109.906	193.1	Not Ok

Table 4 Variation of implicit constraints for slab thickness at Cost2

Slab Thickness, t (mm)	σ_{b1}	$\sigma_{b1(min)}$	$\sigma_{b1(max)}$	$d_{required}$	d_{min}	$d_{provided}$	Comments
253.9	3.12574	-24	3.16228	196.991	110.204	196.9	Not Ok
254.2	3.13517	-24	3.16228	197.007	110.213	197.2	Ok
254.6	3.14777	-24	3.16228	197.027	110.224	197.6	Ok
255	3.16037	-24	3.16228	197.047	110.236	198	Ok
255.1	3.16352	-24	3.16228	197.053	110.239	198.1	Not Ok

Table 5 Variation of implicit constraints for slab thickness at Cost3

Slab Thickness, t (mm)	σ_{b1}	$\sigma_{b1(min)}$	$\sigma_{b1(max)}$	$d_{required}$	d_{min}	$d_{provided}$	Comments
292	3.07015	-24	3.16228	235.096	109.137	235	Not Ok
293	3.09908	-24	3.16228	235.153	109.164	236	Ok
295	3.15697	-24	3.16228	235.269	109.217	238	Ok
296	3.18593	-24	3.16228	235.327	109.244	239	Not Ok

It has been obtained that constraints are violated if slab thickness is-

I. decreased 0.2mm or increased 0.1mm at Cost1.
II. decreased 1.1mm or increased 0.1mm at Cost2.
III. decreased 3mm or increased 1mm at Cost3.

3.2. Sensitivity analysis in terms of percent variation of total cost

In this part, comparison has been made among the sensitivity design parameters for three cost data separately. Figure 2, Figure 3 and Figure 4 represent the percent variations of total cost for percent variations of design parameter values at Cost1, Cost2 and Cost3 respectively. The graphs have been plot for only feasible constraint regions. Smooth straight line indicates that no sudden increase in total cost. From these graphs it can be seen that no sudden increase in total cost occurs for Cost1. However, for Cost2 and Cost3, sudden increase in total cost can occur due to deviations in top flange width, bottom flange width, top flange thickness, top flange transitional thickness. And sudden increase in total cost can occur for deviation in girder spacing for Cost3 regime. Variations in these parameters can cause sudden increase in number of shear bar which consequently can cause sudden increase the total non-prestressing steel cost as well as total cost.

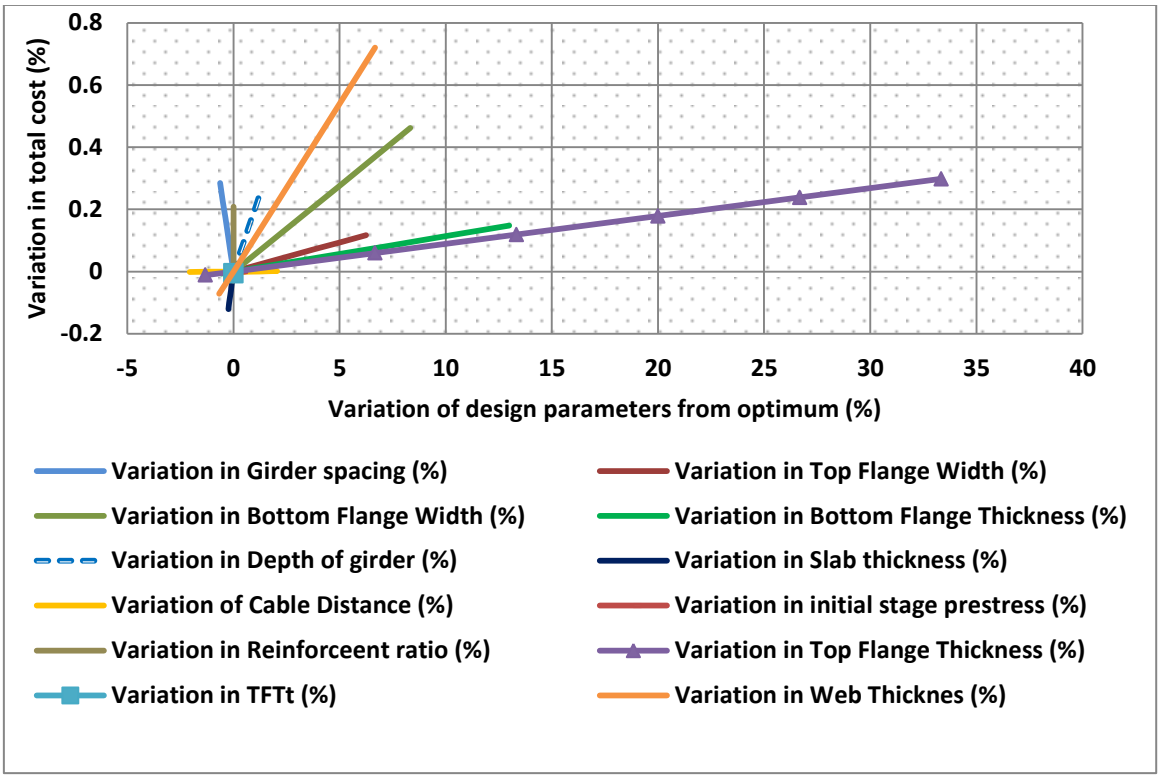

Figure 2. Percent variation of total cost vs percent variation in optimum values of parameters for Cost1

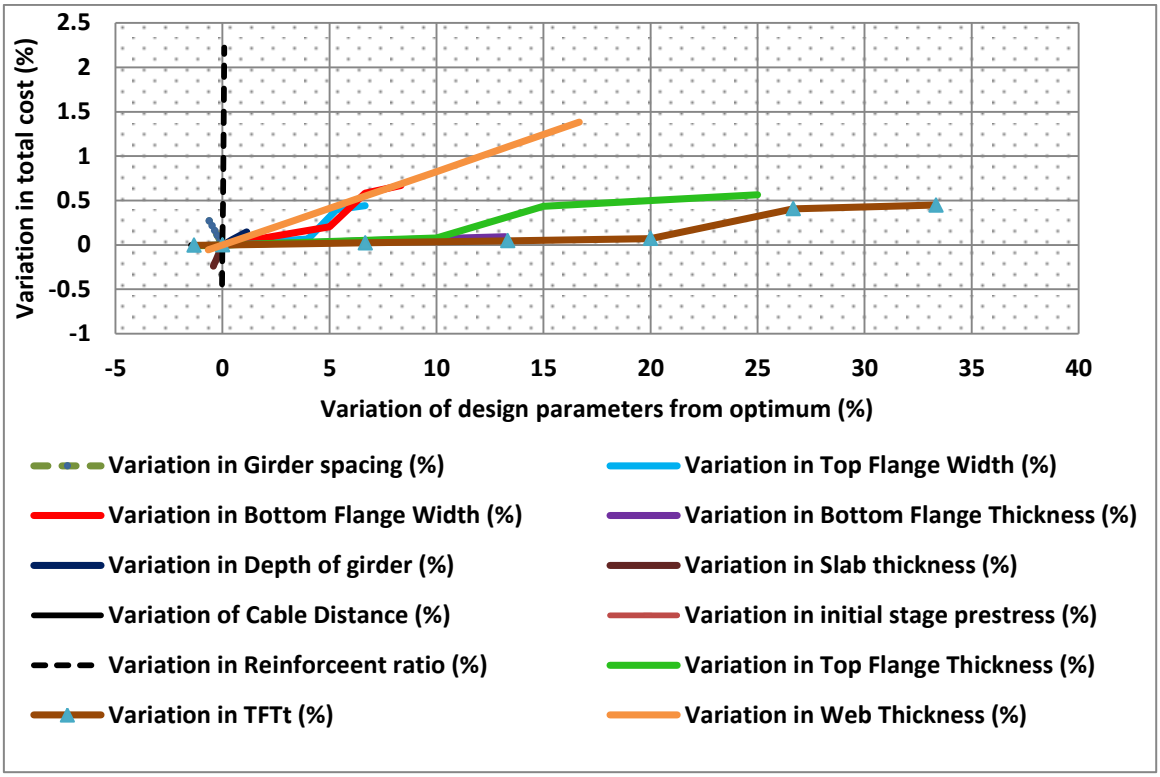

Figure 3. Percent variation of total cost vs percent variation in optimum values of parameters for Cost2

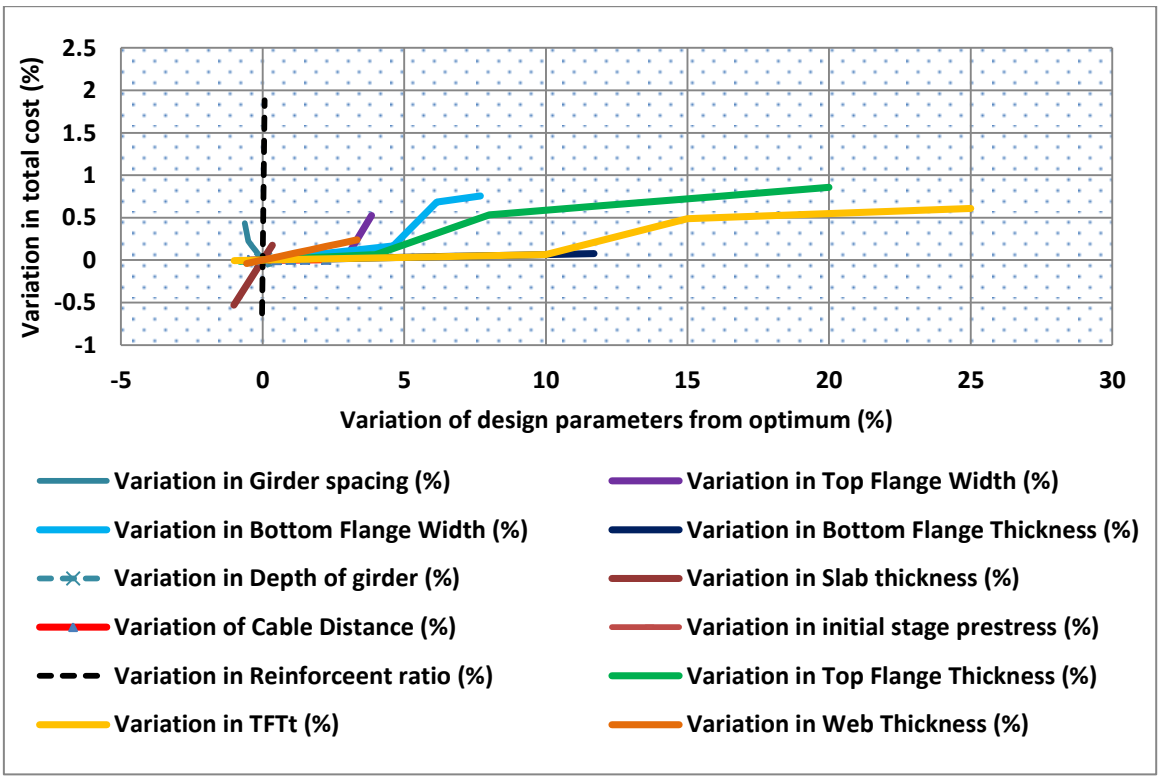

Figure 4. Percent variation of total cost vs percent variation in optimum values of parameters for Cost3

4. CONCLUSIONS

In this paper, sensitivity analyses are done on the cost optimized design parameters of 30m span PC I-girder bridge for three different cost regimes. Then the sensitivity of each parameter is compared for these three cost regimes. These analyses are done based on the modified C++ program and output results are summarized. It has been found that, for cost data with increased steel cost, sudden increase in total cost occurs for variations in girder spacing, top flange width, top flange thickness, top flange transition thickness and bottom flange width which is due to sudden increase of shear bar number. Also for increased steel cost, slab thickness can be decreased up to 3mm whereas slab thickness can be decreased only 0.1mm at lower steel cost without violating any constraint.Hence, it can be concluded that cost of steel can play a significant role in regard to structural safety during sensitivity analyses. For this reason structural sensitivity analyses with respect to different cost regimes should be integral part in any of the design methodology.

REFERENCES

Ahsan R, Rana S and Ghani SN (2012). Cost optimum design of post-tensioned I-girder bridge using global optimization algorithm. Journal of Structural Engineering. American Society of Civil Engineering: 273-284.

Becker W, Rowson J, Oakley JE, Yoxall A, Manson G and Worden K (2011). Bayesian sensitivity analysis of a model of the aortic valve. Journal of biomechanics, 44(8), pp.1499-1506.

Chen X and Yang H (2017). Sensitivity analysis and optimization of a typical passively designed residential building with hybrid ventilation in hot and humid climates. Energy Procedia, 142, pp.1781-1786.

Ghani SN (1989). A versatile algorithm for optimization of a nonlinear nondifferentiable constrained objective function. UKAEA Harwell report number R13714. HMSO Publications Centre, PO Box 276, London SW85DT; ISBN: 0-7058-1566-8.

Nishat TAH and Ahsan R (2018). Sensitivity analyses of cost optimized solution of post-tensioned pre-stressed i-girder bridge system. Accepted for the publication in "4th International Conference on Advances in Civil Engineering".

Rana S and Ahsan R (2010). Design of pre-stressed concrete I-girder bridge superstructure using optimization algorithm, Journal of Bridge Engineering

Yue H, Brown M, He F, Jia J and Kell DB (2008). Sensitivity analysis and robust experimental design of a signal transduction pathway system. International Journal of Chemical Kinetics, 40(11), pp.730-741.

Proc. 2nd International Conference on Structural Engineering Research (iCSER2019)
19-22 Jan 2019, Dhaka, Bangladesh
ISBN: 978-0-6482681-2-3

Detection of FRP Debonding Behaviour in PSC I-girder by using Natural Frequency

Mysura Alam Khan Snigdha[1], Farhat Aziz Sheen[2], U.S.M Dilruba Mahmud[3] and Shohel Rana[4]

[1]Student, Bangladesh University of Engineering & Technology, Dhaka, Bangladesh.
[2, 3] Structural Safety Engineer, Stichting Bangladesh ACCORD Foundation, Dhaka, Bangladesh.
[4]Assistant Professor, Department of Civil Engineering, BUET, Dhaka, Bangladesh.
Corresponding author's E-mail: sheen_770@yahoo.com, snigdhamysura@gmail.com.

Abstract

Nowadays Fibre-Reinforced Polymers (FRP) are widely used in strengthening and retrofitting of concrete elements, such as beams, columns, slabs, bridge girders and bridge decks etc. Failures may be caused in FRP-strengthened prestressed concrete (PSC) members by flexural failures of critical sections or by debonding of FRP plate from the PSC beams. Debonding of FRP from concrete interface region may cause a significant decrease in member capacity leading to a premature failure of the system. As the debonding of FRP cannot be identified visibly from the surface, it is essential to develop appropriate non-destructive evaluation techniques for the assessment of these systems for safe application of strengthening concrete structures using FRP composites. In this paper, a non-destructive method is carried out to detect FRP debonding in a PSC I-girder beam using modal characteristics such as natural frequencies, mode shapes. More specifically, modal analysis of an I-girder PSC beam using Finite Element Modelling is presented here. Finite Element Modelling and modal analysis are done by using ABAQUS and MATLAB software respectively. By observing the change in the modal behaviour of I-beam in case of without debonding of FRP, and in case of debonding of FRP, a detailed analysis and discussions have been established which helps to identify the debonding behaviour of FRP in PSC I-girder beam. Moreover, the change in modal behaviours is observed to be significant in a few modes only which are included in this study.

Keywords: PSC I-Girder, Fibre-Reinforced Concrete (FRP), debonding, frequency, modal analysis.

1. INTRODUCTION

Many structures like bridges, buildings built in the past are estimated to be structurally deficient caused by increased load demands, environmental deterioration and structural aging. For example, Thirty-five percent of all bridges in the U.S. are estimated to be structurally deficient and require repair, strengthening, widening or replacement [Karbhari and Zhao, 2000]. These structures require repairing, strengthening, widening or replacement to overcome deficiencies and for this purpose, the use of composite materials such as fiber reinforced polymers (FRP) is increasing gradually. Carbon-fiber-reinforced polymer (CFRP) is a well-known high-performance composite material used to strengthen reinforced concrete structural components.

Structural components strengthened or retrofitted with FRP behave as composite components, and their strengths are calculated by taking this into account. For flexural strengthening of beams, CFRP plates or sheets are attached to the tension face. Interfacial bonding between the adherents plays a significant role in achieving composite behavior and increasing strength. Unlike steel plates, FRP plates do not undergo corrosion problems. However, the interfacial bond between FRP and concrete can deteriorate due to environmental and load-related issues leading to debonding durability and delamination. Concrete structures with FRP plates can demonstrate a brittle failure mode if the FRP debonds from the concrete. Debonding of the plates and ripping of concrete are common failure modes

in concrete structures rehabilitated with FRP plates [Nguyen et al., 2001]. The ripping of concrete and debonding of the FRP are initiated due to high localized stress concentration in the interface layer [Buyukozturk and Hearing, 1998]. It is therefore of interest to identify the integrity of interfacial bonding between the concrete structure and the FRP. Detection of debonding is crucial in characterizing the strength of the structural composite components since composite action can only be achieved with a strong interfacial bond. Nondestructive evaluation (NDE) techniques can be very useful to detect the debonding between composite materials and concrete structures.

In the past few years, there have been built numerous flyovers in Bangladesh and the material of these flyovers are Pre-Stressed Concrete. To get the best service in our daily life and for safety factors, inspection for damage of these structures and maintenance are very important. Therefore, the present study is emphasized on the numerical simulation of an I-girder beam of PSC beam Type Bridge strengthened using CFRP materials. In this case, Modal analysis of two models of I-Beam- one fully strengthened by CFRP and another debonded in one place, have been developed using ABAQUS 2017 to detect debonding of FRP. The numerical analysis has been performed showing frequency variation and Time History Analysis has been developed using MATLAB.

2. METHODOLOGY

Though in the past experimental studies were popular, numerical analysis using finite element method has become more and more popular nowadays because of a revolutionary advancement in the computer-based programs. Besides computer modeling can avoid a huge cost of experimental work, time and effort to accomplish such work except with drawback lying in the simplification of assumptions that almost certainly have to be made in any of such computer model.
Among many computer modeling methods, Finite Element Method (FEM) is the most popular simulation method to predict the physical behavior of systems and structures. Of all these packages, ABAQUS which is capable of modeling and analyzing a vast range of 2D and 3D practical problems has been chosen for its versatility, reliability and relative ease of use.

For the purpose of carrying out the investigation, firstly a finite element model of a rectangular beam of PSC beam type bridge has been developed using ABAQUS 2017. Verification of this finite element model has been achieved with the theoretical value of the natural frequency of the cross section (using the equation of natural frequency for dynamic structures) and it has shown good agreement between the two results. Then other two models of I-Beam have been developed to proceed with the investigation. Among them, one is fully strengthened by CFRP and another one is debonded in one place. The numerical analysis has been performed showing frequency variation and Time History Analysis has been developed using MATLAB. The comparison of the modal behavior of these two models has been presented graphically and also in tabular form.

2.1. Theoretical calculation of frequency

Verification of the model has been done by using a rectangular Pre-Stressed Beam (Both ends fixed) model which is developed by ABAQUS 2017. Theoretical analysis of the frequency of the same section has been calculated using Microsoft Excel and then got compared it with the frequency obtained from the analysis. The pre-stress effect in case of modeling of the beam in ABAQUS is ignored as it seen from the research of Jeong-Tae Kim and others on pre-stress loss in PSC beams that the effect of pre-stress loss is not significant.

The theoretical equation for dynamic structures which is used for frequency analysis is shown below:

$W_n = K^2 \sqrt{(EI/A\rho L^4)}$ ..... (i)
$f = w/2\pi$ ..... (ii)

Where, K = (2n+1) π/2 and E, ρ, L and A are the modulus of elasticity, density, beam length and the cross-section area of the beam, respectively. Calculation and results obtained from Microsoft Excel are presented below in tabular form:

Table 1: Theoretical calculation of the frequency of a designed beam

Dimensions and Properties of the designed beam		**Calculations**
Length L (m)	0.4	Values used in calculations
Height, h (m)	0.04	Area A = 0.5 and Inertia I (M/m^4) = 0.0416667
Width, w (m)	0.04	Sample Calculation for mode 1 is given below:
density ρ(kg/m^3)	2400	A = h*w =1 * 0.5 = 0.0016
Modulus E (M/m^2)	3.00E+10	I = w * h^3/12= 2.133E^{-07}
Calculated cross-section area (M/m^2)	1.6E^{-03}	w = 5708.28 (using equation (i))
Calculated moment of inertia (M/m^4)	2.133E^{-07}	f = 908.5 Hz (using equation (ii))

2.2. Verification of the model

The following illustration is the 3D model of the beam that has been developed using ABAQUS 2017 for the model verification. Therefore, the obtained frequency of the beam with the illustrations of different modes are presented below:

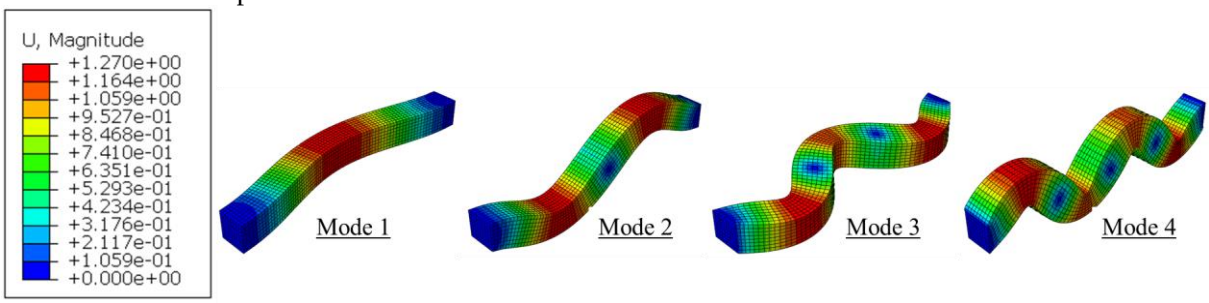

Figure 1: Frequencies and different mode shapes of the beam

Table 2: Frequency obtained from ABAQUS 2017 and the theoretical value of the Frequency.

	Theoretical value of Frequency	Frequency from ABAQUS	Difference (%)
First critical frequency (Hz)	908.5	859.43	5.71
2nd critical frequency (Hz)	2504.4	2213.4	13.15
3rd critical frequency (Hz)	4910.1	4019.6	22.15
4th critical frequency (Hz)	8115.9	6130.2	32.39

Observing the above table, it is seen that the frequency differences in theoretical value from the frequency obtained from ABAQUS 2017 is lower in inferior Mode and almost equivalent. But as the number of modes increases the differences also increases. This is because there are some factors that could affect the free vibration of the structure to some extent such as wind, temperature, loading condition etc. So it can be decided that there is a good agreement between the frequency data. Thus, the finite element model developed is adequate enough to simulate the experimental test results. Hence, developing an I-Beam model by the same process can be used for further numerical study instead of performing experimental works.

3. RESULTS & DISCUSSION

The finite element model of a rectangular beam using ABAQUS 2017 has been verified with the theoretical values of the natural frequency and it shows good agreement. So it is reliable to model

specified beam section and analysis it in the same procedure. So an I-Beam model has been developed and also the modal analysis is done to get the natural frequencies using ABAQUS 2017.

3.1. Properties of I-beam

As this is a pre-stressed concrete beam, it has high strength and high modulus of elasticity. Material property and section properties of this I-beam and FRP that has been used in this study are given in the following table.

Table 3: Material properties of proposed section.

	Pre-stressed Concrete	FRP
Mass Density(kg/m3)	2400	1760
Modulus of Elasticity(GPa)	30	240
Poisson's Ratio	0.2	0.4
Size of the beam	Web- 1m x 0.2m, Flange- 1m x 0.2m, Length-10m	

3.2. The output of I-Beam strengthened with FRP

Considering the above properties an I-girder beam is modeled with FRP and shape of different modes are illustrated below. Also, Natural frequencies of the beam in different modes are given in table 4.

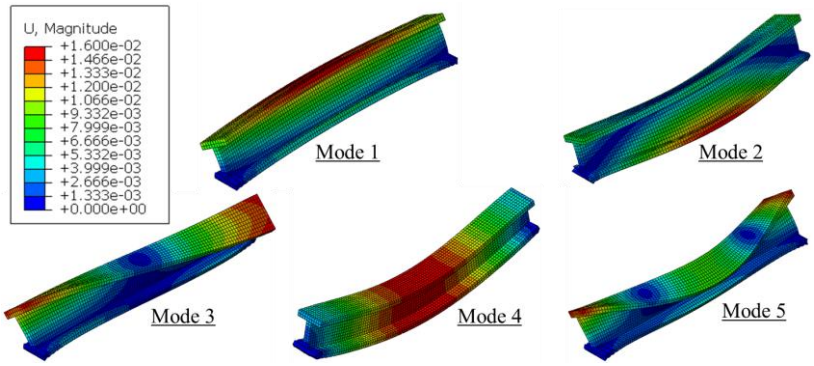

Figure 2: Deformed shapes of the beam in different modes.

3.3. The output of I-Beam after debonding of FRP

Natural frequencies of the beam in different modes are given below in table 4. The shape of different modes is illustrated below in figure 3 after debonding of FRP from the I-girder beam.

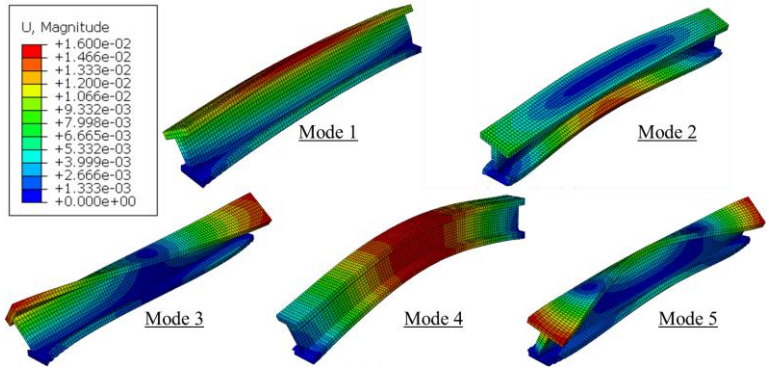

Figure 3: Deformed shapes of the beam in different modes.

From figure 2 and 3, the differences in mode shapes of I-beam strengthened with FRP and FRP debonded condition in different modes are merely visible as frequencies are almost equivalent shown in table 4. But the effect of the debonding of the FRP sheet can be observed from the values of table 4.

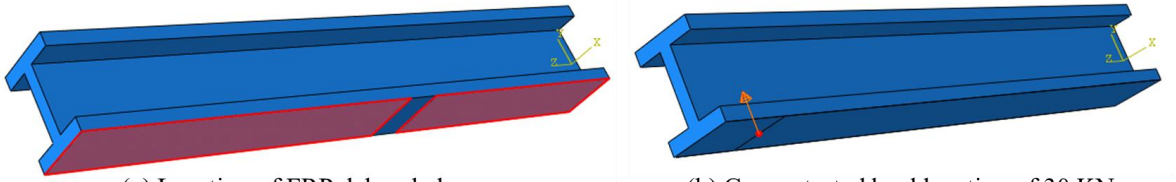

(a) Location of FRP debonded area (b) Concentrated load location of 30 KN

Figure 4: Location of FRP debonded area and location of 30KN concentrated load.

3.4. Comparison of modal behavior of I-beam

Frequencies of the beam strengthened with FRP and FRP debonded condition is compared in table 4.

Table 4: Comparison of natural frequencies.

Mode	Natural Frequency (Hz) (without FRP)	Natural Frequency (Hz) (Strengthened with FRP)	Natural Frequency (Hz) (After debonding of FRP)
1	11.371	12.211	12.209
2	19.593	23.382	23.362
3	24.614	25.504	25.491
4	31.019	33.120	33.111
5	47.526	48.674	48.670

The frequency decreases after debonding of FRP compared to the beam strengthened with FRP. The effect of the debonding of the FRP is quite visible in table 4. So by analyzing Natural frequency one can identify the debonding of the FRP as well as the structural health condition of the structure.

3.5. Developed a time history diagram using MATLAB

To get "Acceleration vs Time" data an impulse load has to create and applied (Hammer load of 30 KN) on the I-Beam as shown in figure 5(b) and then Modal Dynamic analysis has been done. Using those data, a time history diagram has been established by MATLAB. This diagram shows some peak which represents different frequencies of the modes of the beam. Establishing Time History Diagram is important, as, in case of the real-life structure, we will be able to get the natural frequencies by using sensors.

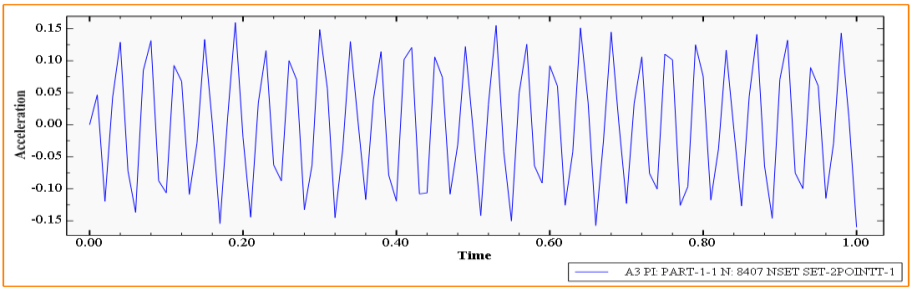

Figure 5: Acceleration vs time graph obtained from ABAQUS 2017.

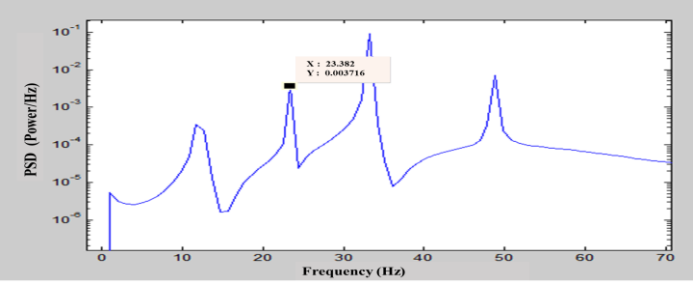

Figure 6: Time History Diagram.

4. CONCLUSION

In this study, a numerical model for I-Beam of PSC bridge has been developed using ABAQUS 2017 for the purpose of evaluating the change of modal characteristics of the beam and the structural health condition of the beam strengthened with FRP. Verification of the model is done by developing a rectangular beam in ABAQUS 2017 and comparing it with the theoretical frequency of that beam. Then using the same procedure, an I-beam is developed and is used for performing the evaluation of debonding of FRP using free vibration. From the analysis, the natural frequencies of that beam are obtained for different mode shapes and a comparison is done between FRP strengthened and FRP debonded condition. A modal dynamic analysis is also done from which "Acceleration vs Time" data have been found. With these "acceleration vs Time" data, numerical analysis is done in MATLAB and a time history diagram is developed. The investigation on the modal behavior of the I-Beam before and after debonding of FRP by finite element method concludes with following outcomes.

- Fiber Reinforced Polymer (FRP) materials are capable of increasing the overall strength of the Pre-Stressed Concrete Structures.
- The differences in mode shapes of I-beam strengthened with FRP and FRP debonded form in different modes are merely visible as frequencies are almost equivalent.
- But the effect of FRP debonding is clearly visible in the frequency data. So by analyzing Natural frequency one can identify the debonding of the FRP and monitor the structural health condition.
- Using natural frequency data, time history diagram has been developed showing different modes.

REFERENCES

ACI 440.4R-04 [2004]. Pre-stressing Concrete Structures with FRP Tendons, American Concrete Institute, Michigan, United States.

Buyukozturk, O. and Hearing, B. [1998]. Failure behavior of pre-cracked concrete beams retrofitting with FRP, Journal of composites for construction pp. 138–144.

Hong S. and Ronald S. H. (2005), Sensors to monitor CFRP/concrete bond in beams using electro-chemical impedance spectroscopy. Journal of Composites for Construction, ASCE, 9(6), 515-523.

Jeong-Tae Kim [2004]. Identification of pre-stress loss in PSC beams using modal information, Structural Engineering and Mechanics, Vol. 17, No. 3-4 (2004) 467-482 467.

Karbhari, V. M. and Zhao, L. [2000]. Use of composites for 21st-century civil infrastructure, Computer Method in Applied Mechanics and Engineering 185: 433–454.

Mirmiran, A., Shahawy, M. and Echary, J. [1999]. Acoustic emission monitoring of hybrid FRP-concrete columns, Journal of Engineering Mechanics 125.

Mirmiran, A. and Yunmei, W. [2001]. Damage assessment of FRP-encased concrete using ultrasonic pulse velocity, Journal of Engineering Mechanics 127: 126–135.

Nguyen, D. M., Chan, T. K. and Cheong, H. K. [2001]. Brittle failure and bond development length of CFRP-concrete beams, Journal of Composites for Construction pp. 12–17.

Proc. 2nd International Conference on Structural Engineering Research (iCSER2019)
19-22 Jan 2019, Dhaka, Bangladesh
ISBN: 978-0-6482681-2-3

Identification of FRP de-bonding of an I-girder Bridge by Vibration-Based Cluster Analysis

Md. Shazzad Hossan[1], Durjoy Goswami[1] and Shohel Rana[2]

[1]Undergraduate Student, Department of Civil Engineering, BUET, Dhaka, Bangladesh
[2]Associate Professor, Department of Civil Engineering, BUET, Dhaka, Bangladesh
Corresponding author's E-mail: Shazzad100@gmail.com

Abstract

Bridges, flyovers that built many years ago, strengthening them with Fiber reinforced polymers (FRP) is very popular and widely used method now a days. But concrete structures with FRP sheets can exhibit a brittle failure mode if the FRP de-bonds from the concrete. There are several types of Structural Health Monitoring (SHM) techniques to assess this condition of structures. Here, the vibration-based method is used to analyze the FRP de-bonding by cluster analysis. Finite element modelling of a three-dimensional concrete I-Girder Bridge is performed. Dynamic analysis is performed before and after the de-bonding of FRP strips. From the analysis, vibration responses such as accelerations are obtained to perform the cluster analysis. From the clustering results, the faulty points of a girder of the bridge is identified, where FRP de-bonded from the concrete.

Keywords: Structural health monitoring, FRP de-bonding, Vibration-based analysis, Cluster analysis, Unsupervised learning.

1. INTRODUCTION

Many structures built in the past need strengthening and retrofitting to overcome deficiencies caused by increased load demands, environmental deterioration and structural ageing. Structural Health Monitoring is a very useful damage detection strategy for civil engineering infrastructures (Farrar and Worden, 2007; Shon et. al. 2003). Many civil engineering structures such as bridges are being used to pass their life expectancy and load capacity. It is not always possible to demolish an old bridge structure and build a new one there. Because it will have both financial burden and negative impact on traffic and environment. In order to improve the safety and reliability of ageing and damaged structure, early identification of damages in structures are important.

In order to strengthening the concrete structures, composite materials such as fiber reinforced polymers (FRP) are being increasingly used. Interfacial bonding between the FRP and concrete plays a significant role in achieving the strength. However, concrete structures with FRP sheets can exhibit a brittle failure mode if the FRP de-bonds from the concrete Nguyen et al., 2001). Thus, it is important to identify the de-bonding between the concrete structure and the FRP.

A number of techniques have been developed as Structural Health Monitoring (SHM) technology to assess the condition of the structure which includes visual inspection, nondestructive evaluation (NDE) and vibration-based methods. The use of vibration measurements in structural monitoring is less subjective than the visual inspection. Vibration based method identifies the structural damages and assesses the structural integrity. There are some researches related to the vibration measurements on FRP rehabilitated concrete structures. Vibration tests have also been used for assessing the effectiveness of strengthening of structural members with FRP. Pascale and Bonfiglioli (2001) studied the effectiveness of modal testing in assessing the overall stiffness changes of RC beams extensively cracked and subsequently repaired with FRP sheets. Zanardo et al. (2007) evaluated the effectiveness of FRP strengthening through dynamic measurements of a bridge before and after strengthening.

Alamdari et al. (2017) performed a spectral-based clustering for structural health monitoring of an arch type bridge in Sydney. In this research, the vibration-based method is used to identify the FRP de-bonding from the concrete surface of an I-girder bridge structure by cluster analysis. The girder surfaces are bonded with FRP strips. Dynamic analysis is performed before and after the de-bonding of FRP strips. After that, cluster analysis is done to detect the faulty points of a girder of the bridge, where FRP de-bonded from the concrete surface.

2. FINITE ELEMENT MODELING

A three-dimensional model of a concrete I-Girder Bridge is developed using Finite Element modelling software as shown in Fig. 1. The dimensions and the properties of the bridge are shown in Table 1.

Table 1. Dimension and Properties of the I-Girder Bridge

Dimension and properties of I-girder	
Dimension	
Length	48m
Height of the girder	2.5m
Height of the web	1.695m
Height of the top flange	0.355m
Height of the bottom flange	0.45m
Properties	
Density of Girder Concrete	2400 Kg/m^3
Modulus of elasticity	30 GPa
Poison's ratio	0.2

Dimension and properties of Slab	
Dimension	
Length	48m
Height	12.11m
Thickness	0.2m
Properties	
Density of Slab concrete	2400 Kg/m^3
Modulus of elasticity	30 GPa
Poison's ratio	0.2

Dimension and properties of FRP	
Dimension	
Length	0.4m
Height	2.5m
Thickness	6mm
Properties	
Density of FRP	1760 Kg/m^3
Modulus of elasticity	240 GPa
Poison's ratio	0.4

To simulate a crack, the value of the Modulus of Elasticity of the concrete in the cracked zone is reduced by 50% as shown in Fig. 2. After that, the bridge is retrofitted with the FRP strips. The de-bonding of two FRP strips from the girder surface is modelled as shown in Fig. 3. The vibration responses such as acceleration of the bridge are obtained after applying ambient excitation for about 10 seconds on the loading points as shown in Fig. 4.

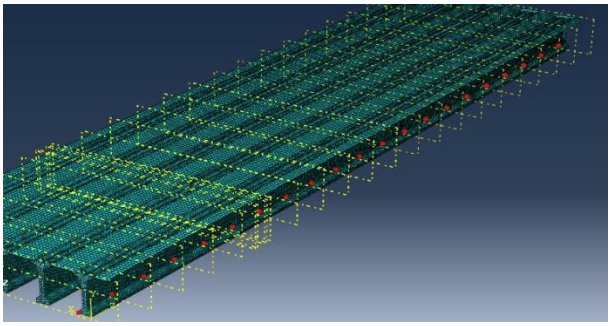

Figure 1. FE Model of the bridge

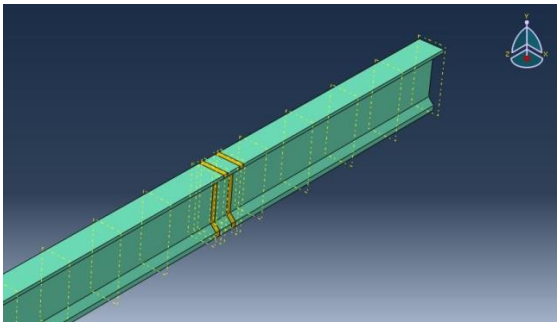

Figure 2. Simulation of crack in the girder

Dynamic analysis such as Modal analysis is performed before and after the de-bonding of FRP strips. The responses are collected from the sensor points as shown in Fig. 1 from a typical girder. A total of 21 sensor points have been considered. A typical response of a certain sensor point is shown in Fig. 5. By using K-means clustering, vibration responses due to de-bonding of FRP is investigated and de-bonding of FRP in the bridge is identified.

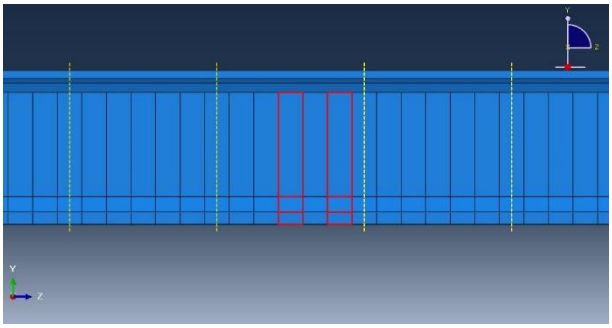

Figure 3. De-bonding of FRP strips

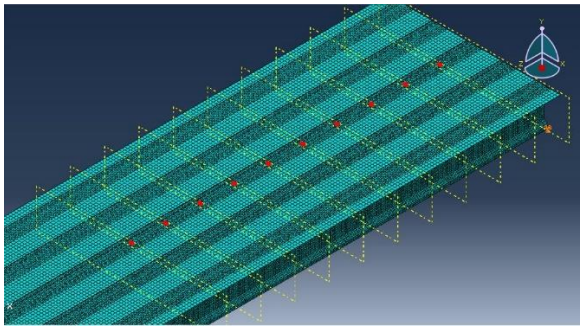

Figure 4. Loading points on the bridge

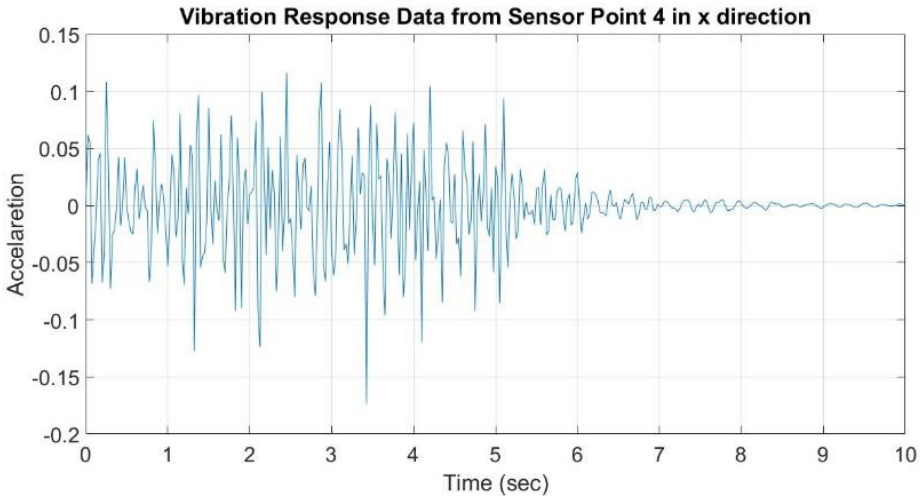

Figure 5. Acceleration response of the a sensor in the girder

3. Feature extraction

The frequency characterization of such random stationary process can be computed using the PSD function which is calculated by taking the Fourier transform of the autocorrelation function,

$$S_{xx}(\omega) = \int_{-\infty}^{\infty} R_{xx}(\tau)\, e^{-i\omega\tau}\, d\tau \qquad (1)$$

Where $S_{xx}(\omega)$ is the PSD of the response at frequency ω. For a given PSD, the nth-order spectral moment, SM can then be computed as,

$$\lambda_x^n = \int_{-\infty}^{\infty} |\omega|^n\, S_{xx}(\omega)\, d\omega \qquad (2)$$

Where n is the order of SM.

Finally, for a discretized signal x, the nth-order SM λ_x^n can be obtained using,

$$\lambda_x^n = \frac{2}{N^{n+1}} \sum_0^{|\frac{N}{2}|} S_{xx}(j)\, (\frac{j}{\Delta t})^n \qquad j \in [1: N/2] \qquad (3)$$

Where S_{xx} is the discrete N-point spectral density obtained by the discrete Fourier transform of the autocorrelation function and Δt is the sampling period.

Here, the studied response signals are the tri-axial (x, y, z) accelerations from a given sensor, which are normalized with respect to their mean and standard deviation as,

$$\bar{x}(t) = \frac{x(t)-\mu}{\sigma} \quad (4)$$

Where μ and σ are the mean and standard deviation of the acceleration, respectively.

For the first, second and the third orders, the SMs are calculated separately for each direction (x, y, z) using Eq. (3), and a resulting 3-dimensional vector is constructed as,

$$\Lambda^n = [\lambda_x^n \;\; \lambda_y^n \;\; \lambda_z^n] \quad (5)$$

The next step is to use this Λ^n vector of all the sensor data as the indicative feature to perform the cluster analysis to identify the de-bonding of FRP strips.

4. K-means clustering

K-means clustering algorithm performs a partition of data space into K clusters. Each cluster is represented by an object, named centroid or the mean point, whose initial value can be randomly set or estimated by applying some kind of heuristic. In an iterative process, each element is assigned to the partition with the least distance between it and the centroid of the partition. Once all elements have been assigned into clusters, cluster centroids are recalculated using the information of the elements that belong to each partition. The process converges to a solution. K-means clustering for damage detection allows detecting anomalies like damage which are usually isolated in small clusters.

5. RESULT

Typical acceleration responses after normalization in x-direction of two sensor points, sensor point 5 and sensor point 10 are shown in Fig. 6. The normalized power spectral density (PSD) vs. Frequency graph between those two sensors points are shown in Fig. 7.

In the first case, FRP strip is de-bonded near sensor point 5. Absolute distance of co-ordinate (SM_x, SM_y, SM_z) is calculated and plotted vs sensor point in Fig. 8. In this case, order of the SM is considered equal to 2. In Fig. 8, it is observed that the red colored line deflects upward near sensor point 5. This represents that the de-bonded FRP is near sensor point 5.

The cluster analysis result using K-mean cluster analysis is plotted in Fig.8. Each point of the cluster indicates the sensor. The FRP strip is de-bonded near sensor points 4 and 5. The cluster represented by black point are seems to be outlier which indicates the faulty points of the girder. The SM values of sense point 4 and sense point 5 are represented in Fig. 9 by '*' shaped points. Total five points can be seen in the black colored cluster, where 2 points (sense point 4 and sense point 5) are nearer to the de-bonded FRP portion. The rest three points of the black colored cluster are near the support of the I-girder where the vibration response is too small. Therefore, if these three points are excluded from the outlier cluster, the remaining two sense point 4 and sense point 5 indicate the de-bonded FRP strip of the girder.

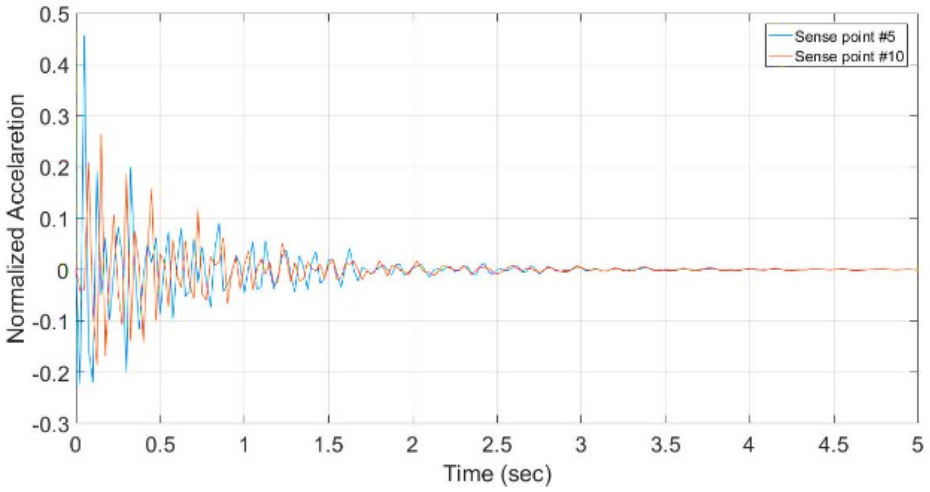

Figure 6. Acceleration responses of the girder at sensor points

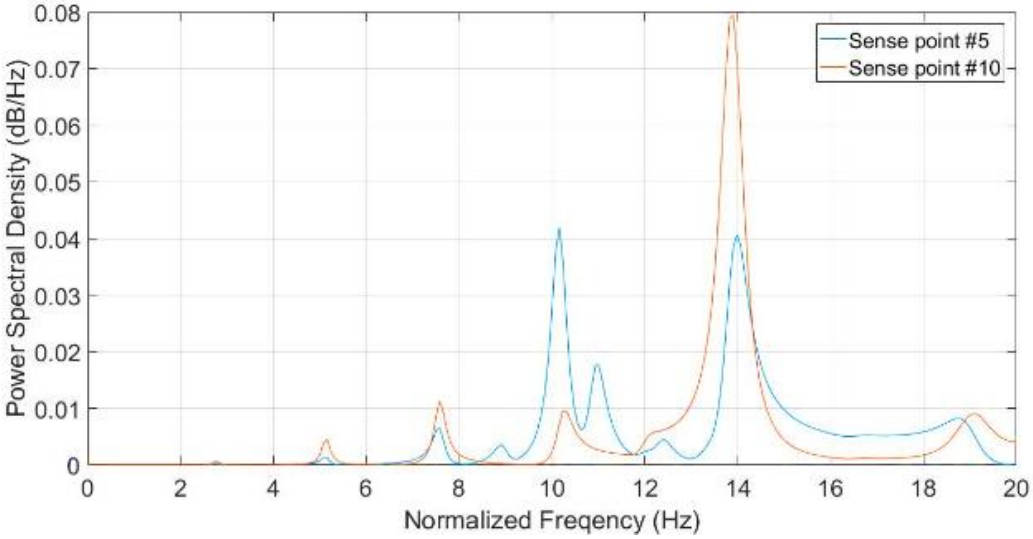

Figure 7. PSD of acceleration responses

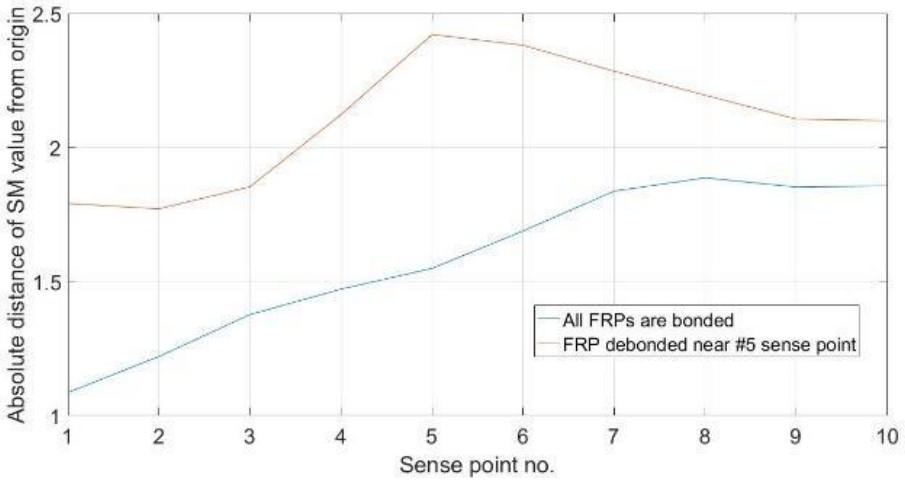

Figure 8. Absolute distance of SM vs sensor points

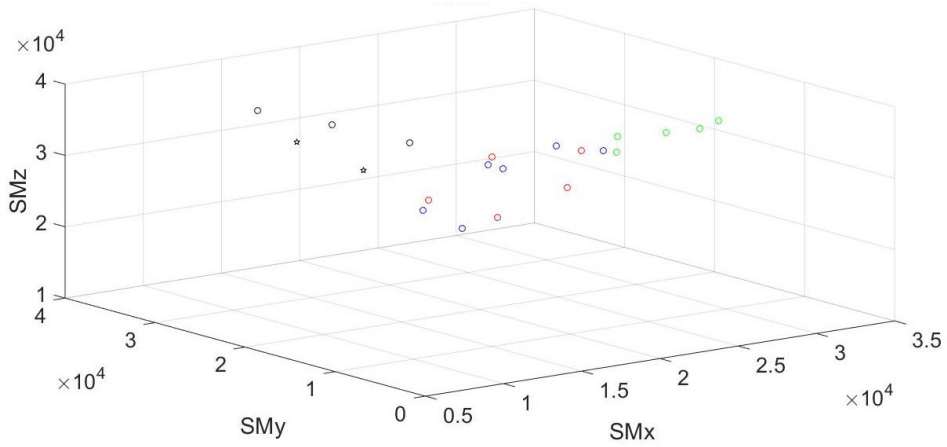

Figure 9. Clusters of sensor points of the girder

6. CONCLUSION

This paper presents an approach to collect the vibration response data from an I-girder bridge, and then investigation of that data to detect anomalies near FRP de-bonded portion. This approach utilizes spectrum-driven features, i.e. the spectral moments, SMs, from measured accelerations from the sensor points. SMs contain information from the entire frequency range, thus subtle differences between the normal signals of bonded FRP and distorted ones due to de-bonding of FRP from the girder surface, could be identified. These SMs are used as inputs to k-means clustering algorithm and faulty points of the girder or de-bonding of FRP is identified.

7. REFERENCES

Alamdari MM, Rakotoarivelo T, and Khoa NLD (2017). A spectral-based clustering for structural health monitoring of the Sydney Harbour Bridge. Mechanical Systems and Signal Processing, 87: 384–40.

Farrar CR, and Worden K (2007). An introduction to structural health monitoring. Philosophical Transaction of Royal Society (1851):303–315. DOI: 10.1098/rsta.2006.1928

Nguyen, D. M., Chan, T. K. and Cheong, H. K. (2001]). Brittle failure and bond development length of CFRP-concrete beams, Journal of Composites for Construction, pp. 12-17.

Sohn H, Farrar CR, Hemez FM, Shunk DD, Stinemates DW, Nadler BR (2004). A review of structural health monitoring literature: 1996–2001. Los Alamos National Laboratory, LosAlamos.

Pascale, G. and Bonfiglioli, B. (2001). Reinforced concrete beams damaged and repaired with CFRP: Dynamic testing and modeling, International Conference on FRP composites in civil engineering, Vol. 42, Elsevier, Hong Kong, pp. 441-448.

Zanardo, G., Hong, H., Xia, Y. and Deeks, A. J. (2006). Stiffness assessment through modal analysis of an RC slab before and after strengthening, Journal of Bridge Engineering (ASCE), 11: 590-601.

Proc. 2nd International Conference on Structural Engineering Research (iCSER2019)
19-22 Jan 2019, Dhaka, Bangladesh
ISBN: 978-0-6482681-2-3

Finite Element Analysis of a Notch Specimen under Monotonic and Cyclic Loading Condition Using a Novel Plasticity Model with Yield Plateau Phenomenon

Md. Tariqujjaman[1] and Nazrul Islam[2]

[1]Undergraduate Student, Civil Engineering Department, Bangladesh University of Engineering and Technology, Dhaka-1000, Bangladesh
2Assistant Professor, Civil Engineering Department, Bangladesh University of Engineering and Technology, Dhaka-1000, Bangladesh
Corresponding author's E-mail: nazrulislam@ce.buet.ac.bd

Abstract

This study analysed various plasticity models to simulate the yield plateau responses of structural mild steel. The plasticity models which have been used for the analysis are bi-linear, multi-linear kinematic, iso-tropic hardening and Chaboche kinematic model available in the FE software package in ANSYS. As neither of these models can simulate the yield plateau phenomena, a novel two surface plasticity model developed by Islam et al. has been used to simulate this response. FE analysis of a single element model has been performed to validate the experimental responses for the yield plateau. Finally, a FE analysis of a notch has been performed under monotonic and cyclic loading condition using the yield plateau model, and the influence of the yield plateau in the structural responses has been investigated.

Keywords: Cyclic Plasticity, Yield Plateau, Mild Steel.

Proc. 2nd International Conference on Structural Engineering Research (iCSER2019)
19-22 Jan 2019, Dhaka, Bangladesh
ISBN: 978-0-6482681-2-3

Damage Identification using Noise Polluted Static Strain Data

NHM Kamrujjaman Serker[1] and Bulbul Ahmed[2]

[1]Professor, Rajshahi University of Engineering & Technology, Rajshahi, Bangladesh
[2] Assistant Professor, Rajshahi University of Engineering & Technology, Rajshahi, Bangladesh

Corresponding author's E-mail: kserker@gmail.com

Abstract

This paper presents a method to detect damage utilizing only the strain data collected from a damage-expected beam structure without intact baseline data. Strain is very sensitive to local damage and relatively easier and cheaper to measure with high accuracy. The presented damage identification technique was verified with the noise polluted experimental data. The structural condition at the intact state is not required for the identification or localization of the damage. The damage identification strategy is also not influenced by the loading condition or loading configuration. Sensor configuration to be installed on the structure along with the measured response can be used to identify and localize presence of any damage. The experimental results show that the damage identification is not affected by the noise in the measured data. Long term monitoring of structure with this technique is also presented in this paper.

Keywords: Damage identification, macro-strain, structural health monitoring.

1. INTRODUCTION

Civil infrastructures are the essential components of the modern civilization and none of these structures is built for eternity. However, the expected service life of these structures is relatively longer compared to other commercial or manufactured products. Uninterrupted performance of these structures is of prime importance for the smooth running of human civilization. Failure of such a structure may cause extreme casualty both in terms of financial as well as live losses. Even a short-term malfunctioning affects the society tremendously. Due to the importance of civil infrastructures structural damage identification has gained increasing attention from the scientific and engineering communities. Therefore safety and integrity of structures can be maintained and uninterrupted service can be ensured through reliable and effective non-destructive damage identification in the structure. Although numerous techniques and algorithm for damage detection can be found in the literatures the most popular method of detecting structural damage is visual inspection where concern people physically observe damage and document its location and severity. Visual inspection technique has many limitations since the process is periodic and dependent on the accessibility to the damage location. The drawbacks of visual inspection can be avoided by using a noninvasive, computational method to detect structural damage i.e. by measuring the structural responses. Structural response based methods usually monitor changes in the response behavior of structural systems to locate and quantify areas of damage.

Doebling et al. (1996) categorized the response based damage identification methods as either local or global damage identification techniques. The vibration-based damage identification methods are considered as global damage identification techniques which consider the modal properties of structure. However, the modal properties especially the modal frequency is highly susceptible to environmental temperature changes. Serker and Wu (2009) evaluated the temperature sensitivity of some vibration based techniques and concluded that the damage localization as well as quantification

can be influenced with the change in temperature. In most local damage identification techniques the vicinity of damage is known a priori and readily accessible for testing, which cannot be guaranteed for most cases in civil engineering.

There are also many other challenges to implement the vibration based damage identification strategy (Farrar and Jauregui, 1998). These challenges include measurement of the structural information as well as post-processing of the measured data. Strain measurement is considered as a solution to these problems due to its simplicity in measurement techniques and damage sensitivity (Jang et al., 2008). In this paper, static macro-strain response based damage identification method is presented. With the proposed method damage detection and/or quantification can be done with no requirement for an analytical model and/or health condition of the intact or undamaged structure. Sensor location ratios are used as the reference to identify the presence of damage. Damage identification can be performed by directly utilizing the strain measurements from various sensors.

2. MACRO-STRAIN BASED DAMAGE IDENTIFICATION APPROACH

For an intact beam the flexural stress or strain at any location along the beam solely depends on the magnitude of the moment. For a given configuration and a set of loads, moment at any location can be expressed as a function of the measurement location. Therefore, the ratio of the strain between two measurement locations can be used as a damage indicator. The strain ratio can help to detect and quantify the damage. In this study macro strain is considered instead of typical strain which can be defined as the average strain over some part as shown in Figure 1(b).

The flexural strain of a beam like structure at any location x can be calculated as

$$\varepsilon_x = \frac{M_x y}{EI} \tag{1}$$

where M_x is the bending moment at any location , and ε_x are the corresponding flexural strain at the same location. y is the distance between the target location and the neutral axis, E is the elastic modulus and I is the moment of inertia of the beam section.

2.1 Damage Localization

Consider the simple supported beam shown in Figure 1(a) with a point load applied at a distance L_P from the left support. Strain at any location x_i can be obtained as

$$\varepsilon_i = \frac{R_L x_i y}{EI} \tag{2}$$

Similarly, the strain at any reference location, x_R, can be written as

$$\varepsilon_R = \frac{R_L x_R y}{EI} \tag{3}$$

Using Equations (2) and (3), ratio of the strain between these two locations can be found as

$$\gamma_i = \frac{\varepsilon_i}{\varepsilon_R} = \frac{x_i}{x_R} \tag{4}$$

From Equation (4), it is clear that for a given configuration of load the ratio of the strain between two measurement locations is equal to the ratio of the distances measured from the

same reference point. The strain ratio is also independent of the applied load. For other measurement locations similar strain ratios can be obtained as

$$\{\gamma_1, \gamma_2 ....., \gamma_i\} = \left\{ \frac{\varepsilon_1}{\varepsilon_R}, \frac{\varepsilon_2}{\varepsilon_R} ..... \frac{\varepsilon_i}{\varepsilon_R} \right\} \tag{5}$$

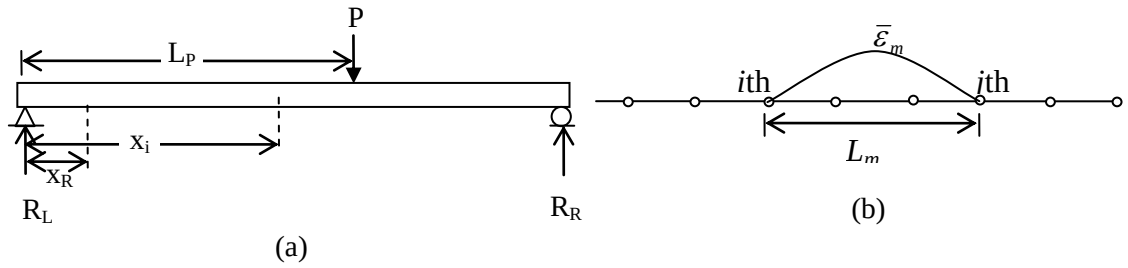

Figure 1. (a) Fundamentals of the strain-ratio approach (b) macro-strain over a long-gage sensor

These strain ratios are all independent quantities and independent of the applied load.
If the damage of an element is defined as a reduction of the flexural rigidity, the damage can be expressed as follows:

$$E^* I^* = \beta EI \tag{6}$$

where E^*I^* and EI are the flexural rigidity of an element under damaged and undamaged state respectively. Here, $\beta \quad (0 \le \beta \le 1)$ is the ratio of the effective flexural rigidity at undamaged and intact conditions. β is 1 with no damage and zero with complete damage in the element. The strain at a location x_i with a reduced stiffness of βEI can be written as

$$\varepsilon_i^* = \frac{R_L x_i y}{\beta EI} \tag{7}$$

The strain ratio between the damaged section and the undamaged reference section can be written using Equations (4) and (8) as

$$\gamma_i^* = \frac{\varepsilon_i^*}{\varepsilon_R} = \frac{1}{\beta} \frac{x_i}{x_R} \tag{8}$$

where γ_i^* is the strain ratio between the damaged section and the reference section. From Equations (4) and (8) it is obvious that the strain ratio value changes as the measurement location receives any damage. Damage is usually identified by comparing the measured response from undamaged and damaged state of any structure. In practice, the structure to be monitored may not be found in undamaged condition which demands some alternatives to obtain the intact state response e.g. analysis through finite element method. In this damage identification process spatial information of the sensors can meet the purpose.

3. APPLICATION IN STRUCTURAL HEALTH MONITORING

It is well known that structural response can be influenced by many factors, for example environmental temperature, humidity and noise etc. This may lead to non-reliable damage identification results if a single measurement is used for damage identification. Erroneous

damage identification can be avoided and thereby the probability of damage detection can also increased by utilizing several sets of measurements and incorporating statistical models into the damage identification scheme. Figure 2 graphically represents the proposed damage identification technique for a set of measurements. Reliability of the damage identification results can be increased by changing the magnitude and position of load. The reference or the critical value of the DI can be obtained from the spatial information of sensors.

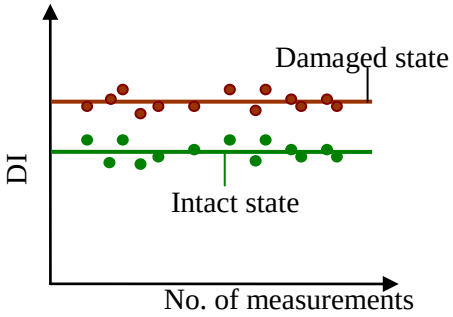

Figure 2. Damage Identification in a Noise Polluted Environment

4. EXPERIMENTAL INVESTIGATION

Experimental investigations were carried out to verify the effectiveness of the proposed damage identification strategy. Tests were performed on simply supported undamaged and damaged beams shown in Figure 3. Test beam was divided into ten zones and two types of sensors were used to measure the strain of different zones. FBG sensors are attached by two-point fixing to measure macro-strain. Gage-length was considered as 200 mm which is equal to the size of the element in the beam model. A single point load of increasing amplitude (30, 50, 75, 100, and 125N) was applied between nodes 3 and 8. Applied loading configuration was same for both intact and damaged beams. Measured strains were recorded in a PC for further processing.

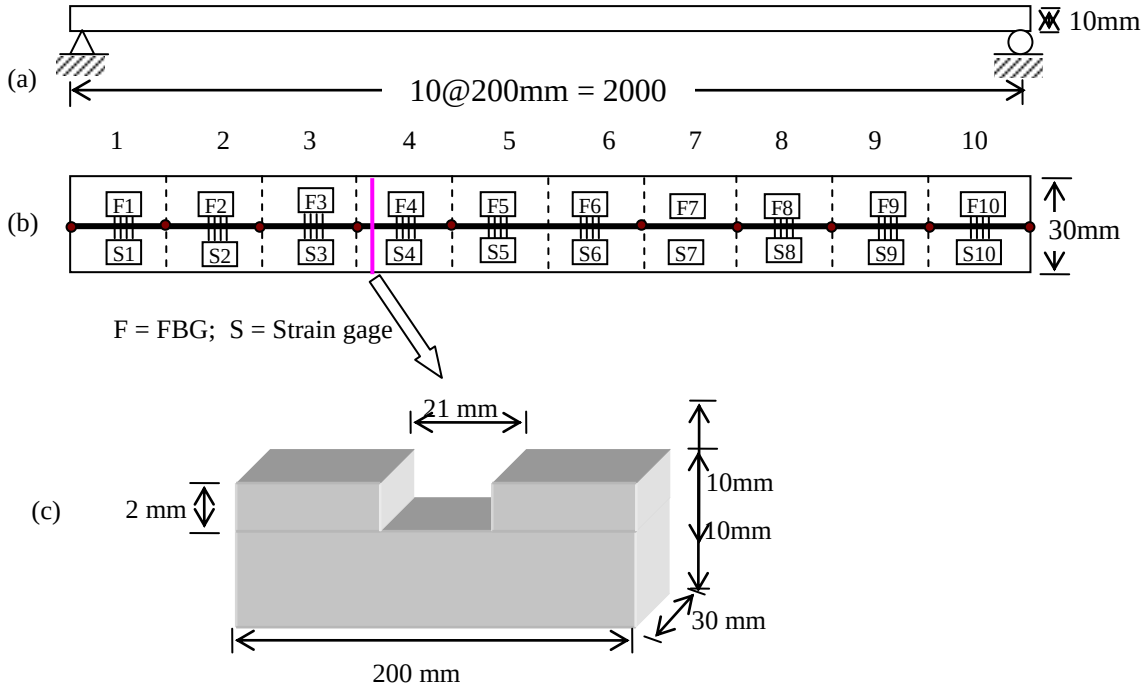

Figure 3. (a) Experimental specimen (b) sensor placement (c) details of damage

For each of the measured strain, simulated random noise was added in the following form

$$\bar{\varepsilon}_i = \bar{\varepsilon}_i * [1 + \beta * \lambda(0,1)] \quad (9)$$

where $\bar{\varepsilon}_i$ is the macro-strain measured at i sensor $\lambda(0,1)$ is a random Gaussian variable with zero-mean and unitary standard deviation and β is the noise amplitude (β = 0.05). Strain ratios, which have been denoted as the damage index (DI), are evaluated for both the noise free and noise polluted measurements. Measured strain ratios are shown in Figures 4 and 5. The location ratio is indicated as the analytical DI and was used as the reference for damage identification.

From Figure 4, it is evident that all the measured points are around the reference line. These data represent the information of the different zones of undamaged beam. Damage identification result for the damaged beam is presented in Figure 5. Damage was applied at zone 4. Figure 5 (c) clearly highlights the presence of the damage in zone 4. In this case all the measured points are lying above the reference. However, the measured data for the other undamaged zones are lying around the reference line indicate 'no damage'.

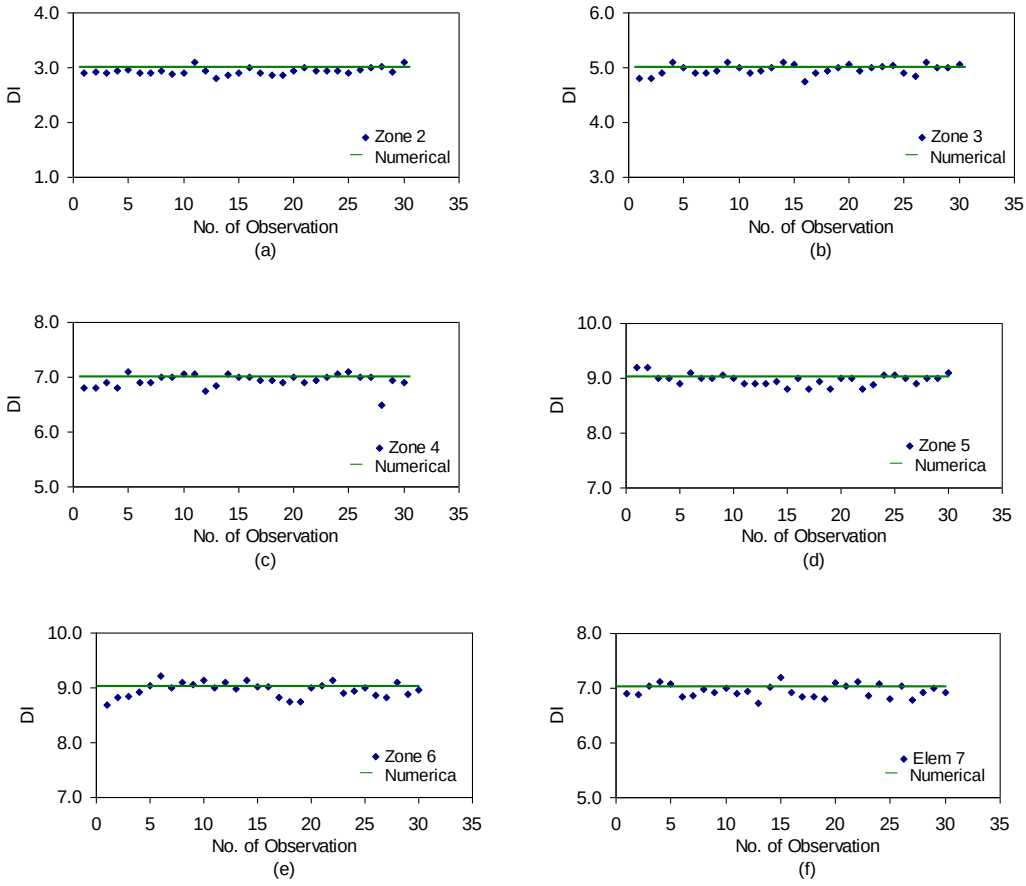

Figure 4. Comparison of the measured DI with the numerical DI of intact beam

5. CONCLUSIONS

In this paper damage identification using the static macro-strain response is presented. The abrupt change in the flexural strain resulted in the neighborhood of the damage region because of the local loss of section. Laboratory experiments are carried out to demonstrate the applicability of the proposed technique with long-gage distributed sensors. Damage identification results for strain gauge aren't presented here. The damage was identified successfully. In addition, the damage identification process is not affected by the introduction of noise to the measured responses. It is noticeable that the method

works well when the magnitude of the load is large enough to produce a large value of strain. In this paper, thirty measured data are used to identify the damage. The more samples data are acquired, the more reliable of the damage identification results are.

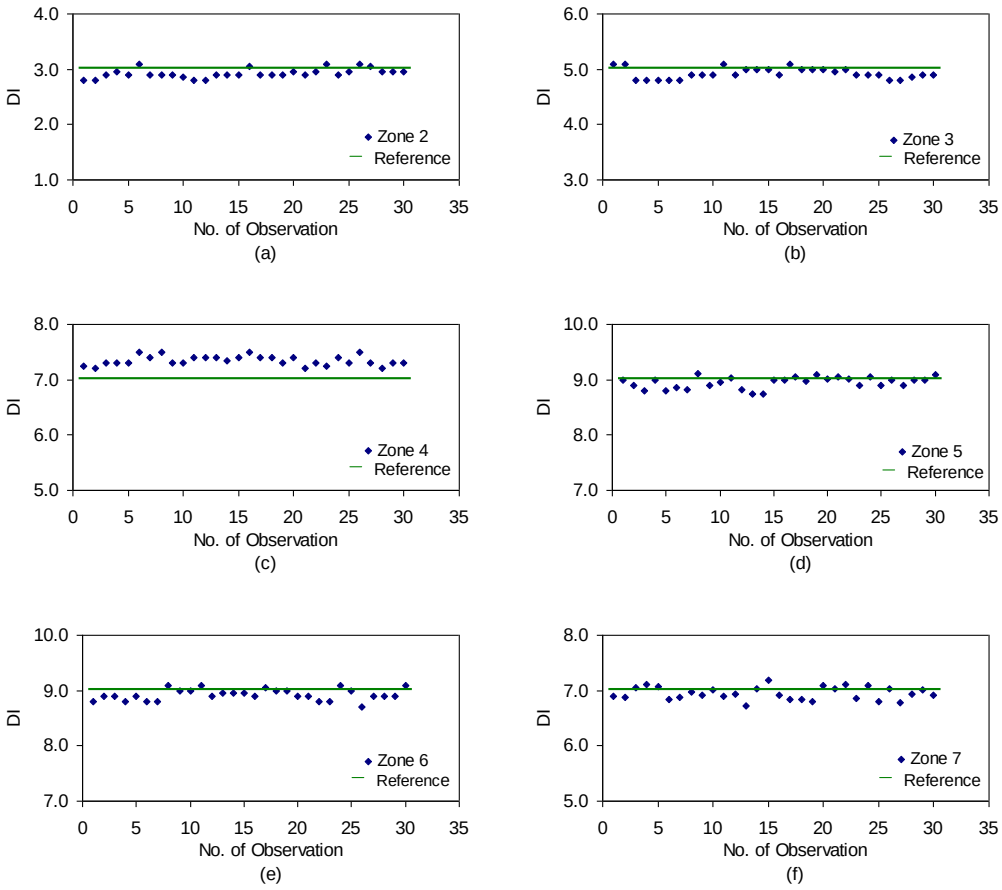

Figure 5. Damage identification using FBG sensors (without noise)

REFERENCES

Doebling SW, Farrar, CR, Prime MB and Shevitz DW (1996). Damage Identification and Health Monitoring of Structural and Mechanical Systems from Changes in their Vibration Characteristics: A Literature Review. Los Alamos National Laboratory report,(LA-13070-MS).

Farrar CR and Jauregui DA (1998). Comparative study of damage identification algorithms applied to a bridge: I. Experiment, Smart Materials and Structures 7 (5), 704.

Jang, SA, Sim SH and Spencer Jr. BF. (2008). Structural Damage Detection Using Static Strain Data Department of Civil and Environmental Engineering, University of Illinois at Urbana-Champaign, Illinois.

Li SZ and Wu ZS (2007). Development of distributed long-gage fiber optic sensing system for structural health monitoring, *Structural Health Monitoring*, 16, 133-143.

Serker, NHMK and Wu ZS (2009). Temperature Sensitivity Assessment of Vibration-based Damage Identification Techniques. *Structural Durability and Health Monitoring*, 5(2), 87-108.

Proc. 2nd International Conference on Structural Engineering Research (iCSER2019)
19-22 Jan 2019, Dhaka, Bangladesh
ISBN: 978-0-6482681-2-3

Geometric Effects of Edge Fairing on Aerodynamic Characteristics of Box Girder Bridge Deck: Influence of Nose Position

Md. Naimul Haque[1], Hiroshi Katsuchi[2] and Md. Basir Zisan[3]

[1]Assistant Professor, Department of Civil Engineering, East West University, Dhaka, Bangladesh
[2]Professor, Department of Civil Engineering, Yokohama National University, Yokohama, Japan
[3]PhD Student, Disaster Prevention Research Institute, Kyoto University, Kyoto, Japan
Corresponding author's E-mail: naimul@ewubd.edu

Abstract

Edge fairing is one of the common aerodynamic countermeasures that is often applied to the box-girder to improve the aerodynamic behaviour of the long-span bridge deck. The aerodynamic response and flow behaviour of bridge deck with edge fairing should be well understood for a better design of the long-span bridges. In this study a numerical investigated was devoted by employing Unsteady RANS to examine the influence of nose position of edge fairing on aerodynamic behaviour of box-girder bridge deck. The nose of the edge fairing was kept on the upper and lower half of the deck for a number of positions and their aerodynamic behaviour was compared to understand the effect of nose position on aerodynamic characteristics. The nose position of the edge fairing was altered by changing the top and bottom plate slopes of the fairing. The steady state behaviour such as the force coefficients, pressure and velocity fields were explored in detail to assess the aerodynamic characteristics of the bridge deck. The results depicted that the nose position of the fairing influences the aerodynamic response significantly and the fairing with nose-down position has a better aerodynamic behaviour than the nose-up position.

Keywords: Aerodynamic response; box girder; fairing; nose position; CFD; Unsteady RANS.

1. INTRODUCTION

With the improvement of material strength and technology, engineers are going for long to longer span cable-supported bridges to improve the navigability. However, as the span length of the bridge increases, the deck becomes flexible in nature and the aeroelastic performance becomes a matter of concern. Various aerodynamic countermeasures are applied to the deck to improve the aerodynamic performance of the long-span bridges. Edge fairing is one of the most common aerodynamic countermeasures that is often applied to the long-span bridge deck to improve the aerodynamic behavior by reducing the along wind load and after-body vortex shedding activity such as the Deer Isle (USA), Bronx-whitestone (USA), Hakucho (Japan) and Tempozan (Japan) bridges possess edge fairing.

For edge fairing, there are a number of important shaping parameters such as the top plate slope (θ_T), bottom plate slope (θ_B) and the nose position (h/D) as shown in Figure 1. The aerodynamic response is quite sensitive to the shape of the fairing. In previous studies (Nagao et al (1993), De Meranda and Bartoli (2001), Sukamta (2008)) only the top (θ_T) and bottom (θ_B) plate slopes were taken into consideration and their influence on aerodynamic responses were investigated experimentally. In their studies few specific combination of top (θ_T) and bottom (θ_B) plate slopes were considered due to expensive nature of the test and showed that edge fairing is efficient in improving the aerodynamic responses. However, no clear recommendation for shaping the edge fairing was provided as it was

difficult to find some optimum shapes in terms of top (θ_T) and bottom (θ_B) plate slopes. In their study, the influence of other important shaping parameters i.e, the nose position (*h/D*) was not taken into

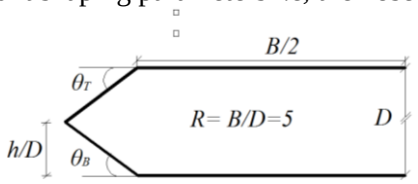

Figure 1. Geometric configuration and important shaing parameters of the considered bridge deck

consideration. Interestingly for edge fairing, the same combination of top (θ_T) and bottom (θ_B) plate slopes can be placed either in the lower half or in the upper half of the deck, hereafter which will be mentioned as nose-down or nose-up position of the fairing respectively as shown in Figure 2. Therefore, along with the top (θ_T) and bottom (θ_B) plate slopes, the influence of nose position (*h/D*) also should be investigated in detail and there is a possibility that some recommendations can be drawn to shape the edge fairing in terms of the nose position (*h/D*) to facilitate the bridge deck shaping procedure. Furthermore, in past studies the discussion was limited to vibration characteristics of the bridge deck only when the velocity was altered for a wide range of values based on a spring supported model without detailed analysis of the flow field for understanding the flow mechanism.

Recently, the Computational Fluid Dynamics (CFD) is becoming a popular research tool in various fields of engineering including bridge and bluff body aerodynamics fields due to its performance. Unsteady RANS is one of the common CFD approach having moderate accuracy and high computational efficiency. A number of researchers have already checked its performance and reliability (Bruno and Mancini (2002) and Sarwar et al (2008), Nieto et al. (2015) and Haque et al (2015a)) and successful application can be found in the field of bridge aerodynamics (Haque et al (2015a) and (2015b)).

With this background, in the present study the influence of nose position (*h/D*) of edge fairing on the aerodynamics of a closed box girder was investigated numerically by CFD. A two-dimensional unsteady RANS simulation with k-ω-SST turbulence model was employed to predict the steady state responses and the flow field around the bridge deck. A comparative study was made among the aerodynamic response of the bridge deck with edge fairing for the nose-up (*h/D*>0.5) and nose-down position (*h/D*<0.5). For each of these two positions of the nose, the top (θ_T) and bottom (θ_B) plate slopes of the fairing was varied from 11^0 to 40^0 as shown in Figure 2. The force coefficients and the flow fields such as the pressure and the velocity distributions were explored in detailed to understand the flow behavior All the simulations were carried out at a Reynolds number (*Re*) of 1.2×10^4.

2. NUMERICAL PROCEDURE

The unsteady Reynolds-Averaged Navier-Stokes (URANS) equations were used to model the flow around the bridge deck. Flow was assumed to be two dimensional and incompressible in nature. The governing equations are as follows:

$$\frac{\partial \overline{U}_i}{\partial x_i} = 0 \tag{1}$$

$$\frac{\partial \overline{U}_i}{\partial t} + \overline{U}_j \frac{\partial \overline{U}_i}{\partial x_j} = -\frac{1}{\rho}\frac{\partial \overline{P}}{\partial x_i} + \frac{\partial}{\partial x_j}\left[\nu\left(\frac{\partial \overline{U}_i}{\partial x_j} + \frac{\partial \overline{U}_j}{\partial x_i}\right) - (\overline{u_i' u_j'})\right] \tag{2}$$

where, $\overline{U}_i$ and x_i are the averaged velocity and position vectors respectively, t is the time, $\overline{P}$ is the

averaged pressure, ρ is the air density, v is the fluid viscosity. Due to time averaging process, the new variable $\overline{u_i'u_j'}$ appeared is known as Reynolds stress. It needs modelling to close the equation, which is

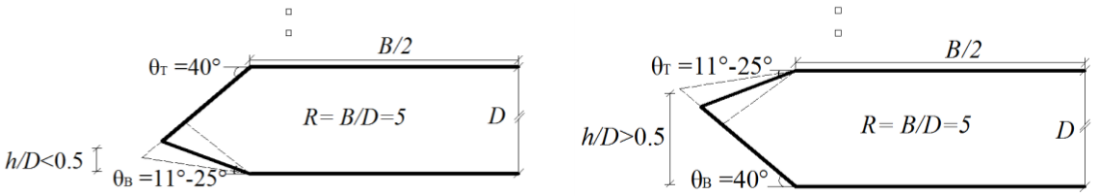

(a) Nose-down position (b) Nose-up position

Figure 2. Considered shapes of the edge fairing and the influence of nose position (*h/D*) on geometric configuration of the bridge deck

known as turbulence modelling. Turbulence modelling was attained by k-ω-SST, a two equations turbulence model (Menter (1994)). All the above mentioned governing equations were discretized by Finite Volume Method (FVM) and an open source code OpenFOAM was used as a solver. The convective and diffusive terms in the governing equation were discretized with second order accurate central differencing schemes. For time integration second order accurate backward differentiation formulae method was utilized. PISO (Pressure implicit with splitting of operator) algorithm was utilized to solve those discretized equations. To maintain stability of the simulations the maximum courant number (*Co*) was maintained well below 1. The domain was sufficiently large to avoid unnecessary disturbance of the boundary conditions. The performance of the utilized numerical model and setup for simulating steady state responses had already been checked previously (Haque et al (2015a) and (2015b)) for a wide range of bluff sections. The discussion about the validation study will not be deepen here, interested readers are referred to Haque et al (2015a and 2015b).

3. RESULTS AND DISCUSSION

3.1. Steady State Force Coefficients)

Both the mean and root means square (rms) values of the time varying steady state force coefficients were evaluated. Figure 3 compares the aerodynamic coefficients for these two cases. At the very first sight it can be easily understood that the nose position has significant influence on the steady state force coefficients. For any value of top (θ_T) or bottom (θ_B) plate slope the fairing with nose-down position has less responses as compared to the fairing with nose-up position. Both for the case of mean drag (C_D) and lift (C_L), the fairing with nose-down position has better aerodynamic responses. The fairing with nose-down position has lower drag value as compared to the fairing with nose-up position. The sign of the mean moment coefficient (C_M) has little significance, yet the sign of the lift force coefficient bears significant meaning in bridge aerodynamics field. The deck with nose-down position has a better aerodynamic behavior as the lift force acts downward (negative value) increasing the cable tension and thereafter the stability of the deck against wind.

The root mean square (rms) value of the aerodynamic coefficients provide a general idea about the dynamic characteristics of the bridge deck against wind. Similar to the mean value of the aerodynamic coefficients, the bridge deck with nose-down position has smaller value of aerodynamic coefficients. As can be seen from Figures 3(d) and (f) that for any value of fairings slope (θ_T or θ_B) the fairing with nose-down position experiences a little bit smaller fluctuations due to after-body vortices. However, the Strouhal number (S_t) shows comparatively lesser sensitivity to the variation of nose position of the edge fairing. For smaller plate slopes (θ_T or θ_B), the nose-down position has higher values of Strouhal number (S_t) which indicates that deck with nose-down position will experience vortex-shedding instability at higher wind speed. This section discusses the influence of nose position (*h/D*) on steady-state force coefficients quantitatively. In the next section the steady state flow field was analyzed in

detailed for a specific shape of the fairing as the influence of the nose position (*h/D*) on the force coefficients remains unchanged for any value of top or bottom plate slopes (θ_T or θ_B).

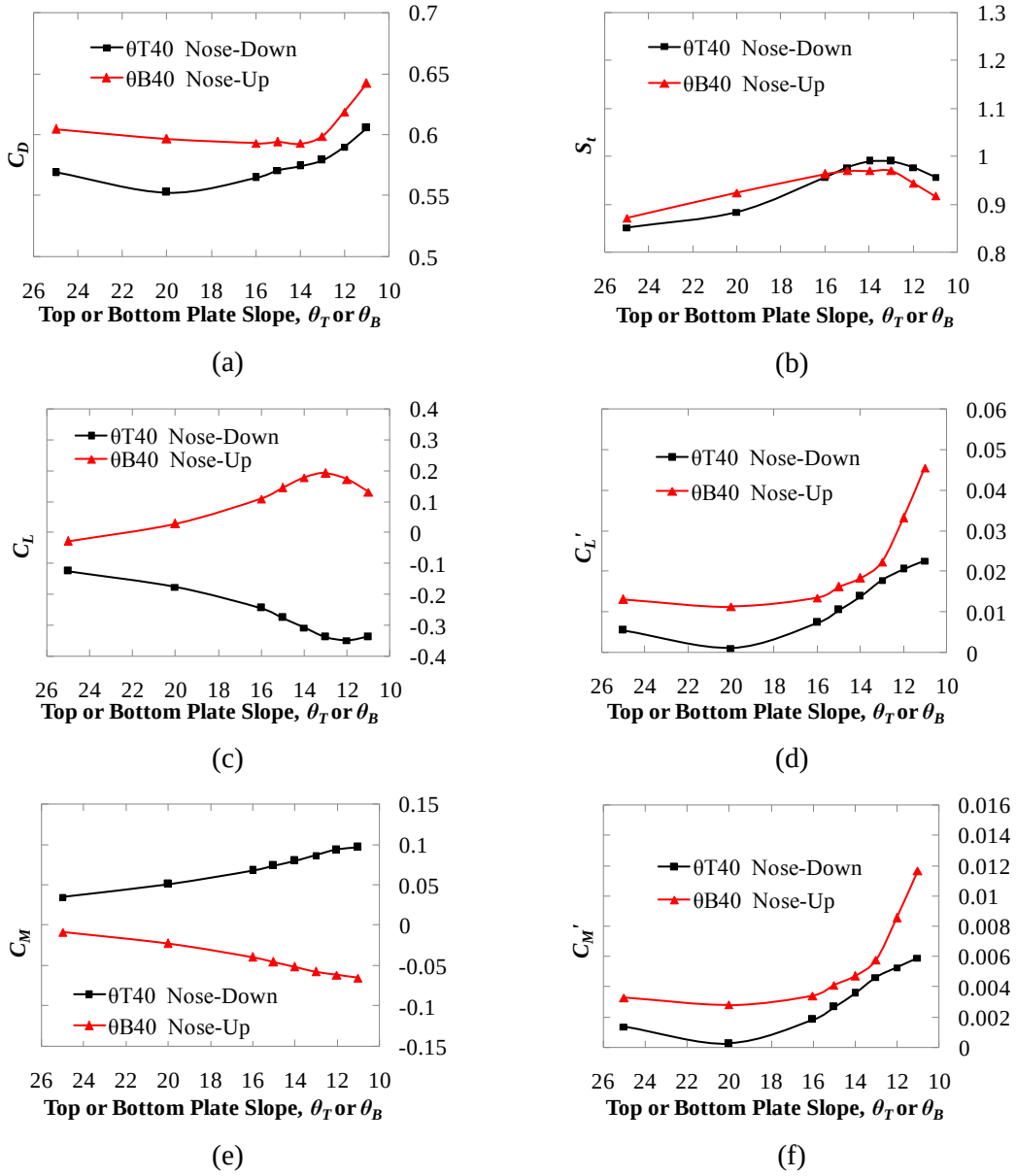

Figure 3. Influence of nose position on steady-state aerodynamic force coefficients

3.2. Flow Field Behavior

The flow field was analyzed for two shapes of fairings: i) Nose-up position (θ_T12-θ_B40; *h/D*>0.5) and ii) Nose-down position (θ_T40-θ_B12; *h/D*<0.5). The mean surface pressures are plotted in Figure 4 for detailed analysis of the flow field. The mean pressures are mainly affected in the leading edge side due to variation of the nose position (*h/D*). The magnitude and sign of the lift and moment coefficients are mainly controlled by the leading edge side pressure distribution. In case of nose-down position (*h/D*<0.5), there is a large negative pressure at the leading edge bottom surface and positive pressure at the leading edge top surface of the deck, as a result the bridge deck experienced negative lift force coefficient (downward) and positive moment coefficient (counterclockwise). Reverse mechanism is true for the case of nose-up position (*h*/D>0.5). To improve the further understanding about the flow field, the time averaged velocity fields are plotted in Figure 5. The general observation that was made in the last section also reflected in Figure 5. The clear shear layer separation and reattachment can be

seen in the leading edge side and after-body vortex shedding can be found. The velocity distribution around the bridge at the vertical plane is plotted in Figure 6. The picture depicts that the flow moves much faster on the bottom deck surface throughout the boundary layer in case of nose-down position and creates suction on the bottom deck surface, increasing the negative lift value of the bridge deck.

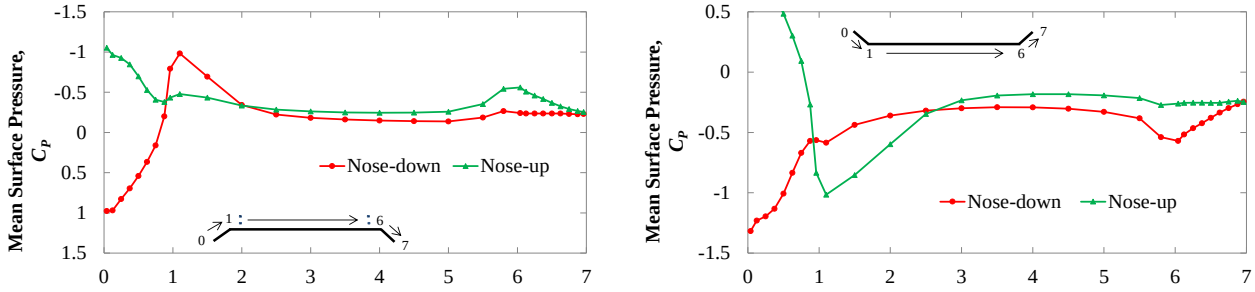

(a) Top surface pressure (b) Bottom surface pressure

Figure 4. Mean surface pressure distribution around the bridge deck

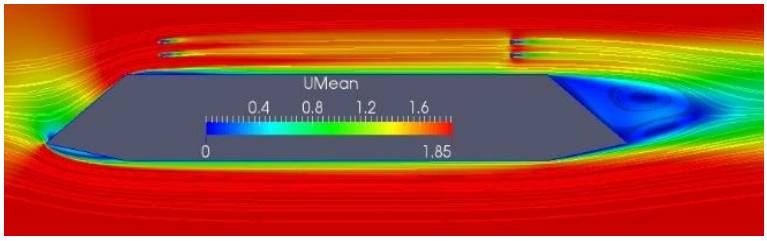

(a) Nose-down position

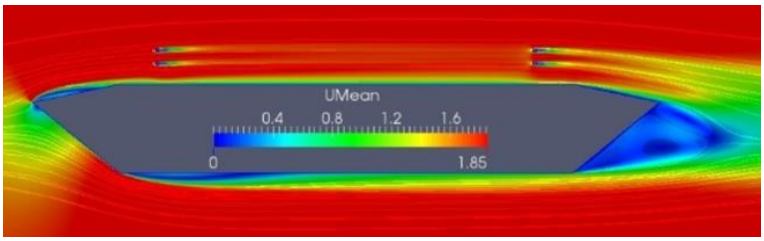

(b) Nose-up position

Figure 5. Time averaged velocity field around the bridge deck

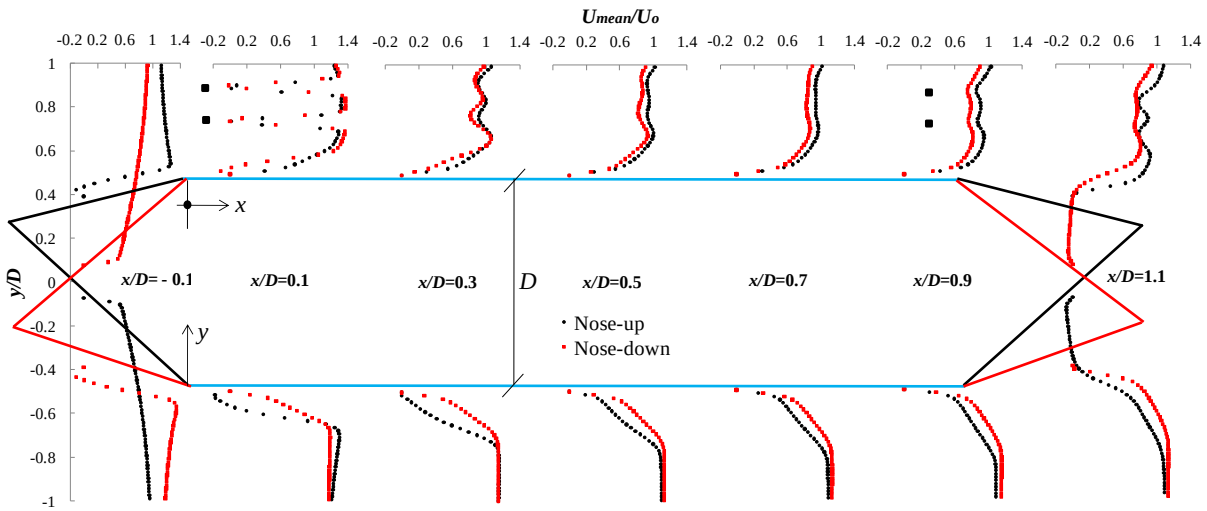

Figure 6. Velocity distribution around the bridge deck at the vertical plane

4. CONCLUSIONS

The influence of edge fairing's nose position (*h/D*) on aerodynamic response of a box girder bridge deck was investigated by employing two-dimensional unsteady RANS simulation. The shapes of the fairing were altered by changing the top (θ_T) and bottom (θ_B) plate slopes to investigate the influence of nose position (*h/D*) on the static behavior of the bridge deck. It was found that the nose-down position of the edge fairing has a better aerodynamic performance. The deck experienced lower aerodynamic loading and fluctuation of flow around the deck during the nose-down position of the edge fairing for any value of the bottom (θ_B) plate slopes. During the nose-down position of the fairing, the deck experiences lesser flow separation at the leading edge side bottom surfaces of the deck as compared to the nose-up position of the fairing and moves much faster at the bottom surface of the deck improving the flow characteristics of the bridge deck. Therefore, for practical bridges the nose of the edge faring can be placed downward to obtain better aerodynamic performance for the long-span cable supported bridge decks.

REFERENCES

Bruno L and Mancini G (2002). Importance of deck details in bridge aerodynamics, Structural Engineering International, 12(4), 289-294.

De Miranda M and Bartoli G (2001). Aerodynamic optimization of decks of cable-stayed bridges. Cable-Supported Bridges – Challenging Technical Limits, Proceeding of IABSE Conference, Seoul Korea, 12-14 June, 34-41 pp.

Haque MN, Katsuchi H, Yamada H, Nishio M (2015a). Flow field analysis of a pentagonal-shaped bridgedeck by unsteady RANS, Engineering Application of Computational Fluid Mechanics, 10(1), 1-16.

Haque MN, Katsuchi H, Yamada H, Nishio M (2015b). Strategy to develop efficient grid system for flow analysis around two-dimensional bluff bodies, KSCE Journal of Civil Engineering, 20(5), 1-12.

Nagao F, Utsunomiya H, Oryu T, Manabe S (1993). Aerodynamic efficiency of triangular fairing on box girder bridge, Journal of Wind Engineering and Industrial Aerodynamics, 49, 565–574.

Sarwar MW, Ishihara T, Shimada K, Yamasaki Y and Ikeda T (2008). Prediction of aerodynamic characteristics of a box girder bridge section using the LES turbulence model, Journal of Wind Engineering and Industrial Aerodynamics, 96,1895-1911.

Sukamta, Nagao F, Noda M, Muneta K (2008). Aerodynamic stabilizing mechanism of a cable stayed bridge with two edge box girder, In Proceedings of 6th International Colloquium on Bluff Body Aerodynamics and Applications, Milano, Italy, 20-24 July.

Menter FR (1994). Two-equation eddy-viscosity turbulence models for engineering application. AIAA Journal. 32, 1589-1605.

Nieto F, Owen JS, Hargreaves DM, Hernandez S (2015). Bridge deck flutter derivatives: efficient numerical evaluation exploiting their independencies, Journal of Wind Engineering and Industrial Aerodynamics, 136,138–150.

ISBN: 978-0-6482681-2-3

Authors Index

ISBN: 978-0-6482681-2-3

ISBN: 978-0-6482681-2-3

ISBN: 978-0-6482681-2-3

THE END